THE UNIVERSITY OF CALGARY

Investigation of C-E Bond Forming Reactions of $[ME_4]^{2-}$ (M = Mo, W; E = O, S, Se)

by

Naomi Louise Kruhlak

A DISSERTATION

SUBMITTED TO THE FACULTY OF GRADUATE STUDIES

IN PARTIAL FULFILLMENT OF THE REQUIREMENTS FOR THE

DEGREE OF DOCTOR OF PHILOSOPHY

DEPARTMENT OF CHEMISTRY

CALGARY, ALBERTA

APRIL, 2001

Abstract

The reactions of $[PPh_4]_2[ME_4]$ (M = Mo, W; E = O, S, Se) with alkyl halides have been investigated and we report the characterization of alkylated intermediates, $[PPh_4][ME_3(ER)]$, and their subsequent decomposition processes. ^1H, ^{77}Se and ^{95}Mo NMR spectroscopy have been used to follow these reactions, and ^{183}W NMR spectroscopy has been used to characterize alkylated products from reactions of $[PPh_4]_2[WS_4]$. The optimum synthetic conditions for alkylated products have been obtained from time dependent NMR spectroscopic data, allowing isolation of $[PPh_4][WS_3(SR)]$ (R = ^{i}Bu, Bz, allyl) and their characterization by X-ray crystallography. In reactions of $[PPh_4]_2[WS_4]$ with alkyl dihalides, monoalkylation is observed to occur readily but bis-alkylation at the same metal centre is not a predominant process. Instead, novel bridging dithiolate species of the formula $[PPh_4]_2[S_3W(SRS)WS_3]$ (R = $CH_2(C_4H_6)CH_2$) are formed and have been isolated and characterized under appropriate conditions.

X-ray crystal structures for the salts $[PPh_4]_2[WO_xS_{4-x}]$ (M = Mo, W; x = 0-2) are reported and include modelling of the rotational disorder observed in the oxothiometallate structures (x = 1, 2). The salts were further characterized by ^{183}W and ^{95}Mo NMR, elemental analysis and IR spectroscopy, and then pure samples were reacted with alkyl halides. Alkylation of $[PPh_4]_2[WO_xS_{4-x}]$ (x = 1, 2) was found to initiate O/S ligand exchange resulting in the formation of $[PPh_4][WS_3(SR)]$, and alkylation with ^{t}BuBr results in the formation of isobutene, presumably by C-S bond cleavage and β-hydrogen transfer, which is not observed in analogous reactions of tetrathio- or tetraselenometallates. Acetonitrile solutions of $[PPh_4]_2[WO_xS_{4-x}]$ (x = 1-3) were found to

be susceptible to aerial oxidation resulting in the formation of $[PPh_4]_2[W_6O_{19}]$, which was characterized crystallographically, and S_8.

Alkylated intermediates, $[PPh_4][ME_3(ER)]$, were found to decrease in stability moving from M = W to M = Mo and E = S to E = Se, making isolation of $[PPh_4][MoSe_3(SeR)]$ a difficult task that has not been successfully achieved. $[PPh_4][MoS_3(SR)]$ and $[PPh_4][WSe_3(SeR)]$ show higher, and comparable, stabilities in solution, but only one member has yet been characterized crystallographically.

Acknowledgements

I would first like to thank my supervisor Dr. Mike Boorman for taking me on as an undergraduate summer student and inviting me back as a graduate student. It has been a pleasurable experience working in his laboratory. I extend my thanks to members of my supervisory committee, Dr. T. Chivers and Dr. R. A. Kydd, for helpful discussion and advice regarding my research, and to Dr. W. Piers and Dr. R. Turner for their contributions to my candidacy exam. I would like to thank past members of the Boorman research group, Dr. Vivian Mozol and Dr. Meiping Wang, for their excellent teaching and patience in the early days, and also Ms. Nana Nguyen and Mr. Clinton Doering for being great summer students to work with.

I would also like to thank Dr. Steve Reid from the University of Saskatchewan, for getting me started in the area of multinuclear NMR spectroscopy and Ms. Dorothy Fox and Ms. Qiao Wu for excellent technical support, particularly with NMR instrumentation. I would like to acknowledge Dr. Deane McIntyre for running ^{183}W NMR spectroscopy and being so generous with instrument time, and Dr. Bob McDonald and Dr. Masood Parvez for successful X-ray crystallography on the most challenging of samples.

I would like to thank Greta Prihodko for being so very helpful and answering the many questions that I had as a graduate student, and other good friends I have made through the Department of Chemistry, Monica Gibson, Nicole Sandblom, Debra McIntosh and Josie Hill. Last, but by no means least, I would like to thank my husband Mike, for his loving support and encouragement throughout my many years of schooling.

To my husband Mike

Table of Contents

Chapter 1 – Biological and Chemical Significance of $[ME_4]^{2-}$

(M = Mo, W; E = O, S, Se)

Chapter 3 – Alkylation reactions of $[PPh_4]_2[WO_xS_{4-x}]$ (M = Mo, W; x = 0-2)

Chapter 4 – Alkylation Reactions of $[PPh_4]_2[WS_4]$ with Alkyl Dihalides and Attempted Complexation to a Second Metal

Chapter 5 – Multinuclear NMR Spectroscopic Studies of $[PPh_4]_2[ME_4]$ (M = Mo, W and E = S, Se) and their Alkylation Reactions

Chapter 6 – Conclusions and Future Work

Symbols and Abbreviations

a, b, c	unit cell dimensions
ADH	aldehyde dehydrogenase
AH	acetylene hydratase
Anal.	elemental analysis
AOR	aldehyde ferredoxin oxidoreductase
avg.	average
b	bridging
Bz	benzyl
Calcd.	calculated
CAR	carboxylic acid reductase
Cp, Cp*	cyclopentadienyl, pentamethylcyclopentadienyl
d	doublet
DMAD	dimethylacetylene dicarboxylate
DMF	N, N-dimethylformamide
DMSO	dimethylsulfoxide
EPR	Electron Paramagnetic Resonance (spectroscopy)
Et	ethyl
EXAFS	Extended X-ray Absorption Fine Structure (spectroscopy)
FDH	formate dehydrogenase
FMDH	N-formylmethanofuran dehydrogenase
Fo, Fc	structure factors, observed and calculated
FOR	formaldehyde ferredoxin oxidoreductase

GAPOR	glyceraldehyde-3-phosphate ferredoxin oxidoreductase
GC-MS	Gas Chromatography-Mass Spectrometry
GOF	goodness of fit
^{i}Bu	isobutyl
^{i}Pr	isopropyl
IR	Infrared (spectroscopy)
m	multiplet
Mol. wt.	molecular weight
NMR	Nuclear Magnetic Resonance (spectroscopy)
ORTEP	Oak Ridge Thermal Ellipsoid Plot
Ph	phenyl
ppm	parts per million
s	solvent (labelled on NMR spectra), or singlet
t, term.	terminal
T	temperature
^{t}Bu	tertiary butyl
THF	tetrahydrofuran
V	volume
vs.	versus
Z	number of molecules in unit cell
α, β, γ	unit cell internal angles
ρ_{calcd}	calculated density
*	impurity (labelled on NMR spectra)

List of Compounds

1 $[PPh_4]_2[WS_4]$

2 $[PPh_4]_2[WOS_3]$

3 $[PPh_4]_2[WO_2S_2]$

4 $[PPh_4]_2[MoS_4]$

5 $[PPh_4]_2[MoOS_3]$

6 $[PPh_4]_2[MoO_2S_2]$

7 $[PPh_4]_2[W_6O_{19}]$

8 $[PPh_4][WS_3(S^iBu)]$

9 $[PPh_4][WS_3(SBz)]$

10 $[PPh_4]_2[WS_3(SC_3H_5)]$

11 $[PPh_4][WS_3(o\text{-}SCH_2(C_6H_4)CH_2Cl)]$

12 $[PPh_4][WS_3(m\text{-}SCH_2(C_6H_4)CH_2Cl)]$

13 $[PPh_4][WS_3(p\text{-}SCH_2(C_6H_4)CH_2Cl)]$

14 $[PPh_4]_2[WS_3(o\text{-}SCH_2(C_6H_4)CH_2S)S_3W]$

15 $[PPh_4]_2[WS_3(m\text{-}SCH_2(C_6H_4)CH_2S)S_3W]$

16 $[PPh_4]_2[WS_3(p\text{-}SCH_2(C_6H_4)CH_2S)S_3W]$

17 $[PPh_4]_2[W_3OS_8(THF)]$

List of Figures

List of Schemes

List of Tables

Chapter 1 – Biological and Chemical Significance of $[ME_4]^{2-}$

(M = Mo, W; E = O, S, Se)

1.1 Introduction

Molybdenum and tungsten are, to date, the only two known examples of transition metals required by nature that are not in the first row of the periodic table.[1] Although they exhibit a number of similarities in their chemistry, they also possess subtle differences that have resulted in the evolution of different roles for the two metals in nature. The biological role of molybdenum has been known in detail for a relatively long period of time. However, the relevance of tungsten was not discovered until quite recently and has sparked a new wave of interest in synthetic chemistry with regard to synthesizing model complexes.[2,3]

The aim of this chapter is to give an overview of the biological and chemical aspects of molybdenum and tungsten enzymes, and then review some related synthetic chemistry, including model compounds.

1.2 Biological Significance of Molybdenum and Tungsten

The solution chemistry of high oxidation state oxothiometallates shows parallels to the chemistry observed in tungsten and molybdenum enzymes. Also, the solid state structural characteristics of coordinated chalcogenide and thiolate ligands are of particular interest when examining the coordination spheres of active metal centres.

Consequently, the chemistry of the simple oxothiometallate $[ME_4]^{2-}$ (M = Mo, W; E = O, S) is particularly intriguing with respect to these issues, and is highly relevant due

to its role as a naturally occurring source of the molybdenum and tungsten in biological systems.

1.2.1 Molybdenum Enzymes

Molybdenum was first discovered to be a requirement for nitrogen fixation in 1930, but it was another fifty years before the element was detected in an enzyme spectroscopically.[2] Molybdenum has widespread biological significance and while it is the most abundant redox-active transition metal in the oceans, its terrestrial abundance is quite low.[4] Molybdenum is present in the oceans as the soluble anion $[MoO_4]^{2-}$, which is incorporated into the active site of an enzyme by transfer mechanisms to form the active metal centre. Molybdenum has been found in more than 30 enzymes to date,[5] which have been isolated from a range of organisms, from bacteria to mammals. The ability of molybdenum (and tungsten) to undergo two-electron transfer reactions, between Mo(IV) and Mo(VI), is exploited in oxygen atom transfer reactions, such as the oxidation of sulfate and the reduction of dimethylsulfoxide (DMSO). The enzymes fall into two distinct classes, characterized by the type of cofactor they contain.[5] The first class contains only one example, nitrogenase, which consists of a heterobimetallic cluster of molybdenum and iron called the iron-molybdenum cofactor, or FeMoco (Figure 1.1). The second class contains examples of a single Mo centre coordinated to an organic ligand, determined by Rajagopalan *et al.* to be a pterin with a dithiolene moiety, and given the name *molybdopterin*.[6-8] The whole entity is described as the molybdenum cofactor or Moco (Figure 1.2).

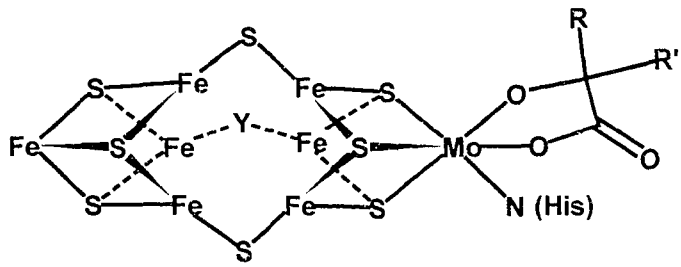

Figure 1.1 The iron-molybdenum cofactor (FeMoco).

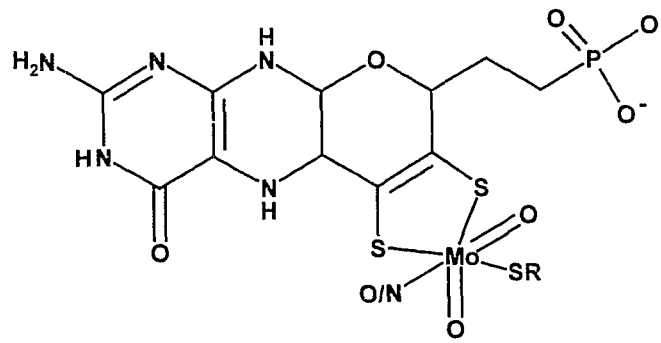

Figure 1.2 The molybdenum cofactor (Moco).

1.2.1.1 Molybdenum Cofactor Containing Enzymes

Variations of the molybdopterin ligand have been found to exist in some classes of organisms.[9,10] Eukaryotic organisms (*e.g.* higher plants and animals) have all been found to contain the unmodified molybdopterin (Figure 1.2), while prokaryotic organisms (*e.g.* bacteria) generally contain dinucleotide modified ligands (Figure 1.3). Tungsten enzymes characterized to date have been found to contain the unmodified molybdopterin ligand.

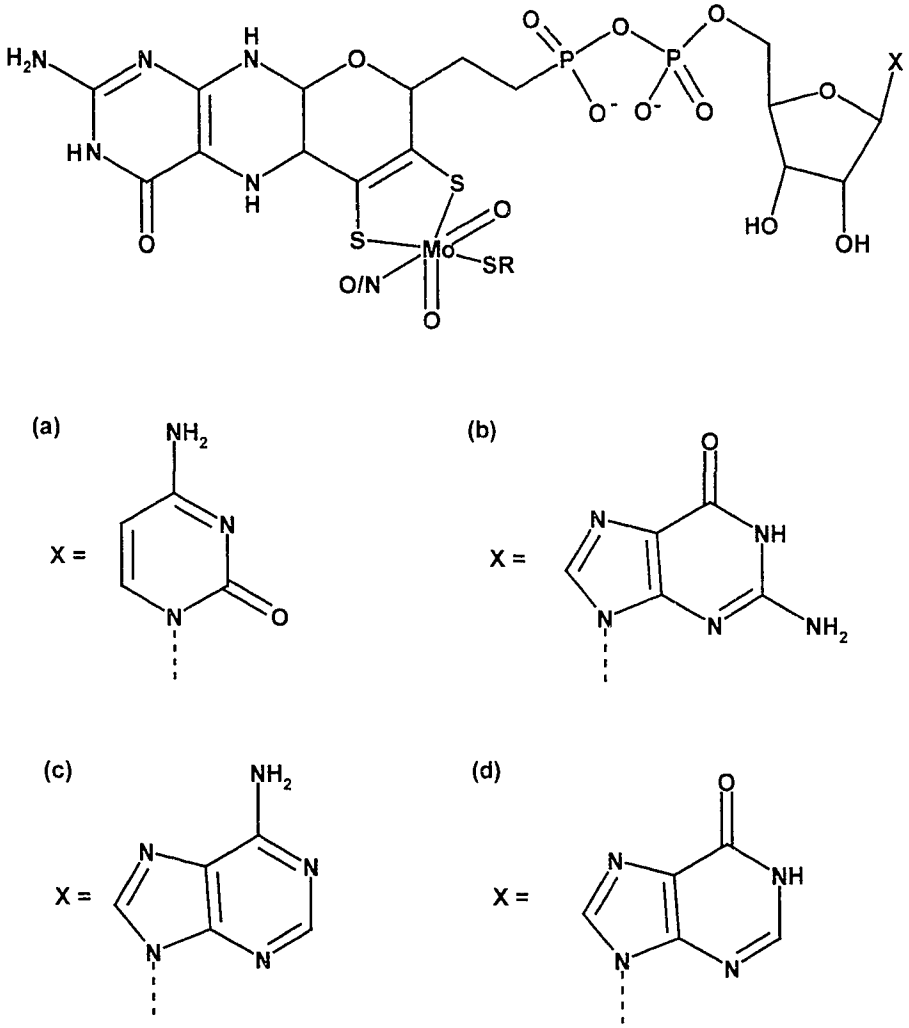

Figure 1.3 Variations on the unmodified molybdopterin, containing (a) cytosine, (b) guanine, (c) adenine and (d) hypoxanthine modified dinucleotides.[11]

Spectroscopic studies have allowed the elucidation of the active metal centres in some enzymes. X-ray crystallographic studies of the oxidized form of aldehyde ferredoxin oxidoreductase from *Pyrococcus furiosus*[11] show that two molybdopterin ligands are chelated to a W centre. This active site is structurally similar to that of

oxidized DMSO reductase from *Rhodobacter sphaeroides*[7] which until recently was also believed to possess two chelated molybdopterin ligands. A new higher resolution crystal structure (1.3 vs. 2.2Å) showed that some disorder was present in the crystals and two different Mo(VI) environments could be located, one with two coordinated molybdopterins and the other with only one.[8] In the latter case, the second dithiolene moiety was still in close proximity to the metal, which caused the authors to remark on the elasticity of the active site coordination sphere. K-edge extended X-ray absorption fine structure spectroscopy (EXAFS) data for DMSO reductase[12] and data from the two Mo sites shown in the table below.

Table 1.1 X-Ray crystallographic[8] and EXAFS[12] bond lengths (Å) for the Mo(VI) coordination sphere in DMSO reductase from *Rhodobacter sphaeroides*. Mo(1) and Mo(2) were refined with site occupancies of 0.6 and 0.4, respectively.

	X-ray cryst. Mo(1)[a]	X-ray cryst. Mo(2)[a]	EXAFS
Mo-$S_{thiolene}$	2.45	2.50	2.435(1)
Mo-$S_{thiolene}$	2.38	2.45	2.435(1)
Mo-$S_{thiolene}$	2.45	not a ligand	2.435(1)
Mo-$S_{thiolene}$	2.42	not a ligand	2.435(1)
Mo-O_{Serine}	1.84	1.92	1.920(15) (O/N)[b]
Mo=O	1.76	1.75	1.683(6)
Mo=O	not a ligand	1.71	not a ligand

[a]Errors in the bond distances are estimated at 0.02-0.04Å, depending on the method of calculation used. [b]The EXAFS data is somewhat ambiguous as to whether a N or O is present at this location.

The EXAFS data compare very favourably with the X-ray crystallographic data for the hexacoordinated Mo environment. The Mo-$S_{thiolene}$ distances are particularly close when the average value of 2.425Å from X-ray crystallography is compared to 2.435Å from EXAFS. The largest deviation occurs in the Mo=O distance, but the authors of the

crystallographic studies explain that this is the least accurate value since the two disordered O sites are within 0.78Å and cannot be resolved. The pentacoordinate structure shows more distinct differences in the proximity of ligands to the metal centre, particularly by the absence of coordinated dithiolene. It would appear that if a disordered crystalline sample was used for acquisition of the EXAFS data, the predominant structure contains the hexacoordinate centre. The pentacoordinate centre may only have been observed in the X-ray crystallographic data due to differences in sample preparation.

Different enzymes require different coordination environments at the metal to allow their catalytic cycles to function. For example, the terminal oxide in DMSO reductase is a consequence of oxygen atom transfer from the substrate to yield the oxidized form of the enzyme. The metal centre is reductively restored by loss of the ligand as water after a series of proton and electron transfer steps. In enzymes responsible for substrate oxidation, such as sulfite oxidase, the reverse process is believed to occur.[13,14] Oxygen atom transfer is facilitated by the oxidized form of the enzyme, which is subsequently reduced, and H_2O is acquired to restore the oxide after a series of proton and electron transfer steps.

Xanthine oxidase uses a more complex mechanism for formation of uric acid,[13] where two sites on the substrate are believed to directly interact with the metal centre. Based on ^{18}O labelling studies, oxygen atom transfer is believed to be facilitated by a terminal oxide after the substrate is coordinatively bound to the metal through a nitrogen (Scheme 1.1). Proton transfer is facilitated by a terminal sulfide, rather than an external source, forming a coordinated hydrosulfide as an intermediate.

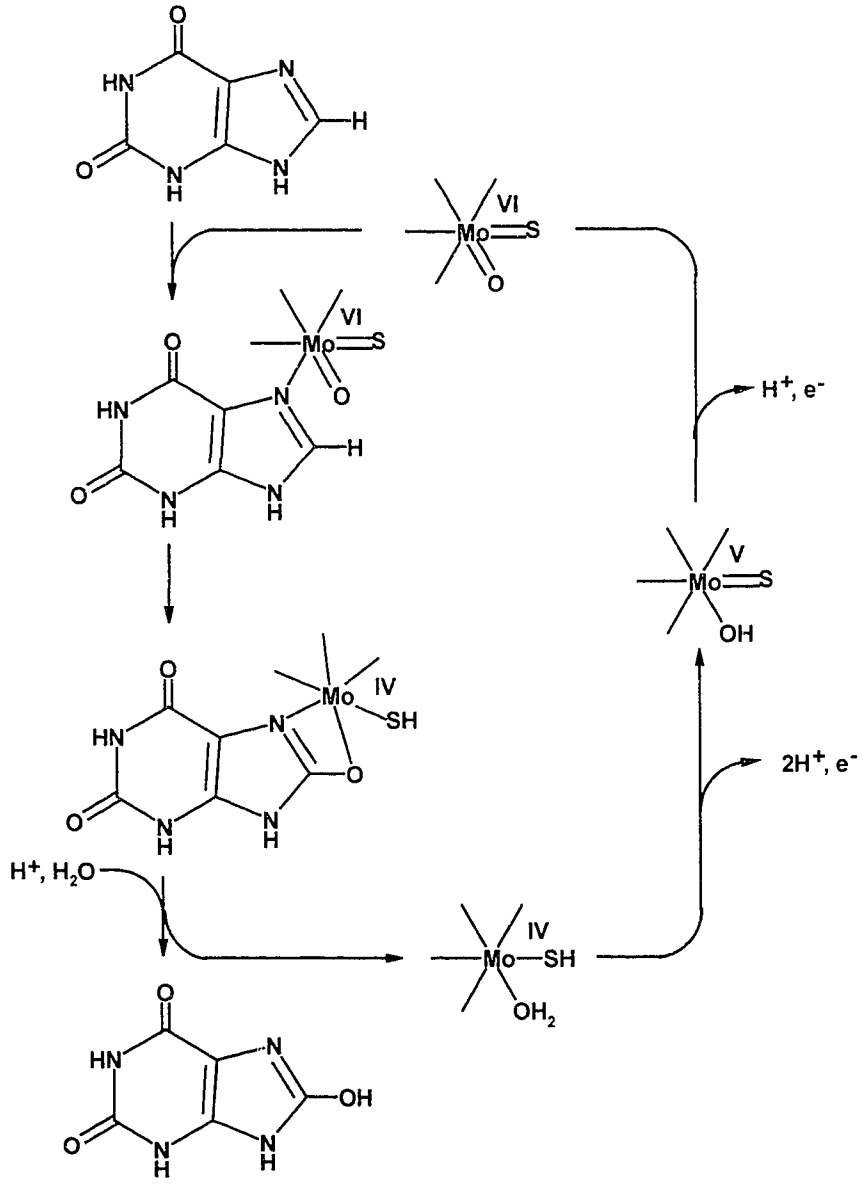

Scheme 1.1 Proposed catalytic cycle for the oxidation of xanthine to uric acid at Mo in xanthine oxidase.[13]

K-edge EXAFS and EPR studies have identified two forms of xanthine oxidase, the desulfo and active forms.[15] The desulfo oxidized (Mo(VI)) form has been characterized crystallographically and found to closely resemble that of sulfite oxidase,[16]

whereas the active form contains a terminal sulfide at 2.15Å in place of one terminal oxide.[17] The terminal sulfide is believed to be highly reactive and, in the reduced form of the enzyme, converts to hydrosulfide (at 2.39Å) as illustrated in Scheme 1.1. The ability of both terminal oxides and sulfides to interconvert to hydroxides and hydrosulfides, respectively, by coupled electron-proton transfer processes, enhances the versatility of the metal centre during its catalytic cycle.

The function of the coordinated pterin dithiolene moiety is not well understood, though it may be present to facilitate electron transfer between the many redox active sites in the enzyme.[2] Alternatively, it may simply be part of an acquisition and storage mechanism for the Mo to prevent formation of polymolybdates at neutral pH.[13]

1.2.1.2 Iron-Molybdenum Cofactor Containing Enzymes

The enzyme nitrogenase is responsible for nitrogen fixation and can be found in bacteria established within the root nodules of legumes, such as pea, bean and clover plants.[18] It contains the iron-molybdenum cofactor, in addition to other iron sulfur clusters, and catalyzes the formation of ammonia from dinitrogen, forming ammonium ions and dihydrogen as by-products.

$$\mathbf{N_2 + 6H^+ + 6e^- \longrightarrow 2NH_3} \qquad \textbf{Equation 1.1}$$

In addition to dinitrogen, nitrogenase is able to reduce a variety of other small unsaturated molecules at ambient temperature. The three types of nitrogenase that exist contain molybdenum/iron, vanadium/iron and iron alone. The enzyme consists of an iron

protein and an iron-molybdenum protein, the former containing a number of iron-sulfur clusters and the latter containing iron sulfide clusters in addition to two FeMoco units. Reduction of dinitrogen occurs after binding to the FeMoco unit, facilitated by electrons transported from the iron protein. It is believed that the reactivity of the protein units is heavily dependent on their spatial orientation within the enzyme.

The structure of FeMoco extracted from *Azotobacter vinelandii* was solved to 2.7 then 2.2Å resolution by Rees and coworkers.[19,20] Based on the structural features of FeMoco, it was suggested that an incoming nitrogen molecule might bind to the iron atoms in the central $Fe_3(\mu\text{-}S)_3Fe_3$ core, which shows a well defined "docking" site suitable for this purpose. It was also suggested that the binding site could not possibly be the molybdenum centre due to its coordinative saturation. This is consistent with the observation that vanadium or iron analogues of nitrogenase still show catalytic behaviour, though less efficient, in the absence of molybdenum.

Based on the X-ray crystallographic data, the molybdenum centre in nitrogenase is believed to be coordinated to three sulfide ligands of the cubane-like cluster, a chelating homocitrate unit and a nitrogen from a histidine amino acid residue.[19,20] The coordination geometry is distorted octahedral, with the sulfides adopting the necessary *facial* arrangement. It is thought that the homocitrate unit plays a critical role in modulating the redox properties of the active site by its involvement in the electron transfer pathway between FeMoco and the iron-sulfur clusters; this is believed to be a highly effective mechanism due to the close proximity (~14Å) of the two components.[19] In addition, the ability of the ligand to undergo protonation suggests that it may be involved in proton transfer to a coordinated substrate.[21] The sulfide ligands are believed

to have both a structural role, in maintaining the cavity for substrate binding, and an electronic role, as part of the iron sulfide cluster undergoing reversible reduction.[22]

EXAFS data for FeMoco suggest that the three bonding Mo-O/N distances are 2.1Å, and three Mo-S distances are 2.3Å. These data are consistent with the previously discussed crystallographic studies with regard to the total number of ligands around Mo but are ambiguous when attempting to distinguish between the number of nitrogen and oxygen ligated functionalities.

1.2.1.3 Molybdenum-Copper Antagonism

An interesting association has been observed in some organisms between the elements Mo and Cu, where a high level of dietary molybdenum can lead to a copper deficiency.[23-25] The other element that must be present for this to occur is sulfur and, consequently, levels of dietary sulfate have been found to affect the extent to which Cu deficiency occurs.[25] This has been extensively observed in cattle and has prompted much interest in Mo/Cu/S coordination chemistry since a direct interaction between each element is implied.

$[MoS_4]^{2-}$ is the best known Cu antagonist[24,25] and studies of its coordination to Cu in the presence of a variety of other ligands has been investigated.[26] A range of structural architectures has been revealed and will be discussed later in this chapter. It has been shown that $[MoS_4]^{2-}$ and its oxo-analogues can be extracted from FeMoco, making them available for complexation to Cu *in vivo*.[27] In addition, thiomolybdates are known to be formed in the digestive tract of ruminants.[25]

The condition has previously been treated by supplementing the diet of the affected animals with $CuSO_4$,[23] which results in sufficiently high levels of copper that depletion by molybdenum does not cause a deficiency. A similar approach has been applied to a related condition in humans, named Wilson's disease after its discoverer Kinnear Wilson in 1912.[23] This condition is caused by the inability to excrete dietary copper, which causes slow neurological and liver degeneration. $[NH_4]_2[MoS_4]$ has been successfully used to treat this condition by converting the copper into a chemically inert form and blocking intestinal absorption.

1.2.2 Tungsten Enzymes

In the early 1970s, it was discovered that the growth of certain organisms was stimulated in the presence of tungstate,[3] and while this did not directly indicate that tungstate was *required* by these organisms, it gave the suggestion that species might exist that naturally utilize the element. Indeed, in 1983, the first example of a naturally occurring tungsten enzyme was isolated and characterized, with more than ten examples having been purified to date.[28] Each type is categorized by the function it performs with particular substrates, and all are implicated in processes involving carboxylic acids and aldehydes. In addition, they are all thermophilic to some degree and function under anaerobic conditions. Tungsten enzymes have been isolated from several different microorganisms, and in some cases more than one has been isolated from the same microorganism.[3] The enzymes can be further categorized by the type of reaction they catalyze. Their catalyzed reactions are listed in the following table.

Table 1.2 The three types of tungsten enzymes, and their respective catalytic reactions.[3,28]

AOR Type	F(M)DH Type
Aldehyde ferredoxin oxidoreductase (AOR)	Formate dehydrogenase (FDH)
	$CO_2 + H^+ + 2e^- \longleftrightarrow HCO_2^-$
Formaldehyde ferredoxin oxidoreductase (FOR)	N-Formylmethanofuran dehydrogenase (FMDH)
Glyceraldehyde-3-phosphate ferredoxin oxidoreductase (GAPOR)	$CO_2 + MFR^+ + H^+ + 2e^- \longleftrightarrow CHO\text{-}MFR + H_2O$ (where MFR is a methanofuran substrate)
Carboxylic acid reductase (CAR)	
Aldehyde dehydrogenase (ADH)	**AH Type**
	Acetylene Hydratase (AH)
$RCHO + H_2O \longleftrightarrow RCO_2^- + 3H^+ + 2e^-$	$C_2H_2 + H_2O \longleftrightarrow CH_3CHO$

Of the above enzymes, AOR, FOR and GAPOR have been found in hyperthermophilic organisms (T > 90°C), and the remainder in moderate thermophilic organisms (T = 45-90°C).[28,29]

To probe the role of tungsten in each of these cases, the organisms were grown in the absence and presence of tungsten and molybdenum. Such studies indicate how the growth of the organism is affected and whether any changes to its catalytic activity occur. It has been found that hyperthermophiles are totally tungsten dependent but some moderate thermophiles grow equally well in an exclusively molybdenum containing environment.[28]

Despite the fact that molybdenum analogues exist for each type of tungsten enzyme, when the molybdenum analogues are grown in the presence of tungsten, they generally become inactive,[30] suggesting a lack of adaptability in changing from molybdenum to tungsten. It is apparent that despite many chemical similarities between the two metals, the fine-tuning of such active sites is dependent on their subtle differences. It is not surprising that the hyperthermophilic organisms are less adaptable than the thermophilic examples, since the former class are found in an exclusively tungsten containing environment. In contrast, thermophiles are exposed to molybdenum as well as tungsten, so would be at an advantage if they could adapt to use either. Such versatility is consistent with the theory that tungsten hyperthermophiles are an earlier life form and that tungsten moderate thermophiles and molybdenum enzymes have evolved from them. An apparent exception is the case of *Methanobacterium wolfeii*, which contains two FMDHs, one of which is molybdenum dependent and the other of which is tungsten dependent.[3] This is an example that the evolutionary theory does not quite accommodate, unless this is a highly versatile system that is dynamic between two separate environments. Such evolutionary considerations will be discussed in more detail later in the chapter.

All of the known tungsten enzymes contain molybdopterin, except in the case of FMDH which contains the molybdopterin guanine dinucleotide variation.[3] All contain iron as a second metal, which is likely in the form of the electron transfer protein ferredoxin.[28] CAR and FDH both have a high iron content, which, coupled with their high molecular weights, is suggestive of a more complex system than seen in other tungsten enzymes. Such complexity tends to make studies of the chemistry associated

with independent tungsten sites more difficult, especially since many of these organisms normally exist at extreme temperatures and pressures. It appears that tungsten has at least two physiological roles, one in catalyzing sugar degradation and the other in peptide degradation. How tungsten is directly involved in these steps on a molecular level, and how this relates to the overall catalytic activity of the enzyme, is not known.

The most widely investigated tungsten enzyme is AOR isolated from *Pyrococcus furiosus*, which is the only enzyme to have been characterized by X-ray crystallography to date.[31] The structure has been determined at 2.3Å resolution and shows a metal centre coordinated to two molybdopterin ligands and two oxygen-containing ligands, where the latter could be terminal oxide, glycerol or both. The possible presence of glycerol could be explained by sample preparation procedures, though it is possible that this ligand occupies the position that a substrate would bind during the catalytic cycle.

EXAFS studies of dithionite reduced AOR from *Pyrococcus furiosus* suggest the presence of three W-$S_{thiolene}$ interactions at 2.41Å, two terminal oxides at 1.74Å and an additional W-O/N at 2.10Å.[28] However, it is now believed that these data represent an inactive species and that subsequent studies showing a single terminal oxide at 1.75Å, four or five W-$S_{thiolene}$ at 2.40Å and a W-O/N interaction at 1.97Å represent the active species. In addition, these data correspond closely with the coordination sphere as determined by X-ray crystallography,[31] which was performed on a sample that had been tested to ensure its catalytic activity.

1.2.3 Evolutionary Considerations

Why is tungsten utilized in place of molybdenum in some biological systems? This has been best explained by comparing their abundance under certain conditions and the redox actvities of the respective metals.[30] The types of environments where tungsten enzymes have been found are either deep sea or shallow volcanic hydrothermal vents.[3] Such places have a very high abundance of sulfur and are essentially anaerobic, so when one considers the types of inorganic tungsten and molybdenum species found in these places they will invariably be metal sulfides. While tungsten sulfide chemistry is very active at the high temperatures found in the thermal vent (*ca.* 100°C in some cases), the molybdenum chemistry is almost non-existent due to the formation of insoluble MoS_3 and MoS_2 which precipitate out of solution.[4] It has been suggested that enzymes in these areas have evolved to take full advantage of the rich tungsten supply, in the absence of molybdenum.

In contrast, it has been suggested that bacteria containing tungsten enzymes are actually an example of prehistoric organisms that have not evolved appreciatively with time, and that molybdenum enzymes have actually evolved from them.[3] This stems from the assumption that the atmosphere in prehistoric times was rich in reducing H_2S, with a very minimal abundance of oxygen. Organisms that evolved at this time were anaerobic and relied heavily upon sources of sulfide. In time, as the atmosphere became richer in oxygen, the formation of tungsten and molybdenum oxides became more significant, forcing some organisms to slowly adapt to using redox active molybdate over the less reactive tungstate. In addition, the formation of H_2O in place of H_2S was believed to have a cooling effect on the surface of the Earth, making the molybdate a more suitable choice

than the now deactivated tungstate. In areas where sulfide concentrations and temperatures remained high, such as in the volcanic thermal vents, the tungsten enzymes continued to flourish.

1.2.4 Selenium versus Sulfur at Active Metal Centres

Sulfur is much more abundant than selenium, which likely contributes to its widespread use in biology, compared to the more specific roles for which selenium is employed.[32,33] The incorporation of selenium into active sites of certain enzymes is thought to have started during the appearance of dioxygen in the evolution of the Earth's atmosphere, which allowed Se to be present as a soluble oxidized form, $[SeO_4]^{2-}$, rather than as insoluble metal selenides.[32] Amino acids such as cysteine and methionine commonly contain sulfur functionalities, but in some cases have adopted selenium to enhance catalytic function. For example, the molybdenum enzyme formate dehydrogenase contains a selenocysteine amino acid residue coordinated to the oxidized metal centre at a distance of 2.7 Å.[34] The only other coordinated ligands are two molybdopterins, making a five-coordinate centre with an available site for substrate binding. Earlier EXAFS data also suggest the presence of a coordinated selenocysteine residue in tungsten containing formate dehydrogenase,[35] showing that both Mo and W are found associated with this element at their active sites. One reason for the switch to selenium is that it has a lower pK_a than sulfur, resulting in it being unprotonated at physiological pH and consequently a better nucleophile for reaction during the catalytic cycle.[33]

1.2.5 Model Systems

With molybdenum, and tungsten to a lesser degree, playing such a major role in biology, the interest in simulating the coordination environment of active metal centres using synthetic inorganic chemistry is widespread.[3,21,36] Model complexes play a role in several different aspects of chemistry and biology, one of which is in the characterization of active metal sites. X-ray crystal structures and EXAFS studies are the most popular methods for determining the coordination geometry at an active centre, but require a certain number of assumptions and approximations to be made in order to obtain a refined solution. Synthetic models of these proposed environments are invaluable in the refinement process, by allowing measurements to be made on small molecules and then comparing them to data obtained for the active centre. Many coordination compounds have been synthesized for the purpose of model studies, and some of the more representative structures are illustrated overleaf.

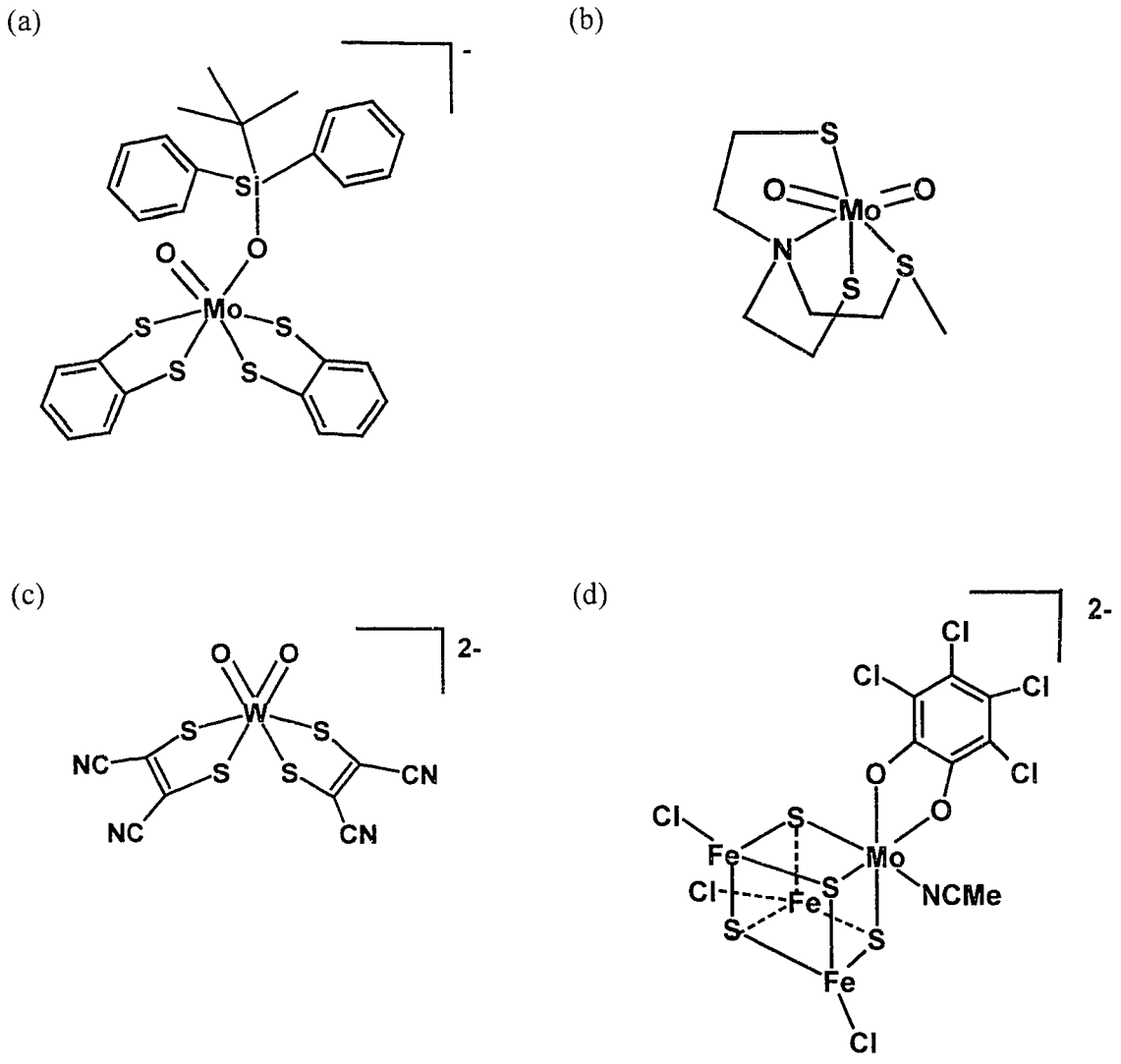

Figure 1.4 Structural model complexes for the active sites in various enzymes: (a) Model for Mo site in DMSO reductase,[37] (b) model for Mo site in sulfate oxidase,[38] (c) model for W site in AOR,[39] (d) model for Mo site in nitrogenase.[40]

While such structures are adequate in simulating the primary coordination sphere of the metal, most are not able to function chemically in the manner of an enzyme, by

facilitating catalytic processes. As a result, another kind of model complex has been developed. Young *et al.* have developed a range of complexes that utilize the tris(pyrazolyl)borate ligand, and in some cases undergo analogous processes to those observed at the active sites in molybdenum and tungsten enzymes.[42,43] The complex $LMo^{VI}O_2(SPh)$ (L = hydrotris(3,5-dimethyl-pyrazolyl)borate) has been shown to undergo coupled protonation and electron transfer to give $LMo^{V}O(OH)(SPh)$, which subsequently yields $[LMo^{V}O_2(SPh)]^-$ on deprotonation.[43] $LMo^{IV}O(SPh)$ can be formed by removal of an oxide using PPh_3, and trapped as a coordinatively saturated solvated species, representing the lower oxidation state of the catalytic cycle in molybdenum enzymes. The analogous tungsten chemistry has been investigated, including the incorporation of a selenolate to represent the active site in formate dehydrogenase,[44,45] but does not show the same chemical reactivity as the molybdenum system due to the higher bond strengths of the W=O bonds.

Coucouvanis and coworkers have developed a system of cubane-like Mo/Fe/S clusters that exhibit catalytic activity related to nitrogenase.[21] A particularly successful example is shown in Figure 1.4(d),[40] which can reduce the unstrained N=N bond in dimethyldiazene to form a mixture of ammonia, methylamine and ethylamine. The only drawback is that catalytic activity undoubtedly occurs at the Mo centre in this model, whereas this is not believed to be the case in the enzyme nitrogenase.

Many of these models contain functional groups or ligands that are not biologically relevant, such as the tris(pyrazolyl)borate ligand, the trademark of Young and coworkers. Such a bulky ligand occupies three coordination sites in a *facial* arrangement allowing stability of terminal oxides and sulfides without polymetallate

formation. While the complexes exhibit some analogous chemical reactivity to that found in biological systems, the ligand itself is not biologically significant in a structural sense.

Some attempts have been made to synthesize biologically relevant ligands, such as the molybdopterin ligand, which defines its class of molybdenum enzymes. Stiefel *et al.* have reported the synthesis of various Mo complexed ligands with structural similarities to molybdopterin.[46] Studies of the chemistry of two of these compounds (Figure 1.5) reveal that they can be chemically oxidized to their respective Mo(V) species and, in the latter case, can be reduced back to their original electronic configuration.

The goal of the total synthesis of molybdenum complexed molybdopterin is important since such a compound might structurally and chemically mimic an active metal centre, and provide valuable insight into the catalytic cycles that occur *in vivo*.

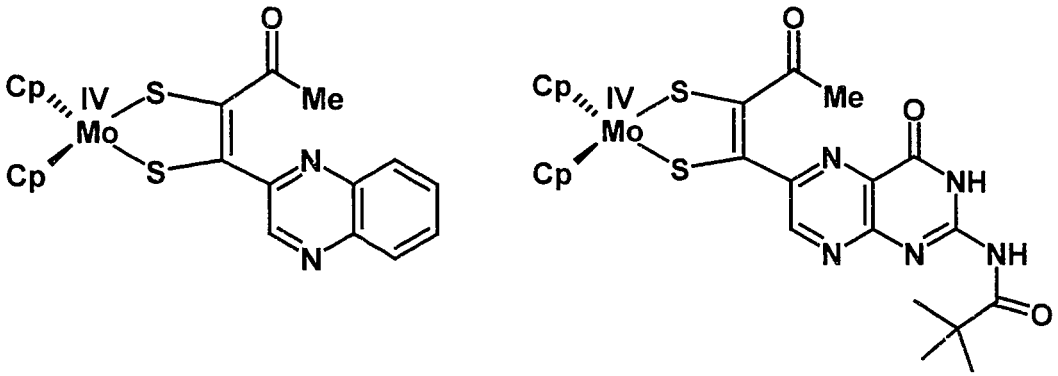

Figure 1.5 Models containing structural analogues of the molybdopterin ligand.[46]

Another class of models is that which contains redox mimics. Biological systems usually undergo highly efficient oxidation and reduction at active sites, often caused by a

highly constrained geometry that favours a normally unfavourable process. The previously discussed $LMo^{VI}O_2(SPh)$ (L = hydrotris(3,5-dimethyl-pyrazolyl)borate) model system also fulfils the requirement of being a redox mimic by undergoing oxidation and reduction at potentials that are biologically accessible.[43]

We have discussed some of the areas of interest in model studies, but a somewhat different approach is to take the source of metal that is available to a particular organism and use this as a precursor to simulate the coordination environment of an active centre. While this is rather a tall order, we might at least be able to investigate chemical differences in the reactivity of the various metal sources and make some suggestions on how an organism might take up and utilize a metal such as molybdenum. We chose to investigate the chemistry of anions that are known to be a source of tungsten and molybdenum for thermophilic and hyperthermophilic bacteria.

Anions of the formula $[MO_xS_{4-x}]^{2-}$, where M = Mo, W and x = 0-4, are known to be found under certain conditions in equilibrium with each other (Eq. 1.2). In such environments, organisms take up these anions and use them to maintain levels of the respective metals at active centres responsible for vital processes within the organism.

$$[MS_4]^{2-} \rightleftharpoons [MOS_3]^{2-} \rightleftharpoons [MO_2S_2]^{2-} \rightleftharpoons [MO_3S]^{2-} \rightleftharpoons [MO_4]^{2-} \qquad \textbf{Equation 1.2}$$

The biosynthetic pathway used to create the active site coordination environment *in vivo* is somewhat ambiguous, which has resulted in the investigation of coordination chemistry of the above anions. The second half of this chapter is a review of the related chemistry of $[ME_4]^{2-}$ anions, with discussion of their relevance to biology.

1.3 Chemical Significance of $[ME_4]^{2-}$ (M = Mo, W; E = O, S, Se)

A vast array of chemistry has previously been explored for the $[ME_4]^{2-}$ (M = Mo, W; E = O, S, Se) anions, which will not all be reviewed here. Instead, the focus will be on reactions that are related to chemistry reported in subsequent chapters of this thesis, and its biological implications. Scheme 1.2 represents the key areas of our review.

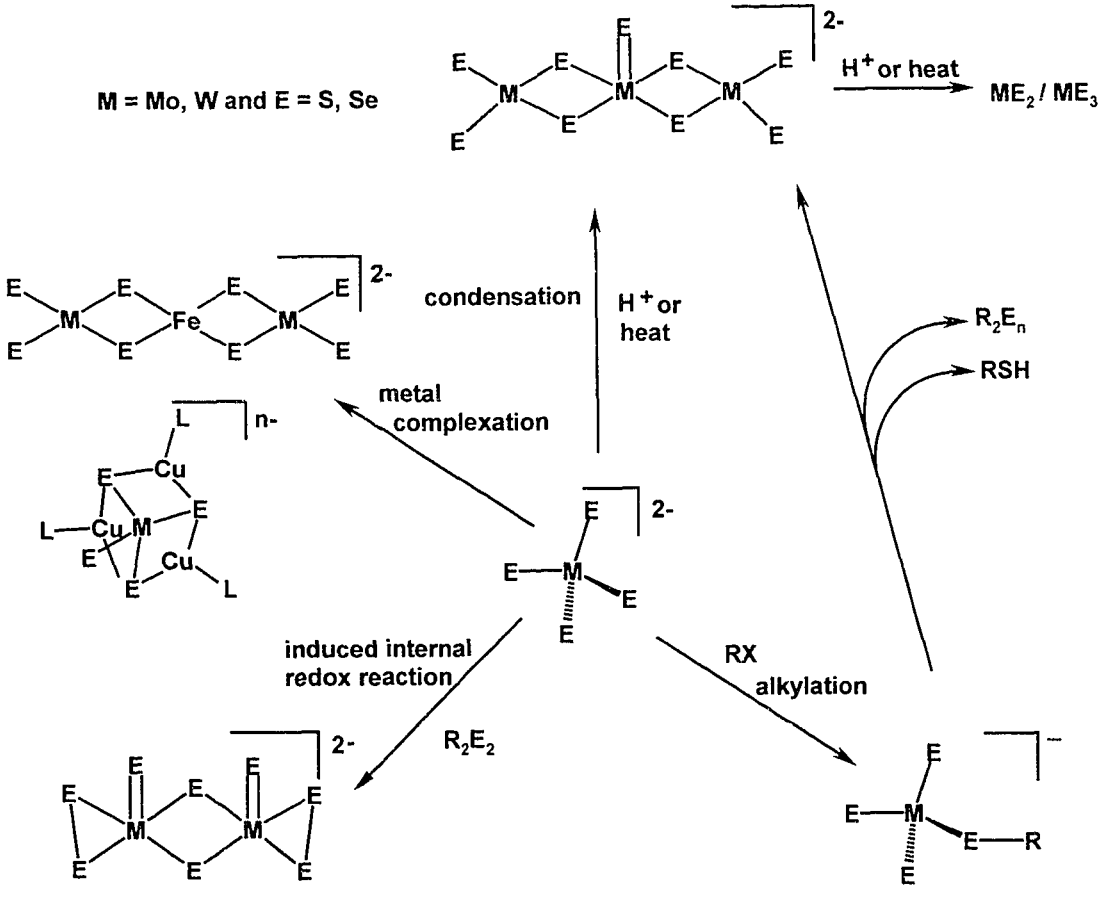

Scheme 1.2 Typical reactions of $[ME_4]^{2-}$ (M = Mo, W; E = O, S, Se) which will be discussed in the chapters of this thesis.

1.3.1 Known Examples of Oxo-, Thio- and Selenomolybdates and Tungstates

The oxothiometallate anions $[MO_xS_{4-x}]^{2-}$ (M = Mo, W; x = 0-4) have all been prepared from strongly basic solutions of the respective metallate and varying amounts of H_2S, with a variety of cations.[47] For the preparation of oxoselenometallate anions $[MO_xSe_{4-x}]^{2-}$ (M = Mo, W; x = 0-4), the use of H_2Se under similar conditions has been successful,[48] and in the case of tetraselenometallates, the reactions of the respective metal carbonyl and potassium triselenide,[49] or oxometallate and bis(dimethyloctylsilyl) selenide[50] have offered less toxic alternatives. In some cases, the resultant anions have been observed *in situ* by UV-Vis spectroscopy and have not been isolated in a pure form due to their instability. The mixed oxothioselenometallates $[MOS_2Se]^{2-}$ and $[MOSSe_2]^{2-}$ (M = Mo, W) have been observed *in situ* from the reaction of oxothiometallates with H_2Se or oxoselenometallates with H_2S.[51,52] The only tellurium analogue of the above anions to be isolated to date is $[WOTe_3]^{2-}$,[53] with $[MTe_4]^{2-}$ being notably absent due to its instability compared to the oxo-analogue.

1.3.2 Condensation Reactions

Condensation of mononuclear (thio)(seleno)metallates to poly(thio)(seleno)-metallates in solution is a thermodynamically favourable process that is commonly observed with loss of small molecules such as H_2E or R_2E_n (E = O, S, Se).[54] Protonation readily initiates such reactions,[55] though heat,[56] oxidation[57] and C-E bond formation[58] may result in similar outcomes, depending on the chalcogen ligands involved.

1.3.2.1 Polyoxometallates

Polymetallates containing only oxide ligands usually consist of high oxidation state metal centres, since reduction of oxide coordinated molybdenum and tungsten centres is generally not a favourable process. Anions consist mainly of "MO_6" units, but tetrahedral "MO_4" units are sometimes incorporated into structures.[71] Compared to sulfide or selenide containing structures, polyoxometallates exhibit much higher nuclearity. In addition, the examples of isolated polytungstate and polymolybdate anions are mostly not isostructural (Figure 1.6).

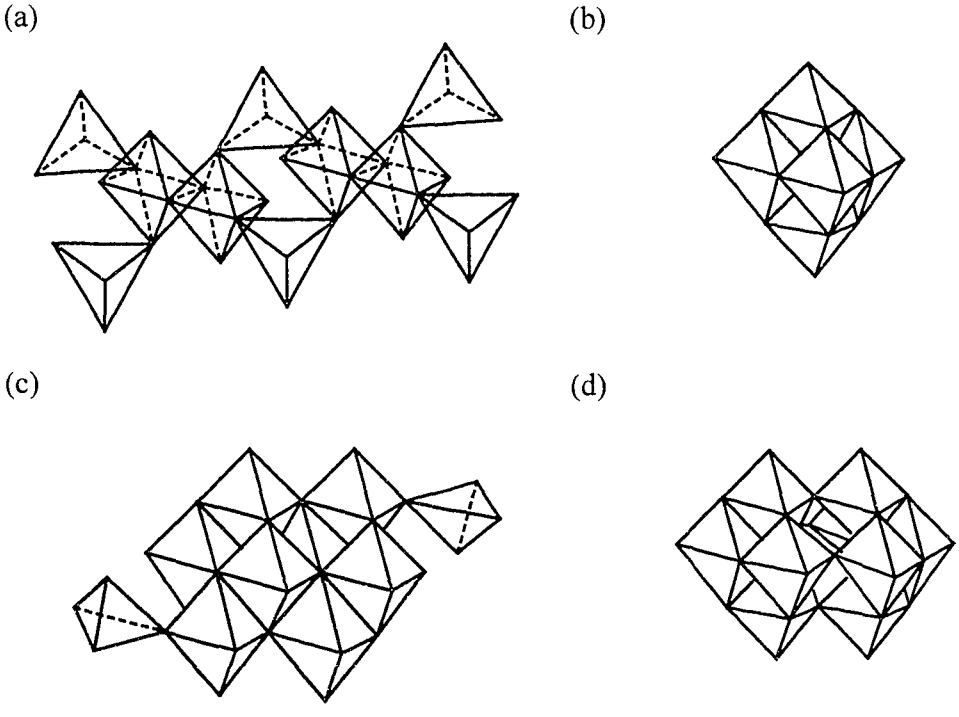

Figure 1.6 Structures of distinct polymolybdates and tungstates that have been isolated and characterized (where "MO_6" and "MO_4" units are represented by octahedra and tetrahedra, respectively):[59] (a) $[Mo_2O_7^{2-}]_n$, (b) $[M_6O_{19}]^{2-}$ (M = Mo, W), (c) $[Mo_{10}O_{34}]^{8-}$, (d) $[W_{10}O_{32}]^{2-}$.

Factors such as pH, temperature and concentration affect the nature of the anionic species in solution, resulting in a range of different species in equilibrium with each other. Since many of these species only exist in solution, studies using ^{183}W NMR spectroscopy have proven useful for characterization purposes.[60] Polymetallate formation can be controlled by pH, resulting in a necessity for high basicity to maintain mononuclear anions in solution.

Due to the propensity for polymetallate formation at neutral pH, living organisms might require a mechanism by which the mononuclearity of molybdate anions can be maintained during the uptake and transportation. It is thought that the molybdopterin ligand may fulfill this role.[13]

1.3.2.2 Polythiometallates

Upon heating or acidification, mononuclear (oxo)thiometallates readily condense in solution to form poly(oxo)thiometallates, with concomitant reduction at some of the metal centres involved.[56] This process has been investigated for many years and a variety of structural architectures have been characterized.[61,62] More examples of molybdenum polythiometallates with lower oxidation states are known, presumably due to the greater tendency for the metal to undergo reduction. The use of ammonium salts in such syntheses is widespread due to their tendency to undergo O/S ligand redistribution, resulting in more variation in the polythiometallates obtained. The most commonly formed anions containing exclusively $[E]^{2-}$ ligands are the linear polymetallates $[M_3E_9]^{2-}$ and $[M_4E_{12}]^{2-}$, where M = Mo, W and E = O, S (Figure 1.7),[63-66] where $[O]^{2-}$ preferentially assumes a terminal versus bridging position.

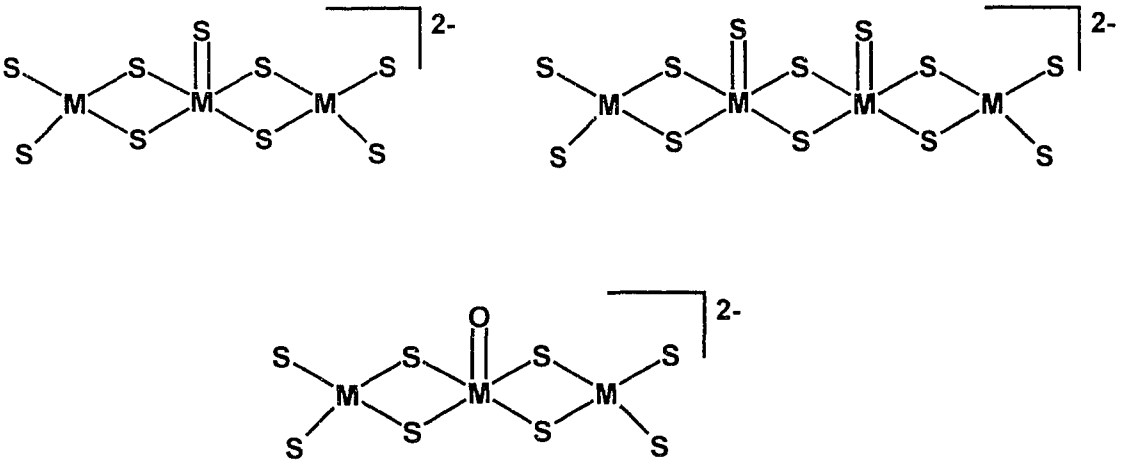

Figure 1.7 Structural geometries of $[M_3S_9]^{2-}$, $[M_4S_{12}]^{2-}$ and $[M_3OS_8]^{2-}$, where M = Mo, W.[63-65]

In some cases, aerial oxidation of sulfide ligands can lead to the formation of coordinated disulfides, $[S_2]^{2-}$, initiating polymetallate formation[57] and resulting in the incorporation of terminal oxide ligands.[63] Coordinated disulfides have also been isolated from reactions of $[MS_4]^{2-}$ or $[MOS_3]^{2-}$ with acetic acid (M = Mo, W) (Figure 1.8(a) and (b)),[67] and coordinated *tetra*sulfide ligands, $[S_4]^{2-}$, have been prepared from solutions of $[MS_4]^{2-}$ (M = Mo, W) or $[MoOS_3]^{2-}$ and elemental sulfur, to yield the structures shown in Figure 1.8(c) and (d).[68,69]

(a) (b)

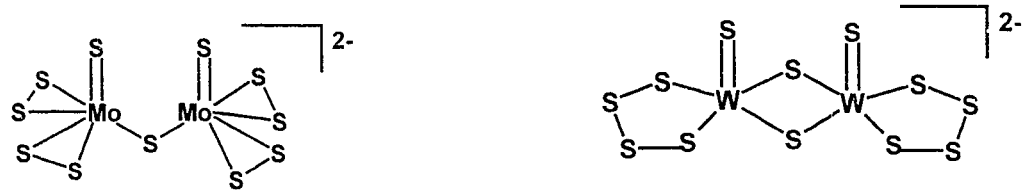

(c) (d)

Figure 1.8 Structural geometries of (a) $[Mo_2(S)_2(\mu\text{-}S)(\eta^2\text{-}S_2)_4]^{2-}$,[67] (b) $[W_2(O)_2(\mu\text{-}S)(\eta^2\text{-}S_2)_4]^{2-}$,[67] (c) $[W_2(S)_2(\mu\text{-}S)_2(\eta_2\text{-}S_4)_2]^{2-}$,[68] (d) $[(S_4)_2Mo(S)]^{2-}$.[69]

A large variety of other structures have been synthesized by using existing polythiometallates as starting points for ligand variation, often by taking advantage of the substitutionally labile polysulfide ligands.[70,71] In addition, structures have been derived from mononuclear building blocks such as $[OMo(SPh)_4]^-$,[72] or by the addition of $[MoS_4]^{2-}$ across coordinated disulfide ligands.[70]

Disulfide ligands have also been synthesized by induced internal redox reactions,[73] where an organic disulfide (R_2S_2) acts as an external oxidant to initiate electron transfer from terminal sulfide to metal, resulting in formation of a dinuclear complex (Scheme 1.3).

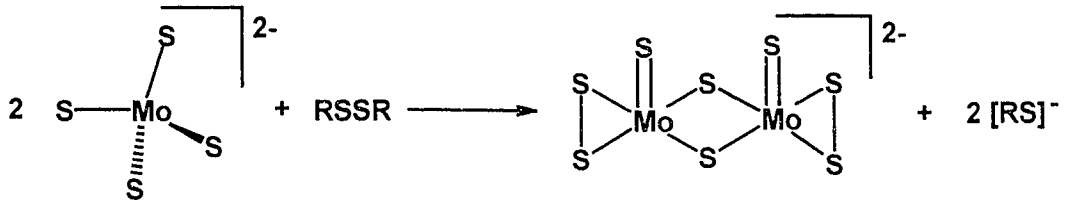

Scheme 1.3 Induced internal redox reaction of $[MoS_4]^{2-}$ and R_2S_2.[75]

Comparisons with the analogous selenide chemistry indicate that $[MoS_4]^{2-}$ can also be activated by organic diselenides,[73] and that $[WSe_4]^{2-}$ can be activated by organic disulfides, resulting in reduction at the metal centre to M(V).[74] In contrast, $[WS_4]^{2-}$ is insufficiently susceptible to reduction under these conditions and remains as W(VI).[74] A particularly novel use of induced internal redox reactions was recently reported by Stiefel *et al.* who describe the treatment of $[WOS_3]^{2-}$ or $[MoO_2S_2]^{2-}$ with constrained cyclic disulfides (Scheme 1.4).[75] The resultant metal coordination spheres shows structural similarities to those observed at the active sites in some molybdenum and tungsten containing enzymes.

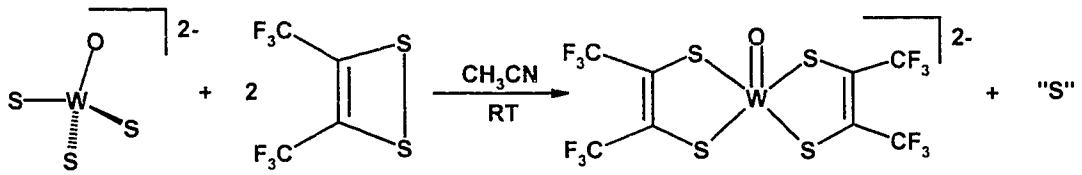

Scheme 1.4 Reaction of $[WOS_3]^{2-}$ and $(CF_3)_2C_2S_2$ (1:2) in acetonitrile at room temperature.[75]

Under extreme conditions, such as excessive heat or acidification, thio- and selenometallates have been shown to form insoluble metal sulfides of the approximate formula MS_2.[76,77] Analysis by electron microscopy and x-ray absorption techniques has shown that these metal sulfides exhibit a range of morphologies, including hollow spheres and microtubules. Recent studies have reported the preparation of these structures at room temperature using ultrasonication, providing a facile route to new materials that are industrially relevant as lubricants.[78,79]

The extreme conditions under which hyperthermophilic bacteria exist result in formation of insoluble metal sulfides, and probably polythiometallates. Coupled with the differences in redox activity between the tungsten and molybdenum sulfides, the chemical differences between the two metals under these conditions have major implications in the evolutionary theory of tungsten and molybdenum enzymes.

1.3.2.3 Polyselenometallates

Polyselenotungstates and molybdates have been investigated more recently and are generally isostructural to the analogous polythiometallates. The added advantage of the ^{77}Se NMR handle has been useful in characterizing mixtures of anions, where terminal selenides are significantly more deshielded than bridging or diselenide ligands,[80] and molybdenum selenides are more deshielded than those in the analogous tungsten complexes. Many polyselenometallates have been synthesized from mononuclear tetraselenometallates under the same reaction conditions as the analogous sulfide complexes. These include $[W_3Se_9]^{2-}$ from acidification reactions[81] or $[Se_4]^{2-}$ ligated complexes by refluxing in the presence of elemental selenium.[50,81] An interesting

example of a complex prepared from the latter reaction is $[W_2Se_{10}]^{2-}$,[81] which exists as two structural isomers. One contains a coordinated diselenide and tetraselenide, whereas the other contains two triselenides (Figure 1.9). This type of isomerism is not observed in the analogous thiometallate system, though identifying the species present in solution is more challenging compared to the selenide analogues which can readily be identified by ^{77}Se NMR.

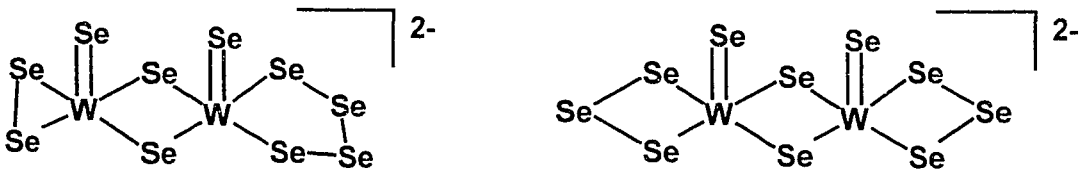

Figure 1.9 The major and minor isomers of $[W_2Se_{10}]^{2-}$, respectively, isolated from the reaction of $[WSe_4]^{2-}$ with elemental selenium.[81]

Mixed oxoseleno- and thioselenometallates have been reported for the mononuclear $[ME(\eta^2\text{-}Se_4)_2]^{2-}$ (M = Mo, W; E = O, S, Se) anions (see Figure 1.8(d) for analogous structure), prepared by the reaction of $[MSe_4]^{2-}$ with $Se_4(NC_5H_{10})_2$, SeS_2, and Se_8, respectively.[50] ^{77}Se NMR spectroscopy shows that the $[Se_4]^{2-}$ selenium atoms become progressively more shielded on moving from a selenide to sulfide to oxide in the apical position on the metal. This is explained based on the relative $p\pi$-$d\pi$ overlap of chalcogenide and metal, which increases from selenide to oxide. The better π-overlap in the oxide case results in more electron density being donated to the metal and less from the $[Se_4]^{2-}$ selenium atoms. A similar approach is used to explain the greater deshielding

in the molybdenum versus tungsten analogues, where the M-Se orbital overlap is more favourable in the former case.

1.3.2.4 C-E Bond Formation and the Chemistry of Related Polymetallates

The bulk of this thesis reports alkylation reactions of $[ME_4]^{2-}$, with alkyl halides, and the ultimate formation of polythio- and polyselenometallates. The related $[Cp^*WS_3]^-$ anion has also been reported to undergo alkylation to $Cp^*WS_2(SR)$ in good yields, though no mention was made of its propensity to form condensation products under these conditions.[82] However, when $Cp^*WS_2(S^tBu)$ is prepared from Cp^*WCl_4 and LiS^tBu, the dinuclear species $Cp^*_2W_2S_2(\mu\text{-}S)_2$ (Figure 1.10(a))[83] is also formed in solution due to the instability of $Cp^*WS_2(S^tBu)$. Formation of the analogous dinuclear selenide species when $LiSe^tBu$ is used under the same conditions supports the formation of $Cp^*WSe_2(Se^tBu)$ as an intermediate.[84] The analogous dinuclear molybdenum sulfide species has been isolated by thermal decomposition of $Cp^*Mo(\eta^2\text{-}SCH_2CH_2S)_2$, and a dinuclear thioselenomolybdate was isolated from the reaction of $Cp^*Mo(S^tBu)_3$ and elemental selenium.

(a)

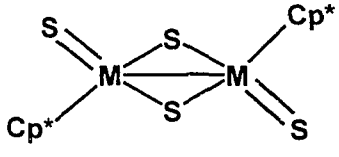

(b)

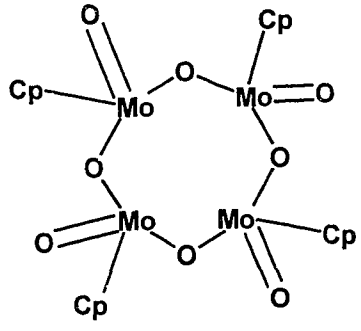

Figure 1.10 Structural geometries of (a) $Cp^*_2M_2S_2(\mu\text{-}S)_2$ (M = Mo, W)[83] and (b) $Cp_4Mo_4O_4(\mu\text{-}O)_4$.[85]

$Cp_2Mo_2O_2(\mu\text{-}O)_2$ (Figure 1.10(b)) has previously been isolated and characterized from the hydrolysis of $CpMoCl_4$ and is believed to form via the tetranuclear molybdate shown in Figure 1.10(b).[86] C-O bond formation has been investigated with the mononuclear $[Cp^*WO_3]^-$ anion and dimethylacetylene dicarboxylate (DMAD), and was found to undergo [2 + 2 + 2] cycloaddition of two acetylene molecules and one W=O unit (Scheme 1.5).[85]

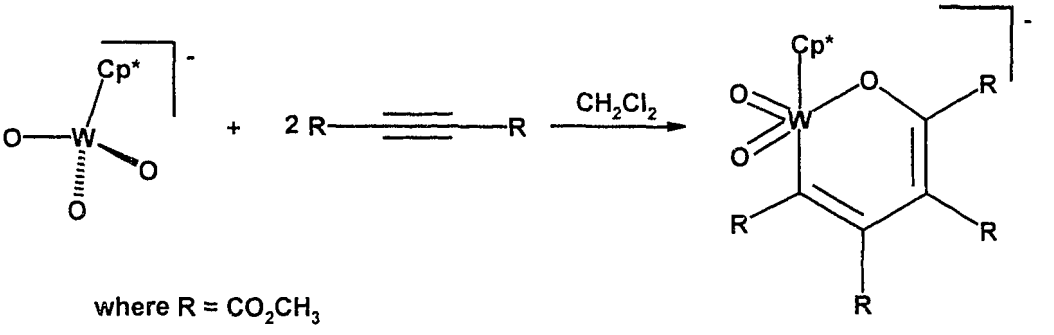

Scheme 1.5 [2+2+2] cycloaddition of $[Cp^*WO_3]^-$ and DMAD (1:2).[85]

In contrast to the oxo-system, reactions of acetylenes with $[Cp^*MS_3]^-$ (M = Mo, W) were found to result in [2 + 3] cycloaddition and reduction at the metal centre (Scheme 1.6).[83] $[Cp^*MS_3]^-$ was sufficiently labile to react with unactivated acetylenes such as PhCCPh and PhCCH, and yield coordinated dithiolene moieties with structural similarities to the active metal sites in tungsten containing enzymes.

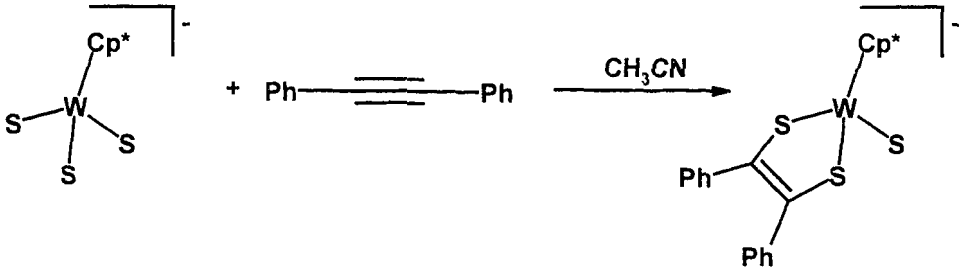

Scheme 1.6 *Reaction of* $[Cp^*MS_3]^-$ *(M = Mo, W) and* PhCCPh (1:1).[82,83]

$[MS_4]^{2-}$ anions are not sufficiently labile to react with unactivated acetylenes, and the only isolable products reported with *activated* acetylenes, such as DMAD, are formed in the presence of BzSSSBz (Scheme 1.7).[87] The resultant mononuclear tris(dithiolene) complex is thought to be produced due to the initial formation of a tetrasulfide ligand containing anion since the same product can be formed by the direct reaction of $[MoS(\eta^2\text{-}S_4)]^-$ and DMAD.

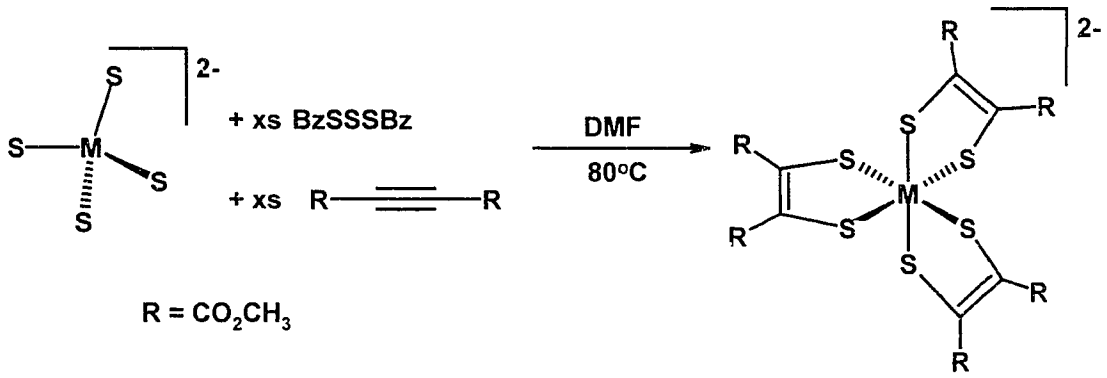

Scheme 1.7 Reaction of $[MS_4]^{2-}$ (M = Mo, W), BzSSSBz and DMAD at 80°C.[87]

1.3.3 Metal Complexation Reactions

Transition metal complexation of thio- and selenomolybdates and -tungstates has been investigated for many years, with much of the interest originating from the biological relevance of metal sulfide clusters.[26] As previously discussed, the active site in nitrogenase contains a cubane-like Mo/Fe/S cluster, and problems associated with copper-molybdenum antagonism in nature are thought to be due to a direct interaction between copper and molybdenum in the presence of sulfide, possibly resulting in formation of a bimetallic cluster. Metal sulfide clusters also have relevance to

hydrodesulfurization chemistry, for example the active Co/Mo/S phase derived from $[MoS_4]^{2-}$ and $CpCo(CO)_2$ at high temperatures.[77]

A common complexation stoichiometry is 1:2, for heterometal to thiometallate, resulting in $[M'(MS_4)_2]^{n-}$ (M = Mo, W) where M' adopts a tetrahedral (*e.g.* M' = Ni, Pd, Pt) or square planar geometry (*e.g.* M' = Ag, Cu, Fe) (Figure 1.11(a))[26,88] By varying the stoichiometry of the complexation reaction, structures containing six-coordinate M' have been obtained, such as in $[Pb_2(MS_4)_4]^{2-}$ (Figure 1.11(b)).[26]

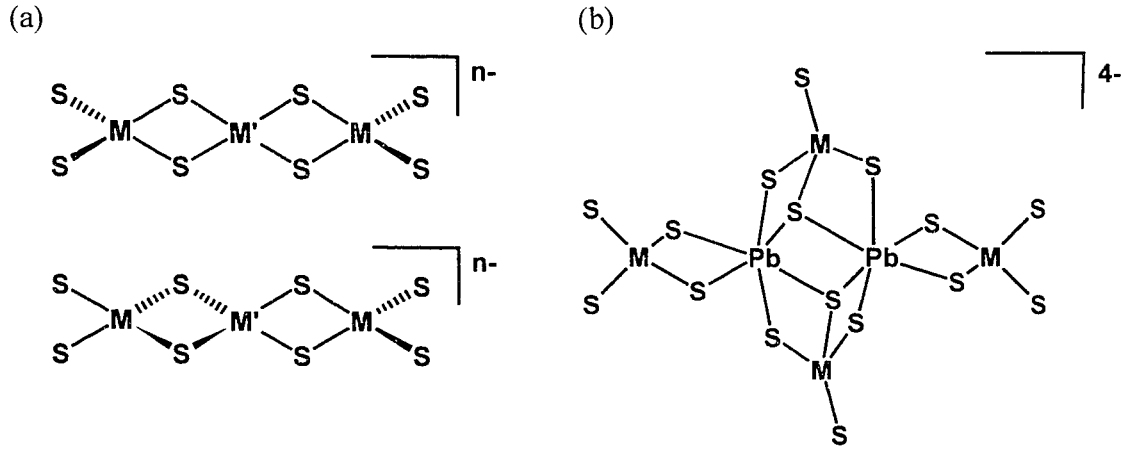

Figure 1.11 Structural geometries of (a) $[M'(MS_4)_2]^{n-}$ and (b) $[Pb_2(MS_4)_4]^{2-}$ (M = Mo, W; *e.g.* M' = Ni, Pd, Pt, Ag, Cu, Fe).[26,88]

Cu(I) and Ag(I) feature heavily in complexation studies of thiomolybdates and tungstates, and frequently result in similar structures. When CuCl is complexed to $[MS_4]^{2-}$ in the presence of $[NCS]^-$, the discrete $[(CuNCS)_2WS_4]^{2-}$ anion is formed.[89] In contrast, when the complexation is performed in the presence of $[SCN]^-$, polymeric $[(CuNCS)_4WS_4]^{2-}$ is formed with tetrahedrally coordinated copper centres (Figure 1.12).

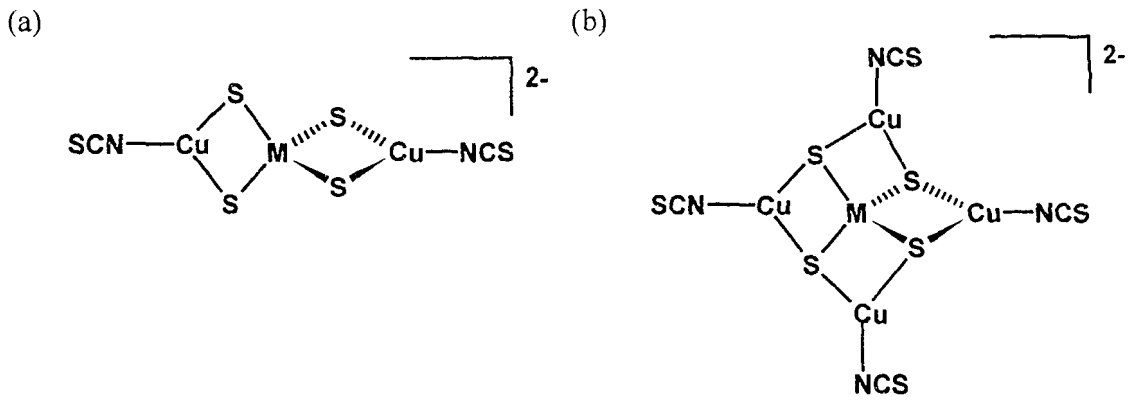

Figure 1.12 Structural features of (a) $[(CuNCS)_2WS_4]^{2-}$ and (b) $[(CuNCS)_4WS_4]^{2-}$.[89]

When $[MoS_4]^{2-}$ is reacted directly with CuCl in a 1:3 ratio, $[MoS_4(CuCl)_3]^{2-}$ is formed, which is structurally related to $[Cu(NCS)_4WS_4]^{2-}$ with the absence of one of the copper centres.[90] Under aerobic conditions, the double cubane-like $[MS_4(CuCl)_5Cl_2]^{4-}$ (M = Mo, W) has been isolated from the same ratio of reagents and is shown in Figure 1.13.

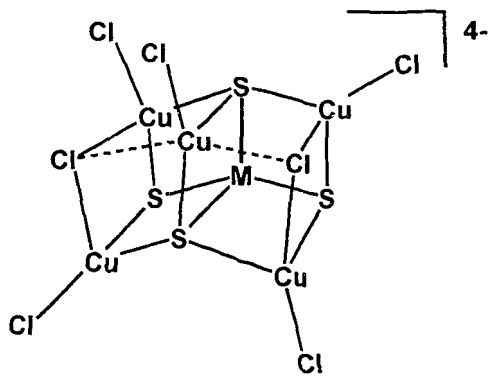

Figure 1.13 Double cubane-like structure of $[MS_4(CuCl)_5Cl_2]^{4-}$ (M = Mo, W).[91]

Highly complex macromolecular structures with cubane-like units have been generated from thiometallates or oxothiometallates and copper halides.[92] The non-coordinating oxide ligands are generally retained during complexation, resulting in a

maximum of three copper centres per molybdenum or tungsten for complexed $[MOS_3]^{2-}$ (Figure 1.14).[26] Interestingly, some reactions of $[MO_2S_2]^{2-}$ (M = Mo, W) have resulted in metal complexes containing $[MOS_3]^{2-}$ units, apparently by O/S ligand exchange in solution.[93]

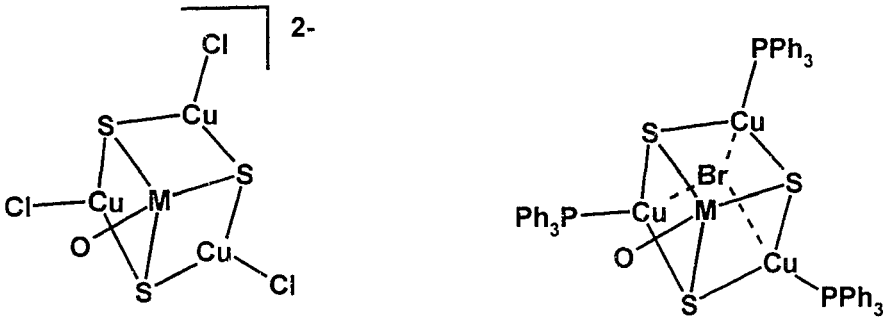

Figure 1.14 Structures containing $[MOS_3]^{2-}$ (M = Mo, W) units.[26]

Structures of the type described above for copper, have all been prepared using silver halides, with the exception of $[MS_4(CuCl)_5Cl_2]^{4-}$ (M = Mo, W). In addition, examples of structures reported only for silver exist, such as the polymeric anion $[AgWS_4]^-$ (M = Mo, W) which was prepared from $[MS_4]^{2-}$ and AgI in the presence of methylpyridine.[94] Under the same conditions, reactions of copper halides in place of AgI result in the formation of discrete anions, which is explained by the preference of Cu^+ ions for the harder basic pyridine ligands, compared to the Ag^+ ions for the softer $[MS_4]^{2-}$ ligands.

Reactions of $[MSe_4]^{2-}$ (M = Mo, W) with copper or silver halides result in formation of many complexes that are isostructural to those previously discussed for $[MS_4]^{2-}$, though some different macromolecular architectures have been reported.[95-97]

Cubane-like structures are commonly featured in iron sulfide chemistry, and the most common building block for bimetallic clusters is the $[MoFe_3S_4]^{n+}$ (n = 3-6) unit which can be prepared from $[MoS_4]^{2-}$ and $FeCl_2$ in the presence of ligands such as dialkyldithiocarbamate[98] or cyclohexanethiolate.[99] Most of the recent model complexes for the active site in nitrogenase incorporate the $[MoFe_3S_4]^{n+}$ core,[100] which appear to have almost endless possibilities for derivatization, and shows chemical reactivity similar to that observed in nature.[40]

1.4 Context of the Work Described in This Thesis

The vast array of unexplored chemistry in the area of metal complexation and condensation product formation that stems from reactions of simple $[ME_4]^{2-}$ anions is proof that this is an important area of study. Advances in the area of biological chemistry are due in part to a better understanding of chemical reactivity of small biologically relevant molecules, such as those containing high oxidation state molybdenum and tungsten centres with sulfur containing ligands.

We have attempted to investigate the formation of C-E bonds by the reaction of $[ME_4]^{2-}$ with alkyl halides, and isolate the alkylated intermediates. Such intermediates contain terminal chalcogenide and chalcogenate ligands at high oxidation state metal centres and exhibit structural similarities to the active sites in tungsten and molybdenum-containing enzymes. Our studies have allowed us to make comparisons in reactivity between the two metals, molybdenum and tungsten, and also the three chalcogenides, oxide, sulfide and selenide.

Chapter 2 – Isolation and Characterization of Oxothiometallates, $[PPh_4]_2[MO_xS_{4-x}]$ (M = Mo, W and x = 0-2)

2.1 Introduction

Investigation into the reactivity of anions of the formula $[MO_xS_{4-x}]^{2-}$, where M = Mo, W and x = 0-4, requires pure, well characterized samples of appropriate salts. A literature procedure for the respective ammonium salts, where x = 0-2 was published by MacDonald *et al.*,[47] which was a refinement of longstanding procedures developed by Krüss[101] and Corleis.[102] The procedure involved passing H_2S through or over a solution of tungstic or molybdic acid, treated with ammonium hydroxide, and the degree of oxo/sulfido ligand exchange was dependent on the amount of H_2S used.

The process of oxo/sulfido ligand exchange in aqueous media has been investigated in much detail by Müller.[24] Müller was able to observe all five $[MO_xS_{4-x}]^{2-}$ anions in solution and was initially able to isolate compounds where x = 0-2. Later, he succeeded in isolating examples where x = 3, but only as alkali metal salts, by utilizing their low solubility. Unfortunately, this does not provide a suitable route to ammonium salts, a finding that was mirrored by the McDonald paper,[47] where practical syntheses were absent for x = 3, 4. Since that time, Reid *et al.* have developed an alternative approach to isolating the missing salts by buffering the pH of a tungstate solution and treating with ammonium sulfide.[103] While this has been satisfactory for isolating solid $Cs_2[MO_3S]$, it is not of particularly high purity and shows a tendency to undergo oxo/sulfido redistribution. In particular, attempts to purify the salt by column chromatography actually decrease its purity.

Another issue that has complicated the synthesis of $[MoO_xS_{4-x}]^{2-}$ salts is the fact that these procedures commonly result in a mixture of anions,[47] except in the case of tetrathiometallates which can be synthesized by bubbling excessive amounts of H_2S until all oxo ligands have been replaced. (The ammonium salts are now commercially available from Aldrich). Any further reactions performed using these salts would require pure samples, to enable accurate comparisons of reactivity to be made.

Harmer *et al.* have investigated the formation kinetics for $[NH_4]_2[MoO_xS_{4-x}]$, from $[MoO_4]^{2-}$, and found that the rate decreases as the number of sulfido ligands increases.[104] It is suggested that increased steric crowding from each additional sulfur atom reduces the ease with which the remaining oxygens can be replaced. In addition, the process is far more facile for molybdenum than tungsten analogs,[105,106] possibly due to the higher bond strengths for W-O versus Mo-O, or the higher bond strength of Mo-S versus W-S in the product. It was deduced that protonation is the first step in oxide replacement, weakening the M-O bond, which is also observed to be the first step in condensation of the anions. In the presence of $[SH]^-$ (from H_2S), exchange of hydroxide with hydrosulfide is favourable (Equation 2.1), and will continue by the same mechanism until all oxide ligands are replaced.

$$[MO_3(OH)]^- + [SH]^- \rightleftharpoons [MO_3S]^{2-} + H_2O \qquad \textbf{Equation 2.1}$$

As expected, further complications when using these salts result from the tendency for samples of ammonium salts to undergo oxo/sulfido exchange in both aqueous and non-aqueous solutions, resulting in changes of the distribution of anions present. When Equation 2.1 occurs from right to left, the presence of H^+ enhances oxide

exchange from water by removing $[SH]^-$ as H_2S and shifting the equilibrium to the left. Newly formed H_2S may subsequently react with $[MoO_2S_2]^{2-}$ or $[MoOS_3]^{2-}$ and the end result is a complex series of equilibia to exchange oxide and sulfide ligands. Since ammonium salts will undergo ligand redistribution even in non-aqueous media, it appears that the cation can behave as a proton source. To avoid unwanted ligand redistribution in this way, we chose to use $[PPh_4]^+$ as a cation in our reactions of interest, which has imparted greater stability on solutions, greater purity in isolated salts, and also has the added advantage of higher solubility in organic solvents.

2.2 Synthesis and Characterization

Although our original intention was to prepare and characterize the complete series, $[PPh_4]_2[MO_xS_{4-x}]$ where M = Mo, W and x =0-4, this proved to be difficult for compounds where x = 3, 4 due to a lack of a practical synthetic approach for the respective ammonium salts. Compounds where x = 0-2 were successfully synthesized by metathetical cation exchange using $[PPh_4]Cl$ in aqueous media. Although anions of the general formula $[MO_xS_{4-x}]^{2-}$ are known to be in equilibrium when in aqueous media,[7,8] redistribution of oxo- and thio-ligands is sufficiently slow that preparation and isolation of the respective $[PPh_4]^+$ salts is possible by rapid precipitation. Characterization of the anions has been performed using IR, NMR and X-ray crystallography, where numbering of the compounds is as follows: $[PPh_4]_2[WO_xS_{4-x}]$ (x = 0 (**1**), 1 (**2**), 2 (**3**)) and $[PPh_4]_2[MoO_xS_{4-x}]$ (x = 0 (**4**), 1 (**5**), 2 (**6**)).

2.2.1 Multinuclear NMR

NMR studies have undoubtedly given the most revealing information about the composition of mixtures, due to the well-defined chemical shifts for each species in solution.

To aid in the structural analysis of products from reactions of these anions, we felt it would be useful to characterize the thiometallates using a common solvent and common cation since it has previously been reported that variations of up to 100ppm in ^{95}Mo chemical shift are observed for $[MoS_4]^{2-}$ due to the use of different solvents, and approximately 10ppm for different cations in dimethylformamide (DMF) solvent.[107-109] Our future reactions were to be performed in acetonitrile due to the enhanced solubility of the salts in this solvent, so we collected solution NMR data for compounds **1-6** in acetonitrile.

^{95}Mo and ^{183}W NMR spectroscopy were used to characterize componds **1-6**; molybdenum has two NMR active nuclei, whereas tungsten has only one. Their nuclear properties are given below (Table 2.1)[110] where it can be seen that although tungsten possesses the desirable spin of ½ and a reasonable natural abundance, it shows very low receptivity compared to carbon. In contrast, both molybdenum nuclei have higher receptivity but are quadrupolar, and the ^{97}Mo exhibits a quadrupole moment that is approximately ten times larger than ^{95}Mo, resulting in broader linewidths. In addition, the natural abundance of ^{95}Mo is 1.5 times that of ^{97}Mo, making ^{95}Mo the nucleus of choice.

The sensitivity of these techniques can be estimated based on signal to noise ratios,[111] and it is calculated that for the thiomolybdates, an impurity of another thiomolybdate would go undetected by ^{95}Mo NMR if present in less than 10%. ^{183}W

NMR offers poorer detection limits, where it is estimated that less that 33% of another thiotungstate would go undetected.

Table 2.1 NMR spectroscopic parameters for ^{95}Mo, ^{97}Mo and ^{183}W nuclei.[110]

Nucleus	^{95}Mo	^{97}Mo	^{183}W
Spin (I)	5/2	5/2	1/2
Natural Abundance (%)	15.72	9.46	14.28
Quadrupole moment	0.12	1.1	------
Receptivity/^{13}C	2.88	1.84	5.89×10^{-2}

We have shown that careful, stepwise recrystallization is a viable means to separate $[PPh_4]_2[MOS_3]$ and $[PPh_4]_2[MO_2S_2]$, and that redistribution of oxo- and thio-ligands does not occur for these compounds in non-aqueous media under an inert atmosphere. Tabulated below are ^{95}Mo and ^{183}W chemical shifts we have measured for compounds **1-6** (Table 2.2). The general trend in chemical shifts is in agreement with results previously published by Wedd *et al.*[107] The counterintuitive decrease in shielding at the metal centre with increasing numbers of terminal thio ligands is due to the large paramagnetic, versus diamagnetic, shielding contribution.[112] The increase in deshielding is consequently explained by an increase in the number of soft ligands around the metal.

Table 2.2 ^{95}Mo and ^{183}W NMR data for the compounds $[PPh_4]_2[MO_xS_{4-x}]$ (where M = Mo, W and x = 0-2) in CD_3CN and CH_3CN, respectively.

	Chemical shift (δ) in ppm[a]	
	M = Mo	M = W
$[MS_4]^{2-}$	2212	3658
$[MOS_3]^{2-}$	1588	2630
$[MO_2S_2]^{2-}$	996	1662

[a]Referenced to 2M $Na_2[MO_4]$ in D_2O and H_2O, respectively.

The linear correlation between ^{95}Mo and ^{183}W chemical shifts can clearly be seen when comparing data collected under the same conditions in both the molybdenum and tungsten cases, most importantly, with the same solvent, cation, and temperature. A graph to represent this relationship is shown below.

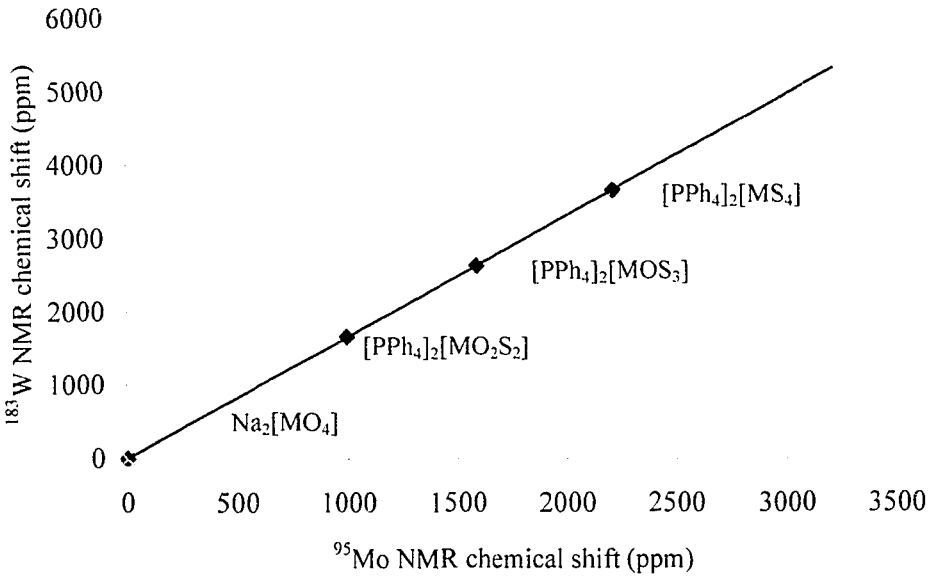

Figure 2.1 Linear correlation of ^{95}Mo and ^{183}W chemical shifts for oxothiometallates.

^{95}Mo and ^{183}W NMR data have been collected for a range of thiomolybdates and tungstates,[107-109,113-116] in the presence of different cations and solvents, and are summarized in the following tables.

Table 2.3 ^{95}Mo and ^{183}W chemical shifts (δ) for compounds $A_2[MO_xS_{4-x}]$ (where M = Mo, W and x = 0-2) in ppm,[a] currently available from this work and the literature.

	$[WO_3S]^{2-}$		$[MoO_3S]^{2-}$	
Cation (A)	MeCN	$H(D)_2O$	MeCN	$H(D)_2O$
$[NH_4]^+$	--------	--------	--------	497[c]
K^+	--------	--------	--------	--------
$[PPh_4]^+$	--------	--------	--------	--------
$[Et_4N]^+$	--------	--------	451[b]	--------
	$[WO_2S_2]^{2-}$		$[MoO_2S_2]^{2-}$	
Cation (A)	MeCN	$H(D)_2O$	MeCN	$H(D)_2O$
$[NH_4]^+$	--------	1787[c]	--------	1066[c.c] 1067[f]
K^+	--------	--------	--------	--------
$[PPh_4]^+$	1662[d]	--------	996[d]	--------
$[Et_4N]^+$	--------	--------	997[b], 964[c]	--------
	$[WOS_3]^{2-}$		$[MoOS_3]^{2-}$	
Cation (A)	MeCN	$H(D)_2O$	MeCN	$H(D)_2O$
$[NH_4]^+$	--------	2760[c]	--------	1654[f]
K^+	--------	2760[g,h]	--------	1654[c,h]
$[PPh_4]^+$	2630[d]	--------	1588[d]	--------
$[Et_4N]^+$	--------	-------	1586[b], 1587[c]	--------

	$[WS_4]^{2-}$		
Cation (A)	MeCN	$H(D)_2O$	DMF
$[NH_4]^+$	--------	3769[c]	3639[i]
K^+	--------	--------	--------
$[PPh_4]^+$	3658[d]	--------	--------
$[Et_4N]^+$	--------	-------	--------

	$[MoS_4]^{2-}$					
Cation (A)	$H(D)_2O$	MeOH	$MeNO_2$	MeCN	DMF	DMSO
$[NH_4]^+$	2258[c] 2259[f]	--------	--------	--------	--------	--------
K^+	2259[e]	--------	--------	--------	--------	--------
$[PPh_4]^+$	--------	--------	--------	2212[d]	--------	--------
$[Et_4N]^+$	2251[c]	2229[c]	2208[c]	2207[c], 2209[b]	2192[c]	2176[c]

[a]Referenced to 2 M Na_2MO_4 in D_2O or H_2O. [b]Reference 113. [c]Reference 107. [d]This work. [e]Reference 114. [f]Reference 115. [g]Reference 108. [h]$K_3[MOS_3]Cl$. [i]Reference 116.

From data obtained for the thiomolybdates, we have observed that our measured chemical shifts for $[PPh_4]_2[MoOS_3]$ and $[PPh_4]_2[MoS_4]$ in acetonitrile correspond closely with the values reported for the respective $[Et_4N]^+$ salts. Two distinctly different values have previously been reported for $[Et_4N]_2[MoO_2S_2]$.[107,113] Our measured value for $[PPh_4]_2[MoO_2S_2]$ in acetonitrile is in good agreement with the value reported in reference 113. The value reported in reference 107, which deviates by 33ppm, appears to be anomalous. It has previously been reported[108,114] that cation dependent variations in chemical shifts of up to 9ppm for $[MoS_4]^{2-}$ and 10ppm for $[WS_4]^{2-}$ occur, although the actual values for each cation have not been reported. When compared to other reported values, our data for $[PPh_4]^+$ salts are well within the respective cation ranges above. In comparing the ^{183}W NMR chemical shifts, it is difficult to make a direct comparison because previously reported values have been for different cations *and* solvents, making the values significantly different from those we have measured.

2.2.2 IR Spectroscopy and Elemental Analysis

Infrared spectra were collected on crystalline samples of **1-6**. The oxothiometallates, **2**, **3**, **5** and **6**, all contain acetonitrile solvent in their crystal structures as determined by X-ray diffraction. In addition, elemental analysis data for these salts correspond closely with the calculated values when acetonitrile solvent is included. It should be noted that elemental analysis would not detect an impurity of another thiometallate if present in less than 10%, owing to the similar molecular weights and elemental composition of the various anions. The presence of a minor impurity has been further investigated by X-ray crystallography and will be discussed later in this chapter.

The M-S and M-O stretches can clearly be observed by infrared spectroscopy in two distinct regions of the spectrum (Table 2.4), the latter being at a higher frequencies due, in part, to increased bond strength.[105] The shorter Mo-S versus W-S distances are reflected in the higher absorption frequencies of the former, as are the shorter W-O versus Mo-O distances. The observation that replacement of terminal oxide ligands by sulfide, using H_2S, proceeds more rapidly for Mo than W is consistent with the M-S and M-O bond strengths for the two metals.[104] This suggests a lower activation energy for Mo-O bond cleavage and formation of more thermodynamically favourable Mo-S bonds.

Table 2.4 Infrared spectroscopy M-O and M-S stretches (in cm^{-1}) for **1-6**.

	1 $[WS_4]^{2-}$	**2** $[WOS_3]^{2-}$	**3** $[WO_2S_2]^{2-}$	**4** $[MoS_4]^{2-}$	**5** $[MoOS_3]^{2-}$	**6** $[MoO_2S_2]^{2-}$
M-S	449	446	444	469	467	459
M-O	--------	880	877, 845	--------	870	868, 855

It can be seen that the presence of two M-O stretches in the cases of **3** and **6** will clearly indicate that $[MO_2S_2]^{2-}$ is present in a sample. Detection of **5** in a sample of predominantly **6** is possible due to the difference in M-S frequencies, but will be more difficult for small amounts of **2** in **3**, since the W-O stretches are very close in frequency. Similarly, detecting impurities of **1** in **2**, or **4** in **5** is also difficult since the M-S bands lie at very similar frequencies. Despite this, infrared spectroscopy provides a suitable means to detect impurities of **2** in **1**, and **5** in **4** or **6**.

2.2.3 X-Ray Crystallography

Crystallographic differences between $[PPh_4]_2[MS_4]$ and $[PPh_4]_2[MO_xS_{4-x}]$ (x = 1, 2) provide an excellent means to separate individual components from the mixture that usually forms during synthesis. The reduced solubility of $[PPh_4]_2[MS_4]$ and its inability to readily form large crystals without first layering with Et_2O allows the recrystallization of the oxothiometallates without contamination from $[PPh_4]_2[MS_4]$. Separation of each of the oxothiometallates, $[PPh_4]_2[MOS_3]$ and $[PPh_4]_2[MO_2S_2]$, is a more difficult task. The best method we have found for ensuring that a pure batch of compound is obtained, is to start with a sample of predominantly one species, as confirmed by IR and ^{95}Mo or ^{183}W NMR spectroscopy, and recrystallize it by the method described above. The first batch of crystals obtained by recrystallization show no detectable impurities by IR or NMR spectroscopy. Subsequent batches of crystals obtained from this same solution yield progressively larger quantities of the minor component.

Analysis of **1-6** by X-ray crystallography has shown all four oxothiometallates to be isomorphous in the space group $P2_1/n$, and the two tetrathiometallates to be isomorphous in the space group C2/c (Table 2.5), confirming the unit cell parameters previously reported for $[PPh_4]_2[MoS_4]$.[117] Compounds of the formula $[PPh_4]_2[MSe_4]$, (where M= Mo, W) have also been reported to be isomorphous with $[PPh_4]_2[MS_4]$, (where M= Mo, W).[117]

Table 2.5 Crystallographic data for $[PPh_4]_2[WO_xS_{4-x}]$ (x = 0 (**1**), 1 (**2**), 2 (**3**)) and $[PPh_4]_2[MoO_xS_{4-x}]$ (x = 0 (**4**), 1 (**5**), 2 (**6**)).

	1	**2**	**3**	**4**	**5**	**6**
Empirical formula	$C_{48}H_{40}P_2S_4W$	$C_{50}H_{43}NOP_2S_3W$	$C_{50}H_{43}NO_2P_2S_2W$	$C_{48}H_{40}MoP_2S_4$	$C_{50}H_{40}D_3MoNOP_2S_3$	$C_{50}H_{43}MoNO_2P_2S_2$
Mol. wt. (g mol^{-1})	990.88	1015.87	999.81	902.97	930.96	911.90
Colour	Yellow	Yellow	Yellow	Orange	Orange	Yellow
Crystal system	Monoclinic	Monoclinic	Monoclinic	Monoclinic	Monoclinic	Monoclinic
Space group	C2/c (#15)	$P2_1/n$ (#14)	$P2_1/n$ (#14)	C2/c (#15)	$P2_1/n$ (#14)	$P2_1/n$ (#14)
a (Å)	11.030(5)	20.788(2)	20.757(3)	11.039(1)	20.923(3)	20.693(6)
b (Å)	19.439(5)	10.517(3)	10.415(3)	19.495(2)	10.527(3)	10.382(3)
c (Å)	20.118(5)	21.189(2)	21.126(3)	20.112(3)	21.188(5)	21.040(5)
β (deg)	91.20(3)	105.71(1)	106.014(11)	91.35(1)	106.20(2)	105.93(2)
V (Å^3)	4313(2)	4459.4(12)	4389.9(15)	4327.0(8)	4481.5(17)	4347(2)
Z	4	4	4	4	4	4
ρ_{calcd} (g cm^{-3})	1.526	1.513	1.513	1.386	1.38	1.393
T (K)	170	170	170	293	295	170
R[a]	0.035	0.050	0.0539	0.043	0.050	0.055
R_w[b]	0.027[b]	0.159[c]	0.1771[c]	0.036[b]	0.121[c]	0.179[c]
GOF[d]	2.30	1.07	1.155	1.36	1.06	0.96

[a] $R = \Sigma \, ||Fo| - |Fc|| / \Sigma \, |Fo|$. [b] $R_w = [\{\Sigma w(|Fo| - |Fc|)^2\} / \Sigma w Fo^2]^{1/2}$. [c] $R_w = [\{\Sigma w(|Fo| - |Fc|)^2\} / \Sigma w(Fo^2)^2]^{1/2}$. [d] $GOF = [\Sigma w(|Fo| - |Fc|)^2 / (n - p)]^{1/2}$ (where n = number of data; p = number of parameters varied).

The crystal structures of **1** – **6** consist of discrete mononuclear $[MO_xS_{4-x}]^{2-}$ anions (where M = Mo, W; x = 0-2) and $[PPh_4]^+$ cations. In the structures of **2**, **3**, **5** and **6** acetonitrile solvent of crystallization is also present. Each metal atom is coordinated by four $[E]^{2-}$ ligands (where E = O, S) in a tetrahedral arrangement, as shown below for $[WS_4]^{2-}$ (Figure 2.2). **1** and **4** are shown to be isomorphous in the space group C2/c and **2**, **3**, **5** and **6** are shown to be isomorphous in the space group $P2_1/n$. The $[PPh_4]^+$ cations show no unusual structural features, however, the M-E bonds in some cases exhibit large variations and will be discussed further.

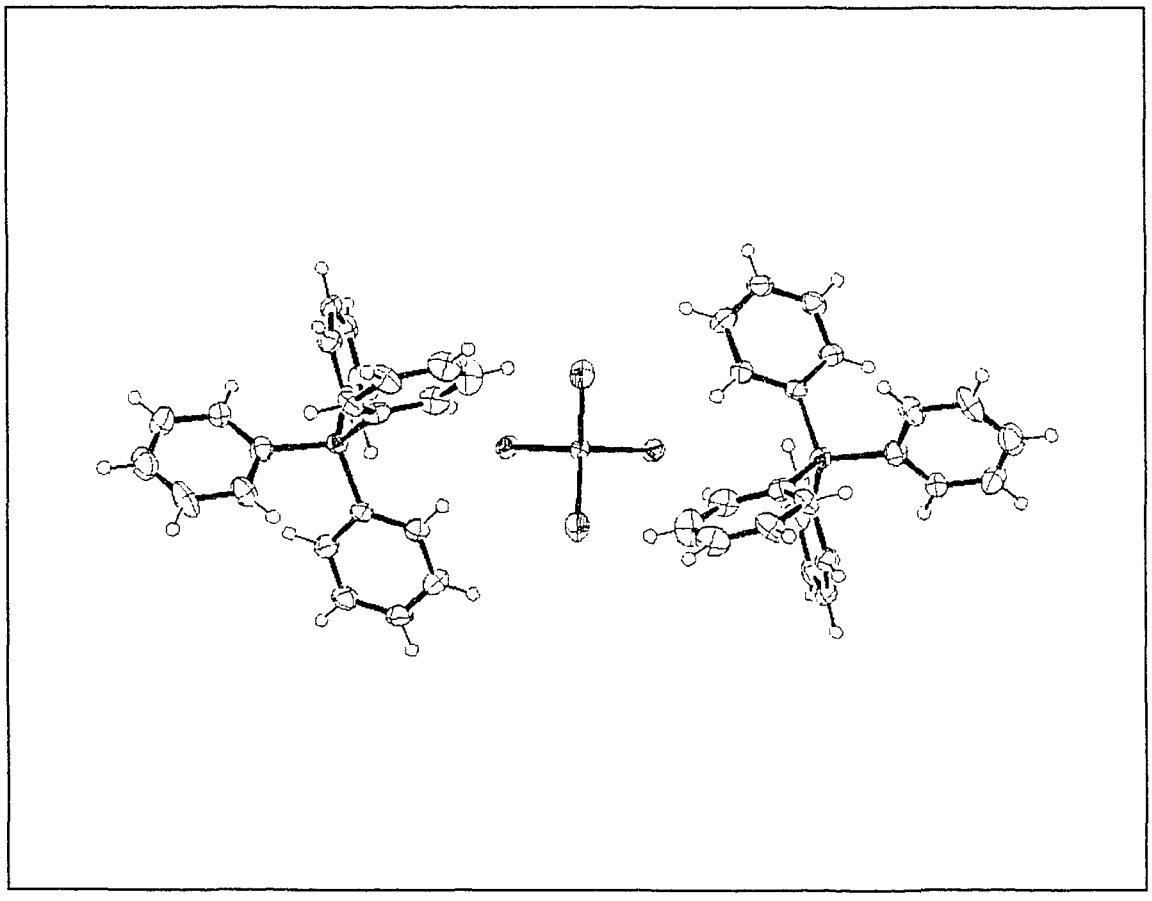

Figure 2.2 ORTEP representation of $[PPh_4]_2[WS_4]$ (**1**) showing symmetry related atoms.

2.2.3.1 $[PPh_4]_2[MS_4]$ (M = Mo, W)

In the tetrathiometallates, all M-S bonds were found to be essentially equal in length, at an average of 2.195Å. It is somewhat surprising that the Mo-S bond lengths of our tetrathiometallates are shorter than the analogous W-S bond lengths (see Tables 2.6 and 2.7) when one considers that the ionic radii of Mo(VI) and W(VI) are nearly identical.[59] The average M-S bond in $[PPh_4]_2[MoS_4]$ is 2.179Å compared to 2.195Å in $[PPh_4]_2[WS_4]$, and our oxothiometallate structures show a similar trend. In contrast, the x-ray crystal structures of $[PPh_4][Cp^*MoS_3]$ and $[PPh_4][Cp^*WS_3]$[83] exhibit similar M-S

bond lengths, a feature that is also observed in the compounds $[PPh_4][MoS_3(S^tBu)]$ and $[PPh_4][WS_3(S^tBu)]$.[118] In the case of compounds of the formula $[NH_4]_2[MS_4]$ (where M = Mo,[119] W[24]) the average Mo-S and W-S are again almost identical (2.178Å and 2.177Å, respectively), but when one compares the W-S bond lengths in $[NH_4]_2[WS_4]$ to those of our respective $[PPh_4]^+$ salt, we observe a difference of almost 0.02Å.

Table 2.6 Selected bond distances (Å) and angles (°) for $[PPh_4]_2[WS_4]$ (**1**).

W-S(1)	2.196(2)	S(1)-W-S(1)*	110.7(1)
W-S(1)*	2.196(2)	S(1)-W-S(2)	108.63(6)
W-S(2)	2.194(2)	S(1)-W-S(2)*	109.36(6)
W-S(2)*	2.194(2)	S(1)*-W-S(2)	109.36(6)
		S(1)*-W-S(2)*	108.63(8)
Average W-S	2.195	S(2)-W-S(2)*	110.19(8)

Table 2.7 Selected bond distances (Å) and angles (°) for $[PPh_4]_2[MoS_4]$ (**4**).

Mo-S(1)	2.178(2)	S(1)-Mo-S(1)*	110.54(10)
Mo-S(1)*	2.178(2)	S(1)-Mo-S(2)	109.33(6)
Mo-S(2)	2.180(1)	S(1)-Mo-S(2)*	108.82(6)
Mo-S(2)*	2.180(1)	S(1)*-Mo-S(2)	108.82(6)
		S(1)*-Mo-S(2)*	109.33(6)
Average Mo-S	2.179	S(2)-Mo-S(2)*	109.99(8)

2.2.3.2 $[PPh_4]_2[MOS_3]$ (M = Mo, W)

Preliminary refinement of the oxotrithiometallates resulted in the appearance of one short and two long M-S bond distances, and for the dioxodithiometallates, one short and one long M-O bond distance. X-ray absorption spectroscopy of $[NH_4]_2[MoO_2S_2]$ single crystals show the anion to be in the more symmetrical C2/c space group and identical bond distances for both Mo-O bonds.[120] The longer M-S bonds were closer in length to those in $[PPh_4]_2[MS_4]$, suggesting a shortening of the third bond. In the case of the M-O bond lengths in $[MO_2S_2]^{2-}$, the shorter bond was closer to that reported for

$[NH_4]_2[MoO_2S_2]$ and the other appeared to be elongated. The data were highly suggestive of disorder within the crystal lattice and so an attempt was made by Dr. M. Parvez to model this.

In the oxotrithiometallates, the disorder could be modelled satisfactorily by slightly lowering the site occupancies of O(1) and S(3) which resulted in the appearance of two new atomic positions, O(1)' and S(3)'. The ratio of the two sites for each disordered atom was found to be 0.93: 0.07, when M = W and 0.85: 0.15, when M = Mo. Figures 2.3(a) and (b) illustrate the spatial relationship between the two positions of the disordered atoms in $[WOS_3]^{2-}$ and $[MoOS_3]^{2-}$, respectively.

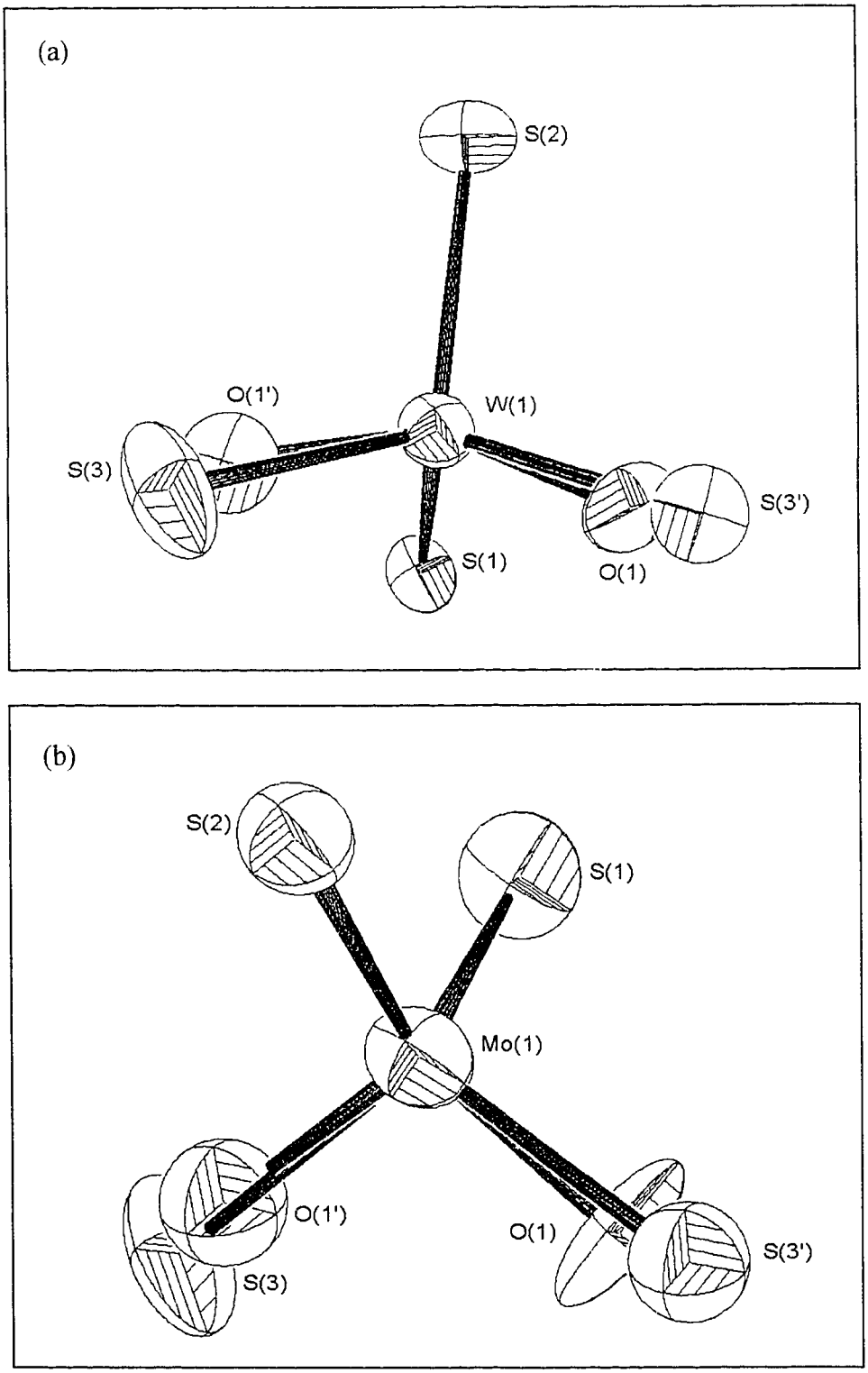

Figure 2.3 ORTEP representations of the anionic portions of (a) $[PPh_4]_2[WOS_3]\cdot CH_3CN$ and (b) $[PPh_4]_2[MoOS_3]\cdot CD_3CN$, showing both positions for disordered atoms.

It can be seen from the ORTEP representations of $[WOS_3]^{2-}$ and $[MoOS_3]^{2-}$ that O(1) and O(1') appear to be exchangeable by a two-fold rotation axis passing through M, as are S(3) and S(3'). Such an operation would exchange positions S(1) and S(2), which would be undetected crystallographically. Structural data shown in Tables 2.8 and 2.9 show that the angles about each symmetry related anion are approximately tetrahedral, with the bond distances and angles in the minor component being more distorted from a regular tetrahedron than in the major orientation. The modelling has also resulted in more consistency between individual M-S and M-O bond distances, which was not found when a site occupancy of one was used for all atoms.

The shorter W-O versus Mo-O bonds are consistent with a stronger dπ-pπ interaction for W and O. The slight elongation of the M-S bonds in $[PPh_4]_2[MOS_3]$ versus $[PPh_4]_2[MS_4]$ may be caused by the localization of more negative charge on the sulfur atoms due to the preference for the oxygen to π-bond with the metal.

Table 2.8 Selected bond distances (Å) and angles (°) for $[PPh_4]_2[WOS_3]\cdot CH_3CN$ (**2**).

W-O(1)	1.690(4)	O(1)-W-S(1)	109.7(3)
W-O(1')	1.699(4)	O(1)-W-S(2)	108.2(3)
W-S(1)	2.203(3)	O(1)-W-S(3)	107.4(4)
W-S(2)	2.210(3)	S(1)-W-S(2)	110.80(11)
W-S(3)	2.198(2)	S(1)-W-S(3)	107.4(4)
W-S(3')	2.207(3)	S(2)-W-S(3)	111.86(14)
O(1') -W-S(1)	109(4)	S(1)-W-S(3')	111.3(13)
O(1') -W-S(2)	109(2)	S(2)-W-S(3')	104.9(6)
O(1') -W-S(3')	112(3)		

Table 2.9 Selected bond distances (Å) and angles (°) for $[PPh_4]_2[MoOS_3]\cdot CD_3CN$ (**5**).

Mo-O(1)	1.725(3)	O(1)-Mo-S(1)	110.24(15)
Mo-O(1')	1.714(2)	O(1)-Mo-S(2)	110.70(15)
Mo-S(1)	2.2000(13)	O(1)-Mo-S(3)	103.89(16)
Mo-S(2)	2.1994(12)	S(1)-Mo-S(2)	110.50(5)
Mo-S(3)	2.1713(10)	S(1)-Mo-S(3)	112.16(7)
Mo-S(3')	2.1776(11)	S(2)-Mo-S(3)	109.18(7)
O(1') -Mo-S(1)	109.6(8)	S(1)-Mo-S(3')	108.0(3)
O(1') -Mo-S(2)	108.9(13)	S(2)-Mo-S(3')	109.2(3)
O(1') -Mo-S(3')	110.7(7)		

If co-crystallization of another member of the oxothiometallate series was occurring, the most likely impurity would be $[PPh_4]_2[MO_2S_2]$ which is isomorphous with $[PPh_4]_2[MOS_3]$. Since our crystal data clearly shows the site occupancy ratio of each pair of disordered atoms is the same, the model is highly suggestive of a rotational disorder rather than a compositional disorder.

2.2.3.3 $[PPh_4]_2[MO_2S_2]$ (M = Mo, W)

When an attempt was made to model the disorder in the dioxodithiometallates, the data suggested disorder of O(2) and S(1), when M = W, and O(2) and S(2), when M = Mo. Two new sites were located in each structure and the site occupancies were optimized at 0.85: 0.15 for each pair of atomic positions. ORTEP representations of the anionic portions of these compounds illustrate the spatial relationship between the two disordered atomic positions (Figure 2.4(a) and (b)).

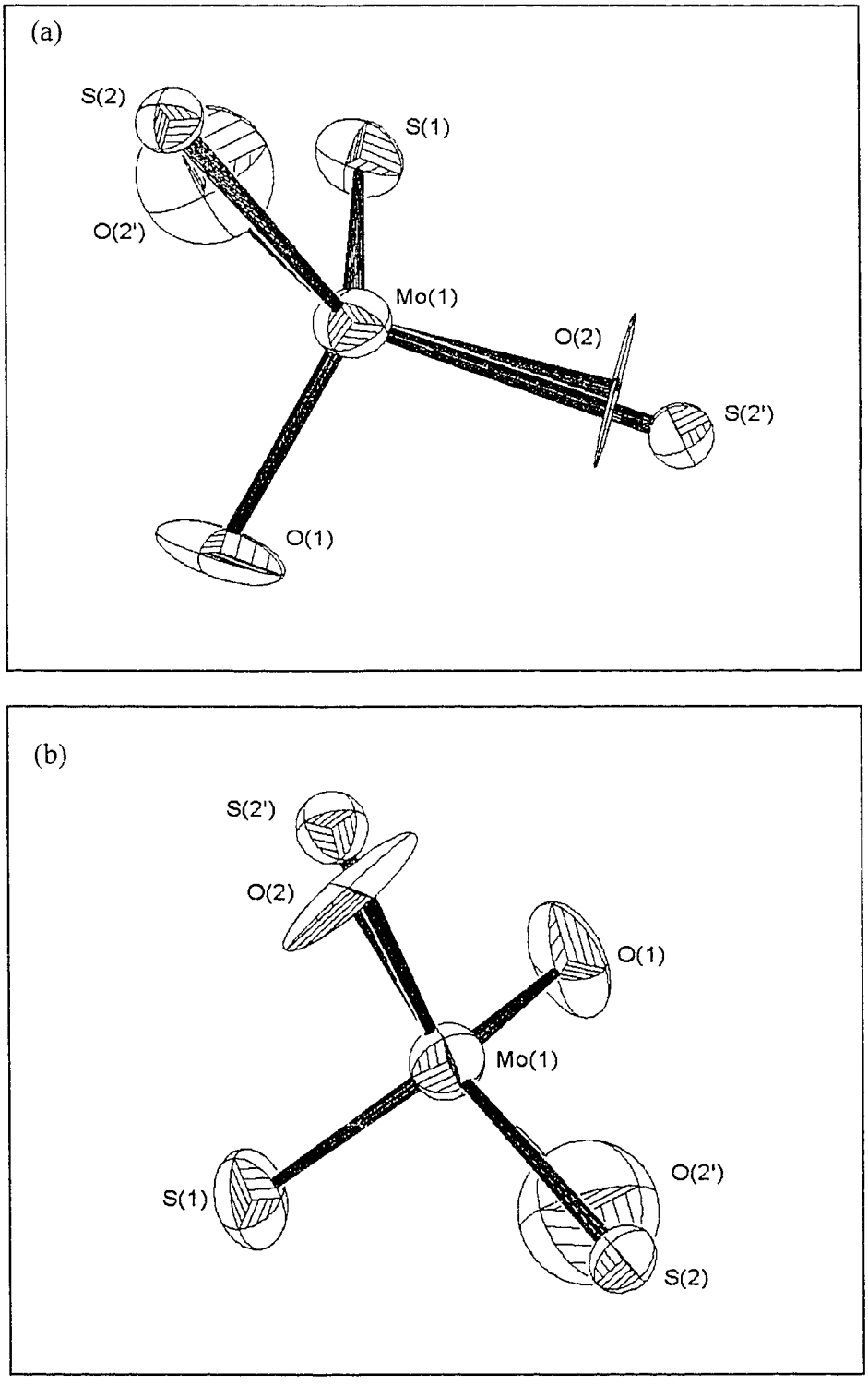

Figure 2.4 ORTEP representations of the anionic portions of (a) $[PPh_4]_2[WO_2S_2]\cdot CH_3CN$ and (b) $[PPh_4]_2[MoO_2S_2]\cdot CD_3CN$, showing both positions for disordered atoms.

The position for each of the disordered atoms is related first by a rotation about a two fold axis running through M, then a reflection in the plane of the four disordered atoms. The first operation exchanges the two non-disordered atoms, and the second brings them back to their original positions.

Table 2.10 Selected bond distances (Å) and angles (°) for $[PPh_4]_2[WO_2S_2]\cdot CH_3CN$ (**3**).

W-O(1)	1.704(4)	O(1)-W-O(2)	107.6(8)
W-O(2)	1.709(4)	O(1)-W-S(1)	109.5(4)
W-O(2')	1.701(4)	O(1)-W-S(2)	109.8(4)
W-S(1)	2.2170(19)	O(2)-W-S(1)	109.9(6)
W-S(1')	2.209(2)	O(2)-W-S(2)	109.3(5)
W-S(2)	2.2121(18)	S(1)-W-S(2)	110.74(14)
O(1)-W-O(2')	118.1(7)	O(2') -W-S(2)	116.5(18)
O(1)-W-S(1')	102.3(8)	S(1') -W-S(2)	110.6(7)
O(2)'-W-S(1')	97.6(18)		

Table 2.11 Selected bond distances (Å) and angles (°) for $[PPh_4]_2[MoO_2S_2]\cdot CH_3CN$ (**6**).

Mo-O(1)	1.716(3)	O(1)-Mo-O(2)	107.9(5)
Mo-O(2)	1.733(4)	O(1)-Mo-S(1)	109.1(3)
Mo-O(2')	1.722(4)	O(1)-Mo-S(2)	108.8(2)
Mo-S(1)	2.2000(17)	O(2)-Mo-S(1)	110.8(4)
Mo-S(2)	2.2035(19)	O(2)-Mo-S(2)	109.5(4)
Mo-S(2')	2.189(2)	S(1)-Mo-S(2)	110.68(11)
O(1)-Mo-O(2')	107(3)	O(2') -Mo-S(2')	113(3)
O(1)-Mo-S(2')	103.5(6)	S(1') -Mo-S(2)	112.2(6)
O(2)'-Mo-S(1)	112.2(6)		

The bond angles in the major constituent for each structure are approximately tetrahedral, however, deviation from a regular tetrahedron is observed in the minor constituent and is particularly pronounced in $[PPh_4]_2[WO_2S_2]$. As in the

oxotrithiometallates, the site occupancies of each pair of disordered atoms is the same, suggesting that the disorder is of a rotational nature, rather than being compositional.

Our spectroscopic and elemental analysis data indicate that, within our detection limits, we have obtained pure oxothiometallates, and our attempts to model disorder in the crystal structures of **2**, **3**, **5** and **6** have indicated that our crystalline samples contain single compounds.

2.3 Stability to O/S Redistribution

Due to the absence of ligand redistribution in non-aqueous solutions of the $[PPh_4]^+$ salts under an inert atmosphere, we have been unable to even observe $[PPh_4]_2[MO_3S]$ and $[PPh_4]_2[MO_4]$ *in situ*. In addition, ammonium salts of $[MO_3S]^{2-}$ and discrete $[MO_4]^{2-}$ do not exist in appreciable concentrations in neutral aqueous media, and so do not provide a viable route to preparation of their respective $[PPh_4]^+$ salts by metathetical cation exchange.

The isolable $[PPh_4]^+$ salts, where x = 0-2, are readily soluble in acetonitrile and do not appear to undergo ligand redistribution in the absence of air, which appears to be due to the lack of a proton source from either the solvent or cation.

2.3.1 Formation of $[PPh_4]_2[W_6O_{19}]$

It was found that the thiomolybdates are relatively air stable when in solution, however, the tungsten analogues are quite sensitive. Acetonitrile solutions of **1**, **2** and **3** turn almost colourless when exposed to air for a period of 12-24 hours. The same colourless compound in all three cases was isolated and crystallized, and was shown by

X-ray crystallography to be the condensation product $[PPh_4]_2[W_6O_{19}]\cdot 2CH_3CN$ (**7**). The structure was solved by Dr. M. Parvez and crystallographic data and selected structural parameters are given in the following tables.

Table 2.12 X-ray crystallographic data for $[PPh_4]_2[W_6O_{19}]\cdot 2CD_3CN$ (**7**).

Empirical formula	$C_{52}D_6H_{20}NO_{19}P_2W_6$	β (°)	101.126(12)
Molecular wt (g mol^{-1})	2174.04	V ($Å^3$)	2877.3(9)
Colour	red	Z	2
Crystal system	monoclinic	T (K)	170
Space group	$P2_1/n$ (#14)	ρ_{calcd} (g cm^{-3})	2.509
a (Å)	13.102(3)	R[a]	0.035
b (Å)	11.570(2)	Rw[b]	0.022
c (Å)	19.345(3)	GOF[c]	1.31

[a] $R = \Sigma \, ||Fo|- |Fc||/\Sigma \, |Fo|$. [b] $R_w = [\{\Sigma w(|Fo|- |Fc|)^2\}/\Sigma wFo^2]^{1/2}$. [c] $GOF = [\Sigma w(|Fo| - |Fc|)^2/(n-p)]^{1/2}$ (where n = number of data; p = number of parameters varied).

Table 2.13 Selected bond distances (Å) and angles (°) for $[PPh_4]_2[W_6O_{19}]\cdot 2CD_3CN$ (**7**).

W(1)-O(1)	2.3198(6)	W(2)-O(9)	1.727(9)
W(1)-O(2)	1.928(9)	W(3)-O(1)	2.3189(6)
W(1)-O(3)	1.925(9)	W(3)-O(3)	1.896(8)
W(1)-O(5)	1.901(9)	W(3)-O(4)	1.944(9)
W(1)-O(6)	1.697(8)	W(3)-O(7*)	1.930(8)
W(1)-O(7)	1.901(9)	W(3)-O(8*)	1.903(9)
W(2)-O(1)	2.3292(6)	W(3)-O(10)	1.718(10)
W(2)-O(2)	1.907(7)		
W(2)-O(4)	1.910(9)	W(1)-O(1)-W(2)	89.93(3)
W(2)-O(5*)	1.919(7)	W(2)-O(1)-W(3)	90.10(3)
W(2)-O(8)	1.939(9)	W(3)-O(1)-W(1*)	90.07(3)

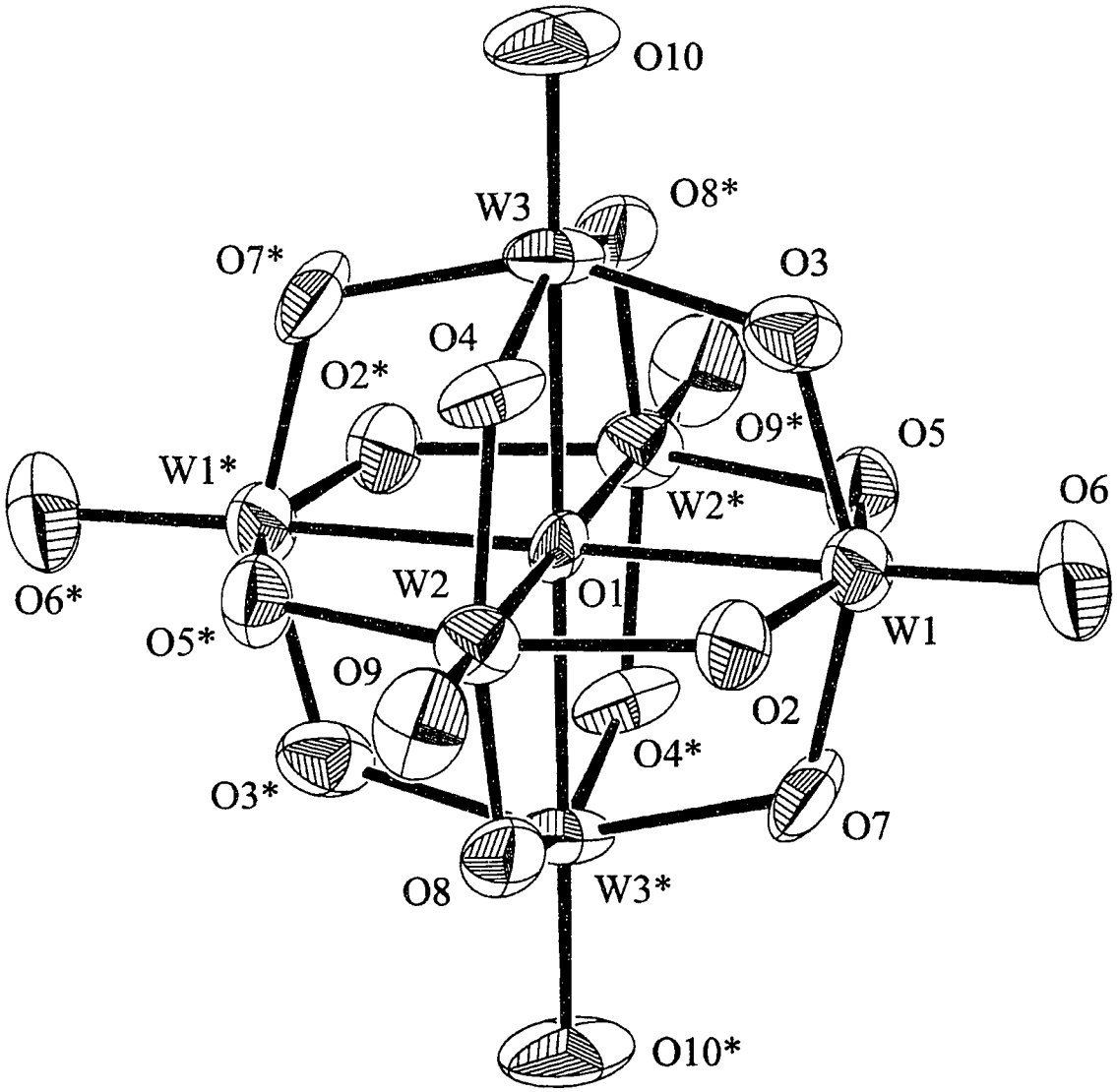

Figure 2.5 ORTEP representation of the anionic portion of $[PPh_4]_2[W_6O_{19}]\cdot 2CD_3CN$ (**7**).

The structure consists of $[W_6O_{19}]^{2-}$ anions (Figure 2.5), $[PPh_4]^+$ cations and CD_3CN molecules of solvation, all separated by normal van der Waals distances. In the anion, the central O atom, which lies on an inversion centre, is bonded to six W atoms in an octahedral arrangement, and these are each bonded to one terminal and four bridging O atoms. The average W-O distances are 2.323(4), 1.917(15) and 1.714(13) Å for W-$O_{central}$, W-O_b and W-O_t bonds, respectively. W-$O_{central}$-W angles are in the narrow range 89.89(2)-90.11(2). Many structures containing $[M_6O_{19}]^{2-}$ (M = Mo, W) have previously been reported, but none with $[PPh_4]^+$ cations.[121-123] The cations in **7** show average P-C and C-C distances of 1.80(2) and 1.38(2) Å, which are well within the expected range, and exhibit no unusual features.

We believe that another product from this decomposition is S_8, which has been isolated as a crystalline solid in some cases. We have previously reported the single crystal structure of $[PPh_4]_2[W_6O_{19}]\cdot 2CD_3CN$, which was obtained from the reaction of $[PPh_4]_2[WO_2S_2]$ with excess ^{t}BuBr in CD_3CN, a day after completion of an NMR experiment.[124] Under such conditions, the compound was isolated as a red crystal, in contrast to the colourless crystals isolated from solutions of thiometallates after exposure to air. We now believe that the apparently red crystal was actually colourless but with a coating of red $[PPh_4]_2[W_3S_9]$, which was also in solution. Several attempts were made to simulate the same reaction environment in the hope of producing another red crystal of $[PPh_4]_2[W_6O_{19}]\cdot 2CD_3CN$, but in each case the only crystals formed were colourless. It is most likely that formation of $[W_6O_{19}]^{2-}$ was the result of a small amount of air entering the reaction tube, causing stepwise replacement of the sulfide ligands by oxide, and condensation of the tungstate ion which is known to occur when the pH is not high.

$$[WS_4]^{2-} + 2O_2 \longrightarrow [WO_4]^{2-} + {}^1/_2S_8 \qquad \textbf{Equation 2.2}$$

$$[WO_4]^{2-} \xrightarrow{pH > 7} \textbf{polytungstates} \qquad \textbf{Equation 2.3}$$

7 has previously been synthesized under different conditions[125] and isolated as a white powder, but no crystal structure was reported. In each case, acidification or the presence of water initiated the decomposition of an oxometal species and in none of the cases was the decomposition of a thiometal species reported. In addition, it was also reported that such chemistry is only observed when M = W, which is in agreement with our own observations. Solutions of thiomolybdates are stable for several days when exposed to air, and over a period of weeks, form polythiomolybdates instead of polymolybdates.

^{183}W NMR studies have previously been used to characterize polytungstates.[126] $[N^nBu_4]_2[W_6O_{19}]$ is reported to exhibit a single resonance at a chemical shift of 47ppm in CH_3CN, where all tungsten atoms are in identical environments. A spectrum of **7** in CH_3CN showed a single resonance at 54ppm, illustrating the influence a different cation has on ^{183}W chemical shift. After crystallization of **7** and redissolution in DMF, a spectrum containing resonances at 56, -23, -107 and –168ppm was obtained (Figure 2.6), with integration close to 3:4:1:1, respectively. The signal at 56ppm is likely $[W_6O_{19}]^{2-}$, now in the presence of a different solvent, and is apparently only present in a third of its original concentration. The other signals are suggestive of the formation of one or more different polytungstates, though comparison to literature values[126] does not indicate that

one single structure can account for all the observed signals. Perhaps the most appropriate interpretation is the formation of $[W_{10}O_{32}]^{4-}$ and another unidentified species. Literature for $[W_{10}O_{32}]^{4-}$ reports that, as a $[N^nBu_4]^+$ salt in CH_3CN, it exhibits two signals at –30 and –174ppm with an integration of 4:1, respectively.[126] When one considers that the signal due to $[W_6O_{19}]^{2-}$ as a $[PPh_4]^+$ salt, in DMF, was 9ppm further upfield than that as a $[N^nBu_4]^+$ salt, in CH_3CN, it seems reasonable that our observed signals at –23 and –168ppm correspond to the reported literature values for $[W_{10}O_{32}]^{4-}$, shifted by 6 or 7ppm upfield due to the presence of the $[N^nBu_4]^+$ cation and DMF solvent. The remaining signal in our spectrum at 107ppm is likely due to low concentrations of a third polytungstate, of which the largest signal is the only one observed. There are several species which might fit this description and it is therefore unreasonable to speculate which might be present.

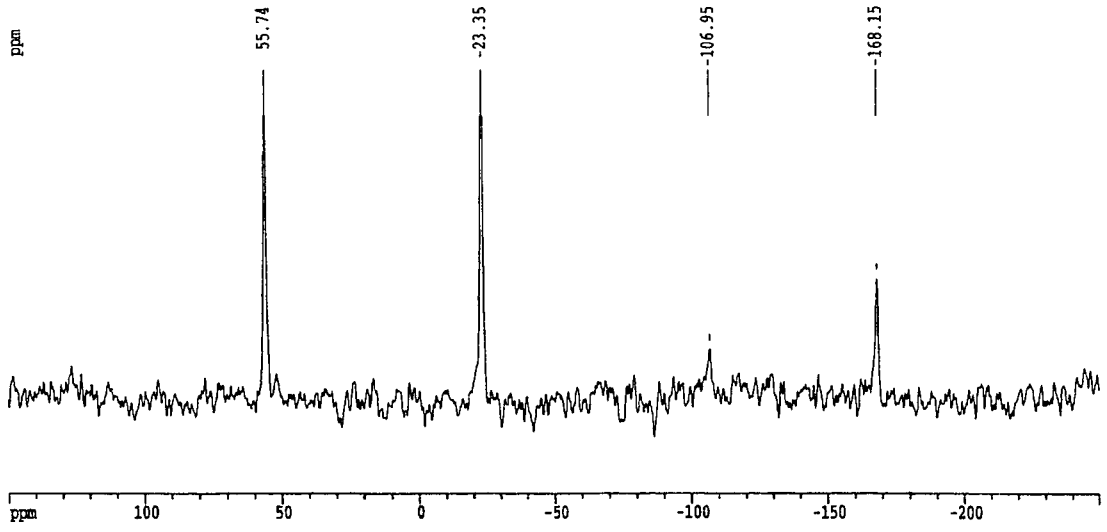

Figure 2.6 ^{183}W NMR spectrum of **7** in DMF.

2.4 Summary

It has been found that compounds of the formula $[PPh_4]_2[MO_xS_{4-x}]$ (M = Mo, W and x = 0-2) can be isolated and purified satisfactorily for use in further reactions. ^{183}W and ^{95}Mo NMR have proved to be useful tools in characterizing the oxothiometallates, and in combination with elemental analysis and IR spectroscopy, have shown the samples to be pure within the detection limits of each technique. While oxothiometallates are often observed to undergo O/S ligand substitution, solutions of $[PPh_4]^+$ salts in acetonitrile, under dinitrogen, exhibit an absence of ligand exchange and their high stability can be utilized to our advantage when characterizing and using them for further reactions. When the $[PPh_4]^+$ salts of oxothiotungstates in acetonitrile are intentionally exposed to aerial oxygen, the $[S]^{2-}$ ligands appear to be oxidized to S_8, and the resultant tungstate anions form hexatungstate, $[W_6O_{19}]^{2-}$. $[PPh_4]_2[W_6O_{19}]\cdot 2CH_3CN$ was readily crystallized from acetonitrile solutions and was characterized by X-ray crystallography, EA, IR and ^{183}W-NMR. Using ^{183}W NMR, it was also observed that, in DMF, $[W_6O_{19}]^{2-}$ equilibrated to more than one other polymetallate, including $[W_{10}O_{32}]^{4-}$.

Single crystal X-ray structures were obtained for all six compounds and on initial refinement exhibited anomalous bond lengths for some of the M-E bonds. Further investigation by modelling of the X-ray data suggested that a rotational disorder was present, and that any kind of compositional disorder was absent. The rotational disorder was further modelled and refined to give alternate sites for the O or S atoms involved. The lack of a compositional disorder has allowed us to be certain that one or more oxothiometallates do not co-crystallize, and that crystalline samples are of high purity.

2.5 Experimental

General Procedures

$[NH_4]_2[MoS_4]$, $[NH_4]_2[WS_4]$ and $[PPh_4]Cl$ were used as purchased from Aldrich, and $[NH_4]_2[MO_xS_{4-x}]$ (where M = Mo, W; x = 1, 2) were synthesized by the literature method.[47] Solutions for NMR and crystallization were manipulated under an atmosphere of dry dinitrogen using standard Schlenk and glovebox techniques. Acetonitrile was distilled over P_2O_5 then CaH_2, and diethyl ether was distilled over Na/benzophenone, respectively. Solvents were stored over molecular sieves and degassed before use. CD_3CN was stored over molecular sieves under dry dinitrogen before use.

Physical Measurements

^{183}W NMR measurements were performed by Dr. Deane McIntyre in the Department of Biological Sciences using a wide-bore Bruker AM-400 spectrometer operating at a resonance frequency of 16.7 MHz and equipped with a horizontal solenoid probe. Samples were run in cylindrical Pyrex tubes with an outside diameter of 17mm and a length of about 4cm. The field stability of the Supercon made it possible to acquire all spectra unlocked. Spectra were referenced to an external standard of 2 M $Na_2[WO_4]$ in H_2O at 0ppm by sample replacement. All spectra were acquired at room temperature (21 ± 1°C) with a pulse length of 20 μs (30° pulse), a relaxation time of 0.327s and a sweep width of 25kHz. Generally, 16 K complex data points were used for each pulse. Each sample was run twice to ensure reproducibility of the signal.

^{95}Mo NMR measurements were performed using Bruker AMX-300 and DRX-400 spectrometers operating at resonance frequencies of 19.5 and 26.0 MHz, respectively.

Samples were run in 5mm tubes and the magnetic field was locked and shimmed using the ^{2}H resonance of the deuterated solvent. Chemical shifts were referenced externally to 2M $Na_2[MoO_4]$ solution in $^{2}H_2O$ at 0ppm by sample replacement. All spectra were acquired at room temperature (21 ± 1°C) with a pulse length of 23 μs (90° pulse), a relaxation time of 0.7μs, and a sweep width of 17.6 to 32.3 kHz. 32K data points were used for each pulse.

NMR measurements for the oxothiometallates were taken using saturated solutions of each compound in CH_3CN; ~3×10^{-3} M for $[PPh_4]_2[MS_4]$ and ~ 6×10^{-3} M for $[PPh_4]_2[MOS_3]$ and $[PPh_4]_2[MO_2S_2]$. ^{183}W NMR measurements for $[PPh_4]_2[W_6O_{19}]$ were taken using ~ 1×10^{-3} M solutions in CH_3CN or DMF. Infrared spectra were recorded using a Mattson 4030 FT-IR spectrometer.

Syntheses of $[PPh_4]_2[MO_xS_{4-x}]$ (M = W, x = 0 (1), 1 (2) and 2(3); M = Mo, x = 0 (4), 1 (5), 2 (6))

All $[PPh_4]^+$ salts were prepared from the respective $[NH_4]^+$ salts. A typical procedure for the preparation of $[PPh_4]_2[WS_4]$ (**1**), based on that described by Sécheresse *et al.*,[124] involved dissolving $[NH_4]_2[WS_4]$ (1.01g, 2.90mmol) in a minimal amount of distilled water (65 ml) to give a yellow solution. In a separate beaker, $[PPh_4]Cl$ (2.21g, 5.9mmol) was dissolved in distilled water (160 ml) to give a colourless solution. On mixing of the two solutions, precipitation of a fine yellow solid occurred, leaving behind an almost colourless solution. The precipitate of $[PPh_4]_2[WS_4]$ was filtered, washed with water (3 × 10ml) then acetone (3×10ml), and dried *in vacuo* to give a yield of 2.57g (89.5%). IR (KBr pellet):[127] 449 ($\nu_{W=S}$) cm^{-1}. Anal. Calcd. for $[PPh_4]_2[WS_4]$: C

58.18%; H 4.07%. Found: C 58.21%; H 3.92%. ^{183}W NMR (400MHz, CH_3CN): δ 3658 ppm.

Data for 2. IR (KBr pellet): 446 ($\nu_{W=S}$), 880 ($\nu_{W=O}$) cm^{-1}. Anal. Calcd. for $[PPh_4]_2[WOS_3]\cdot CH_3CN$: C 59.12%; H 4.27%; N 1.38% Found: C 59.00%; H 4.26%; N 1.52%. ^{183}W NMR (400MHz, CH_3CN): δ 2630 ppm. **Data for 3.** IR (KBr pellet): 444 ($\nu_{W=S}$), 845 ($\nu_{W=O}$), 877 ($\nu_{W=O}$) cm^{-1}. Anal. Calcd. for $[PPh_4]_2[WO_2S_2]\cdot CH_3CN$: C 60.07%; H 4.33%; N 1.40% Found: C 59.87%; H 4.27%; N 1.50%. ^{183}W NMR (400MHz, CH_3CN): δ 1662 ppm. **Data for 4.** IR (KBr pellet):[127] 469 ($\nu_{Mo=S}$) cm^{-1}. Anal. Calcd. for $[PPh_4]_2[MoS_4]$: C 63.85%; H 4.46%. Found: C 63.77%; H 4.47%. ^{95}Mo NMR (300MHz, CD_3CN): δ 2212 ppm. **Data for 5.** IR (KBr pellet): 467 ($\nu_{Mo=S}$), 870 ($\nu_{Mo=O}$) cm^{-1}. Anal. Calcd. for $[PPh_4]_2[MoOS_3]$: C 64.72%; H 4.67%; N 1.51% Found: C 64.70%; H 4.54%; N 1.62%. ^{95}Mo NMR (300MHz, CD_3CN): δ 1588 ppm. **Data for 6.** IR (KBr pellet): 459 ($\nu_{Mo=S}$), 855 ($\nu_{Mo=O}$), 868 ($\nu_{Mo=O}$) cm^{-1}. Anal. Calcd. for $[PPh_4]_2[MoO_2S_2]$: C 65.85%; H 4.75%; N 1.53% Found: C 65.31%; H 4.73%; N 1.59%. ^{95}Mo NMR (300MHz, CD_3CN): δ 996 ppm.

Crystals of $[PPh_4]_2[MOS_3]$ and $[PPh_4]_2[MO_2S_2]$ (where M = Mo, W) were grown from saturated solutions of each salt in acetonitrile under nitrogen, which was maintained at −10°C for 24 hours. The large rectangular blocks were suitable for analysis by single crystal X-ray diffraction. Crystals of $[PPh_4]_2[MS_4]$ were prepared from saturated solutions of each salt in acetonitrile by layering with diethyl ether under nitrogen. After 2-3 days at −10°C, the crystals were of a suitable size for single crystal X-ray crystallography.

Preparation of $[PPh_4]_2[W_6O_{19}]$ (7)

The first crystals of $[PPh_4]_2[W_6O_{19}]$ were prepared by the following procedure: To an NMR tube containing $[PPh_4]_2[WO_2S_2]$ (0.005g, 0.0052 mmol), 0.8 ml of CD_3CN was added under dinitrogen to give a green solution. ^tBuBr (10 μl, 0.0867 mmol) was added by syringe and the reaction maintained at room temperature. After 5 hours, an orange colour was observed, and after 18 hours, a red precipitate and red crystals had formed in the NMR tube. One of the crystals was subjected to an X-ray diffraction study.

It was later found that **7** could be prepared by a simpler procedure: $[PPh_4]_2[WO_xS_{4-x}]$ (0.1 g) was mixed with *ca.* 5 ml of CH_3CN and ultrasonicated until dissolved, to give a green solution. Air was bubbled through the solution for 30 minutes and then a septum with needle was used to cover the reaction vessel. The solution was left for 24 hours, after which it had turned almost colourless, with large colourless crystals adhering to the side of the vessel. In some cases, yellow crystals were also observed, and shown by single crystal X-ray diffraction to be S_8. An X-ray study of the colourless crystals revealed them to be identical in composition to those obtained by the first synthesis. Characterization by EA and IR revealed that **7** was the major product from the aerial decomposition of all three thiotungstates, $[PPh_4]_2[WO_xS_{4-x}]$ (x = 0-2). ^{183}W NMR data was collected on the near-colourless solution obtained by the above synthesis, with ultrasonication to partially dissolve the colourless crystals. A yield of 10.9 mg (29.6 %) was obtained, based on $[PPh_4]_2[WOS_3]$. IR (KBr pellet):[125] 1115 (s), 1000 (w), 980 (s), 815 (s), 750 (w), 720 (s), 695 (m), 590 (w), 520 (s), 440 (s), 360 (w) cm^{-1}. Anal. Calcd. for $[PPh_4]_2[W_6O_{19}]\cdot 2CH_3CN$: C 29.66%; H 2.20%; N 1.33%. Found: C 29.51%; H 2.28%; N 1.48%. ^{183}W NMR (400MHz, CH_3CN): δ 54 ppm.

X-Ray Crystallography

X-ray crystallography was performed by Dr. Masood Parvez, including modelling of disordered structures. Crystals of **1**, **3**, **5** and **7** were mounted directly onto a glass fiber, **4** and **6** were coated in Paratone-8277 oil and then mounted on a glass fiber, and **2** was sealed in a glass capillary under argon. Data for **1**, **2**, **3**, **6** and **7** were collected using a Rigaku AFC6S diffractometer with graphite monochromated Mo Kα radiation at –103 ± 1°C. Data for **4** and **5** were collected using an Enraf-Nonius CAD-4 diffractometer with graphite monochromated Cu Kα radiation at room temperature. The ω-2θ scan technique was used in all cases. Cell constants and an orientation matrix for data collection were obtained from a least squares refinement using the setting angles of 22 or 25 carefully centreed reflections. The intensities of three representative reflections, measured every 200 reflections, showed slight variation over the course of the data collection. A linear correction was applied to account for this phenomenon. An empirical absorption correction based on azimuthal scans of several reflections was applied. Data were also corrected for Lorentz and polarization effects.

Calculations were performed using the TEXSAN[128] package for **1-5** and **7**, and using SHELXL97[129] for **6**. Structures **1-5** and **7** were solved by direct methods and the heavy atom method was used to solve **6**. Atoms were located using Fourier expansion techniques and were refined using full-matrix least-squares. All non-hydrogen atoms were refined anisotropically and hydrogen atoms were included at geometrically idealized positions.

Structures **2**, **3**, **4** and **6** were furthered refined using SHELXL97, in an attempt to model the observed disorder that previously resulted in anomalous bond lengths. By varying the site occupancies of each of the atoms, an optimum occupancy could be determined, which was constrained during the final stages of refinement to allow multiple positions for some of the atoms to be located.

In **2**, O(1) and S(3) were each found to be disordered over two sites, with occupancy factors of 0.928(10) for O(1) and S(3), and 0.072(10) for O(1') and S(3'). During the refinements, the W-O and W-S bond distances for these atoms were, in turn, constrained at 1.690(4)Å and 2.210(3)Å, respectively. The phenyl rings were constrained as regular hexagons.

In **3**, O(2) and S(1), were each found to be disordered over two sites, with occupancy factors of 0.852(5) for O(2) and S(1), and 0.148(5) for O(2') and S(1'). During the refinements, the W-O and W-S bond distances for these atoms were constrained, In turn, at 1.700(4)Å and 2.210(2)Å, respectively. The phenyl rings were constrained as regular hexagons.

In **5**, O(1) and S(3) were each found to be disordered over two sites, with occupancy factors of 0.852(5) for O(1) and S(3), and 0.148(5) for O(1') and S(3'). During the refinements, the Mo-O and Mo-S bond distances for these atoms were constrained, in turn, at 1.710(3)Å and 2.180(1)Å, respectively. The phenyl rings were constrained as regular hexagons.

In **6**, O(2) and S(2), were each found to be disordered over two sites, with occupancy factors of 0.852(5) for O(2) and S(2), and 0.148(5) for O(2') and S(2'). During the refinements, the Mo-O and Mo-S bond distances for these atoms were constrained, in

turn, at 1.720(4)Å and 2.190(2)Å, respectively. The phenyl rings were constrained as regular hexagons.

Chapter 3 – Alkylation reactions of $[PPh_4]_2[WO_xS_{4-x}]$ (M = Mo, W; x = 0-2)

3.1 Introduction

Our original interest in C-S bonds stemmed from the chemistry of dinuclear W(III) bridging thioether complexes, which were observed to undergo C-S bond cleavage in the presence of nucleophiles.[130] Seeking to study the reverse process of C-S bond formation in a simpler system, $[PPh_4]_2[WS_4]$ was chosen as a suitable candidate for reactions with alkyl halides. Reactions of $[N(C_5H_{10})H_2]_2[WS_4]$ (piperidinium tetrathiotungstate) with alkyl halides had previously been reported, where the major organic products were disulfides.[131,132] In addition, $[R_4X]_2[W_3S_9]$ was formed in reactions of $[NH_4]_2[WS_4]$ with ammonium, phosphonium and arsonium salts, $[R_4X][Y]$ (where Y = OH, Cl, I).[63] In each of these cases an alkylated intermediate was suggested, though none had been isolated under the reported conditions. The goal of isolating and characterizing an intermediate species from the alkylation of $[WS_4]^{2-}$ is particularly challenging due to the tendency for high oxidation state mononuclear thiolate complexes to undergo reductive elimination, forming organic disulfides and lower valent metal centres. Also, since sulfide ligands have a propensity to bridge between metal centres the formation of polythiometallates is highly favoured.

Preliminary studies into the alkylation of $[PPh_4]_2[WS_4]$ by Meiping Wang proved that $[PPh_4][WS_3(SEt)]$ could be isolated from the reaction of $[PPh_4]_2[WS_4]$ with EtBr,[133] and that formation of organic sulfides and polythiometallates occurred by decomposition of the alkylated product (Scheme 3.1).

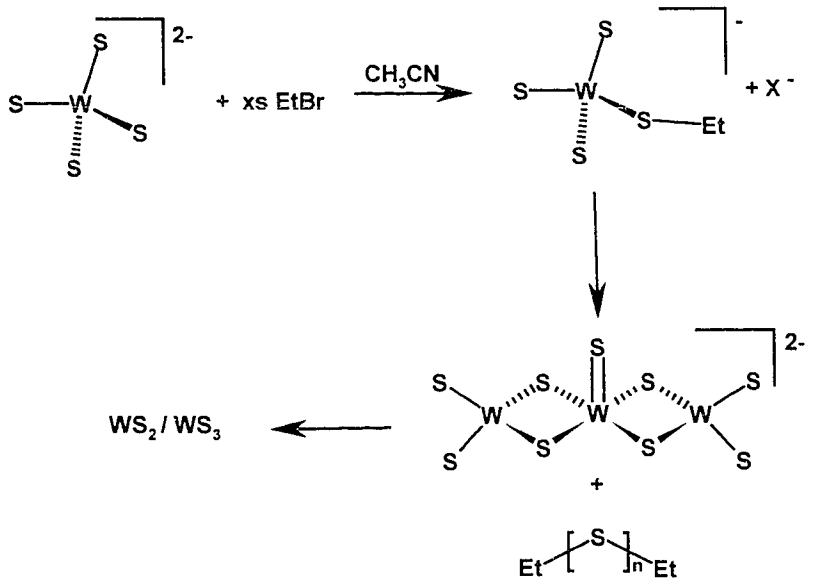

Scheme 3.1 $[PPh_4]_2[WS_4]$ and EtBr (1:10) in CH_3CN.

Kinetic studies on the formation and decomposition of this salt and the ^{t}Bu analogue were carried out using UV/Vis and NMR spectroscopy.[58] The data suggest that formation of the Et analogue proceeds by an associative nucleophilic substitution mechanism (S_N2) in contrast to the bulkier ^{t}Bu analogue which reacts by a dissociative nucleophilic substitution mechanism (S_N1). Decomposition kinetics for $[WS_3(SEt)]^-$ suggest that the first step involves the association of two such anions and although data for the decomposition of $[WS_3(S^tBu)]^-$ was inconclusive, it suggests that a different mechanism was involved for the more bulky alkyl group.

Successful isolation and characterization by X-ray crystallography has since been achieved for $[PPh_4][WS_3(SR)]$, where R = ^{i}Pr, ^{t}Bu and for $[PPh_4][MoS_3(SR)]$, where R = ^{t}Bu. We decided to investigate the chemistry with several *new* alkylating agents to

broaden our understanding of the formation and decomposition of alkylated species. Our findings will be reported in this chapter.

3.2 New Alkylated $[WS_4]^{2-}$ Complexes

3.2.1 Reactions with BzCl

In order to devise a synthetic strategy that would allow us to isolate these species, the reactions were followed by ^{1}H-NMR spectroscopy to determine the optimum conditions for synthesis and isolation. Benzyl halides are particularly suitable for ^{1}H NMR studies since the methylene protons adjacent to the halide are represented as a singlet in the spectrum, and replacement of the halide by other subtly different groups is reflected by distinct chemical shift changes that can be used to identify the species.

Alkyl bromides were the alkylating agents of choice for the initial studies into these reactions. They resulted in faster reaction times than the corresponding chlorides and avoided unwanted redox reactions as observed with iodides forming triiodide ions.[134] However, in the benzyl halide case, BzBr was found to be unsuitable due to the rapid decomposition of reaction mixtures resulting in black precipitates of WS_3/WS_2. Reactions at low temperature could be maintained without visible decomposition, but when concentrated to remove solvent during the work-up procedure, decomposition could not be avoided. As a result, we have used BzCl as the alkylating agent in this case, and have achieved much success. Figure 3.1 shows time dependent ^{1}H NMR spectra for a typical alkylation reaction of $[PPh_4]_2[WS_4]$ with one equivalent of benzyl chloride injected at 0°C and maintained room temperature for the remainder of the experiment.

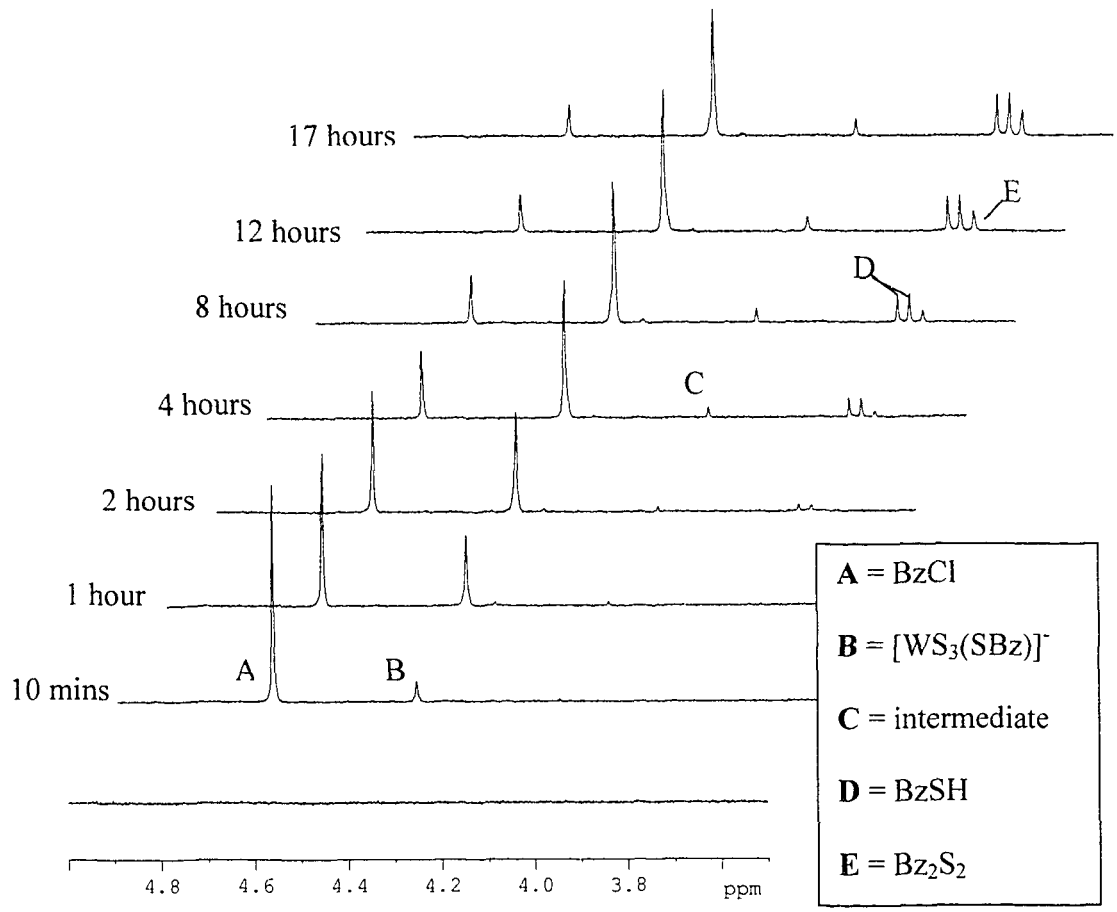

Figure 3.1 Time dependent ^{1}H NMR series for $[PPh_4]_2[WS_4]$ and BzCl (1:1) in CD_3CN at room temperature.

The series of spectra clearly shows the benzyl chloride (BzCl, 4.67ppm) being consumed and the formation of the alkylated species at a more upfield position (4.36ppm). The major organic decomposition product in this case is benzyl thiol (BzSH, 3.74ppm, doublet, $^{3}J_{HH}$ = 7.7Hz), which originates from reaction of the alkylated species with the small amount of residual water present in the deuterated solvent. The signal at 3.70ppm represents benzyl disulfide (Bz_2S_2), and the additional decomposition peak at 4.05ppm is believed to be due to an as yet unidentified intermediate, which we have

independently generated by the reaction of Bz_2S_2 and $[WS_4]^{2-}$, or Bz_2S_2 and $[WS_3(SBz)]^-$. From these data, we can deduce that the optimum reaction time, when one equivalent of benzyl chloride is used at room temperature, is 10 hours. When a large excess of benzyl chloride is used, the optimum reaction time is reduced to 2 hours, and significant decomposition has not occurred by this time, making a more desirable set of reaction conditions. Figure 3.2 shows the ^1H NMR spectrum of crystals of $[PPh_4][WS_3(SBz)]$ in CD_3CN, which was used to confirm the identity of signal B in Figure 3.1.

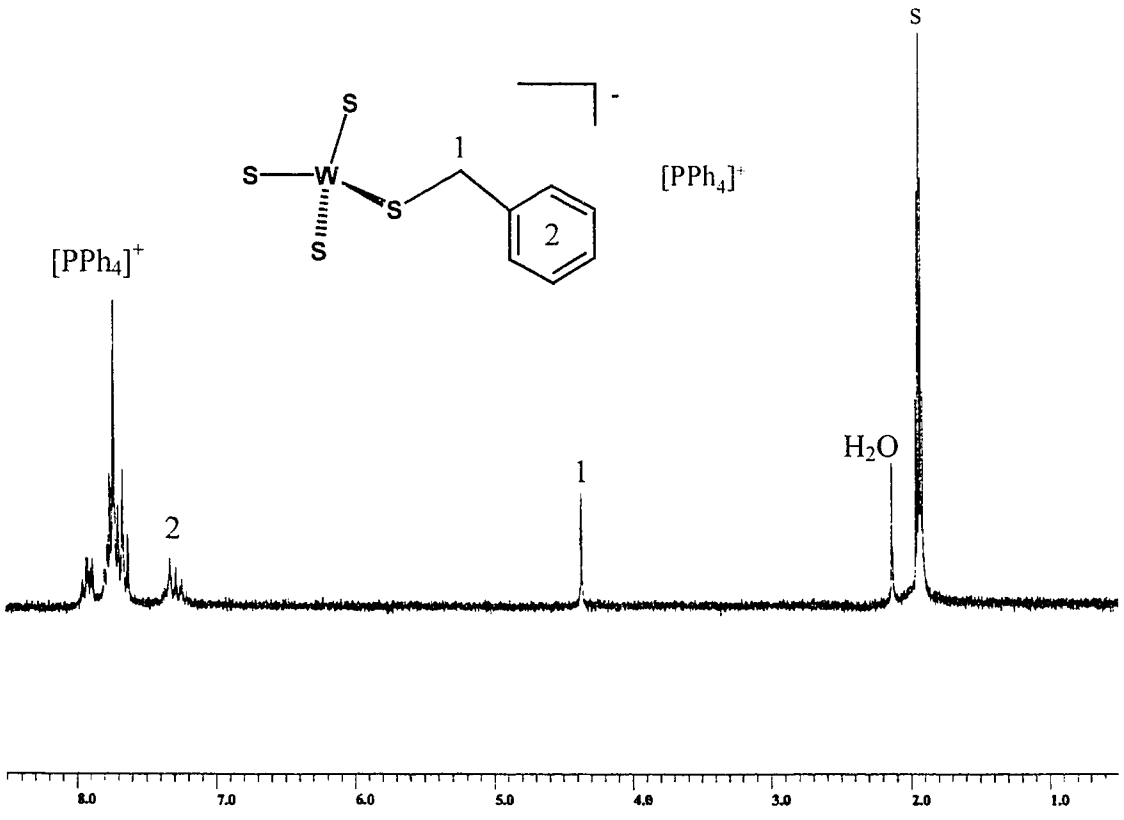

Figure 3.2 ^1H NMR spectrum of $[PPh_4][WS_3(SBz)]$ in CD_3CN at room temperature.

When crystals of $[PPh_4][WS_3(SBz)]$ were left in solution at room temperature for three days, decomposition occured to yield BzSH and Bz_2S_2, as observed in Figure 3.2 (signals D and E respectively), in addition to the unidentified intermediate at 4.05ppm (signal C). The appearance of this intermediate by decomposition of $[PPh_4][WS_3(SBz)]$ rules out the possibility that signal C is a bis-alkylated product. It is more likely that signal C is due to a polythiometallate species with a coordinated $[BzS]^-$ ligand. No evidence exists for the presence of free $[BzS]^-$ in solution, which would give a more upfield signal than the respective sulfides.[135]

The X-ray crystal structure of $[PPh_4][WS_3(SBz)]$ was solved and a detailed analysis will be presented later in this chapter with comparisons to other related structures.

3.2.2 Reactions with ^{i}BuBr

^{i}BuBr would be expected to react with $[WS_4]^{2-}$ by an S_N2 mechanism, as observed for EtBr, since the bromide is at a primary carbon. Such a mechanism would result in $[WS_3(S^iBu)]^-$ being the major product. If ^{i}BuBr was to react by an S_N1 mechanism, isomerization to the more stable carbocation would occur after dissociation of the halide before nucleophilic attack (Scheme 3.2).[136] The result would be formation of $[WS_3(S^tBu)]^-$ as the major product in the latter case.

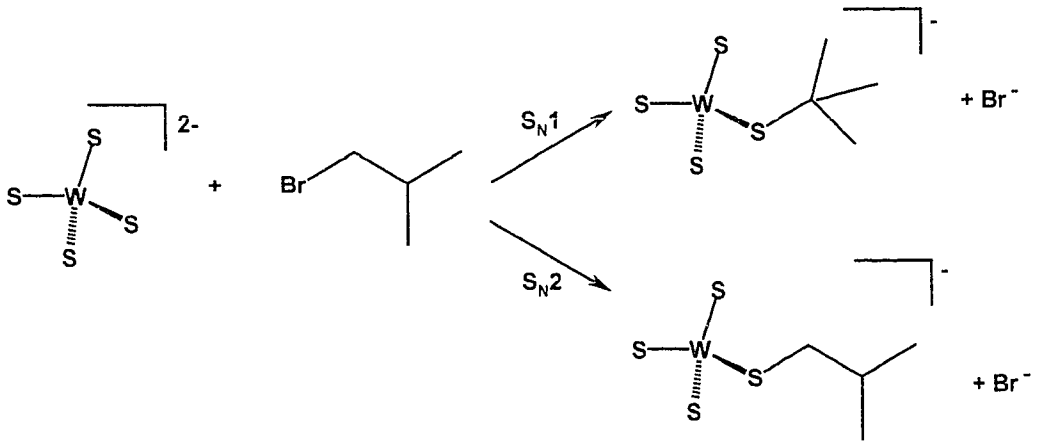

Scheme 3.2 Possible reaction mechanisms for $[WS_4]^{2-}$ and ^{i}BuBr.

Since the reaction with ^{t}BuBr, which proceeds by an S_N1 mechanism, is optimal after 6-8 hours, we settled on 6 hours as an appropriate reaction time for ^{i}BuBr. It should be noted that attempts to follow the reaction by time dependent ^{1}H NMR were not useful due to the small intensity of the coupled signals. In addition, the CD_3CN signal overlapped with one of the product signals and the only other suitable solvent, in terms of solubility, was CD_2Cl_2. Chlorinated solvents such as CD_2Cl_2 and $CDCl_3$ have been avoided due to their tendency to decompose both thiometallates and alkylated products over time. It is likely that these solvents are actually behaving as alkylating agents, forming highly unstable methylated intermediates that rapidly decompose.

After working-up the reaction mixture, a small quantity of THF extract was analyzed by ^{1}H NMR and was shown to contain only one alkylated product, $[WS_3(S^{i}Bu)]^{-}$. In addition, crystals were isolated from this solution, and shown to be $[PPh_4][WS_3(S^{i}Bu)]$ by ^{1}H NMR, with an absence of a signal at 1.55ppm due to $[PPh_4][WS_3(S^{t}Bu)]$ (Figure 3.3). We can now rule out the possiblity of the alkylation

reaction proceeding by an S_N1 mechanism, in agreement with the kinetic data acquired for reaction of EtBr.

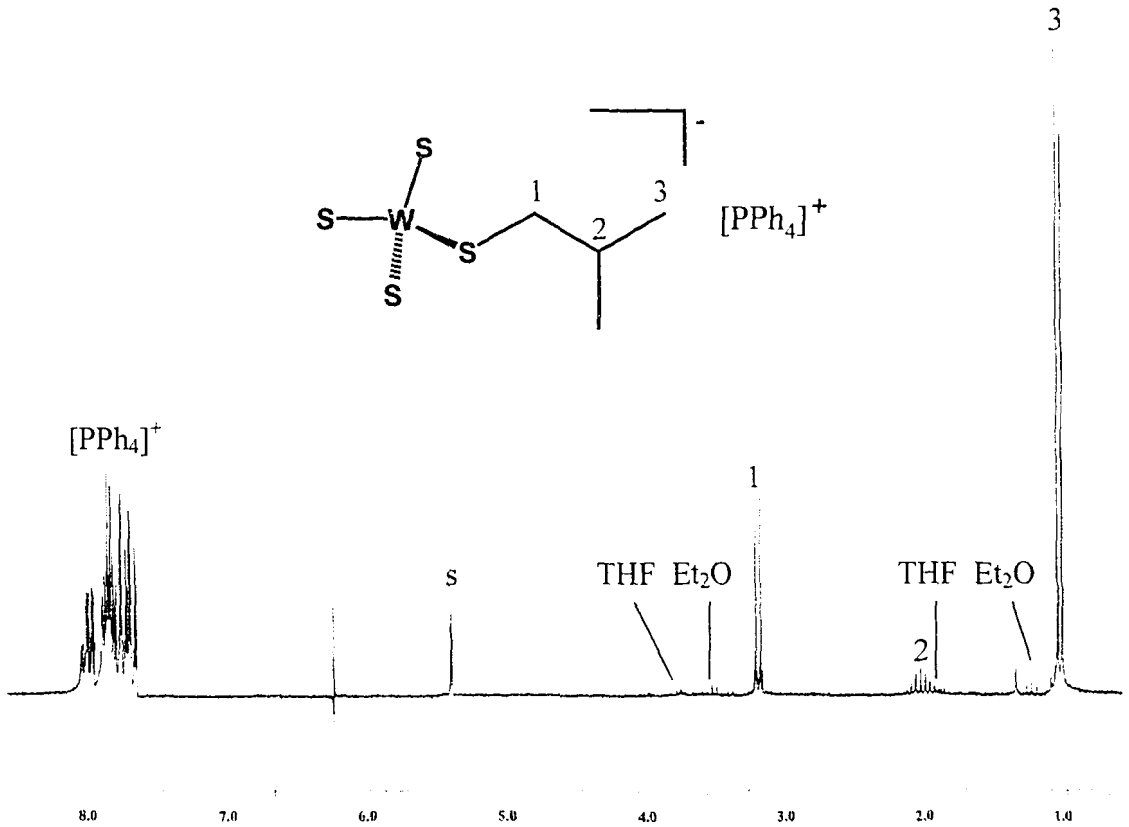

Figure 3.3 ^{1}H NMR of $[PPh_4][WS_3(S^iBu)]$ in CD_2Cl_2 at room temperature.

Crystals of $[PPh_4][WS_3(S^iBu)]$ were subjected to analysis by X-ray crystallography and found to contain disorder at the tertiary carbon. The disorder was modelled satisfactorily with two atomic positions, each with an occupancy of 0.5. The data showed no indication that an impurity of $[PPh_4][WS_3(S^tBu)]$ was present in the crystal lattice and structural comparisons will be made later in this chapter.

3.2.3 Reactions with Allyl Bromide (C_3H_5Br)

Initial attempts to follow the reaction of $[PPh_4]_2[WS_4]$ and C_3H_5Br by time dependent ^1H NMR were unsuccessful due to the complex array of signals observed and the unusual broadening observed for the signal believed to be the alkylated product. Instead, reaction conditions were optimized by varying the reaction time and comparing yields of crystals. Crystals of $[PPh_4][WS_3(SC_3H_5)]$ were subjected to a variable temperature ^1H NMR study which confirmed that the broadening was caused by fluxional behaviour at room temperature (Figure 3.4).

The spectra were collected in CD_3CN due to limited solubility of $[PPh_4][WS_3(SC_3H_5)]$ in other common solvents. At –40°C, the coupling resembles that of allyl bromide at room temperature but clearly with a second order pattern. The α-protons (signal 1) are coupled to the β-proton (signal 2) with a coupling constant of 7.32Hz. The γ-protons (signals 3a and 3b) are both coupled to the β-proton with coupling constants of 16.88 and 9.89Hz, respectively, the *trans* coupling being greater than the *cis*. Other fine structure can be observed for signals 1 and 3 and must consequently be due to long range coupling between the α- and γ-protons. This is more pronounced than in the allyl bromide spectrum and suggests a closer interaction through space.

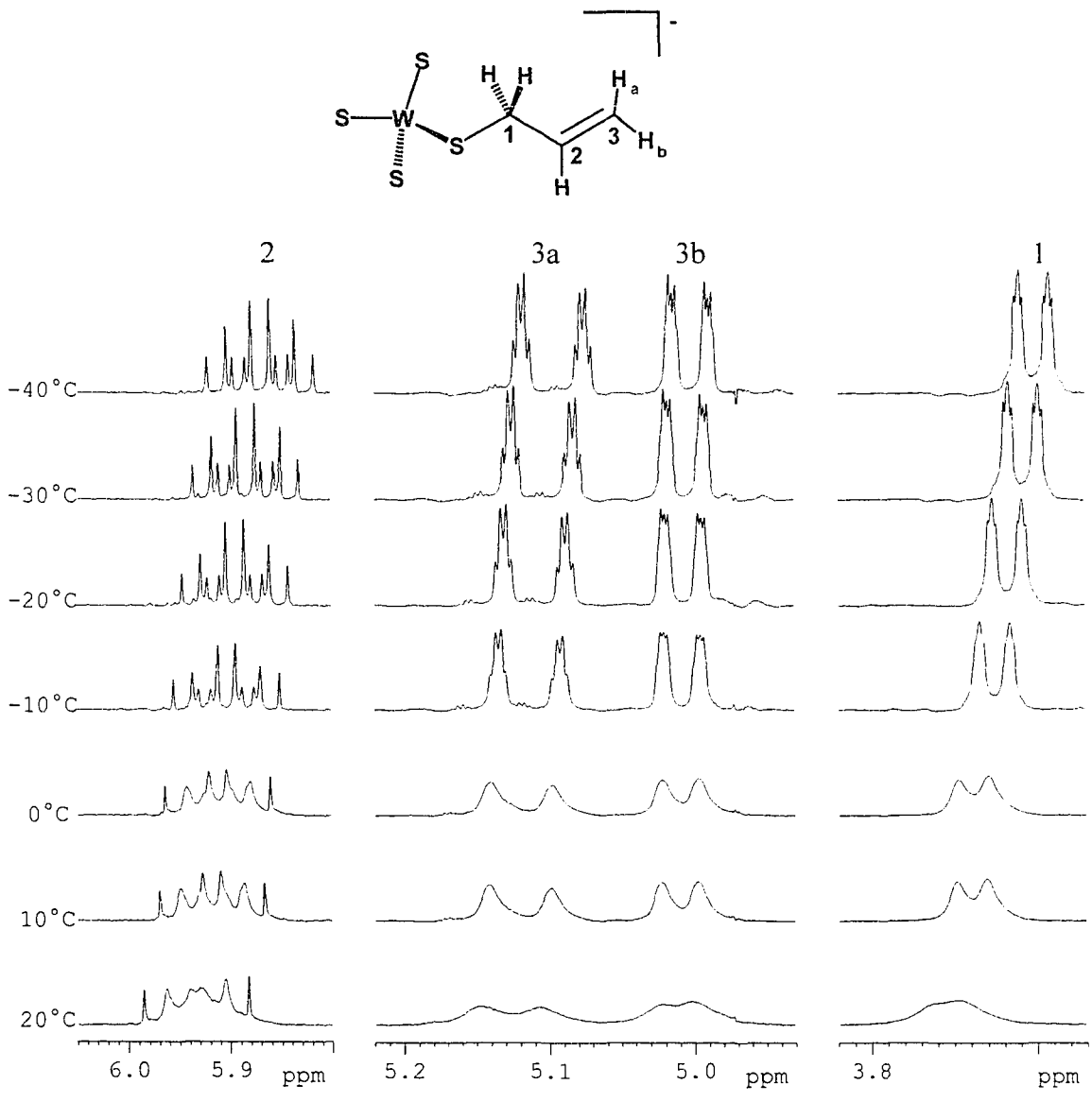

Figure 3.4 Variable temperature ^{1}H NMR series for $[PPh_4][WS_3(SC_3H_5)]$ in CD_3CN.

All of the signals become more resolved at –40°C, with signal 2 being the clearest at all temperatures. While rotation about the C-S and/or C-C single bonds could result in broadened signals, such a phenomenon is not observed for any of the other alkyl groups investigated or for the allyl bromide prior to C-S bond formation. It would also seem

unlikely that signal 2 would be best resolved if this process were occurring. Fluxionality where α- and γ-carbons are exchanged would result in enhanced resolution for signal 2 over 1 and 3, consistent with our observations, and would also explain the stronger coupling between α- and γ-protons compared to allyl bromide. This could occur by two possible mechanisms (Scheme 3.3): (a) α- and γ-carbons exchange via a four-membered cyclic transition state involving the same sulfur atom at all times, or (b) migration of the allyl group over the four sulfurs via a six-membered cyclic transition state. Our current data do not allow us to determine which of these two mechanisms is occurring, however, the allyl migration over all four sulfurs is more attractive due to the more sterically accessible transition state invoked.

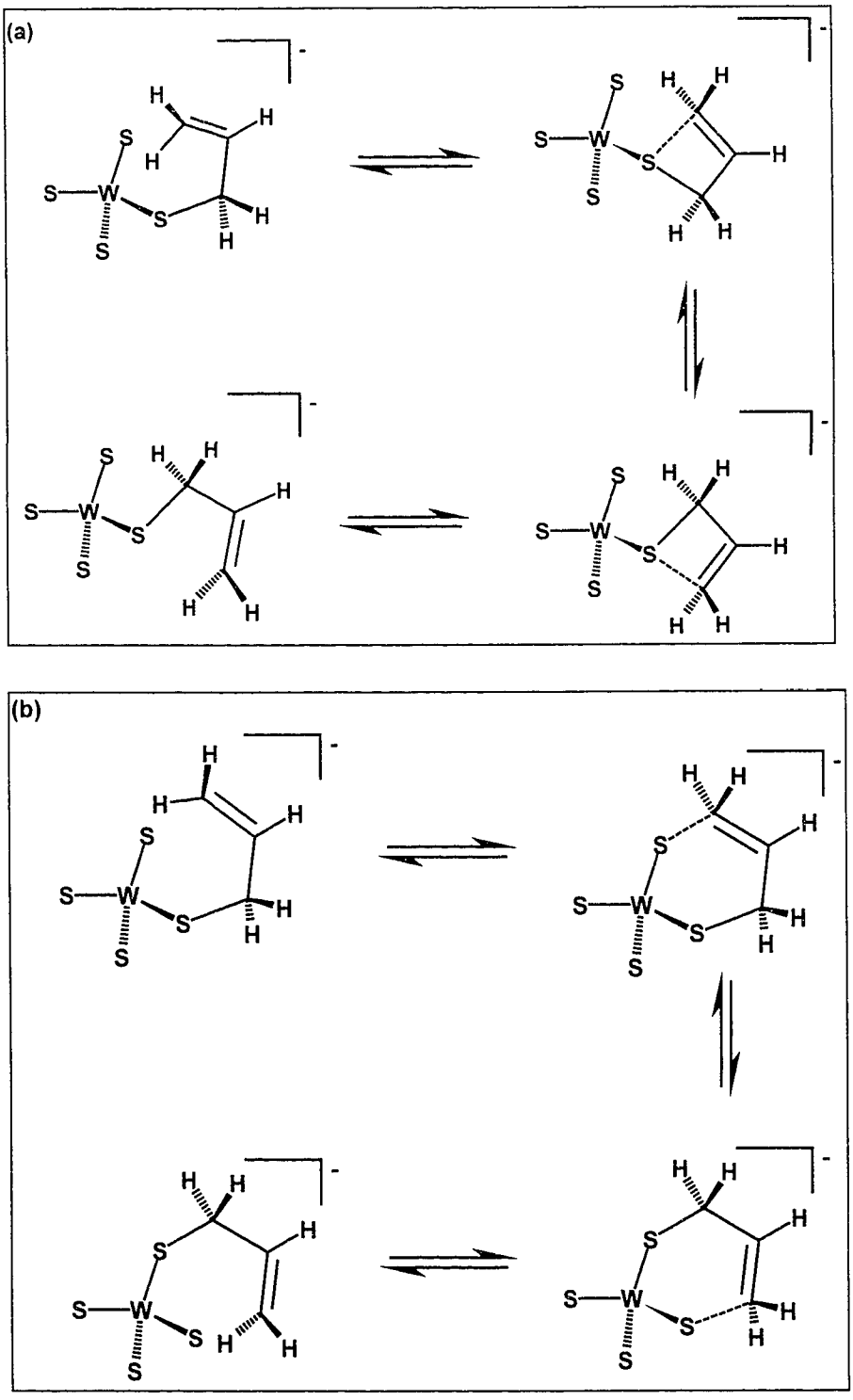

Scheme 3.3 Possible modes of fluxionality for $[PPh_4][WS_3(SC_3H_5)]$, (a) via a four-membered transition state and (b) via a six-membered transition state.

An X-ray crystal structure was obtained for $[PPh_4][WS_3(SC_3H_5)]$ and comparisons with related structures will now be made.

3.2.4 X-Ray Crystallography of $[PPh_4][WS_3(S^iBu)]$(8), $[PPh_4][WS_3(SBz)]$ (9) and $[PPh_4][WS_3(SC_3H_5)]$ (10)

Crystallographic parameters for **8-10** are shown in Table 3.1 and ORTEP representations are shown in Figures 3.5-3.7.

Table 3.1 Crystallographic data for $[PPh_4][WS_3(SR)]$ (R = ^{i}Bu (**8**), Bz (**9**), C_3H_5(**10**)).

	8	**9**	**10**
Empirical formula	$C_{28}H_{29}PS_4W$	$C_{31}H_{27}PS_4W$	$C_{27}H_{25}PS_4W$
Molecular wt (g mol^{-1})	708.57	742.59	692.53
Colour	red	red	red
Crystal system	triclinic	monoclinic	triclinic
Space group	$P\bar{1}$ (#2)	$P2_1/n$ (#14)	$P\bar{1}$ (#2)
a (Å)	11.0377(6)	16.2111(9)	9.4716(9)
b (Å)	11.1307(5)	11.0080(6)	10.4336(10)
c (Å)	13.6286(7)	18.1339(10)	14.4186(14)
α (°)	82.941(1)		100.183(2)
β (°)	84.877(1)	111.722(1)	90.457(2)
γ (°)	60.826(1)		91.747(2)
V (Å^3)	1450.05(13)	3006.2(3)	1401.7(2)
Z	2	4	2
ρ_{calcd} (g cm^{-3})	1.623	1.641	1.641
T (K)	193	193	193
R[a]	0.0282	0.0409	0.0413
R_w[b]	0.0717	0.0659	0.0968
GOF[c]	1.015	0.819	0.976

[a] $R = \Sigma \| |Fo| - |Fc| \| / \Sigma |Fo|$; [b] $R_w = [\{\Sigma w(Fo^2 - Fc^2)^2\}/\Sigma w(Fo^4)]^{1/2}$; [c] $[\Sigma w(Fo^2 - Fc^2)^2/(n-p)]^{1/2}$ (n = number of data; p = number of parameters varied).

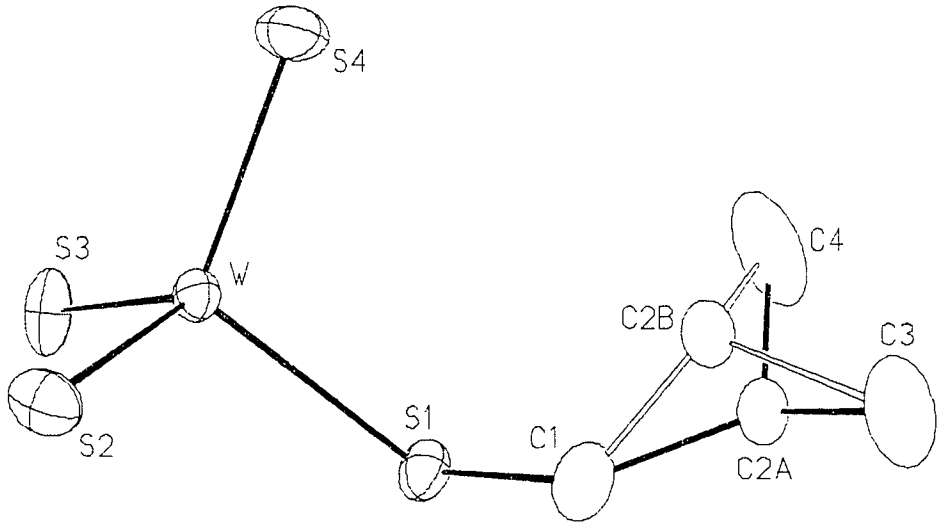

Figure 3.5 ORTEP representation and labelling scheme for the anionic portion of $[PPh_4][WS_3(S^iBu)]$ (**8**), illustrating disorder at C2 (hydrogen atoms omitted for clarity).

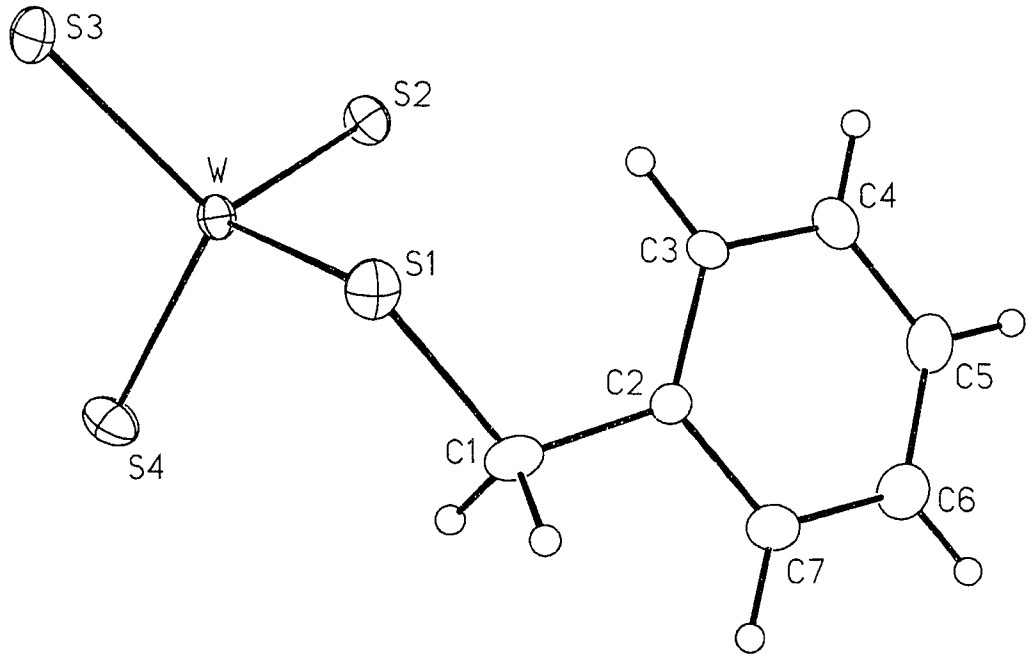

Figure 3.6 ORTEP representation and labelling scheme for the anionic portion of $[PPh_4][WS_3(SBz)]$ (**9**).

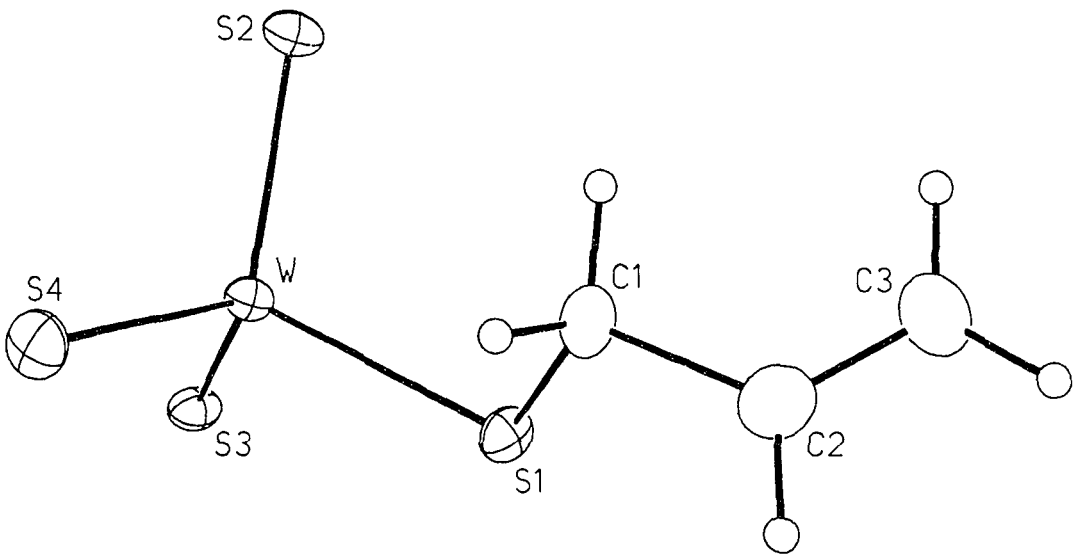

Figure 3.7 ORTEP representation and labelling scheme for the anionic portion of $[PPh_4][WS_3(SC_3H_5)]$ (**10**).

The structures consist of $[PPh_4]^+$ cations and $[WS_3(SR)]^-$ (R = ^{i}Bu, Bz, C_3H_5) anions. The absence of any solvate molecules is observed in structures where R = ^{i}Pr and ^{t}Bu,[58] and in contrast to the R = Et structure,[133] which contains a molecule of THF in the unit cell. The ^{i}Bu structure (**8**) exhibits disorder of the tertiary carbon (C2) and has been modelled satisfactorily using occupancy factors of 0.5 for each of the two sites. In all cases, the geometry at the metal centre is approximately tetrahedral (see Table 3.2) and the bond lengths and angles fall in the ranges of related structures. The $[PPh_4]^+$ cations are unremarkable, and show no close contacts with the anions.

Table 3.2 Selected bond lengths (Å) and bond angles (°) for $[PPh_4][WS_3(SR)]$ (R = ^{i}Bu (**8**), Bz (**9**), allyl (**10**)).

	8	**9**	**10**
W-S(1)	2.3231(10)	2.3376(18)	2.3295(18)
W-S(2)	2.1499(11)	2.1475(18)	2.1583(16)
W-S(3)	2.1476(13)	2.1523(17)	2.1530(17)
W-S(4)	2.1471(13)	2.1532(19)	2.1538(18)
S(1)-C(1)	1.825(5)	1.819(7)	1.850(7)
S(1)-W-S(2)	109.87(5)	109.58(7)	109.59(7)
S(1)-W-S(3)	102.80(5)	102.89(7)	104.43(7)
S(1)-W-S(4)	109.33(5)	109.88(8)	109.39(7)
S(2)-W-S(3)	111.06(5)	110.74(7)	110.57(7)
S(2)-W-S(4)	110.03(5)	110.63(7)	110.65(8)
S(3)-W-S(4)	113.50(7)	112.84(7)	112.02(8)
W-S(1)-C(1)	104.85(18)	106.3(3)	103.9(2)

The average W-$S_{terminal}$ bond distances for **8-10** range from 2.148-2.155 Å and all other species of the formula $[PPh_4][WS_3(SR)]$, except R = ^{t}Bu, show distances within this range. These also compare favourably with the analogous $Cp^*MS_2(SR)$ (M = Mo, W; R = ^{t}Bu, Bz)[11,12] species which range from 2.136-2.149 Å (Table 3.3).

Table 3.3 Average and representative bond distances (Å) for **8-10** and related compounds.

Compound	$M\text{-}S_{terminal}$	$M\text{-}S_{thiolate}$	S-C	Ref.
$[PPh_4][WS_3(SEt)]$	2.153 (avg.)	2.323(3)	1.86(1)	133
$[PPh_4][WS_3(S^iBu)]$ (**8**)	2.148 (avg.)	2.3231(10)	1.825(5)	This work
$[PPh_4][WS_3(S^iPr)]$	2.155 (avg.)	2.326(3)	1.833(9)	58
$[PPh_4][WS_3(S^tBu)]$	2.146 (avg.)	2.354(4)	1.86(2)	"
$[PPh_4][MoS_3(S^tBu)]$	2.148 (avg.)	2.341(2)	1.882(8)	"
$[PPh_4][WS_3(SBz)]$ (**9**)	2.151 (avg.)	2.3376(18)	1.819(7)	This work
$[PPh_4][WS_3(SC_3H_5)]$ (**10**)	2.155 (avg.)	2.3295(18)	1.850(7)	This work
$[PPh_4][WS_3(SH)]$[a]	2.171(2)	2.171(2)		137
$[PPh_4]_2[WS_4]$	2.195 (avg.)			138
$[PPh_4]_2[MoS_4]$	2.180 (avg.)			"
$Cp^*WS_2(S^tBu)$	2.147(2)	2.345(2)	1.850(9)	82
$Cp^*WS_2(SBz)$	2.149 (avg.)	2.328(4)	1.861(1)	"
$Cp^*MoS_2(S^tBu)$	2.136(1)	2.354(1)	1.874(5)	83
$Cp^*Mo(S^tBu)_3$		2.296 (avg.)	1.871 (avg.)	"
$[PPh_4][Cp^*WS_3]$	2.192 (avg.)			"
$[PPh_4][Cp^*MoS_3]$	2.188 (avg.)			"
$W(S^tBu)_4$		2.236(4)	1.871(18)	139
$Mo(S^tBu)_4$		2.235(3)	1.84(2)	140

[a] Thiol proton is disordered over four crystallographically equivalent sites.

It is noted that $[MS_3(SR)]^-$ exhibits terminal Mo-S and W-S distances that are almost identical, in contrast to the Cp* analogs which exhibit shorter terminal Mo-S distances than W-S, as also observed in the compounds $[PPh_4]_2[MS_4]$,[138] and $[PPh_4][Cp^*MS_3]$ (M = Mo, W).[83] In the case of $[MS_3(SH)]^-$, a M-S bond distance of 2.171(2) is observed,[137] however this apparent lengthening is due to disorder of the thiol proton over the four S sites, giving an average distance of three $M\text{-}S_{terminal}$ and one M-S(H).

It is apparent that as the number of terminal sulfides increases on a single metal centre, the amount of π-donation that each can provide is reduced, thus lengthening the

$M\text{-}S_{terminal}$ bond distances. In reverse, structural data for Cp* polythiolate compounds show that as the number of thiolate ligands increases, the $M\text{-}S_{thiolate}$ bond distance becomes shorter. It appears that the lack of competing π-donation from terminal sulfides allows more donation from the thiolate, thus shortening the $M\text{-}S_{thiolate}$ bonds. In the M(IV) compounds $M(S^tBu)_4$ (M = Mo, W), the π-donation is less pronounced due to the partially filled d-orbitals on the metal.[139,140]

The slight variations in $M\text{-}S_{thiolate}$ bond distances in $[MS_3(SR)]^-$ (M = Mo, W; R = Et, ^{i}Bu, ^{i}Pr, ^{t}Bu, Bz, C_3H_5) are likely due to the nature of the alkyl group present. The effect appears to be predominantly steric, with the bulky ^{t}Bu structures exhibiting the longest $M\text{-}S_{thiolate}$ bonds and no apparent lengthening due to the presence of electron withdrawing Bz or allyl groups. The steric bulk of the alkyl groups is also reflected in the M-S-C bond angles, where the largest value is observed for ^{t}Bu (111.8(5)° and 111.8(2)° for W and Mo, respectively) and the smallest for allyl (103.9(2)°).

The S-C bond distances compare favourably with other related structures containing one or more thiolate ligands. The S-M-S angles vary by *ca.* 11° in each structure, with the smaller angles at S(1) reflecting the presence of the thiolate ligand.

3.2.5 Reactions with Vinyl and Phenyl Halides

Attempts were made to react vinyl and phenyl bromides with $[WS_4]^{2-}$ under similar reaction conditions to those used for isobutyl bromide, but no reaction was observed (Scheme 3.8). A coordinated vinyl or phenyl thiolate is highly desirable since it would show a closer resemblance to the thiolene coordination of metal bound molybdopterin than ligands such as allyl thiolate.

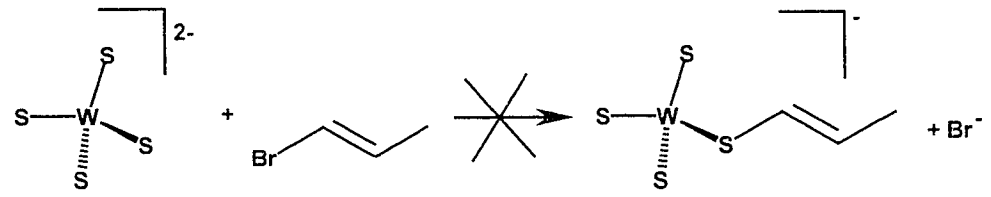

Scheme 3.4 Attempted reaction for $[PPh_4]_2[WS_4]$ and *trans*-1-bromo-propene bromide.

In light of our alkylation reactions proceeding by nucleophilic substitution, it is actually not surprising that vinyl and phenyl halides do not react. S_N2 reactions require that the α-carbon be accessible to the incoming nucleophile, but in the case of an unsaturated α-carbon, the π-electron density around the double bond repels the nucleophile. S_N1 reactions require that the carbocation generated by loss of the halide be sufficiently stable, but in the case of vinyl or phenyl halides this would result in the positive charge residing on an unsaturated carbon, which is highly unfavourable.

3.3 Attempts to Alkylate $[WS_4]^{2-}$ with 1-Adamantyl Halides ($C_{10}H_{15}X$)

3.3.1 X = Br, I, OTs

1-Adamantyl halides were chosen for the above reactions in the hope that they might impart better stability to the alkylated product as observed with another tertiary alkyl group, ^{t}Bu. Using the same conditions as reactions of ^{t}BuBr (two-fold excess of ^{t}BuBr in CH_3CN at RT for 8 hours), reactions were attempted first with 1-adamantyl bromide and then 1-adamantyl iodide, but no sign of 1-adamantyl sulfides was present in the THF extract to suggest C-S bond formation (Scheme 3.5).

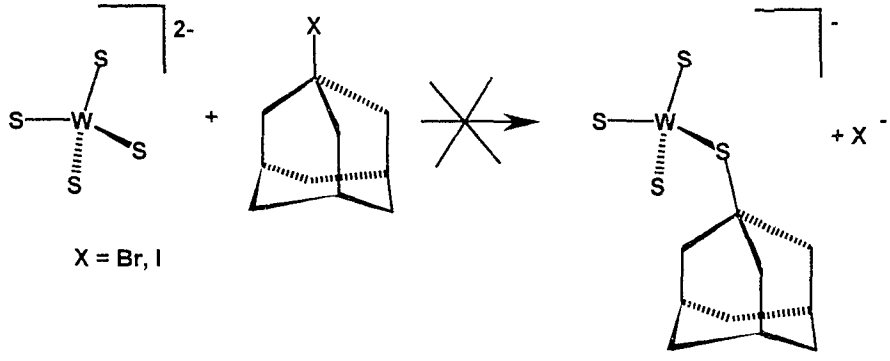

Scheme 3.5 Attempted reaction for $[PPh_4]_2[WS_4]$ and 1-adamantyl halides.

It was believed that, by improving the leaving group on the alkylating agent, the reaction might be more favourable, so 1-adamantyl tosylate was synthesized and used in place of the 1-adamantyl halide. The reaction appeared to proceed with the expected colour change from yellow to orange to red, but after pumping to dryness and extraction with THF, it only produced a pale orange solution. The residue after extraction with THF was identified as a mixture of unreacted $[PPh_4]_2[WS_4]$ and $[PPh_4]_2[W_3S_9]$ based on solubility and IR data. On analysis by ^1H NMR, the orange THF extract was found to contain small amounts of $[PPh_4]_2[WS_4]$ and $[PPh_4]_2[W_3S_9]$, unreacted 1-adamantyl tosylate, and various other species believed to be sulfides. No alkylated product was observed.

The activation energy barrier for an S_N1 reaction when R = 1-adamantyl is likely much higher than when R = ^{t}Bu, due to the contraint imposed on the α-carbon and subsequent restriction of planarity required for carbocation intermediate. However, formation of $[PPh_4]_2[W_3S_9]$ from $[PPh_4]_2[WS_4]$ in the presence of 1-adamantyl tosylate

suggests that a reaction is occurring between the two reagents and that under appropriate conditions an intermediate might be isolated.

3.3.2 Silver Assisted Halide Abstraction

It was surmised that if dissociation of the leaving group could be made more facile, then formation of an adamantylated $[WS_4]^{2-}$ might be more favourable, provided the intermediate carbocation could be stabilized. Friedel-Crafts reactions utilize an alkyl halide in the presence of a Lewis acid to generate a stabilized carbocation (Scheme 3.6),[141] and Olah *et al.* have reported the formation of a stabilized ^{t}Bu cation from the respective iodide using a silver salt (Equations 3.1 and 3.2).[142]

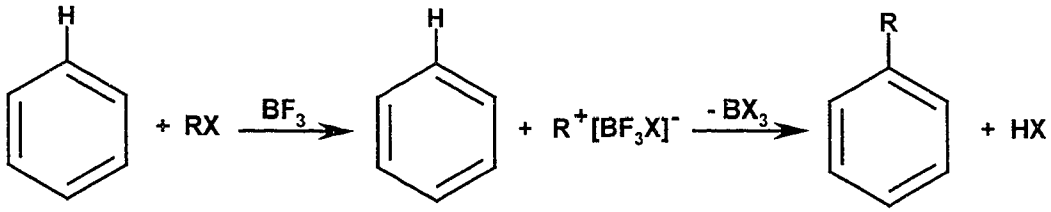

Scheme 3.6 Generation of a stabilized carbocation in a Friedel Crafts reaction.[141]

$$^t\text{BuI} + \text{AgF} \longrightarrow \text{AgI(s)} + {}^t\text{BuF} \qquad \textbf{Equation 3.1}$$

$$^t\text{BuF} + \text{BF}_3 \longrightarrow {}^t\text{BuF} \cdot \text{BF}_3 \rightleftharpoons {}^t\text{Bu}^+ \text{BF}_4^- \qquad \textbf{Equation 3.2}$$

We subsequently developed a similar approach to stabilizing a 1-adamantyl carbocation using silver assisted halide abstraction by $AgBF_4$ (Scheme 3.7).

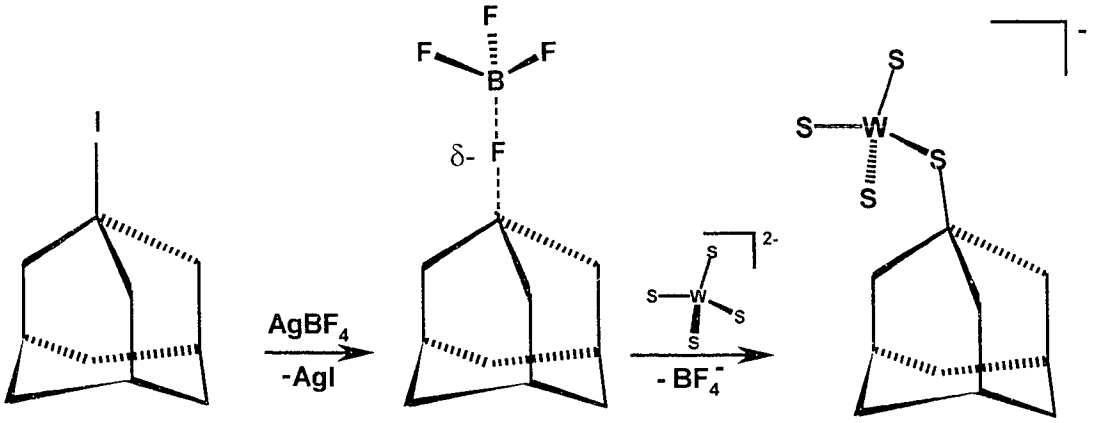

Scheme 3.7 Possible synthetic route to $[PPh_4][WS_3(SC_{10}H_{15})]$ using $AgBF_4$.

On an NMR scale, 1-adamantyl iodide was dissolved in $CDCl_3$ and mixed with $AgBF_4$ in a 3:1 ratio in $CDCl_3$. Immediately a yellow precipitate of AgI formed, which was filtered to leave "$[C_{10}H_{15}][BF_4]$" in solution. It was critical to use an excess of 1-adamantyl iodide in preparing the "$[C_{10}H_{15}][BF_4]$" solution to ensure that no unreacted Ag^+ remain in solution, which rapidly forms an insoluble complex with $[WS_4]^{2-}$. An upfield change in chemical shift was observed for the adamantyl on abstraction of the halide, and was most predominant for the β-protons. (Figure 3.8(a)).

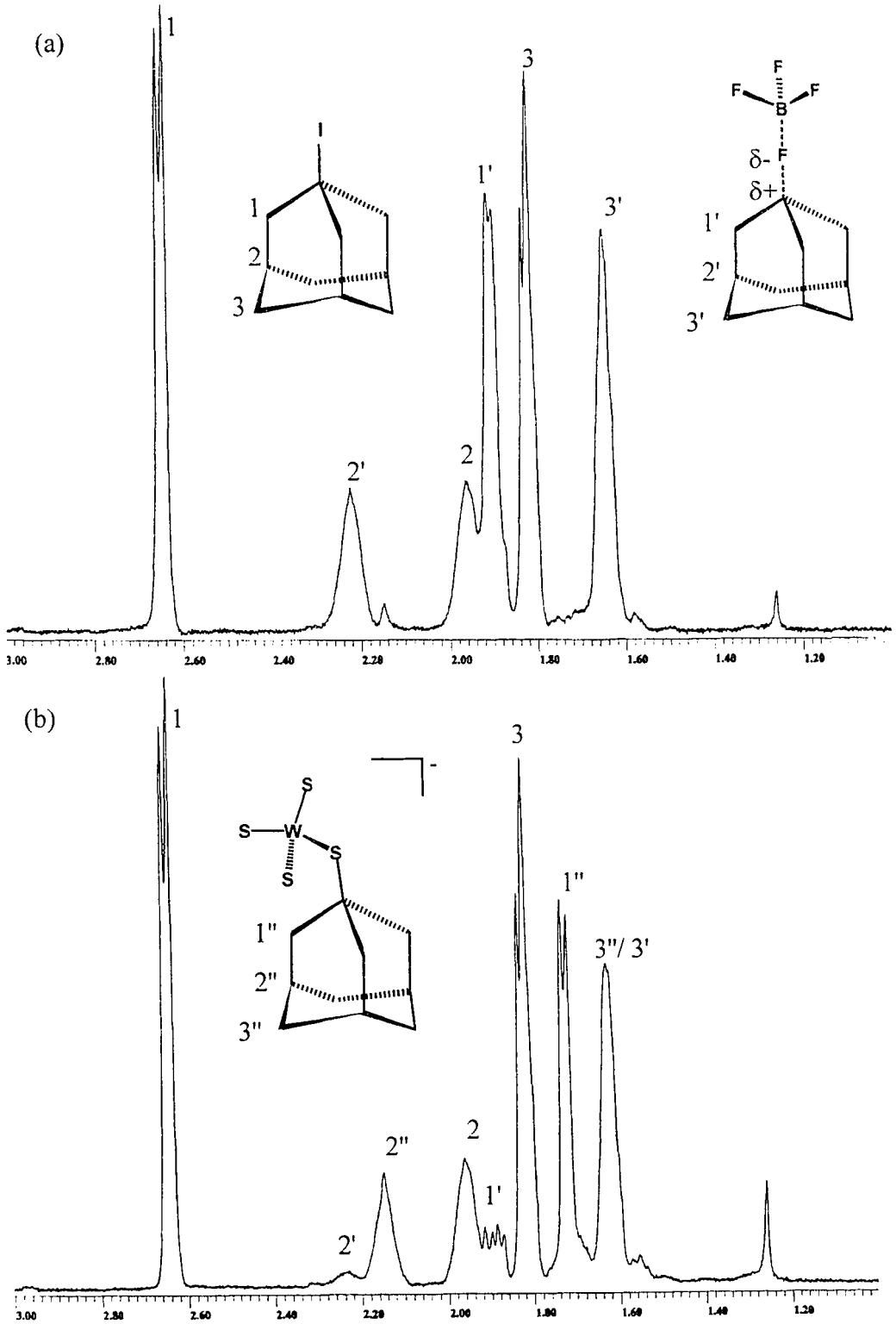

Figure 3.8 ^{1}H NMR spectra of (a) "$[C_{10}H_{15}][BF_4]$" with a slight excess of 1-adamantyl iodide, and (b) $[WS_3(SC_{10}H_{15})]^-$ *in situ*.

The six equivalent methylene protons closest to the iodide (signal 1) are significantly more deshielded at 2.65ppm than the three protons on the adjacent tertiary carbon, at 1.96ppm. The other six equivalent methylene protons (signal 3) are observed to be slightly more upfield at 1.82ppm. On reaction with $AgBF_4$, new methylene signals appear upfield at 1.91ppm (signal 1', 6H) and 1.65ppm (signal 3', 6H). Curiously, the new proton signal for the tertiary carbon appears *downfield* at 2.23 ppm (signal 2', 3H). On addition of this sample to $[PPh_4]_2[WS_4]$ in $CDCl_3$, a red solution was immediately formed and shown to contain a new set of resonances that can be assigned to an alkylated product (Figure 3.8b). New signals appear at 1.82ppm (1", 6H), 2.15ppm (2", 3H) and 1.63ppm (3", 6H). The latter signal overlaps with a small amount of unreacted "$[C_{10}H_{15}][BF_4]$" and consequently integration for signal 3" was measured by subtracting the area due to "$[C_{10}H_{15}][BF_4]$" based on its other adamantyl signals.

On scaling up the reaction in the hope of isolating an adamantylated species, the red solution was pumped to dryness and washed with Et_2O to remove excess 1-adamantyl iodide. The THF extract was red but the ^1H NMR showed no signs of an adamantylated species. The only crystals that could be isolated from the THF extract were of $[PPh_4]_2[W_3S_9]$.

Although it appears that we have synthesized $[WS_3(SC_{10}H_{15})]^-$ *in situ*, it has not been possible to isolate the $[PPh_4]^+$ salt under these or similar conditions.

3.4 Alkylation of Oxothiotungstates

A natural progression from alkylation reactions of $[WS_4]^{2-}$ is to vary the type of chalcogenide ligands at the metal centre. Mixed oxothiometallates are of particular

interest since active sites in tungsten and molybdenum enzymes sometimes contain terminal oxide and sulfide ligands at the same centre, often in combination with a thiolate ligand. Alkylation reactions at a mixed oxothiometallate could either occur at the sulfide or oxide ligands. Based on the ability of the oxygen to π-bond with the metal more effectively than sulfur, more of the negative charge will reside on the sulfur.[143] That is, the sulfur is more nucleophilic than oxygen and will more readily react with an alkyl halide by a nucleophilic substitution mechanism.

Since the tetrathiotungstate system has been investigated in much detail, we predicted that reactions of the closely related oxothiotungstates would be relatively straightforward to follow and decomposition products readily identified. Once again, ^{1}H NMR was employed to follow the alkylation reactions with some interesting results.

3.4.1 Reactions of $[PPh_4]_2[WO_2S_2]$ and $[PPh_4]_2[WOS_3]$ with EtBr

Investigations commenced using ethyl bromide and $[PPh_4]_2[WO_2S_2]$, and time dependent ^{1}H NMR spectra immediately showed many similarities with the analogous $[WS_4]^{2-}$ reactions with respect to the species formed in solution.[118] Subsequent experimental scale reactions using rigorously dried solvent to prevent formation of ethyl thiol were performed but showed signs of decomposition during work-up, yielding insoluble tungsten sulfides and $[PPh_4]_2[W_3S_9]$. GC-MS confirmed the presence of organic sulfides in the Et_2O extract and ^{1}H NMR showed an absence of alkylated product in the THF extract.

Reactions of ethyl bromide and $[PPh_4]_2[WOS_3]$ again showed similar time dependent ^{1}H NMR spectra, and apparent formation of $[WS_3(SEt)]^-$ (*ca.* 3.18, 1.29ppm)

could clearly be observed (Figure 3.9), though in smaller yields than in the analogous $[WS_4]^{2-}$ reactions. In addition, larger volumes of ethyl sulfides were observed in the $[WOS_3]^{2-}$ reactions compared to $[WS_4]^{2-}$. This indicates that while alkylation at sulfur is certainly occurring, decomposition is very rapid via W-S bond cleavage. In Figure 3.9, the reaction mixture was spiked with a small amount of Et_2O to observe whether the signal increased in intensity due to some alkylation and subsequent decomposition at the oxide in $[WOS_3]^{2-}$. Since the Et_2O signal remained constant in intensity throughout the experiment, our belief that alkylation would occur at the sulfur atom preferentially was confirmed.

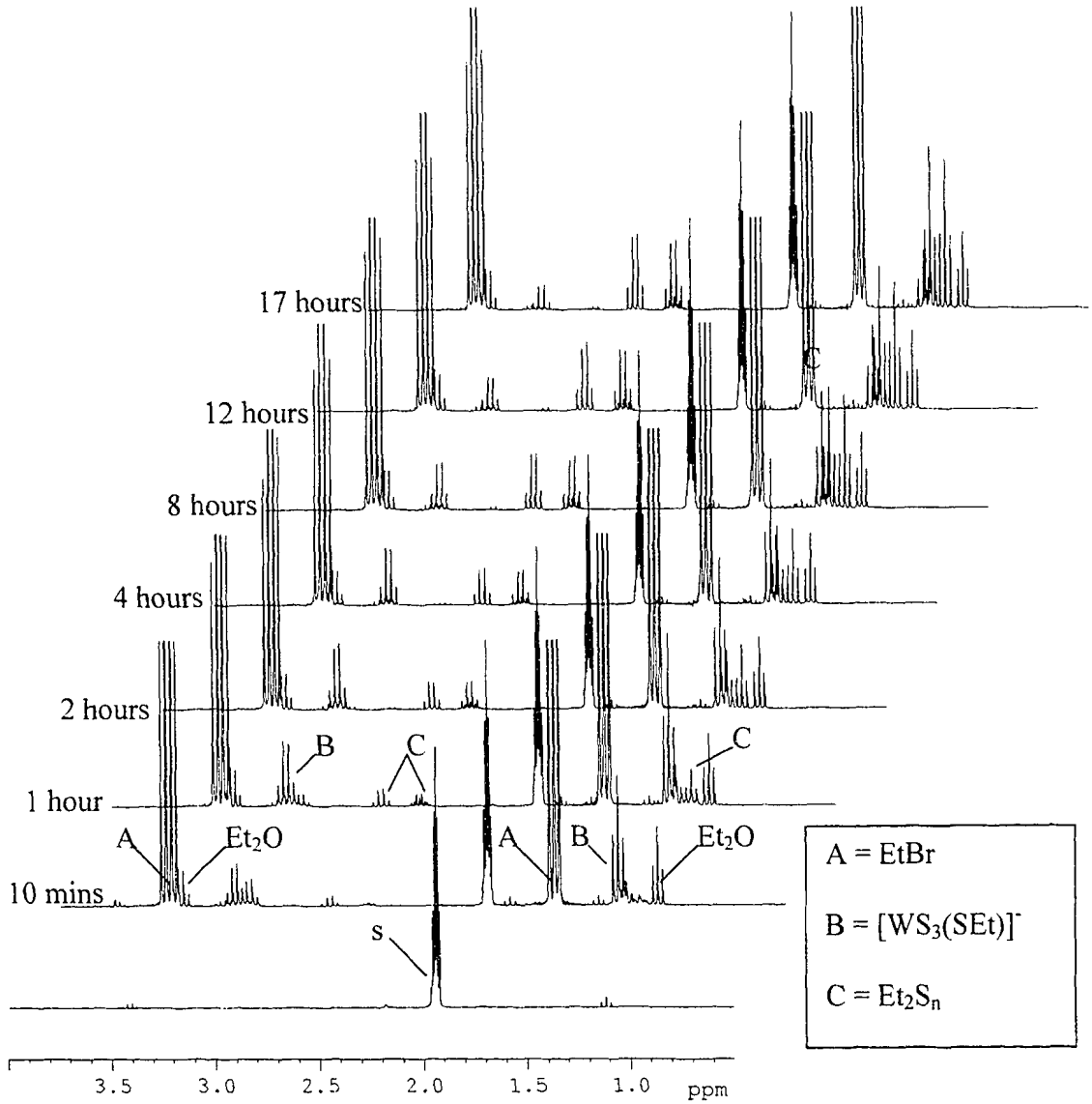

Figure 3.9 Time dependent ^{1}H NMR spectra of $[PPh_4]_2[WOS_3]$ and EtBr (1:5) in CD_3CN at 0°C.

On a synthetic scale it was possible to isolate red crystals from the THF extract of the reaction of $[PPh_4]_2[WOS_3]$ and EtBr. ^{1}H NMR of these crystals showed that the chemical shift corresponded exactly with that of $[PPh_4][WS_3(SEt)]$ (Figure 3.10), and IR data showed the absence of a W-O bond, suggesting that the crystals were not of

$[PPh_4][WOS_2(SEt)]$. Unfortunately, we were unable to confirm this by X-ray crystallography due to the poor quality of the crystals.

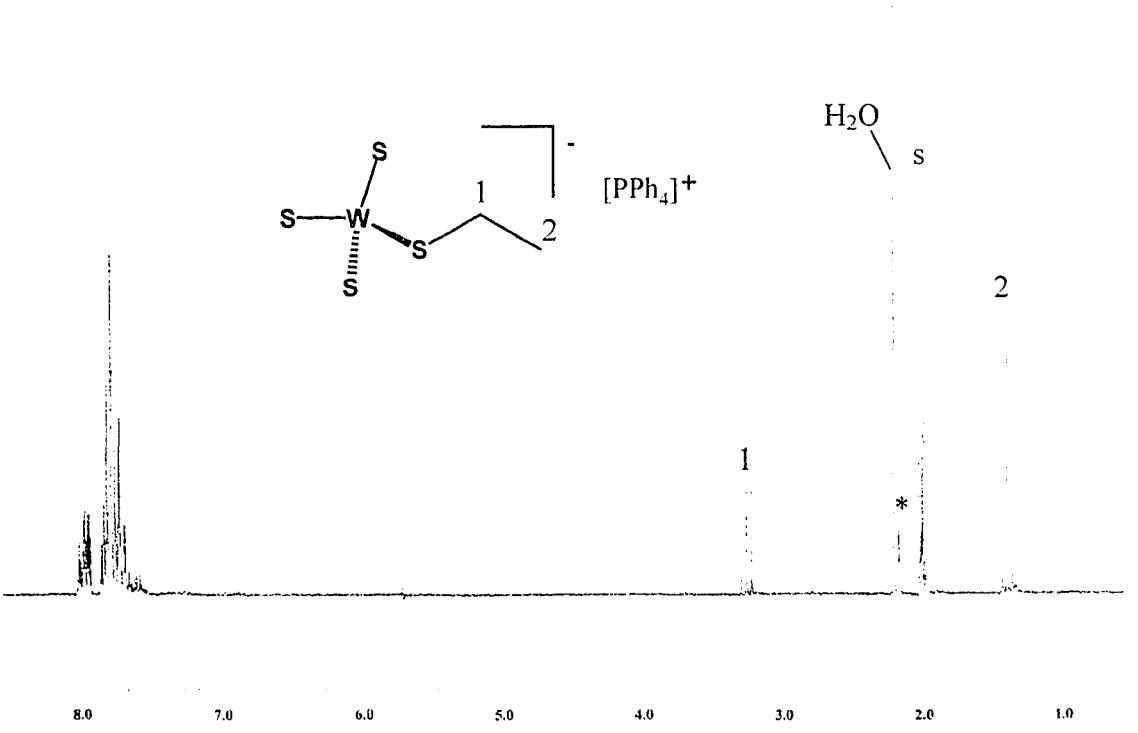

Figure 3.10 ^{1}H NMR spectrum of red crystals obtained from the reaction of $[PPh_4]_2[WOS_3]$ and EtBr (1:5) in CD_3CN.

3.4.2 Reactions of $[PPh_4]_2[WO_2S_2]$ and $[PPh_4]_2[WOS_3]$ with ^{t}BuBr

Time dependent ^{1}H NMR studies of the reaction of $[PPh_4]_2[WO_2S_2]$ or $[PPh_4]_2[WOS_3]$ with ^{t}BuBr show the appearance of a signal at 1.67ppm consistent with isobutene formation, where the methyl proton signal expected at *ca.* 1.8ppm is obscured by excess ^{t}BuBr (Figure 3.11). In addition, GC-MS of the reaction vessel headspace gas on an experimental scale shows a M^+ peak at 56, suggesting the presence of isobutene.

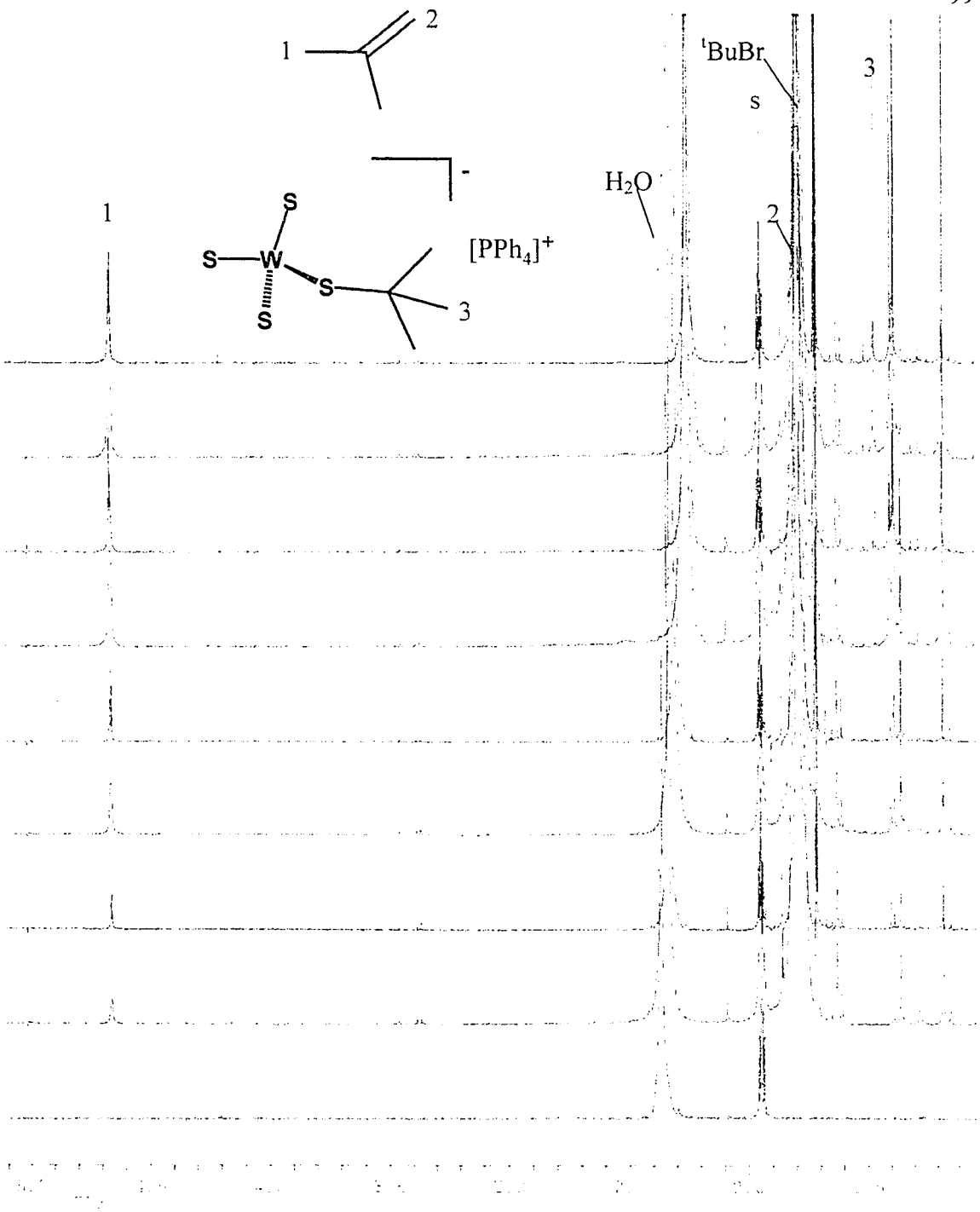

Figure 3.11 ^{1}H NMR spectra of the reaction of $[PPh_4]_2[WO_2S_2]$ and ^{t}BuBr (1:10), showing formation of isobutene.

Such a product could only be formed by C-S bond cleavage, in contrast to the $[WS_4]^{2-}$ system where observed decomposition products are consistent only with a W-S bond cleavage pathway. As with ethyl bromide, the THF extract from an experimental scale reaction suggests formation of an alkylated $[WS_4]^{2-}$, in this case $[WS_3(S^tBu)]^-$ at 1.49ppm in CD_3CN. A possible mechanism for isobutene formation involves elimination of a β-hydrogen to an adjacent terminal chalcogenide ligand (Scheme 3.8).

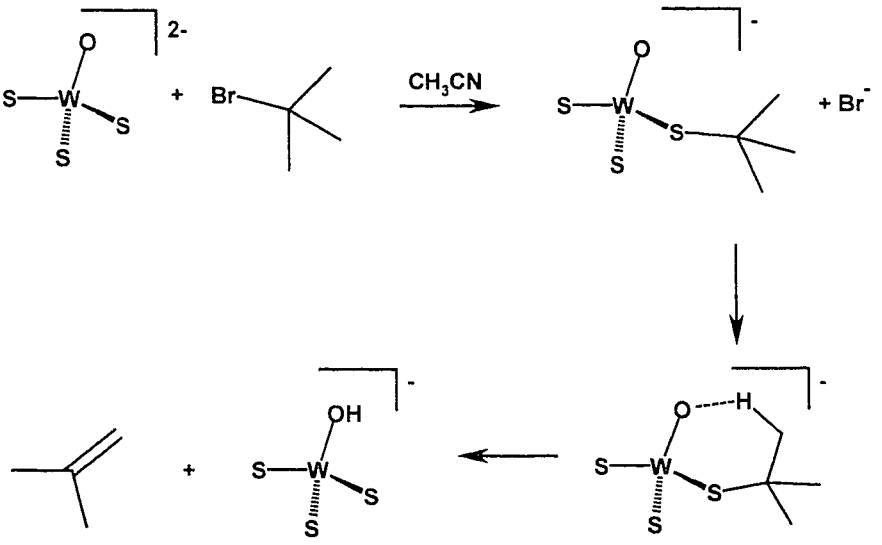

Scheme 3.8 Possible mechanism for formation of isobutene from $[PPh_4]_2[WOS_3]$ and ^tBuBr.

Since this process is only observed in the presence of a terminal oxide ligand, we hypothesize that protonation of the oxide occurs in preference to sulfide. Formation of a protonated oxothiometallate is not unreasonable since a protonated tetrathiotungstate has previously been characterized.[137] In addition, such a species is implicated in O/S ligand

exchange[104] and might explain the formation of $[WS_4]^{2-}$ and its subsequent alkylation in our experiments.

3.4.3 Reactions of $[PPh_4]_2[WO_2S_2]$ and $[PPh_4]_2[WOS_3]$ with BzCl

To avoid a decomposition pathway by β-hydrogen elimination, we chose to next examine reactions of benzyl chloride, which has the advantage of exhibiting distinctive signals in the ^1H NMR spectrum for each species formed in solution. In time dependent ^1H NMR studies of $[PPh_4]_2[WO_2S_2]$ or $[PPh_4]_2[WOS_3]$ and benzyl chloride, the appearance of a small singlet at 4.36ppm suggests formation of $[PPh_4][WS_3(SBz)]$ (Figure 3.12). In addition, the same decomposition products observed compared to the analogous $[WS_4]^{2-}$ reaction. While there is certainly an absence of a decomposition pathway by β-hydrogen elimination, we are still apparently observing formation of a $[WS_4]^{2-}$ benzylated product.

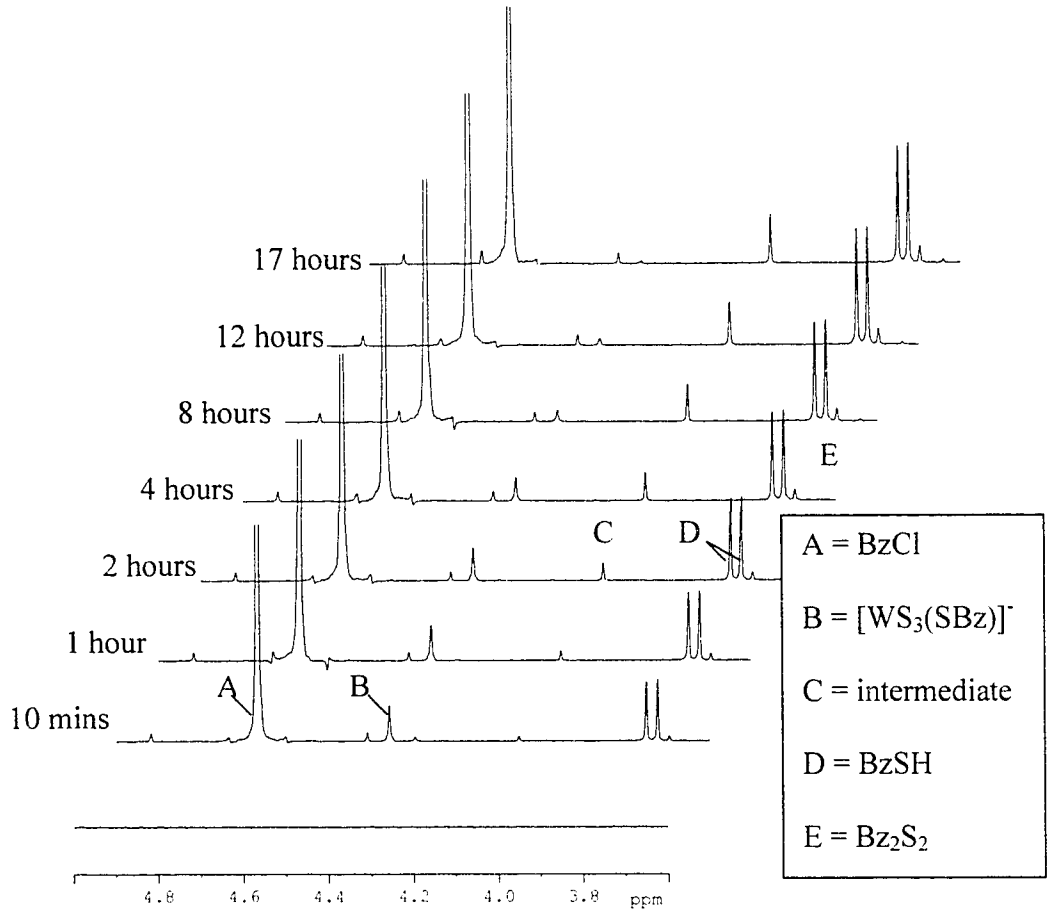

Figure 3.12 ^{1}H NMR spectra of the reaction of $[PPh_4]_2[WOS_3]$ and benzyl bromide (1:10) in CD_3CN at room temperature.

We have confirmed this finding by successfully characterizing a crystal of $[PPh_4][WS_3(SBz)]$, isolated from the ^{1}H NMR scale reaction of a single crystal of $[PPh_4]_2[WOS_3]$ and benzyl chloride, by X-ray crystallography. Our previous investigations into the purity of crystalline oxothiometallates, discussed in Chapter 2, suggest that a single crystal of oxothiometallate contains only one type of molecule, and we are certain that observation of alkylated $[WS_4]^{2-}$ arises from alkylation induced O/S

redistribution, rather than by an impurity of $[WS_4]^{2-}$ being present in the crystal lattice. A naïve explanation might suggest that the presence of small amounts of water in the NMR solvent could cause protonation at the oxide ligand and subsequent replacement by a sulfide ligand from another anion. This would favour a mechanism where alkylation does not even occur until after O/S redistribution has occurred. We are certain that this is not the case since no O/S redistribution is observed for an identical sample in the absence of alkyl halide, even over a period of several days.

3.5 Summary

We have demonstrated that alkylation of $[WS_4]^{2-}$ using alkyl halides results in the formation of transient $[MS_3(SR)]^-$ (R = ^{i}Bu, benzyl, allyl) which can be isolated as a $[PPh_4]^+$ salt under controlled conditions. These conditions have been identified by time dependent ^{1}H NMR studies, which have also provided insight into the stability and decomposition pathways to polythiometallates, organic sulfides and thiols. Vinyl, phenyl and adamantyl halides have shown no reactivity towards $[PPh_4]_2[WS_4]$, which is consistent with a nucleophilic substitution mechanism. However, we believe we have successfully formed adamantylated $[WS_4]^{2-}$ *in situ* by the use of $AgBF_4$ for halide abstraction and stabilization of the carbocation intermediate.

Attempts to alkylate $[WO_xS_{4-x}]^{2-}$ have shown formation of C-S bonds but have not resulted in isolation of $[PPh_4][WO_xS_{3-x}(SR)]$. Instead it appears that O/S ligand substitution is initiated by alkylation as we have isolated $[PPh_4][WS_3(SBz)]$ from the reaction of pure $[PPh_4]_2[WOS_3]$ and BzCl. Furthermore, in contrast to $[WS_4]^{2-}$, reactions of ^{t}BuBr result in some C-S instead of W-S bond cleavage occurring and the elimination

of an unsaturated organic fragment. Clearly, oxothiometallates react by a more complex route than the better understood tetrathiometallates.

3.6 Experimental

General Procedures

All manipulations were performed under an atmosphere of dry dinitrogen or argon, using standard Schlenk and glovebox techniques. All solvents were distilled over appropriate drying agents[144] onto molecular sieves, and degassed with dinitrogen prior to use. All liquid alkyl halides were purchased from Aldrich and stored over molecular sieves under dinitrogen. These were degassed by freeze-pump-thaw techniques prior to use. Thiometallates $[PPh_4]_2[MO_xS_{4-x}]$ (where M = Mo, W and x = 0-2) were prepared as described in Chapter 2 and stored under dinitrogen. Dimethylaminopyridine was provided by Christophe Taeschler. 1-Adamantanol and tosyl chloride were purchased from Aldrich and used without further purification. NEt_3 was dried over molecular sieves and degassed prior to use.

Physical Measurements

Elemental analyses were performed by the University of Calgary, Department of Chemistry, Analytical Services Laboratory. GC-MS data were recorded using a system consisting of a Packard Bell HP Chromatograph equipped with a 5790 mass detector. ^1H and ^{13}C NMR spectra were recorded using Bruker ACT-200 or DRX-400 spectrometers.

Time dependent ^1H-NMR studies were performed on either a Bruker AMX-300 or DRX-400 spectrometer. A typical experiment used 5mg of $[PPh_4]_2[WO_xS_{4-x}]$ (x = 0-2)

dissolved in *ca.* 0.7ml CD_3CN under dinitrogen in a 5mm tube fitted with a rubber septum. An appropriate amount of alkylating agent was injected through the septum, (while the sample was in an ice bath in some cases) and the sample returned to the probe to start data acquisition at predetermined intervals.

^{183}W NMR spectra were collected by Dr. Deane McIntyre in the Department of Biological Sciences using an identical protocol to that described in Chapter 2. THF extract containing the appropriate alkylated species was used directly to prepare samples in cylindrical Pyrex tubes, with an outside diameter of 17mm and a length of about 4cm.

Syntheses of $[PPh_4][WS_3(S^iBu)]$ (8), $[PPh_4][WS_3(SBz)]$ (9) and $[PPh_4][WS_3(SC_3H_5)]$ (10)

$[PPh_4]_2[WS_4]$ (0.128g, 0.129mmol) was placed in a Schlenk tube and dissolved in *ca.* 20ml of CH_3CN. A 10-fold excess of ^iBuBr (141µl, 1.29mmol) was added by syringe and the mixture allowed to stir at room temperature. After six hours, the yellow solution had turned orange, and the solvent and excess ^iBuBr were removed *in vacuo*. In addition, volatile by-products of the formula $^iBu_2S_n$ (where n = 1-3) were removed by pumping. THF (2 × 20ml) was used to extract the red residue to yield a red solution of **8**, leaving $[PPh_4]_2[W_3S_9]$ and unreacted $[PPh_4]_2[WS_4]$ behind. The THF solution was filtered then concentrated to about half its original volume, placed in crystallization tubes and layered with diethyl ether under dinitrogen. After 3 days, bright red crystals of crystallographic quality were obtained in a 63% yield. Anal. Calcd. for $C_{28}H_{29}PS_4W$: C, 47.46; H, 4.12. Found C, 47.47; H, 4.04. ^1H NMR (200MHz, CD_2Cl_2): δ 7.99-7.57 (m, 20H, PPh_4^+), 3.12 (d, 2H), 1.95 (m, 1H), 0.95 (d, 6H). ^{183}W NMR (400MHz, THF): δ 3708ppm.

9 was synthesized by a procedure similar to **8**, except benzyl chloride (148μl, 1.29mmol), instead of ^{i}BuBr, was added at 0°C and the mixture allowed to warm to room temperature. The solvent and volatiles were removed *in vacuo* after stirring for two hours (Note: the mixture was only pumped until a sticky residue remained as pumping to complete dryness resulted in partial decomposition of **9**) and the residue was extracted with THF (2 × 20ml) to give a red solution. After filtration, the solution was layered with Et_2O and maintained at –20°C for 3 days. Bright red crystals of **9** were obtained in a 73% yield. Anal. Calcd. for $C_{31}H_{27}PS_4W$: C, 50.14; H, 3.66. Found C, 49.93; H, 3.55. ^{1}H NMR (200MHz, CD_3CN): δ 7.97-7.60 (m, 20H, P*Ph*$_4^+$), 7.39-7.20 (m, 5H), 4.36 (s, 2H). ^{183}W NMR (400MHz, THF): δ 3712ppm.

10 was synthesized by a procedure similar to **8** except allyl bromide (22μl, 0.26mmol), instead of ^{i}BuBr, was added at 0°C and the mixture allowed to warm to room temperature. The solvent and volatiles were removed *in vacuo* after stirring for two hours and the residue was extracted with THF (2 × 20ml) to give a red solution. After filtration, the solution was layered with Et_2O and maintained at –20°C for 4 days. Bright red crystals of **10** were obtained in a 67% yield. Anal. Calcd. for $C_{27}H_{25}PS_4W$: C, 46.83; H, 3.64. Found C, 46.67; H, 3.57. ^{1}H NMR (400MHz, CD_3CN, -40°C): δ 7.95-7.62 (m, 20H, P*Ph*$_4^+$), 5.87 (m, 1H), 5.10 (d of m, 1H, *cis* to CH_2), 5.00 (d of m, 1H, *trans* to CH_2), 3.70 (d of m, 2H, C*H*$_2$).

Crystal Structure Determinations for 8, 9 and 10

X-ray crystallography was performed by Dr. Robert McDonald at University of Alberta, Department of Chemistry. Crystals of **8**, **9** and **10** were coated in Paratone-8277

oil and then mounted on a glass fiber. Data were collected using a Bruker P4/RA diffractometer with a SMART 1000 CCD detector, using monochromated Mo Kα radiation at –80°C. Programs for diffractometer operation, data collection, data reduction and absorption correction were those supplied by Bruker. Data were integrated to a maximum 2θ value of 51.40° for **8** and **9**, and 51.60° for **10**. The data were corrected for absorption through use of Gaussian integration for **8** and **10**, and through use of the *SADABS* procedure for **9**. The structure of **9** was solved using the program *SHELXS-86*,[145] while the solutions for **8** and **10** were obtained though use of the *DIRDIF-96* program system.[146] The structure refinements were completed by subsequent Fourier syntheses and refined using full-matrix least-squares methods.[147] All non-hydrogen atoms were refined anisotropically and all hydrogen atoms were placed in idealized positions. In the structure of **8**, the isobutyl group exhibited disorder at the tertiary carbon. The alternate positions of this atom were refined satisfactorily with occupancy factors of 0.5.

Attempted Synthesis of [PPh$_4$][WS$_3$(SCHCHCH$_3$)] and [PPh$_4$][WS$_3$(SPh)]

$[PPh_4]_2[WS_4]$ (0.048g, 0.048mmol) was placed in a Schlenk tube and dissolved in *ca.* 10ml of CH_3CN and a 10-fold excess of *trans*-1-bromo-1-propene (41μl, 0.48mmol) was added by syringe. The mixture was allowed to stir at room temperature but after 8 hours, remained yellow. The solvent and volatiles were removed *in vacuo* and THF (1 × 20ml) was used to extract the residue to yield a pale yellow solution. On pumping to dryness, a small amount of fine yellow solid was isolated. ^{1}H NMR of the solid showed only resonances due to $[PPh_4]^+$, which was believed to be $[PPh_4]_2[WS_4]$.

The same reaction conditions were used for attempted alkylation with phenyl bromide (51 μl, 0.48mmol), except that Et_2O (2 × 10ml) was used to remove phenyl bromide from the reaction mixture after pumping to dryness.

Attempted Synthesis of $[PPh_4][WS_3(SC_{10}H_{15})]$ using Adamantyl Halides

$[PPh_4]_2[WS_4]$ (0.050g, 0.05mmol) was placed in a Schlenk tube and dissolved in *ca.* 10ml of CH_3CN. A 10-fold excess of 1-adamantyl bromide (0.109g, 0.50mmol) was dissolved in *ca.* 2ml CH_3CN and cannulated into the $[PPh_4]_2[WS_4]$ solution. The mixture was allowed to stir at room temperature but after 8 hours, remained yellow. The solvent was removed *in vacuo* and Et_2O (2 × 10 ml) was used to remove unreacted 1-adamantyl bromide, which was the only compound found when the washings were analyzed by GC-MS. THF (1 × 20ml) was used to extract the residue to yield a pale yellow solution. On pumping to dryness, a small amount of fine yellow solid was isolated. ^1H NMR of the solid showed only resonances due to $[PPh_4]^+$, which was believed to be $[PPh_4]_2[WS_4]$.

The same reaction conditions were used for attempted alkylation with 1-adamantyl iodide (0.132g, 0.50mmol).

Attempted Synthesis of $[PPh_4][WS_3(SC_{10}H_{15})]$ using 1-Adamantyl Tosylate

1-Adamantyl tosylate was synthesized according to a procedure described by Christophe Taeschler.[148] 1-Adamantanol (0.10g, 0.72mmol) was mixed with tosyl chloride (0.165g, 0.86mol) and dimethylaminopyridine (0.009g, 0.082mmol) in 5 ml CH_2Cl_2 under dinitrogen. NEt_3 (0.16ml, 1.15mmol) was added by syringe and the mixture stirred for 12 hours. A further 5ml CH_2Cl_2 was added and then the organic phase

was washed with 5 ml H_2O, 5 ml 1M HCL and a further 10ml (2 × 5ml) of H_2O. The organic phase was dried with Na_2SO_4 and filtered, and the solvent was removed *in vacuo*. A white solid was obtained in a yield of 68.2%. ^{1}H NMR (200MHz, $CDCl_3$): δ 7.92 (d, 2H, *Ph*), 7.42 (d, 2H, *Ph*), 2.50 (s, 3H, C*H*$_3$), 2.15 (br , 3H, C*H*), 1.72 (d, 6H, C*H*$_2$), 1.63 (br, 6H, C*H*$_2$). ^{13}C{^{1}H} (200MHz, $CDCl_3$): δ 143.4, 141.0, 130.1, 127.5 (*C*$_6$H$_4$), 44.8, 38.0, 30.9 (*C*$_{10}$H$_{15}$, quaternary carbon signal not observed), 22.1(*C*H$_3$).

$[PPh_4]_2[WS_4]$ (0.07g, 0.071mmol) was placed in a Schlenk tube and dissolved in *ca.* 10ml of CH_3CN and cooled to 0°C. 1-Adamantyl tosylate (0.02g, 0.071mmol) was dissolved in *ca.* 5ml CH_3CN at 0°C and cannulated into the $[PPh_4]_2[WS_4]$ solution. The mixture was allowed to warm to room temperature and stir. After 10 minutes the solution had turned orange and was red after 1 hour. The solvent was removed *in vacuo* leaving a dark red residue and then extracted with THF (3 × 10 ml) to give a pale orange solution. ^{1}H NMR of the dried THF extract showed the presence of unreacted 1-adamantyl tosylate and $[PPh_4]^+$, but no evidence for $[WS_3(SC_{10}H_{15})]^-$. The $[PPh_4]^+$ was likely from $[PPh_4]_2[WS_4]$ or $[PPh_4]_2[W_3S_9]$ in the extract. The red residue after extraction was identified as a mixture of $[PPh_4]_2[WS_4]$ and $[PPh_4]_2[W_3S_9]$ based on solubility and IR data.

NMR Scale In Situ Formation of [PPh$_4$][WS$_3$(SC$_{10}$H$_{15}$)]

$AgBF_4$ (0.006g, 0.03mmol) was dissolved in 0.5ml $CDCl_3$ under nitrogen. 1-adamantyl iodide ($C_{10}H_{15}I$) (0.024g, 0.09mmol) was also dissolved in 0.5ml $CDCl_3$ under nitrogen and the two solutions mixed. Immediately a yellow precipitate formed and was left to settle for 10 minutes before filtering. The filtrate, containing "$[C_{10}H_{15}][BF_4]$" and

excess $C_{10}H_{15}I$ was collected in a 5mm NMR tube and subjected to analysis by ^1H NMR. ^1H NMR (200MHz, $CDCl_3$) of "$[C_{10}H_{15}][BF_4]$": δ 2.23 (br, 3H, C*H*), 1.91 (br d, 6H, CH_2), 1.65 (br, 6H, CH_2).

$[PPh_4]_2[WS_4]$ (0.005g, 0.005mmol) was dissolved in 0.7ml $CDCl_3$ in a 5mm NMR tube. A portion of the "$[C_{10}H_{15}][BF_4]$" solution (166μl, 0.005mmol) was added and the yellow solution turned red immediately. The sample was immediately subjected to analysis by ^1H NMR and confirmed the presence of $[PPh_4][WS_3(SC_{10}H_{15})]$. ^1H NMR (200MHz, $CDCl_3$): δ 7.58-7.95 (m, 20H, P*H*$_4^+$), 2.15 (br, 3H, C*H*), 1.82 (d, 6H, CH_2), 1.63 (br, 6H, CH_2).

Reactions of $[PPh_4]_2[WO_xS_{4-x}]$ (x = 1, 2) with Alkyl Halides

$[PPh_4]_2[WO_xS_{4-x}]$ (0.05mmol) was placed in a Schlenk tube and dissolved in *ca.* 10ml of CH_3CN and cooled to 0°C. A 10-fold excess of alkyl halide (0.05mmol) was aded by syringe and the mixture allowed to warm to room temperature and stir until turning a red colour (varies from 2-8 hours depending on the alkylating agent). The solvent was removed *in vacuo* leaving a dark red residue and in some cases was subjected to an Et_2O extraction (2 × 10 ml). All residues were then extracted with THF (3 × 10 ml) to give a solution varying from pale orange to red, depending on the alkyl halide and oxothiometalate combination used. The Et_2O extract was analyzed by GC-MS and the THF extract by ^1H NMR. In some cases, red crystals were obtained by layering the concentrated THF extract with Et_2O in crystallization tubes and storing at -20°C for several days. The yield of crystals ranged from 10-20% based on $[PPh_4]_2[WO_xS_{4-x}]$.

Chapter 4 – Alkylation Reactions of $[PPh_4]_2[WS_4]$ with Alkyl Dihalides and Attempted Complexation to a Second Metal

4.1 Introduction

Based on our success with alkylation of $[PPh_4]_2[WS_4]$ using alkyl monohalides, we decided to explore the possibility of using alkyl dihalides, in an attempt to form bis-alkylated products. Our previous experience with alkylation reactions indicated that when a ten-fold excess of alkyl halide was employed, the reaction rate increased but bis-alkylation at the same metal centre did not occur. Indeed, yields of greater than 65% monoalkylated thiotungstate were isolated from these reactions. The likelihood that bridging dithiolates might form instead of bis-alkylated products seemed reasonably high, though we faced the possibility that these products could be unstable due to the close proximity of the two $[WS_4]^{2-}$ groups, facilitating formation of polythiometallates and disulfides.

Many examples of polymetallate structures have been characterized with bridging bi- or tridentate thiolate and dithiolate ligands between metals, generally isolated from alkali metal (di)thiolate salts and the corresponding metal chlorides.[62] In many of these cases, more than one bridging (di)thiolate or a close M-M interaction is required to stabilize the complex. In fact, dithiolates are frequently used in the preparation of metal cluster compounds, and the architecture of the cluster can be controlled by the chelating, versus bridging, ability of the dithiolate used.[149]

Much time has been invested in using chelating dithiolates to simulate the 1,2-dithiolene moiety found at the active sites of Mo and W enzymes.[36] Again, such approaches generally involve the use of lithium dithiolate salts with metal chlorides,[150] or

the [2 + 3] addition of alkynes across S-M-S units.[82,83] The use of nucleophilic substitution of alkyl halides in the formation of chelating dithiolates has not previously been reported.

Dithiolates in combination with other appropriate terminal ligands, have formed single bridges between two metal centres, but this usually involves electron rich, low valent metals, such as in $[Au_2(1,3\text{-}S_2C_6H_4)(PPh_3)_2]$.[36] Since high oxidation state terminal thiolate complexes are prone to reductive elimination, with loss of ligands as sulfides or disulfides,[62] a bridging dithiolate acting as the only link between two W(VI) centres is particularly novel.

To investigate bridging versus chelating dithiolate formation, we chose the α,α'-dichloroxylene system due to its structural similarity to the highly successful benzyl chloride, which proved to be the easiest to follow by ^{1}H NMR and gave more stable alkylated products.

4.2 Reactions of α,α'-Dichloro-*o*-, *m*- and *p*-xylenes

4.2.1 α,α'-Dichloro-*o*-xylene

We initially hypothesized that since bis-alkylation was not observed to occur with a second equivalent of an alkyl monohalide, such a reaction might be more favourable if the second halide was in close proximity to the metal centre. This could be achieved by intramolecular alkylation to give a cyclic species containing W, S and C (Figure 4.1), which shows similarities to the coordination environment of tungsten in molybdopterin-containing enzymes.[3] Based on our previous success with benzyl chloride as a rapid alkylating agent (including distinct methylene proton signals in the ^{1}H NMR spectrum

and enhanced stability of the alkylated product), we decided to investigate the reaction with α,α'-dichloro-*o*-xylene. Our ^{1}H NMR experiments suggested that, when a 1:1 ratio of reagents is used, the dihalide reacts with two $[WS_4]^{2-}$ anions to form a bridging, rather than a chelating, dithiolate ligand (Scheme 4.1).

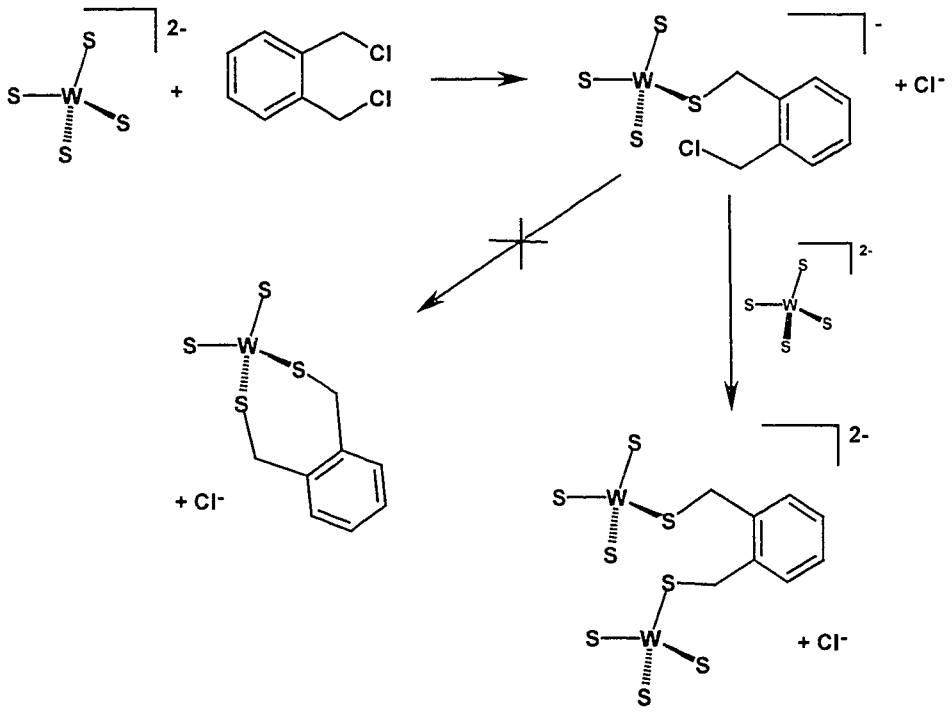

Scheme 4.1 Bis-alkylation versus bridging alkylation.

Alkylation reactions of primary alkyl halides have been shown to proceed by associative nucleophilic substitution (S_N2),[58] where $[WS_4]^{2-}$ acts as the nucleophile. The absence of a second alkylation at the same metal centre suggests that $[WS_3(SR)]^-$ is not a sufficiently good nucleophile for this to occur. Such a reaction may be even less favourable since a neutral metal species would consequently be formed, which does not

favour loss of the halide leaving group. Despite this, the formation of a somewhat stable bridging dithiolate is an interesting observation due to the high oxidation state of the metals involved. Time dependent ^{1}H NMR spectra of $[PPh_4]_2[WS_4]$ with α,α'-dichloro-*o*-xylene in a 2:1 ratio clearly indicate the formation of the monoalkylated and bridging species, as well as giving some insight into the various decomposition products in solution (Figure 4.1).

The dichloroxylene (A) is consumed and the monoalkylated species starts to form, as indicated by the appearance of two new signals (B1 and B2). B1 represents the methylene protons adjacent to the chlorine atom and B2 represents those adjacent to the sulfur of $[WS_4]^{2-}$ after C-S bond formation. The bridging species exhibits one resonance since both sets of methylene protons are now adjacent to the sulfur of a $[WS_4]^{2-}$. The bridging species signal is at a maximum after 8 hours.

After 1 hour of reaction, a signal at 4.12ppm (D) is also observed, which increases in intensity for the duration of the experiment. We believe that this signal is due to the formation of 1,3- dihydrobenzo[c]thiophene by W-S bond cleavage of the monoalkylated product to form the free thiolate then rapid intramolecular nucleophilic substitution of the adjacent benzylic chloride. Metal assisted C-S bond formation and cyclization has previously been reported for α,α'-dihalo-*o*-xylenes,[151] and the chemical shifts for the methylene protons are consistent with those measured in our experiment.

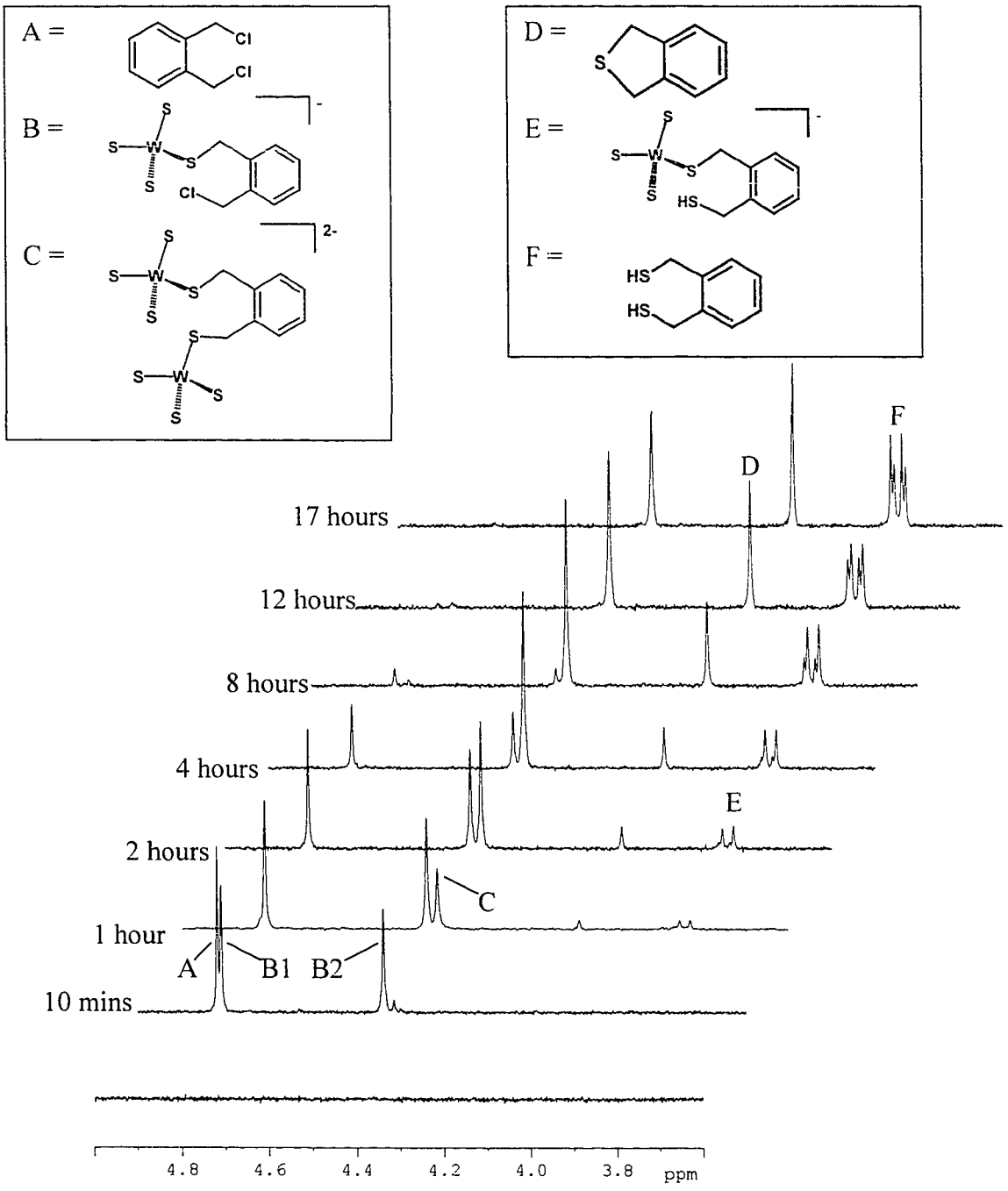

Figure 4.1 Time dependent ^{1}H NMR spectra of $[PPh_4]_2[WS_4]$ with α,α'-dichloro-*o*-xylene (2:1) in CD_3CN at room temperature.

The final set of signals is observed in the region 3.8-3.9ppm and clearly contains two overlapping doublets (E and F). These signals can be assigned to thiols, with the corresponding protons being observed as triplets around 1.9ppm. Signal E is believed to be due to decomposed bridging species containing one thiol functionality, and signal F is believed to be a dithiol. A monalkylated thiol that resulted in signal E would also, by necessity, give a second signal at a different chemical shift due to the methylene protons closest to the metal. Comparative studies with other dichloroxylene isomers suggest that such a signal would be very close to that of the bridging species. Since no other signals are observed in our studies using dichloro-*o*-xylene, we believe that the bridging species (signal C) may be superimposed on the alkylated thiol species. The scheme below illustrates the possible series of steps leading to the signals observed in the ^{1}H NMR spectra when a 2:1 ratio of $[WS_4]^{2-}$ to dichloroxylene is used.

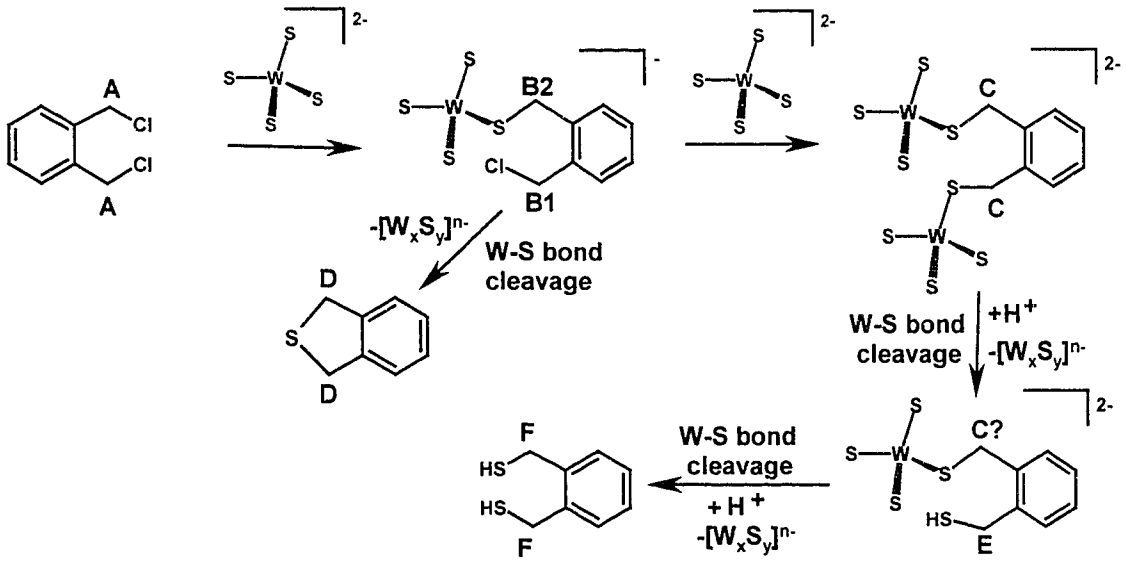

Scheme 4.2 Possible reaction scheme for $[PPh_4]_2[WS_4]$ and α,α'-dichloro-*o*-xylene (2:1) with ^{1}H NMR assignments.

When a two-fold excess of dichloroxylene is used, there is an absence of bridging species, as well as other observable differences.

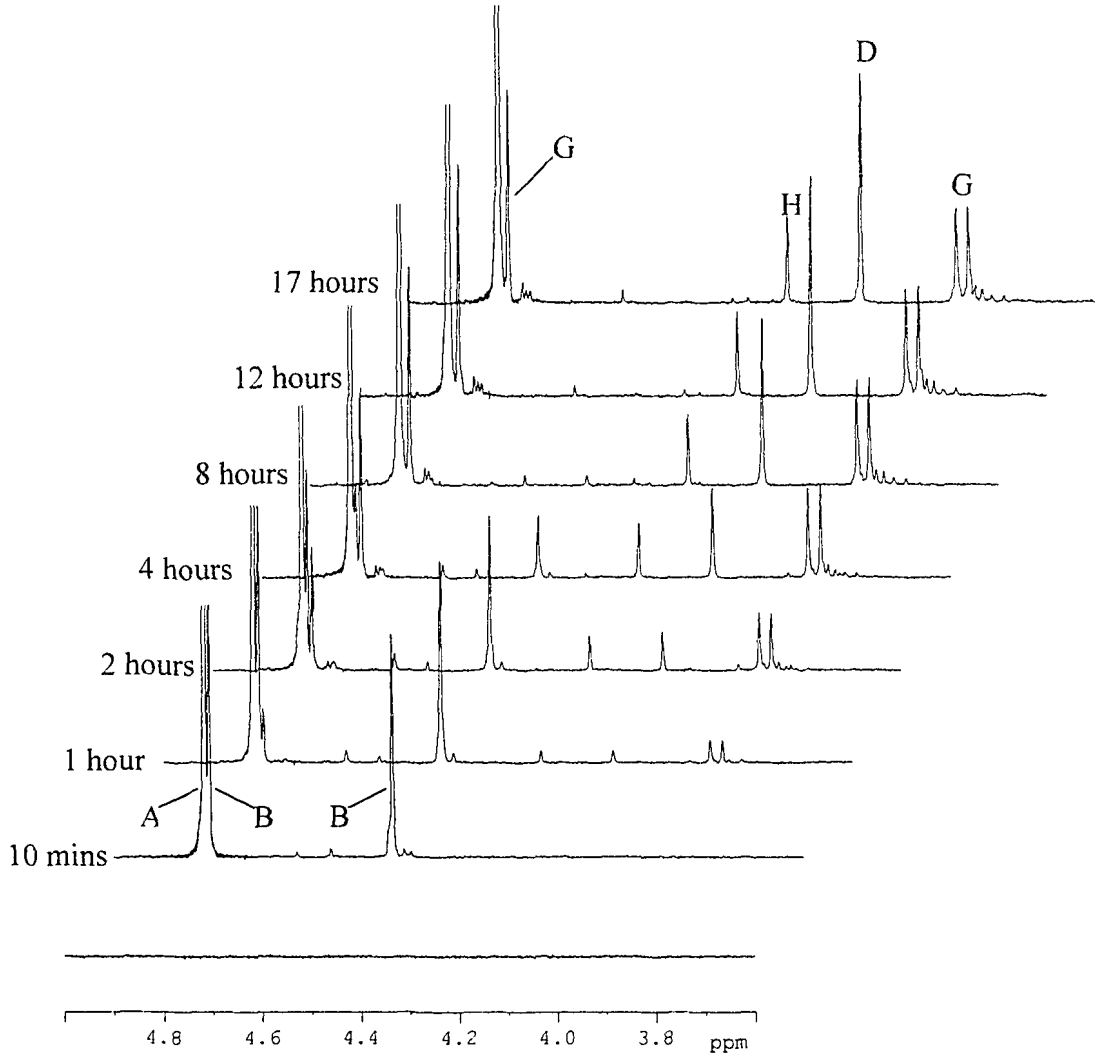

Figure 4.2 Time dependent ^{1}H NMR spectra of $[PPh_4]_2[WS_4]$ with α,α'-dichloro-*o*-xylene (1:2) in CD_3CN at room temperature.

The signal due to 1,3-dihydrobenzo[c]thiophene is again present, which is expected since this product appears to evolve from the monoalkylated species. Only one

doublet is observed in the thiol region at a more downfield chemical shift than in Figure 4.1, and correlates to the singlet at 4.80ppm. These signals (G) are due to alkylation of $[WS_4]^{2-}$ and subsequent thiol formation resulting in a thiol/chloride species (Scheme 4.3). One final unexplained signal appears at 4.23ppm (H), which could be attributed to a decomposition intermediate.

A proposed reaction scheme is shown below for the reaction of $[PPh_4]_2[WS_4]$ with excess dichloroxylene.

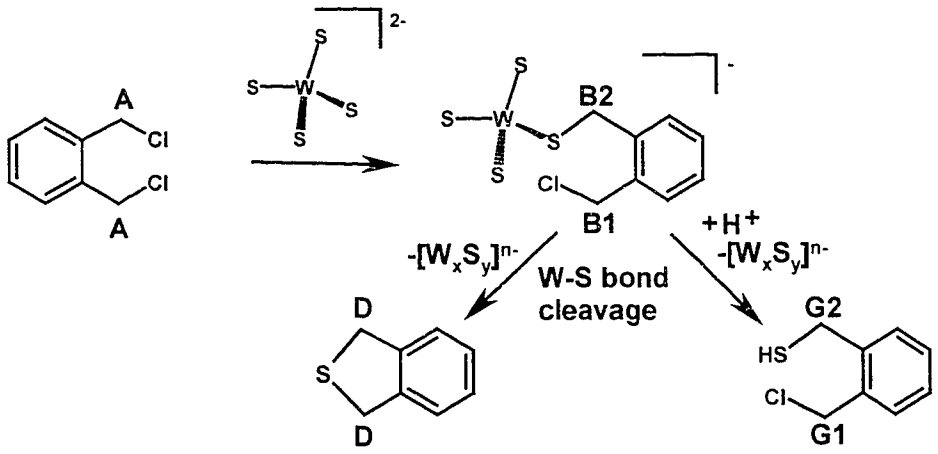

Scheme 4.3 Proposed reaction pathway of $[PPh_4]_2[WS_4]$ and α,α'-dichloro-*o*-xylene (1:2) with ^1H NMR assignments.

Decomposition of both the monoalkylated and bridging species are significant but alkylation of the second metal centre apparently occurs before such decomposition has a chance to occur. Acquisition of a proton, from H_2O in solution, leads to formation of thiols as the major decomposition products.

The spectra in Figure 4.2 were used to determine the optimum reaction time for the monoalkylated species as approximately 2 hours, which led to the isolation and characterization of a crystalline product. A ^{1}H NMR spectrum of the crystals confirmed that the monoalkylated species is correctly identified in Figures 4.1 and 4.2, and is shown below.

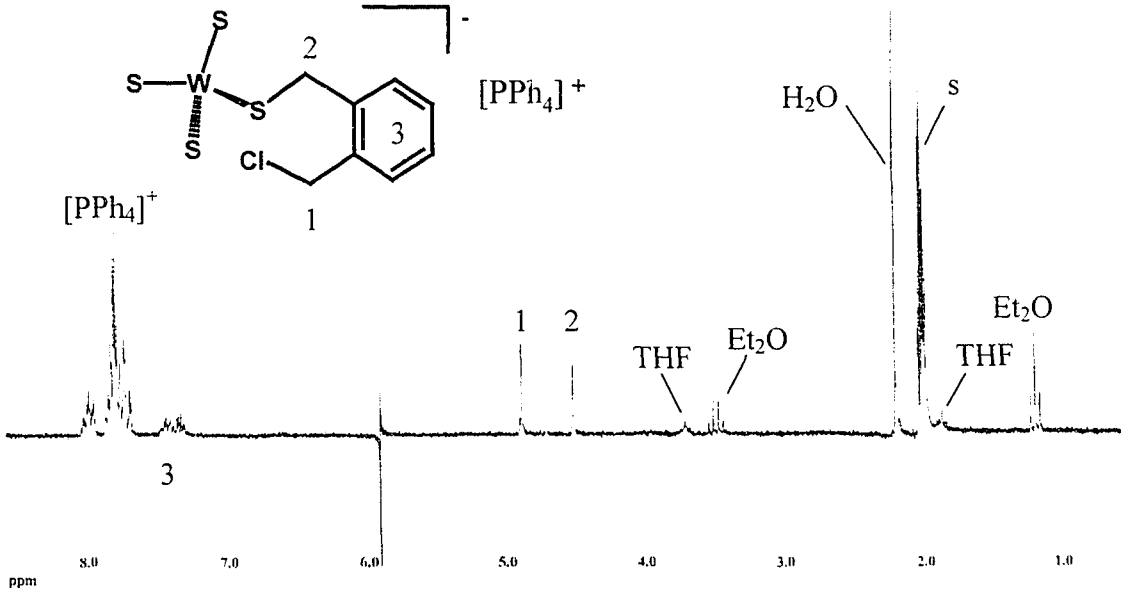

Figure 4.3 ^{1}H NMR spectra of crystalline $[PPh_4][WS_3(o\text{-}SCH_2(C_6H_4)CH_2Cl)]$.

When the above crystals were left to decompose at room temperature for 24 hours, the resulting signals corresponded to chloride/thiol (signal G in Figure 4.2), and 1,3-dihydrobenzo[c]thiophene (signal D) as the two major products. A small amount of the unidentified intermediate in Figure 4.2 (signal H) was also present. We are confident that our assignment of decomposition products from bridging complexes is correct in Figure 4.1 since none of these species were observed in the decomposition spectra of

$[PPh_4][WS_3(o\text{-}SCH_2(C_6H_4)CH_2Cl)]$. X-ray crystallography was successfully performed on $[PPh_4][WS_3(o\text{-}SCH_2(C_6H_4)CH_2Cl)]$ to confirm its structure. Crystallographic parameters are given below.

Table 4.1 Crystallographic data for $[PPh_4][WS_3(o\text{-}SCH_2(C_6H_4)CH_2Cl)]$ (**11**).

	11
Empirical formula	$C_{32}H_{28}ClPS_4W$
Molecular wt. (g mol^{-1})	791.05
Colour	red
Crystal system	monoclinic
Space group	$P2_1/n$ (#14)
a (Å)	16.1381(8)
b (Å)	11.4197(6)
c (Å)	17.4072(9)
β (°)	103.2706(10)
V ($Å^3$)	3122.3(3)
Z	4
ρ_{calcd} (g cm^{-3})	1.683
T (K)	193
R^a	0.0280
$R_w{}^b$	0.0686
GOF^c	0.941

$^a R = \Sigma \,||Fo| - |Fc||\,/\Sigma\,|Fo|$; $^b R_w = [\Sigma w(Fo^2 - Fc^2)^2/\Sigma w(Fo^4)]^{1/2}$; $^c[\Sigma w(F_o^2 - F_c^2)^2/(n-p)]^{1/2}$ (n = number of data; p = number of parameters varied).

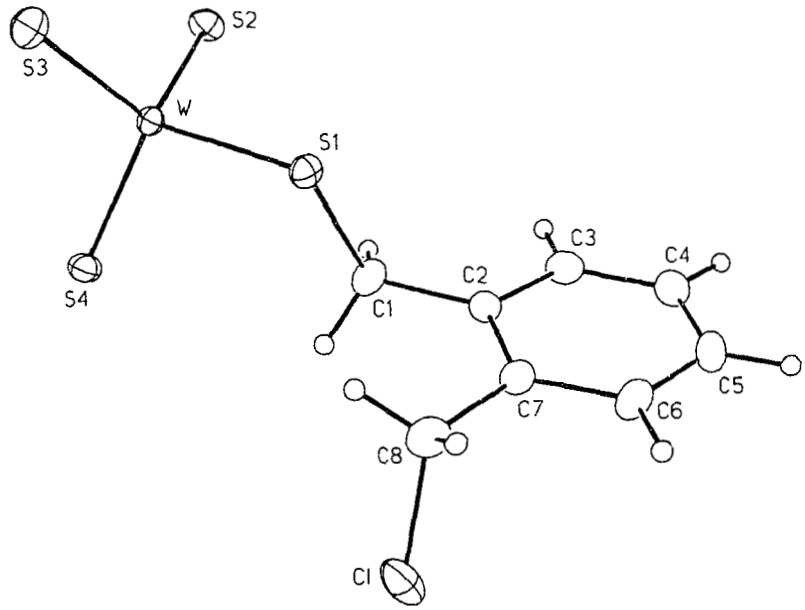

Figure 4.4 ORTEP representation of the anionic portion of $[PPh_4][WS_3(o\text{-}SCH_2(C_6H_4)CH_2Cl)]$ (**11**).

The structure consists of $[PPh_4]^+$ cations and $[WS_3(o\text{-}SCH_2(C_6H_4)CH_2Cl)]^-$ anions. No solvate molecules were found in the unit cell, consistent with analogous structures where R = ^{i}Bu, ^{i}Pr , ^{t}Bu, benzyl and allyl, discussed in Chapter 3. In all cases, the geometry at the metal centre is approximately tetrahedral (see Table 4.2) and the bond lengths and angles fall in the ranges of related structures. The $[PPh_4]^+$ cations are unremarkable, and show no close contacts with the anions.

Table 4.2 Selected bond lengths (Å) and bond angles (°) for $[PPh_4][WS_3(S(o\text{-}SCH_2(C_6H_4)CH_2Cl)]$ (11) and $[PPh_4][WS_3(SBz)]$ (**9**).

	11	**9**
W-S(1)	2.3307(10)	2.3376(18)
W-S(2)	2.1602(10)	2.1475(18)
W-S(3)	2.1425(13)	2.1523(17)
W-S(4)	2.1635(11)	2.1532(19)
S(1)-C(1)	1.854(4)	1.819(7)
S(1)-W-S(2)	108.63(4)	109.58(7)
S(1)-W-S(3)	105.06(5)	102.89(7)
S(1)-W-S(4)	107.32(4)	109.88(8)
S(2)-W-S(3)	112.08(5)	110.74(7)
S(2)-W-S(4)	111.60(5)	110.63(7)
S(3)-W-S(4)	111.77(5)	112.84(7)
W-S(1)-C(1)	102.25(14)	106.3(3)

When the $[PPh_4][WS_3(S(o\text{-}SCH_2(C_6H_4)CH_2Cl)]$(**11**) structure is compared to the isomorphous $[PPh_4][WS_3(SBz)]$(**9**), a few subtle differences can be seen. One of the terminal W-S bonds in **11** is slightly shorter than the other two, whereas in **9**, all three bonds fall within the two extremes observed for **11**. In addition, the W-S-C angle in **11** is somewhat greater than in **9**. Apparently the presence of the *ortho*-chloromethyl group on the benzene ring causes these observed variations in bonding distances and angles, though due to the orientation of this group with respect to the terminal sulfide ligands, none of the variations are particularly large. For instance, we do not observe a significant increase in the W-S bond and W-S-C angle as observed in $[PPh_4][WS_3(S^tBu)]$, where the bulky ^{t}Bu group increases these parameters to 2.354(4)Å and 111.8(5)°, respectively.

The time dependent ^{1}H NMR studies shown in Figure 4.1 allow the optimum reaction time for isolation of the bridging species, in the absence of monoalkylated product, to be determined as 12 hours. On an experimental scale, the reaction mixture was pumped to a sticky residue after 12 hours and the resulting THF extract was deep orange in colour, indicating the presence of an alkylated product. The THF extract was mixed with Et_2O and the resulting red precipitate was dissolved in CH_3CN, placed in crystallization tubes, layered with Et_2O and left at –20°C for a week. The crystals obtained gave the following ^{1}H NMR spectrum, confirming the chemical shift assignment in Figures 4.1, though attempts to obtain an X-ray crystal structure were unsuccessful due to the small size and poor quality of the crystals.

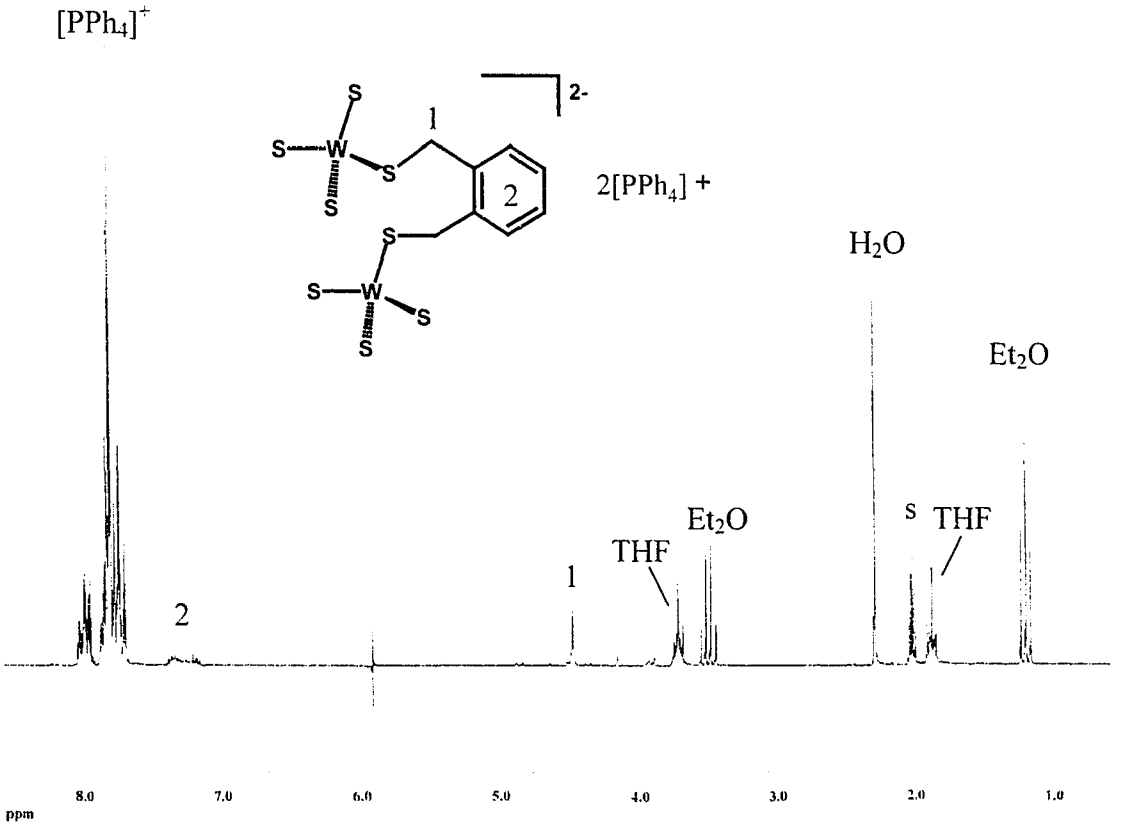

Figure 4.5 ^{1}H NMR spectrum of crystalline $[PPh_4]_2[WS_3(S(o\text{-}SCH_2(C_6H_4)CH_2S)S_3W]$.

4.2.2 α,α'-Dichloro-*p*-xylene

To further probe reactions where W(VI) bridging thiolate complexes were formed, we decided to extend our studies to other dichloroxylene isomers. The *para* isomer was the obvious choice since it provided simpler ^{1}H NMR spectra in the phenyl region, allowing the reactions to be followed in two chemical shift regions.

^{1}H NMR studies were performed under identical conditions to those using α,α'-dichloro-*o*-xylene, starting with a 2:1 ratio of $[PPh_4]_2[WS_4]$ to alkyl dihalide. The spectra clearly show the dichloroxylene being consumed (signal A) giving rise to two new signals of the monoalkylated species, where signal B1 is the methylene group adjacent to the chloride and B2 is the alkylated methylene group. After 1 hour, formation of the bridged dithiolate species can be observed, giving rise to signal C, which is at a maximum after about 8 hours.

After only one hour, we already see the appearance of a signal due to decomposed monoalkylated species, which is suggestive of an organic fragment containing chloride (signal D1) and thiol (signal D2) functionalities. After 2 hours, we also observe the appearance of a monoalkylated species containing a thiol, which could be formed either from decomposition of the bridged species or by subsequent alkylation of the organic thiol/chloride species. The final set of thiol signals appears superimposed on the two previous sets and is due to formation of an organic dithiol (signal F). The three corresponding triplets can be seen at *ca.* 1.9ppm in agreement with our methylene proton assignments.

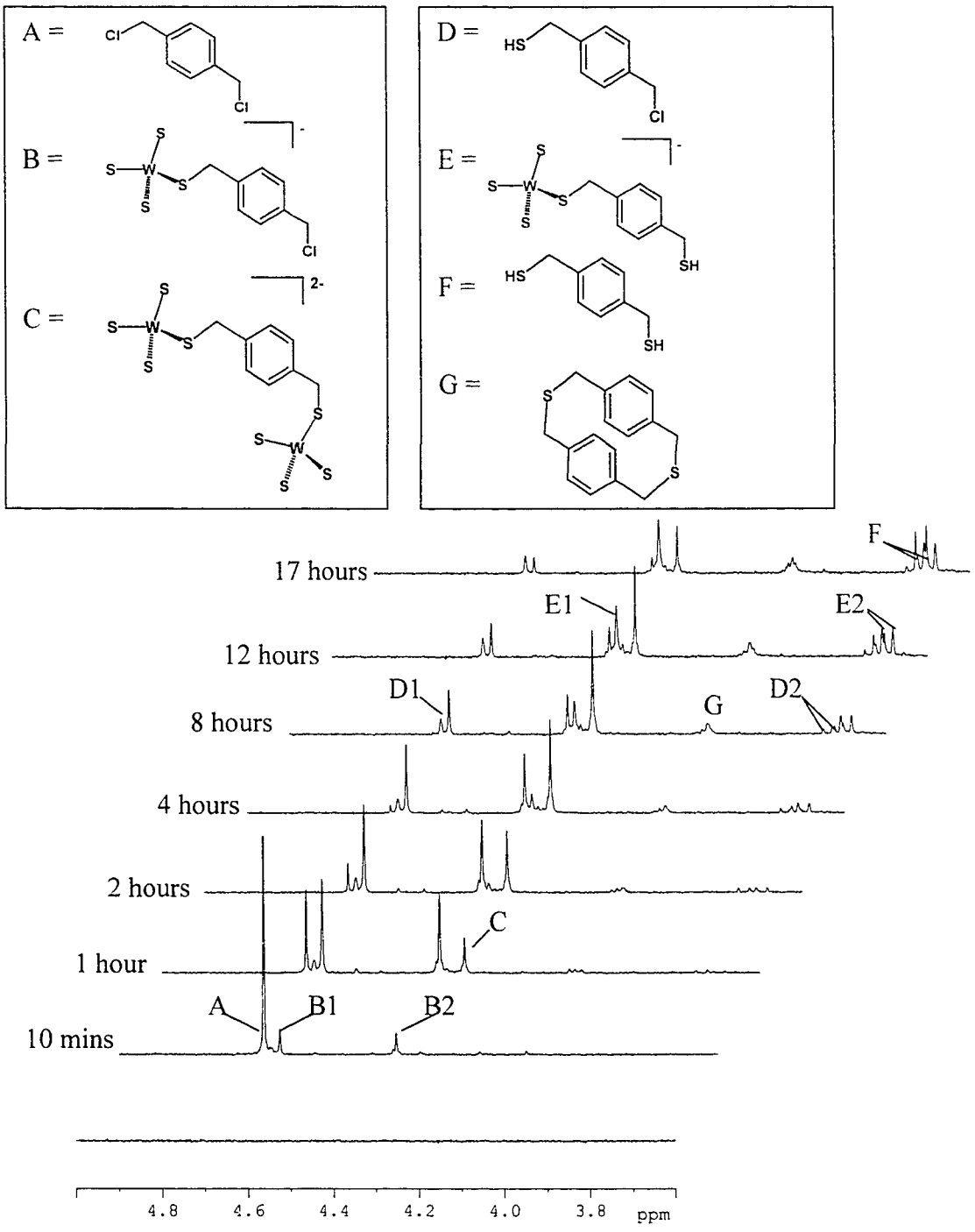

Figure 4.6 Time dependent ^{1}H NMR spectra of $[PPh_4]_2[WS_4]$ with α,α'-dichloro-*p*-xylene (2:1) in CD_3CN at room temperature.

A set of signals at 4.05ppm has been tentatively assigned to macrocyclic species resultant from the associative decomposition of two alkylated species (see Scheme 4.4). Since a collection of very weak signals is observed around this chemical shift, there lies the possibility that more than one macrocyclic species is forming (e.g. trimer versus dimer, or sulfide versus disulfide), resulting in a series of small singlets. Another possibility is that the signals represent inequivalent methylene protons in the dimer, due to puckering of the ring.

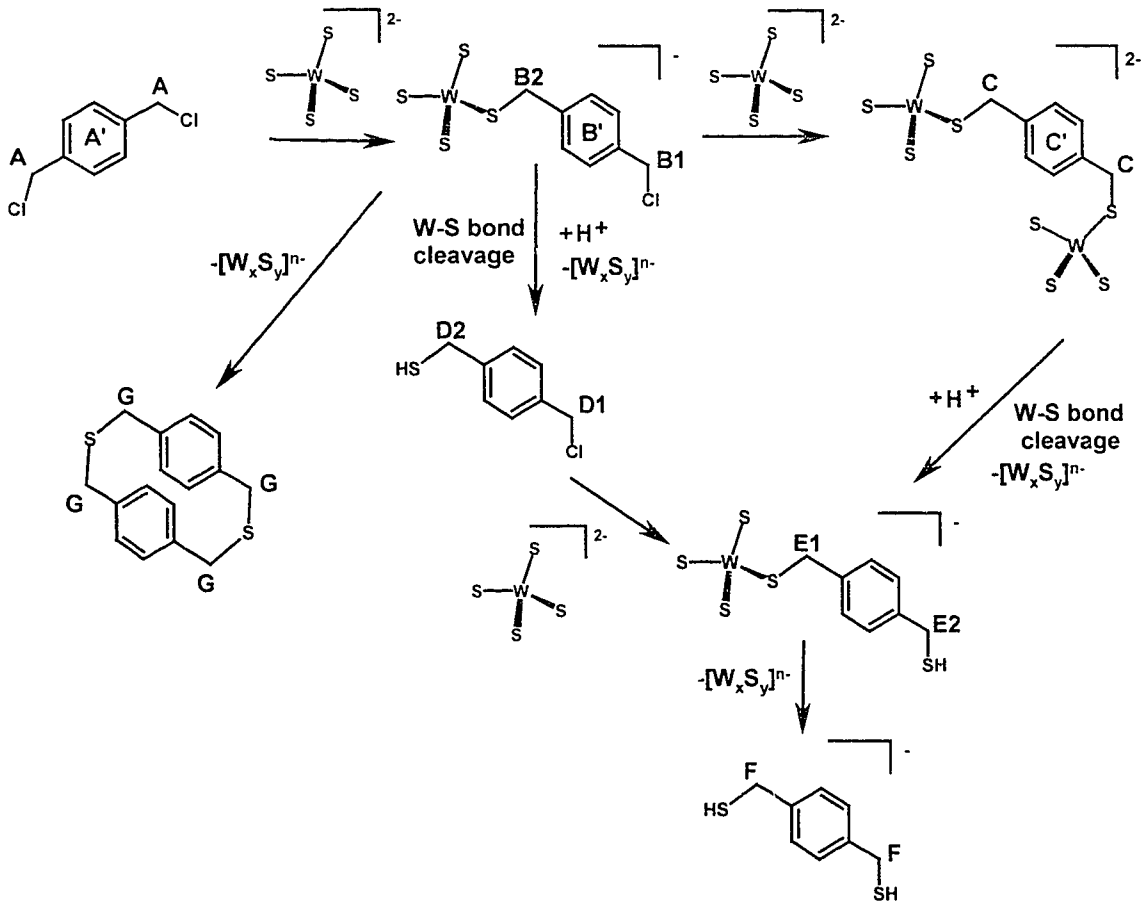

Scheme 4.4 Proposed reaction pathway for $[PPh_4]_2[WS_4]$ and α,α'-dichloro-*p*-xylene (2:1) with ^1H NMR assignments.

In the phenyl region we can follow the above reaction using the more simplified signals of the dichloro-*p*-xylene, in contrast to those of the *ortho* isomer. Reaction of the alkyl dihalide can clearly be seen (signal A'), and subsequent formation of the monoalkylated, then bridged, species (signals B' and C', respectively). These signals correlate well with those observed in the methylene region, confirming our chemical shift assignments for the monoalkylated and bridged species. Various other signals due to decomposition products are observed in this region but are seen to overlap, and are consequently difficult to assign.

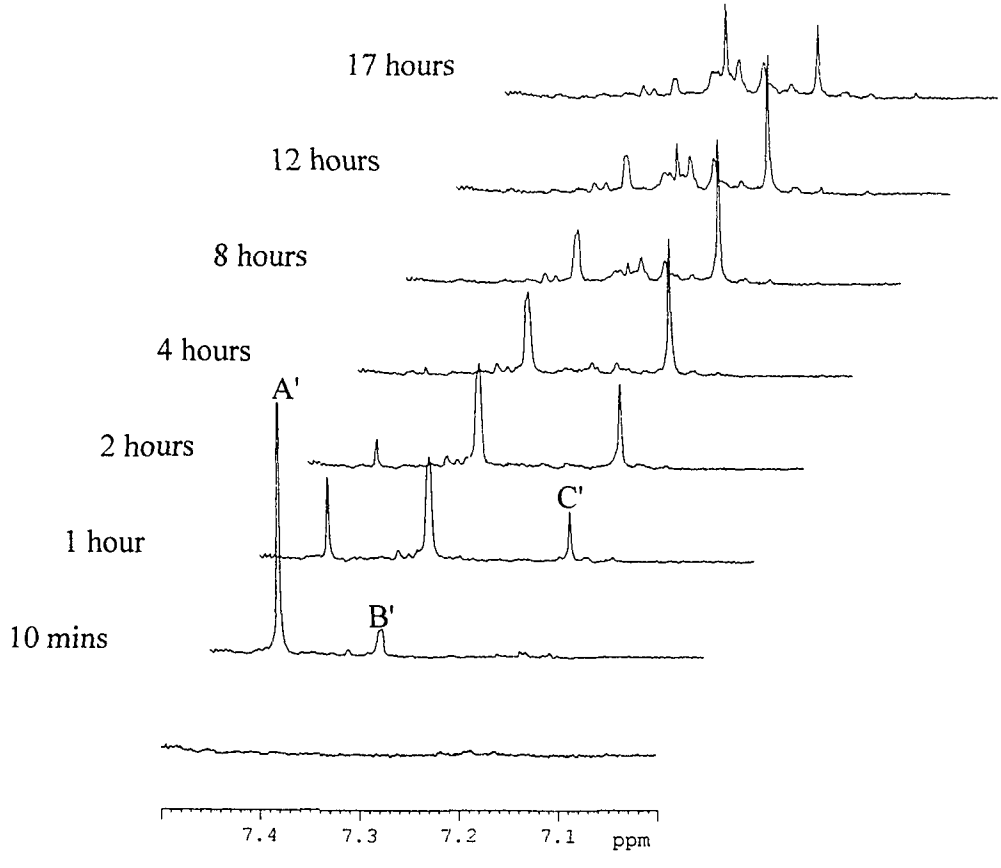

Figure 4.7 ^{1}H NMR of the phenyl region in the reaction of α,α'-dichloro-*p*-xylene and $[PPh_4]_2[WS_4]$ (1:2).

When a two-fold excess of alkyl dihalide is used, there is only a very small amount of bridged species formation (Figure 4.8, signal C), and consequently, the major organic decomposition product is the chloride/thiol (signal D). Due to the excess of alkyl dihalide present, alkylation by the chloride/thiol does not occur, resulting in an absence of alkylated thiol. As the small amount of bridged species decomposes, we start to see the appearance of signal F, which could either be dithiol, which is known to give a doublet at this chemical shift, or a singlet from a disulfide with the corresponding chloromethyl signal being obscured in the 4.7ppm region. A singlet at 4.05ppm (signal G) can be seen where previously a small cluster of signals was observed in Figure 4.6, suggesting that a macrocyclic organic sulfide may be present. Since only tiny quantities of bridged dithiolate species are formed when an excess of alkyl dihalide is used, we can rule out the possibility of forming large amounts of cyclic *di*sulfides, which may have resulted in the several signals observed in Figure 4.6.

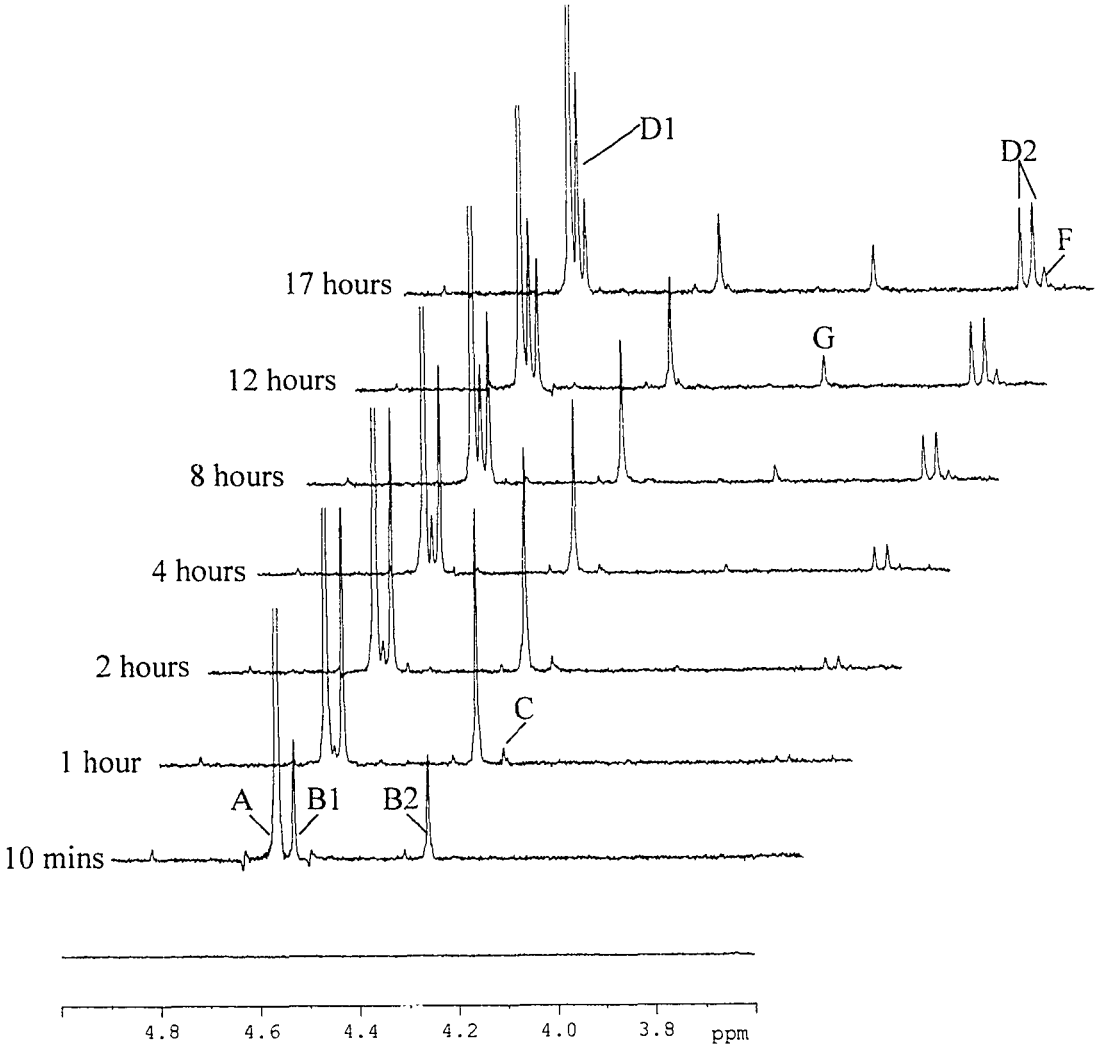

Figure 4.8 Time dependent ^{1}H NMR spectra for $[PPh_4]_2[WS_4]$ and α,α'-dichloro-*p*-xylene (1:2) in CD_3CN at room temperature.

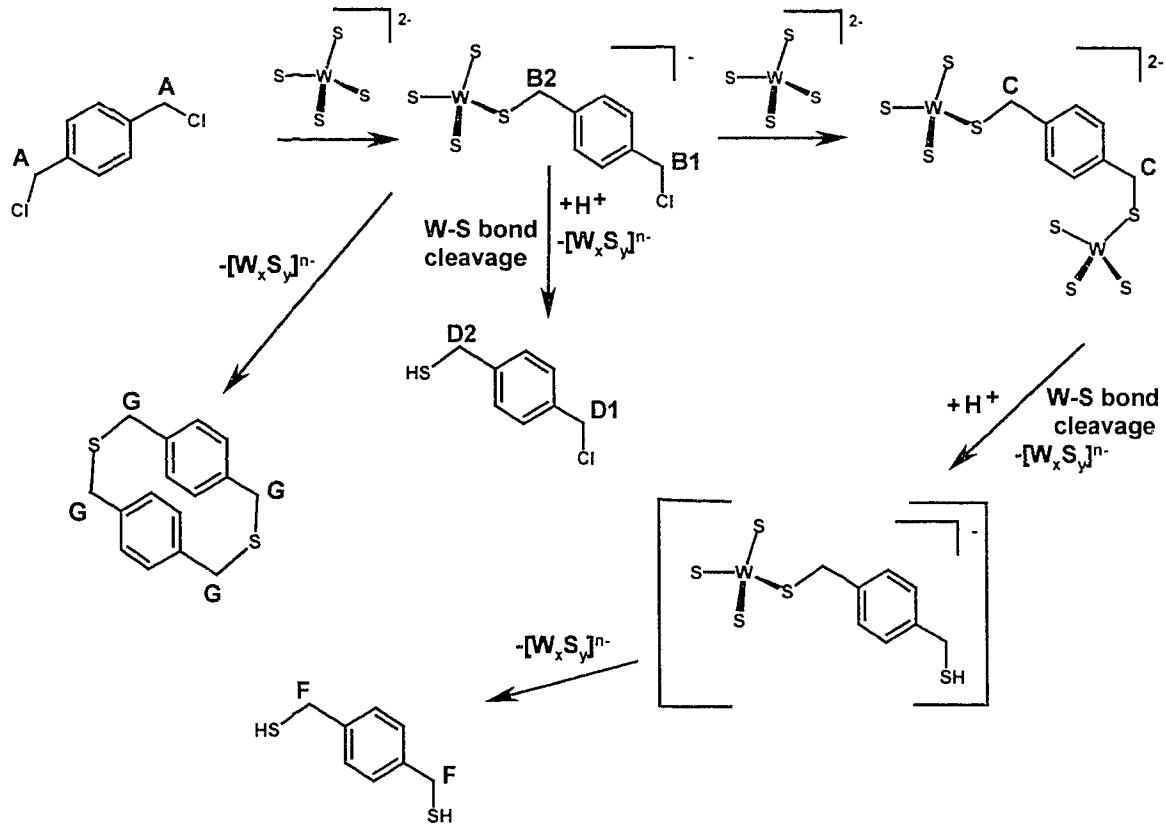

Scheme 4.5 Proposed reaction pathway for $[PPh_4]_2[WS_4]$ and α,α'-dichloro-*p*-xylene (1:2) with ^1H NMR assignments.

A number of significant differences can be seen between reactions of the *ortho* and *para* dichloroxylene isomers. The first alkylation of the *ortho* isomer can be seen to proceed more rapidly than that of the *para* isomer. When one considers the chemical shift of the two dichloroxylenes, the methylene protons appear at a more downfield chemical shift in the *ortho* case, probably due to the closer proximity of the other chloromethyl group. The electron withdrawing effect from the adjacent group apparently deshields the α-carbon, making it more electrophilic and more reactive towards nucleophilic substitution by $[WS_4]^{2-}$. Another distinct difference is in the types of decomposition

products formed by the two reactions. 1,3-dihydrobenzo[c]thiophene is formed in reactions of the *ortho* isomer, but due to steric constraints, macrocyclic sulfides containing two xylene groups are apparently formed in the *para* case. Since no chloro/thiol organic product is observed in reactions of dichloro-*o*-xylene and $[PPh_4]_2[WS_4]$ in a 1:2 ratio, it might be concluded that 1,3-dihydrobenzo[c]thiophene formation from the monoalkylated product is highly favourable, compared to formation of macrocyclic sulfides in the *para* case, where a slower associative mechanism would likely occur.

Based on optimum reaction times of two and 10 hours for monoalkylated and bridging species, respectively, crystalline products could be obtained and their ^1H NMR spectra were used to confirm the chemical shift assignments in previous experiments.

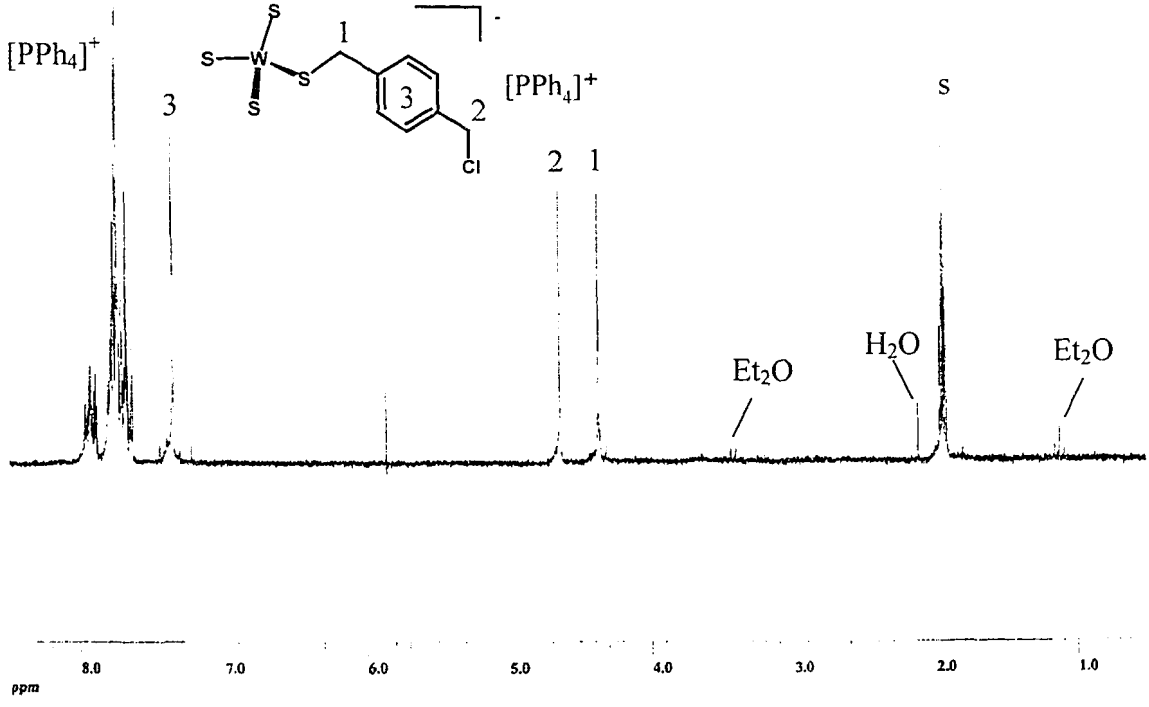

Figure 4.9 ^1H NMR spectrum of crystalline $[PPh_4][WS_3(p\text{-}SCH_2(C_6H_4)CH_2Cl)]$ in CD_3CN.

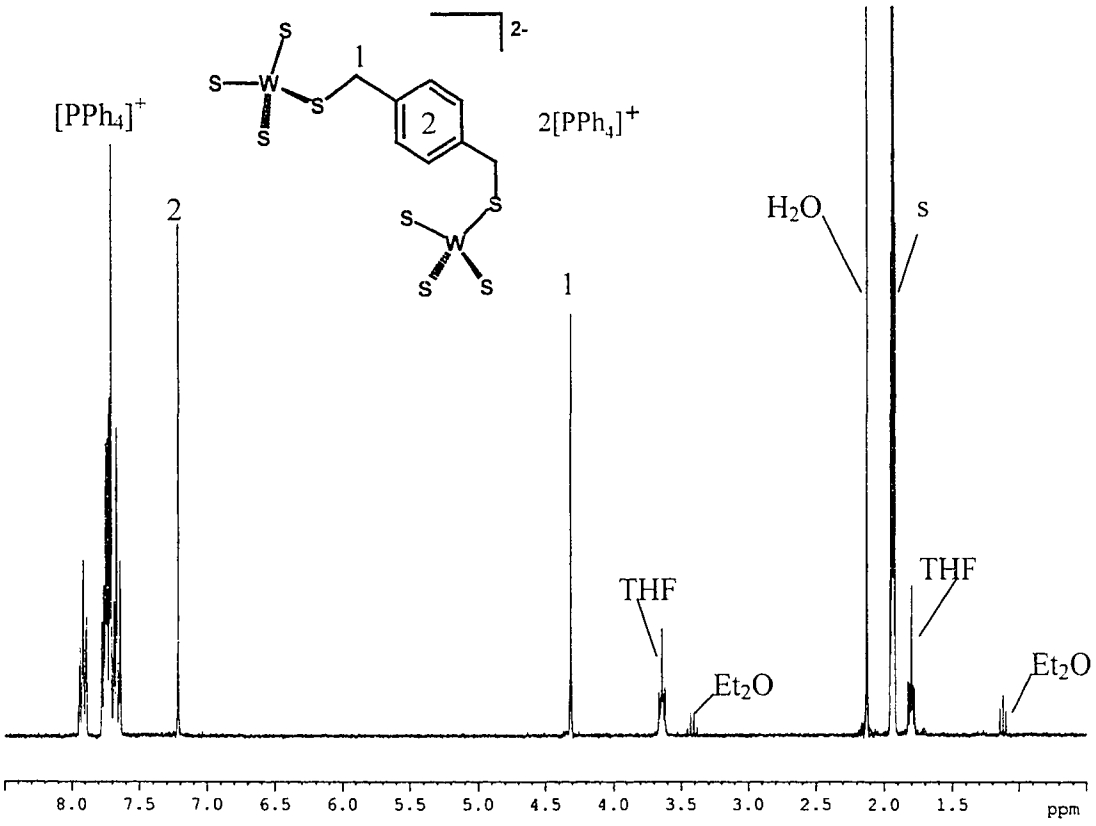

Figure 4.10 ^{1}H NMR spectrum of crystalline $[PPh_4]_2[WS_3(p\text{-}SCH_2(C_6H_4)CH_2S)S_3W]$ in CD_3CN.

When crystals of $[PPh_4][WS_3(p\text{-}SCH_2(C_6H_4)CH_2Cl)]$ were left in CD_3CN solution to decompose, new signals appeared corresponding to the chloro/thiol organic product and a macrocyclic sulfide at 4.05ppm. In contrast, when crystals of $[PPh_4]_2[WS_3(p\text{-}SCH_2(C_6H_4)CH_2S)S_3W]$ were left in solution for a week, the major organic decomposition product was the dithiol and the only other gave a signal at 4.04ppm which could be assigned to a macrocyclic *di*sulfide, being at a slightly different chemical shift than the macrocyclic sulfide from decomposition of $[PPh_4][WS_3(p\text{-}SCH_2(C_6H_4)CH_2Cl)]$.

4.2.3 α,α'-dichloro-*m*-xylene

To complete our studies of the dichloroxylenes, we investigated reactions of the *meta* isomer to allow comparisons to be made with the other two systems. It was evident after our initial time dependent ^{1}H NMR study of $[PPh_4]_2[WS_4]$ and α,α'-dichloro-*m*-xylene (2:1) that the reaction profile was very similar to that of dichloro-*p*-xylene.

The dichloroxylene (signal A, Figure 4.11) starts being consumed on mixing, resulting in formation of two new signals of the monoalkylated species (signals B1 and B2). With time, we start to see formation of the bridged species (signal C) and also two other decomposition products. The first to appear can be assigned to the organic chloro/thiol product (signals D1 and D2), as seen in the dichloro-*p*-xylene experiments, and the second is due to the monoalkylated thiol product (signals E1 and E2).

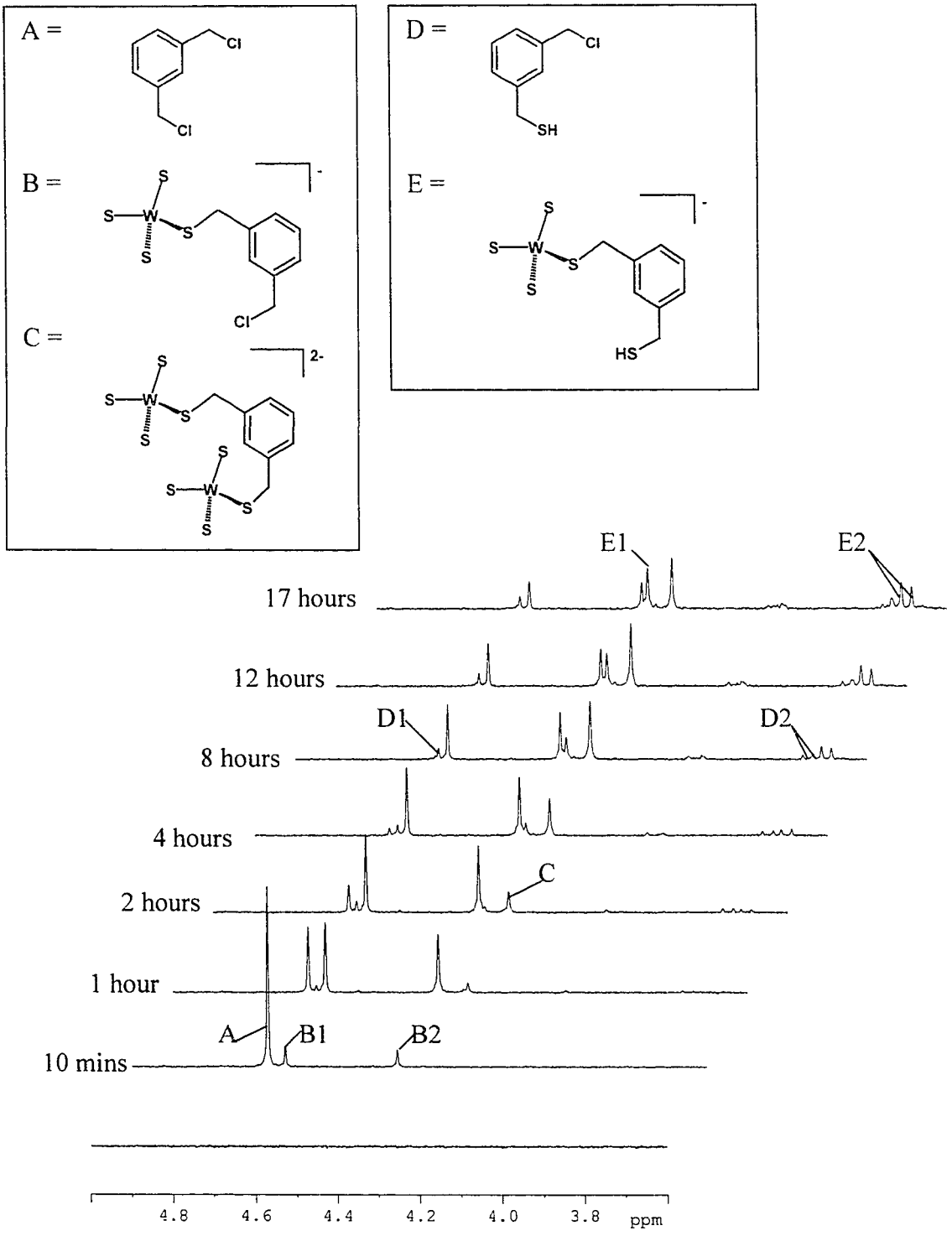

Figure 4.11 Time dependent ^{1}H NMR spectra of $[PPh_4]_2[WS_4]$ and α,α'-dichloro-*m*-xylene (2:1) in CD_3CN at room temperature.

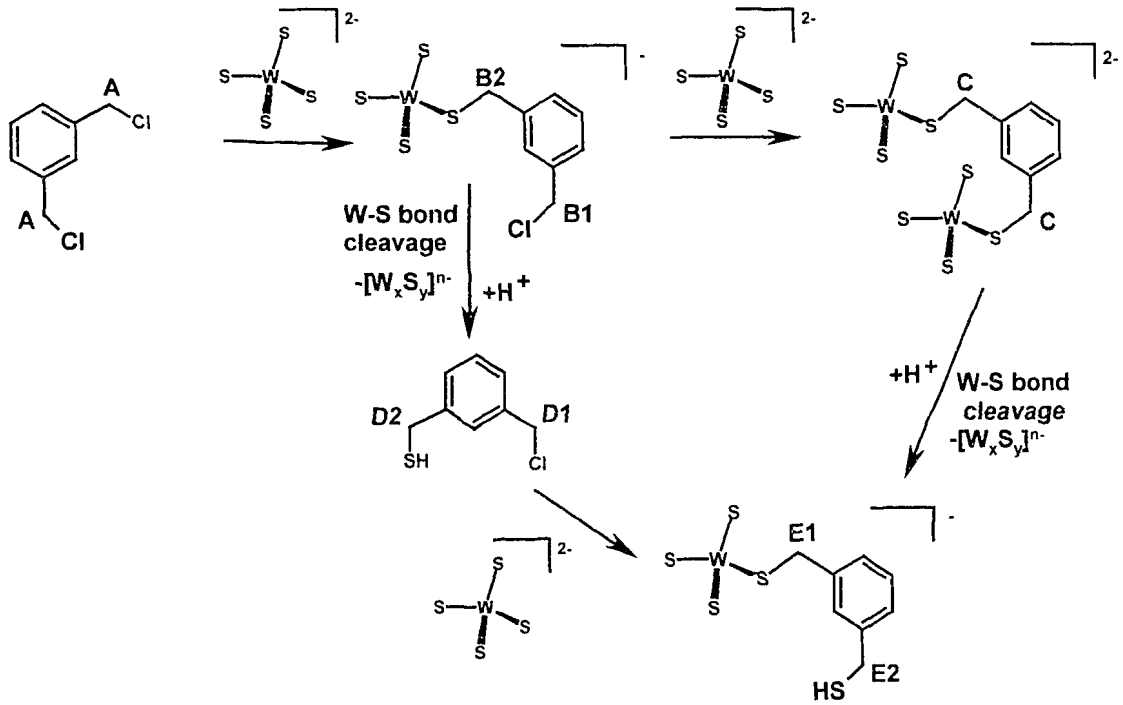

Scheme 4.6 Possible reaction pathway for $[PPh_4]_2[WS_4]$ and α,α'-dichloro-*m*-xylene (2:1) with ^1H NMR assignments.

In the analogous dichloro-*p*-xylene reactions, a dithiol signal appears towards the end of the experiment, superimposed on the other thiol signals in that region. With the dichloro-*m*-xylene reactions, we believe that only small amounts of dithiol have been formed by the end of the experiment and the signal is obscured by other thiol signals making it difficult to detect. This is consistent with less decomposition having taken place after 17 hours compared to the *para* analogue. This is also supported by the presence of only very small amounts of macrocyclic decomposition products at *ca.* 4.05ppm.

When a 1:2 ratio of $[PPh_4]_2[WS_4]$ and α,α'-dichloro-*m*-xylene is reacted, the resulting spectra are essentially identical to those obtained from the analogous dichloro-*p*-xylene reactions (Figure 4.8). Monoalkylation occurs and then decomposition to the chloro/thiol product is observed. Only tiny amounts of bridged product are formed and these appear to result in the formation of dithiol, though as discussed previously, this signal could also be due to organic chloro/disulfide. Only one singlet in the macrocyclic sulfide region at 4.05ppm is observed, which is consistent with formation of a decomposition product from the monoalkylated species.

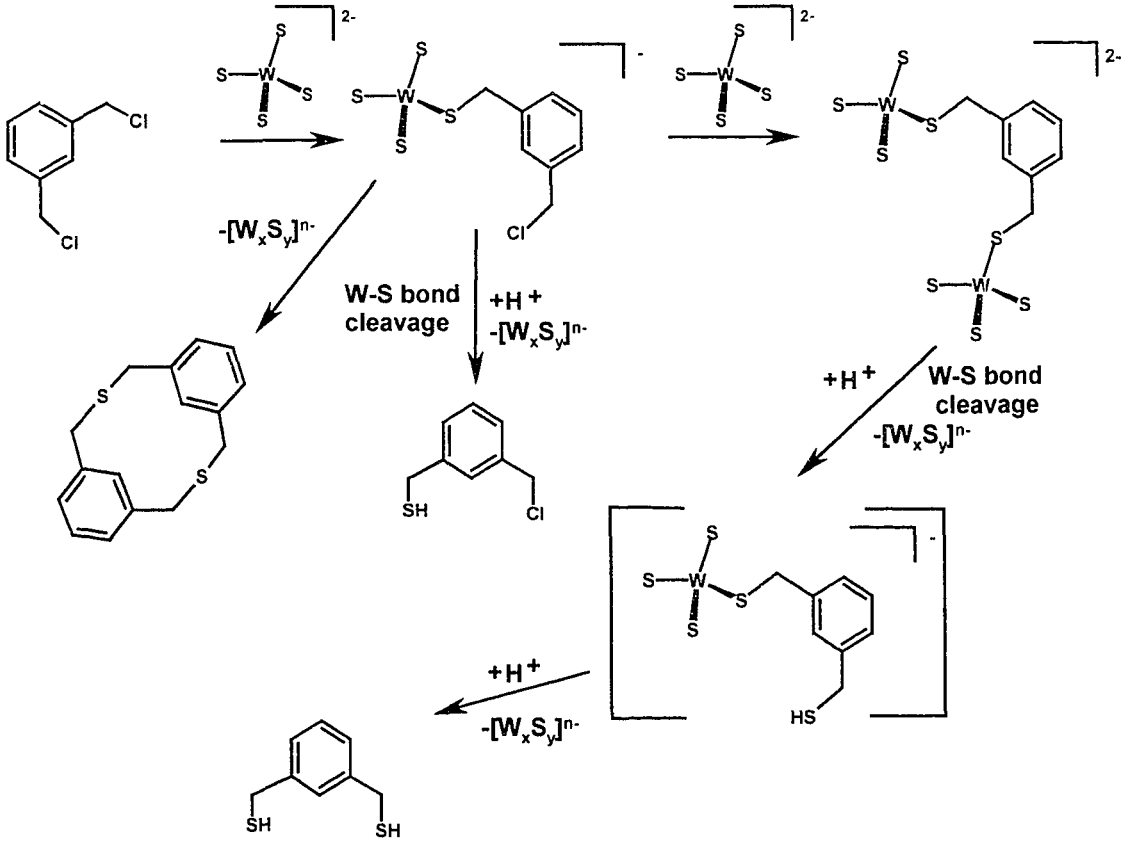

Scheme 4.7 Proposed reaction pathway for $[PPh_4]_2[WS_4]$ and α,α'-dichloro-*m*-xylene (1:2).

The inability of the monoalkylated dichloro-*m*-xylene to intramolecularly form a cyclic sulfide, as seen with dichloro-*o*-xylene, seems to prompt formation of macrocyclic species, as observed with dichloro-*p*-xylene. The observed decomposition products appear to be determined by sterics rather than electronics as we would expect to see more similarities between *ortho* and *para* isomers if the latter were true.

The optimum reaction times for preparation of the monalkylated and bridged species using dichloro-m-xylene were determined from the time dependent ^{1}H NMR studies as two and 12 hours, respectively. ^{1}H NMR of crystals isolated from these reactions allowed confirmation of chemical shift assignments in previous spectra.

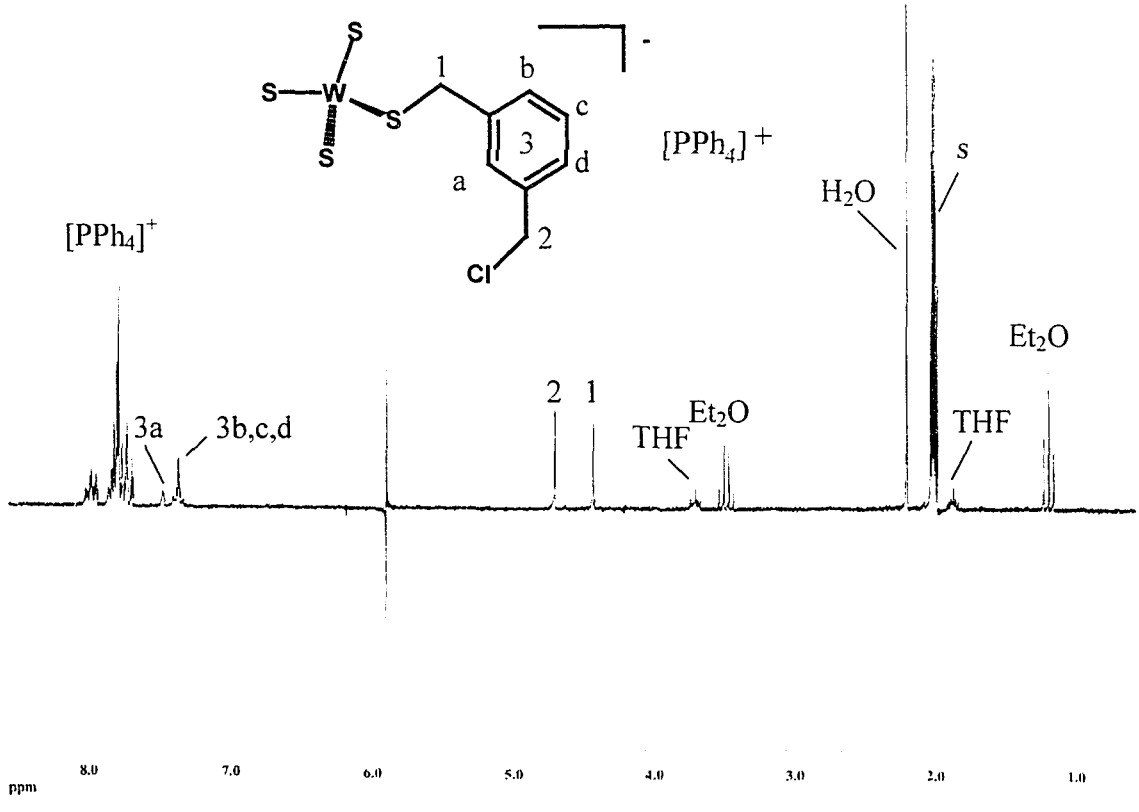

Figure 4.12 ^{1}H NMR spectrum of crystalline $[PPh_4][WS_3(m\text{-}SCH_2(C_6H_4)CH_2Cl)]$ in CD_3CN

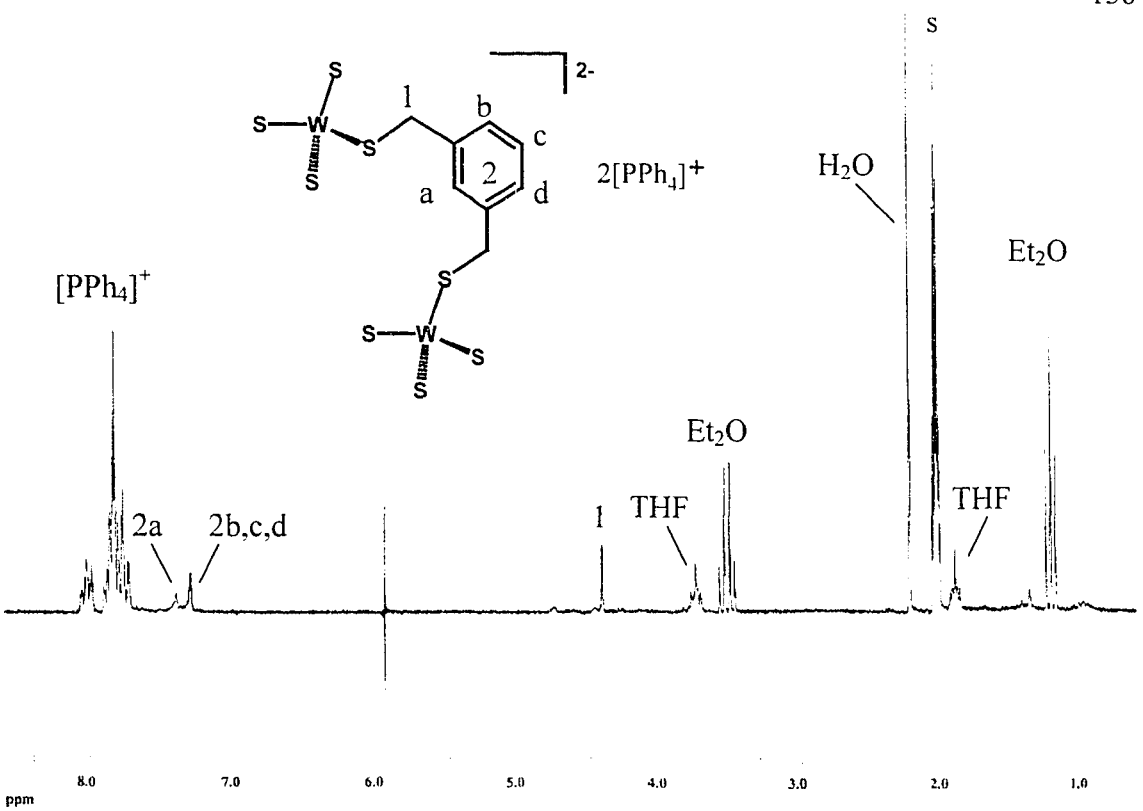

Figure 4.13 ^{1}H NMR spectrum of crystalline $[PPh_4]_2[WS_3(m\text{-}SCH_2(C_6H_4)CH_2S)S_3W]$ in CD_3CN.

When crystals of the monoalkylated and bridged compounds were each left in solution for 24 hours, the same types of decomposition products were observed as in the *para* case. $[PPh_4][WS_3(m\text{-}SCH_2(C_6H_4)CH_2Cl)]$ decomposed to the chloro/thiol organic product and macrocyclic sulfide, whereas $[PPh_4]_2[WS_3(m\text{-}SCH_2(C_6H_4)CH_2S)S_3W]$ gave dithiol and apparent macrocyclic *di*sulfide at a slightly more upfield chemical shift.

Single crystals of $[PPh_4]_2[WS_3(m\text{-}SCH_2(C_6H_4)CH_2S)S_3W]$ were of poor quality, but were isolated in the hope of obtaining at least a partial structure by X-ray crystallography. One of the crystals from the sample was found to diffract well enough for structural analysis but, to our surprise, was found to be of the compound $[PPh_4]_2[W_3OS_8(THF)]$.

Table 4.3 Crystallographic data for $[PPh_4]_2[W_3S_8O(THF)]$ (**17**).

	17
Empirical formula	$C_{52}H_{48}O_2P_2S_8W_3$
Molecular wt. (g mol^{-1})	1574.87
Colour	red
Crystal system	monoclinic
Space group	Cc (#9)
a (Å)	19.6249(16)
b (Å)	11.0538(9)
c (Å)	25.477(2)
β (°)	107.3080(16)
V ($Å^3$)	5276.5(7)
Z	4
ρ_{calcd} (g cm^{-3})	1.982
T (K)	193
R^a	0.0401
$R_w{}^b$	0.0721
GOF^c	0.975

$^a R = \Sigma \,||Fo| - |Fc||\,/\Sigma\,|Fo|$; $^b R_w = [\Sigma w(Fo^2 - Fc^2)^2/\Sigma w(Fo^4)]^{1/2}$; $^c[\Sigma w(Fo^2 - Fc^2)^2/(n-p)]^{1/2}$ (n = number of data; p = number of parameters varied).

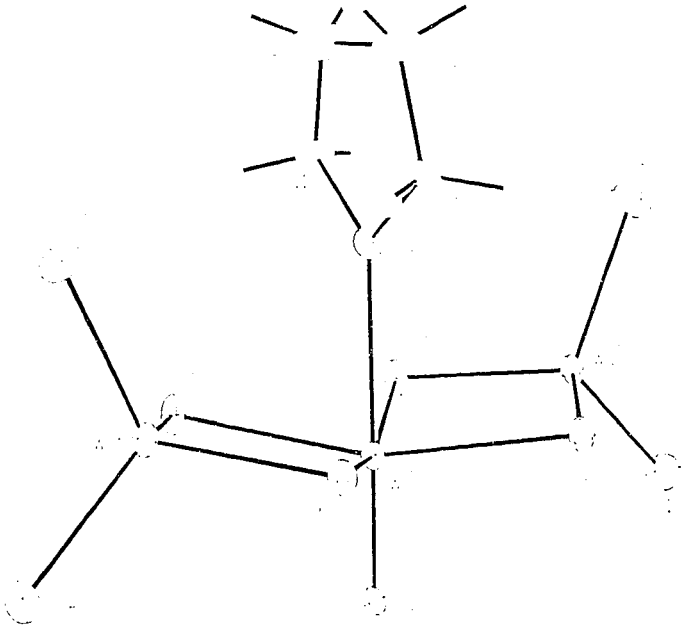

Figure 4.14 ORTEP representation of the anionic portion of $[PPh_4]_2[W_3OS_8(THF)]$ (**17**).

The structure consists of $[PPh_4]^+$ cations and $[W_3OS_8(THF)]^{2-}$ anions, where the THF molecule is coordinated to the central W atom of the anion. The two terminal W atoms are approximately tetrahedral and can be considered as chelating $[WS_4]^{2-}$ ligands on a $[W{=}O]^{2+}$ core. The geometry at the central W is approximately octahedral, with the THF solvate occupying the site *trans* to the terminal oxide. The $[PPh_4]^+$ cations are unremarkable, and show no close contacts with the anions.

Table 4.4 Selected bond distances (Å) and angles (°) for **17.**

W(1)-S(1)	2.437(3)	S(1)-W(1)-S(2)	95.43(10)	S(1)-W(2)-S(2)	105.89(11)
W(1)-S(2)	2.438(3)	S(1)-W(1)-S(5)	81.63(11)	S(1)-W(2)-S(3)	110.22(14)
W(1)-S(5)	2.441(3)	S(1)-W(1)-S(6)	162.33(11)	S(1)-W(2)-S(4)	110.41(14)
W(1)-S(6)	2.427(3)	S(1)-W(1)-O(1)	81.6(2)	S(2)-W(2)-S(3)	110.31(13)
W(1)-O(1)	2.424(7)	S(1)-W(1)-O(2)	100.0(3)	S(2)-W(2)-S(4)	110.43(14)
W(1)-O(2)	1.707(8)	S(2)-W(1)-S(5)	163.01(12)	S(3)-W(2)-S(4)	109.55(17)
		S(2)-W(1)-S(6)	82.31(10)		
W(2)-S(1)	2.259(3)	S(2)-W(1)-O(1)	81.59(18)	S(5)-W(3)-S(6)	105.79(11)
W(2)-S(2)	2.260(3)	S(2)-W(1)-O(2)	98.7(3)	S(5)-W(3)-S(7)	109.48(14)
W(2)-S(3)	2.161(4)	S(5)-W(1)-S(6)	95.40(10)	S(5)-W(3)-S(8)	110.86(13)
W(2)-S(4)	2.105(4)	S(5)-W(1)-O(1)	81.42(19)	S(6)-W(3)-S(7)	110.87(12)
		S(5)-W(1)-O(2)	98.3(3)	S(6)-W(3)-S(8)	109.70(13)
W(3)-S(5)	2.258(3)	S(6)-W(1)-O(1)	80.77(19)	S(7)-W(3)-S(8)	110.06(14)
W(3)-S(6)	2.257(3)	S(6)-W(1)-O(2)	97.6(3)		
W(3)-S(7)	2.163(3)	O(1)-W(1)-O(2)	178.3(3)	W(1)-S(1)-W(2)	79.33(10)
W(3)-S(8)	2.137(4)			W(1)-S(2)-W(2)	79.29(9)
				W(1)-S(5)-W(3)	79.22(9)
				W(1)-S(6)-W(3)	79.54(9)

The terminal W-S bonds have an average length of 2.142Å, whereas the bridging W-S bonds are significantly longer with an average of 2.347Å. The bridging W-S bonds in **17** are very similar in length to those found at the σ-bonded thiolate sulfur in $[PPh_4][WS_3(o\text{-}SCH_2(C_6H_4)CH_2Cl)]$ (**11**), at 2.3307(10)Å. The terminal W-S bonds in **17** also compare favourably with those in **11**, which show an average of 2.155Å. The angles

about the terminal W atoms are approximately tetrahedral, with a slight narrowing between the bridging sulfides due to constrain imposed by the W_2S_2 rings. The central W, with a formal oxidation state of +4, adopts a distorted octahedral arrangement, where the π-bonded terminal oxide shows a significantly shorter W-O distance than the σ-bonded THF molecule. The angles about this central W range from 80.77(19) to 100.0(3)Å.

Within error, the bond distances and angles in **17** are identical to those in the structure of $Cs_2[W_3OS_8(H_2O)]\cdot 2H_2O$ described by Müller *et al.*[64] with the exception of the W-(H_2)O distance which is slightly longer at 2.47(2)Å than at the coordinated THF in **17** at 2.424(7)Å.

A partial structure of $[PPh_4]_2[W_3OS_8(DMF)]$ was previously determined from red crystals obtained from the reaction of $Cl_3W(\mu\text{-}C_4H_8S)_3WCl_3$ with $[PPh_4]_2[WS_4]$ in CH_3CN/DMF.[118] Considerable disorder was observed around the central W atom, making bonding parameters unavailable for comparison with **17**. However, it is likely that the DMF and THF adducts arose from decomposition of alkylated $[WS_4]^{2-}$ in the presence of small amounts of oxygen. This illustrates the sensitivity of these reactions to formation of condensation products, especially if an inert atmosphere is not maintained.

4.3 Attempted Complexation of a Second Metal

As discussed in Chapter 1, there is considerable interest in the chemistry of bimetallic sulfide clusters, commonly investigated with Cu(I), Ag(I) and Fe(II). We were interested to see if our alkylated species could be used as synthons for cluster formation with these metals, in the hope of synthesizing some novel bimetallic thiolato compounds.

When a solution of $AgBF_4$, in CD_3CN, was mixed with a solution of $[PPh_4][WS_3(S(p\text{-}SCH_2(C_6H_4)CH_2Cl)]$ (1:1), in CD_3CN, a red precipitate immediately formed. After removal of the precipitate, ^1H NMR of the remaining solution showed an absence of any methylene signals from alkylated species, but showed a new set of signals attributed to α-chloro-*o*-xylyl disulfide in the methylene region (Figure 4.15). In addition, a multiplet in the phenyl region attributed to $[PPh_4][BF_4]$ was also observed. The methylene signals confirm the possibility that the small signal, labelled F, in Figure 4.8 could either be due to α-chloro-*o*-xylyl disulfide (singlet) or the dithiol (overlapping doublet).

The precipitate showed the same solubility characteristics and physical appearance as that formed in the reaction of $AgBF_4$ and $[PPh_4]_2[WS_4]$, so we believe that, the labile W-S(R) bond is immediately cleaved to allow formation of an Ag/W/S polythiometallate with associated $[PPh_4]^+$ cations, possibly of the formula $[PPh_4][AgWS_4]$.[152] Indeed, the ^1H NMR spectrum of the sparingly soluble precipitate in DMF-d_7 shows an absence of any proton signals except from $[PPh_4]^+$.

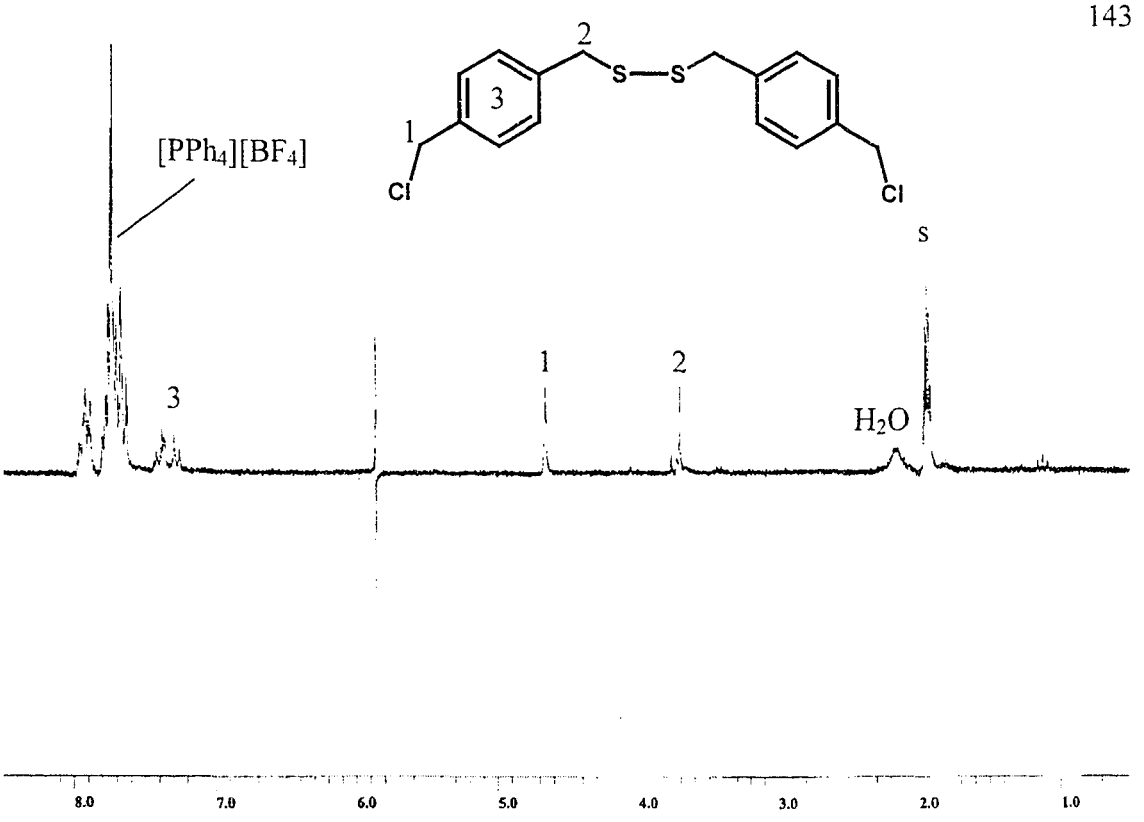

Figure 4.15 ^{1}H NMR spectrum of the reaction mixture from $[PPh_4][WS_3(S(p\text{-}SCH_2(C_6H_4)CH_2Cl)]$ and $AgBF_4$ after removal of precipitate.

When the above reaction was repeated using one molar equivalent of CuCl, a brown precipitate formed on standing and was filtered after 15 minutes to yield a colourless solution. As with the $AgBF_4$ reaction, the only signals observed in the ^{1}H NMR spectrum of the precipitate in DMF-d_7 were due to $[PPh_4]^+$, indicating that no complexed thiolate remained. The filtrate was analyzed by ^{1}H NMR and found to contain predominantly disulfide and small amounts of chloro/thiol.

Finally, attempts were made to react alkylated products with Fe salts. $[PPh_4][WS_3(SBz)]$ was dissolved in DMF-d_7 and $FeCl_2$ (1:1) in DMF-d_7 was injected. A yellow/brown solution immediately formed, which was suggestive that some oxidation of

Fe(II) to Fe(III) had occurred resulting in reduction of W. The ^{1}H NMR spectrum of the solution indicated that no complexed thiolate remained and that Bz_2S_2 and BzSH were the predominant organic decompostion products.

From our preliminary studies we did not pursue metal complexation reactions any further due to the sensitivity of alkylated products to loss of complexed thiolate. However, from the point of view of synthesizing disulfides in high yields, metal complexation may prove a useful strategy.

4.4 Summary

Our ^{1}H NMR spectroscopic studies of the reactions of $[PPh_4]_2[WS_4]$ and alkyl dihalides have shown that bis-alkylation is not a favourable process even when a second halide is suitably located for intramolecular nucleophilic substitution. Instead, formation of novel bridging dithiolate complexes is observed and using time dependent data, the optimum conditions for their isolation could be determined. Using ^{1}H NMR, we have observed a wide variety of organic sulfur-containing decomposition products, which have mostly been identified. The nature of the products formed appears to be dependent on the steric properties of the alkyl dihalide, and in all cases, thiol formation caused by residual water is a predominant process.

We have isolated and characterized monoalkylated and bridged complexes from all three α,α'-dichloroxylene isomers by elemental analysis and ^{1}H NMR. We have obtained an X-ray crystal structure of monoalkylated α,α'-dichloro-*o*-xylene but are yet to obtain one of a bridged complex. Our most recent attempt yielded the structure of

$[PPh_4]_2[W_3OS_8(THF)]$ which illustrated the sensitivity of these compounds to aerial oxidation and consequent polythiometallate formation.

Our attempts to complex a second metal to these alkylated species have unfortunately resulted in the rapid formation of bimetallic sulfides that show an absence of thiolate ligands. The organic fragments are detected in the form of organic sulfides, disulfides and thiols, depending on the reaction conditions.

4.4 Experimental

General Procedures

$[PPh_4]_2[WS_4]$ was prepared as described in Chapter 2. α,α'-Dichloro-*o*-xylene, α,α'-dichloro-*m*-xylene, α,α'-dichloro-*p*-xylene, CuCl and $FeCl_2$ were used as purchased from Aldrich. $AgBF_4$ was used as purchased from Pennwalt Chemicals. Solutions for NMR and crystallization were manipulated under an atmosphere of dry dinitrogen using standard Schlenk and glovebox techniques. Acetonitrile was distilled over P_2O_5 then CaH_2. Diethyl ether and THF were distilled over Na/benzophenone. Solvents were stored over molecular sieves and degassed before use. CD_3CN was stored over molecular sieves under dry dinitrogen before use. Elemental analyses were performed by the University of Calgary, Department of Chemistry, Analytical Services Laboratory. ^1H NMR spectra were recorded using Bruker ACT-200 or AMX-300 spectrometers. Time dependent ^1H-NMR studies were performed on a Bruker AMX-300 spectrometer.

Time Dependent ^1H NMR

A typical experiment involved $[PPh_4]_2[WS_4]$ (5.0 mg, 5.0 μmol) dissolved in *ca.* 0.7ml CD_3CN under dinitrogen in a 5mm tube fitted with a rubber septum. A NMR spectrum of this sample was collected at room temperature. α,α'-Dichloroxylene (4.4 mg, 25 μmol) was dissolved in 100 μl CD_3CN, and after removal of the $[PPh_4]_2[WS_4]$ sample from the spectrometer, the sample was cooled in an ice bath for two minutes and 10 μl of α,α'-dichloroxylene solution (2.5μmol) was injected through the septum. The sample was returned to the spectrometer and allowed to warm to room temperature before commencement of data acquisition at predetermined intervals.

Syntheses of $(PPh_4)[WS_3(SCH_2(C_6H_4)CH_2Cl)]$, o (11), m (12) and p (13)

Synthesis of 11

11 was synthesized by a procedure similar to $[PPh_4][WS_3(SBz)]$ (Chapter 3). $[PPh_4]_2[WS_4]$ (0.102 g, 0.103 mmol) was placed in a Schlenk tube, dissolved in *ca.* 20 ml of CH_3CN then cooled to 0°C. A two-fold excess of α,α'-dichloro-*o*-xylene (0.180 g, 1.03 mmol) was dissolved in *ca.* 5ml CH_3CN then added to the first solution by cannula. The mixture was allowed to warm to room temperature and within 5 minutes the yellow solution had turned red. After two hours the solvent was removed *in vacuo* (Note: the mixture was only pumped until a sticky residue remained as pumping to complete dryness resulted in partial decomposition of **11**). THF (2 × 20ml) was used to extract the red residue to yield a red solution of **11**, leaving $[PPh_4]_2[W_3S_9]$ and unreacted $[PPh_4]_2[WS_4]$ behind. The THF solution was filtered, concentrated to about half its original volume, and placed in crystallization tubes and layered with diethyl ether under

dinitrogen. After 3 days, bright red crystals of crystallographic quality were obtained in a 65 % yield. Anal. Calcd. for $C_{32}H_{28}ClPS_4W$: C, 48.59; H, 3.57. Found C, 49.12; H, 3.71. ^1H NMR (200MHz, CD_3CN): δ 7.99-7.64 (m, 20H, PPh_4^+), 7.41-7.21 (m, 4H, C_6H_4), 4.82 (s, 2H, $ClCH_2$), 4.45 (s, 2H, SCH_2).

Synthesis of 12

12 was synthesized by a procedure similar to **11**, except α,α'-dichloro-*m*-xylene (0.180 g, 1.03 mmol) in CH_3CN, instead of α,α'-dichloro-*o*-xylene, was added at 0°C. The mixture was allowed to warm to room temperature and stirred for 1.5 hours before the solvent was removed *in vacuo*. The residue was extracted with THF (2 × 20ml) to give a red solution and after filtration, the solution was layered with Et_2O and maintained at –20°C for 3 days. Bright red crystals of **12** were obtained in a 69 % yield. Anal. Calcd. for $C_{32}H_{28}ClPS_4W$: C, 48.59; H, 3.57. Found C, 48.71; H, 3.51. ^1H NMR (200MHz, CD_3CN): δ 7.99-7.63 (m, 20H, PPh_4^+), 7.47-7.43 (m, 1H, C_6H_4), 7.40-7.29 (m, 3H, C_6H_4), 4.65 (s, 2H, $ClCH_2$), 4.39 (s, 2H, SCH_2).

Synthesis of 13

13 was synthesized by a procedure similar to **11**, except α,α'-dichloro-*p*-xylene (0.180 g, 1.03 mmol) in CH_3CN, instead of α,α'-dichloro-*o*-xylene, was added at 0°C. The mixture was allowed to warm to room temperature and stirred for 2 hours before the solvent was removed *in vacuo*. The residue was extracted with THF (2 × 20ml) to give a red solution and after filtration, the solution was layered with Et_2O and maintained at –20°C for 3 days. Bright red crystals of **13** were obtained in a 71 % yield. Anal. Calcd.

for $C_{32}H_{28}ClPS_4W$: C, 48.59; H, 3.57. Found C, 48.66; H, 3.43. ^1H NMR (400MHz, CD_3CN): δ 7.96-7.63 (m, 20H, PPh_4^+), 7.33 (br s, 4H, C_6H_4), 4.63 (s, 2H, $ClCH_2$), 4.36 (s, 2H, SCH_2).

Synthesis of $(PPh_4)_2[WS_3(SCH_2(C_6H_4)CH_2S)S_3W]$, o (14), m (15) and p (16)

Synthesis of 14

14 was synthesized by a procedure similar to **11**. $(PPh_4)_2[WS_4]$ (0.122 g, 0.123 mmol) was placed in a Schlenk tube, dissolved in *ca.* 25 ml of CH_3CN then cooled to 0°C. α,α'-Dichloro-*o*-xylene (0.011 g, 0.063 mmol) was dissolved in *ca.* 5ml CH_3CN then added to the first solution by cannula. The mixture was allowed to warm to room temperature and after several hours the solution had turned orange. After 12 hours the solvent was removed *in vacuo* (Note: the mixture was only pumped until a sticky residue remained as pumping to complete dryness resulted in partial decomposition of **14**) and THF (1 × 20 ml) was used to extract the red residue to yield a red solution of **14**, leaving $[PPh_4]_2[W_3S_9]$ and unreacted $[PPh_4]_2[WS_4]$ behind. The THF solution was filtered then concentrated to about a third its original volume, and then diethyl ether (*ca.* 10 ml) was added. An orange solid immediately started to precipitate and the mixture was left to stand for 30 minutes. The precipitate formed a layer on the inside of the flask and the solution was removed by cannula. The solid was redissolved in *ca.* 15 ml of CH_3CN, then placed in crystallization tubes and layered with diethyl ether under dinitrogen. After 7 days at –20°C, a bright red microcrystalline solid was obtained in a 23% yield. Anal. Calcd. for $C_{56}H_{48}P_2S_8W_2$: C, 47.80; H, 3.44. Found C, 48.12; H, 3.51. ^1H NMR

(200MHz, CD_3CN): δ 7.99-7.62 (m, 20H, PPh_4^+), 7.33-7.14 (m, 4H, C_6H_4), 4.42 (s, 4H, SCH_2).

Synthesis of 15

15 was synthesized by a procedure similar to **14**, except that α,α'-dichloro-*m*-xylene was used. The reaction was allowed to stir at room temperature for 12 hours before the solvent was removed *in vacuo.* After the THF extraction, and addition of Et_2O, the resultant red solid was isolated by filtration, redissolved in *ca.* 15 ml of CH_3CN, placed in crystallization tubes and layered with diethyl ether under dinitrogen. After 7 days at −20°C, a bright red microcrystalline solid was obtained in a 25% yield. Anal. Calcd. for $C_{56}H_{48}P_2S_8W_2$: C, 47.80; H, 3.44. Found C, 48.21; H, 3.49. ^1H NMR (200MHz, CD_3CN): δ 7.98-7.60 (m, 20H, PPh_4^+), 7.33-7.28 (m, 1H, C_6H_4), 7.26-7.19 (m, 3H, C_6H_4), 4.31 (s, 4H, SCH_2).

Synthesis of 16

16 was synthesized by a procedure similar to **14**, except that α,α'-dichloro-*p*-xylene was used. The reaction was allowed to stir at room temperature for 10 hours before the solvent was removed *in vacuo.* After the THF extraction, and addition of Et_2O, the resultant orange solid was isolated by filtration, redissolved in *ca.* 15 ml of CH_3CN, placed in crystallization tubes and layered with diethyl ether under dinitrogen. After 7 days at -20°C, bright red crystals were obtained in a 44% yield. Anal. Calcd. for $C_{56}H_{48}P_2S_8W_2$: C, 47.80; H, 3.44. Found C, 47.80; H, 3.37. ^1H NMR (400MHz, CD_3CN): δ 7.95-7.63 (m, 20H, PPh_4^+), 7.22 (s, 4H, C_6H_4), 4.32 (s, 4H, SCH_2).

Crystal Structure Determinations for 11 and 17

X-ray crystallography was performed by Dr. Robert McDonald at University of Alberta, Department of Chemistry. Crystals of **11** and **17** were coated in Paratone-8277 oil and then mounted on a glass fibre. Data were collected on **11** using a Bruker P4/RA diffractometer and on **17** using a Bruker PLATFORM diffractometer, in both cases with a SMART 1000 CCD detector, using monochromated Mo Kα radiation at –80°C. Programs for diffractometer operation, data collection, data reduction and absorption correction were those supplied by Bruker. Data were integrated to a maximum 2θ value of 52.80° for **11** and 52.82° for **17**. The data were corrected for absorption through use of the *SADABS* procedure. The structure of **11** was solved using the *DIRDIF-96* program system,[146] while the solution for **17** was obtained though use of the program *SHELXS-86*.[145] The structure refinements were completed by subsequent Fourier syntheses and refined using full-matrix least-squares methods.[147] All non-hydrogen atoms were refined anisotropically and all hydrogen atoms were placed in idealized positions.

Complexation Reaction of $AgBF_4$ and $[PPh_4][WS_3(S(p\text{-}SCH_2(C_6H_4)CH_2Cl)]$(11)

11 (5.0mg, 6.3μmol) was dissolved in ca. 0.7ml CD_3CN under dinitrogen and a ^1H NMR spectrum was collected. $AgBF_4$ (12mg, 63μmol) was dissolved in CD_3CN (100μl) under dinitrogen then a 10μl aliquot was injected into the solution of **11**. Immediately a dark red precipitate started to form, which was filtered off under dinitrogen, leaving a clear colourless solution. The solution was analyzed by ^1H NMR

spectroscopy, and showed signals due to (p-$SCH_2(C_6H_4)CH_2Cl)_2$. The precipitate was dissolved in DMF-d_7 and showed only $[PPh_4]^+$ signals in its ^1H NMR spectrum.

Complexation Reaction of CuCl and [PPh$_4$][WS$_3$(S(p-SCH$_2$(C$_6$H$_4$)CH$_2$Cl)](11)

11 (5.0mg, 6.3μmol) was dissolved in ca. 0.7ml CD_3CN under dinitrogen and a ^1H NMR spectrum was collected. CuCl (6.0mg, 63μmol) was dissolved in CD_3CN (100μl) under dinitrogen then a 10μl aliquot was injected into the solution of **11**. Immediately a brown precipitate started to form, which was left to stand for 15 minutes then filtered under dinitrogen. The resultant clear colourless solution was analyzed by ^1H NMR spectroscopy, and showed signals due to (p-$SCH_2(C_6H_4)CH_2Cl)_2$ and p-$HSCH_2(C_6H_4)CH_2Cl$. The precipitate was dissolved in DMF-d_7 and showed only $[PPh_4]^+$ signals in its ^1H NMR spectrum.

Complexation Reaction of FeCl$_2$ and [PPh$_4$][WS$_3$(SBz)] (9)

9 (5.0mg, 6.7μmol) was dissolved in ca. 0.7ml DMF-d_7 under dinitrogen and a ^1H NMR spectrum was collected. $FeCl_2$ (8.5mg, 67μmol) was dissolved in DMF-d_7 (100μl) under dinitrogen then a 10μl aliquot was injected into the solution of **9**. Immediately a yellow/brown solution formed, which was analyzed by ^1H NMR spectroscopy. The signals observed were assigned to $[PPh_4]^+$, Bz_2S_2 and BzSH.

Chapter 5 – Multinuclear NMR Spectroscopic Studies of $[PPh_4]_2[ME_4]$ (M = Mo, W and E = S, Se) and their Alkylation Reactions

5.1 Introduction

Alkylation studies have previously been performed using $[PPh_4]_2[MoS_4]$ with EtBr and ^{t}BuBr,[118] and have shown higher reactivity compared to the analogous W system. This has made isolation of an alkylated Mo intermediate quite difficult, though the compound $[PPh_4][MoS_3(S^tBu)]$ has been successfully isolated and characterized by X-ray crystallography.[58] Reactions of $[PPh_4]_2[WSe_4]$ with EtBr were also previously investigated and were found to yield a variety of organic selenides.[118] No alkylated species could be isolated under the reaction conditions used and as a result the research was not pursued further.

Based on the higher stability of the BzCl reaction products with $[PPh_4]_2[WS_4]$ and the ease with which they can be followed using ^{1}H NMR, we decided to revisit studies of $[PPh_4]_2[MoS_4]$ and $[PPh_4]_2[WSe_4]$ using BzCl. In addition to using ^{1}H NMR spectroscopy, we hoped to take advantage of the additional handles of ^{95}Mo and ^{77}Se NMR spectroscopy to observe the reaction products *in situ*. The nuclear properties of the two nuclei are shown below.[110]

Table 5.1 NMR parameters for ^{95}Mo and ^{77}Se nuclei.[110]

Nucleus	^{95}Mo	^{77}Se
Spin (I)	5/2	1/2
Natural Abundance (%)	15.72	7.58
Quadrupole moment	0.12	------
Receptivity/^{13}C	2.88	2.98

The table above shows that while the relative receptivity of the two nuclei is comparable, the natural abundance of the ^{95}Mo nuclei is twice that of ^{77}Se. However, the quadrupolar moment of ^{95}Mo makes acquisition times longer compared to ^{77}Se due to significant line broadening. The long acquisition times required for compounds of the formula $[PPh_4]_2[MO_xS_{4-x}]$ (M = Mo, W; x = 0-2) in CD_3CN (Chapter 2) led us to chose DMF-d_7 as a solvent for our multinuclear NMR spectroscopic alkylation studies to improve the concentration of starting materials and products.

Stiefel and coworkers have reported similarities in the reactivities of $[MoS_4]^{2-}$ and $[WSe_4]^{2-}$ with organic disulfides,[73,74] forming M(V) mononuclear complexes with coordinated $[E_2]^{2-}$ ligands in contrast to reactions of $[WS_4]^{2-}$ which show no reduction at the metal centre. These examples of internal electron transfer reactions, initiated by an external oxidant, illustrate that W tends not to accept an electron from a coordinated sulfide ligand in contrast to Mo centres with coordinated sulfides, which are more readily reduced. Moving down the group to selenides facilitates reduction at the W centre. It is clear from our studies that alkylated $[WS_4]^{2-}$ can be isolated at room temperature but that the analogous $[MoS_4]^{2-}$ and $[WSe_4]^{2-}$ alkylated products rapidly decompose with reduction at the metal. Consequently, we were interested to discover whether the reaction pathways of $[MoS_4]^{2-}$ and $[WSe_4]^{2-}$ were the same, and whether we could determine the optimum reaction conditions for isolation of their benzylated products.

5.2 Reactions of $[PPh_4]_2[ME_4]$ (M = Mo, W and E = S, Se) with BzCl

5.2.1 $[PPh_4]_2[WS_4]$

Since the reactions with $[PPh_4]_2[MoS_4]$ and $[PPh_4]_2[WSe_4]$ were to be carried out using DMF-d_7 on an NMR scale, but CH_3CN on a synthetic scale, we felt it would be

appropriate to follow the reaction of $[PPh_4]_2[WS_4]$ and BzCl in DMF-d_7 to determine whether any differences in reaction products were observed compared to the CD_3CN scheme shown in Figure 3.2.

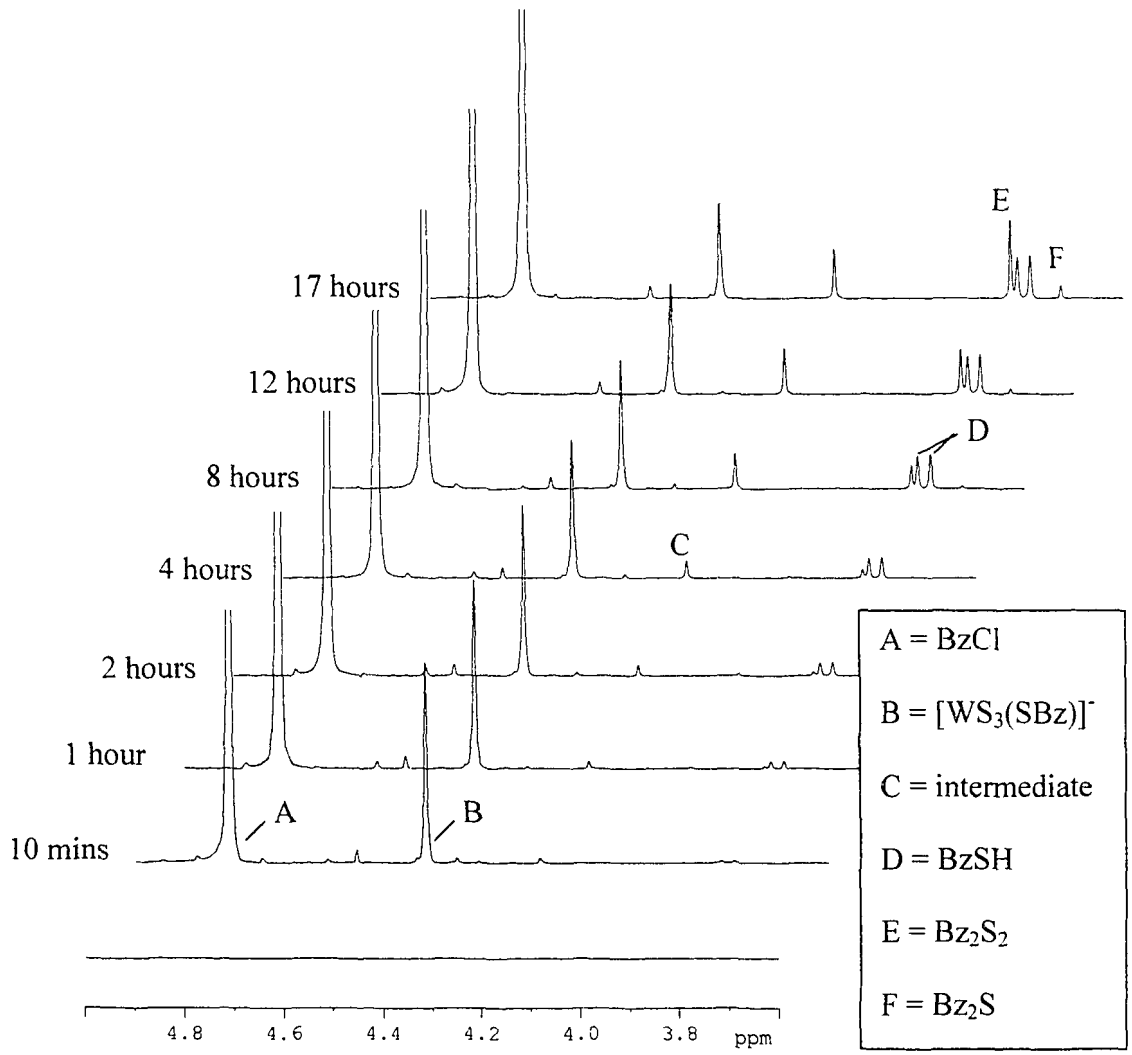

Figure 5.1 Time dependent ^1H NMR spectra from the reaction of $[PPh_4]_2[WS_4]$ and BzCl (1:10) in DMF-d_7.

After accounting for a slight variation in chemical shift due to different solvent effects, we can see that the decomposition products are the same as those observed when

the reaction is performed in CD_3CN, with benzyl thiol being the major organic species. This allows us to be confident that if we determine the optimum reaction conditions for benzylation of $[PPh_4]_2[MoS_4]$ or $[PPh_4]_2[WSe_4]$ in DMF-d_7, these should also apply to the reaction on a synthetic scale in CH_3CN.

In order for us to be able to observe the alkylated product from the reaction of $[PPh_4]_2[MoS_4]$ and BzCl using ^{95}Mo NMR spectroscopy, we first needed to determine the approximate chemical shift window in which the signal would appear. Since there is a linear correlation between ^{183}W and ^{95}Mo chemical shifts, we were able to predict where the ^{95}Mo signal would appear based on the chemical shift of an analogous W species. Attempts to measure the ^{183}W NMR chemical shift using crystals of alkylated species were not successful due to difficulty in obtaining a high enough concentration in solution to observe a signal. In addition, due to the lack of a low temperature capability of this particular NMR probe, some samples decomposed too rapidly to observe a signal. Since this probe did not require a deuterated solvent in sample preparation, we decided to take advantage of this fact and place the concentrated THF extract from the reaction work-up directly in an NMR tube. Using this approach we were able to measure the chemical shifts of $[PPh_4][WS_3(SBz)]$ and $[PPh_4][WS_3(S^iBu)]$ as 3712 and 3708ppm, respectively.

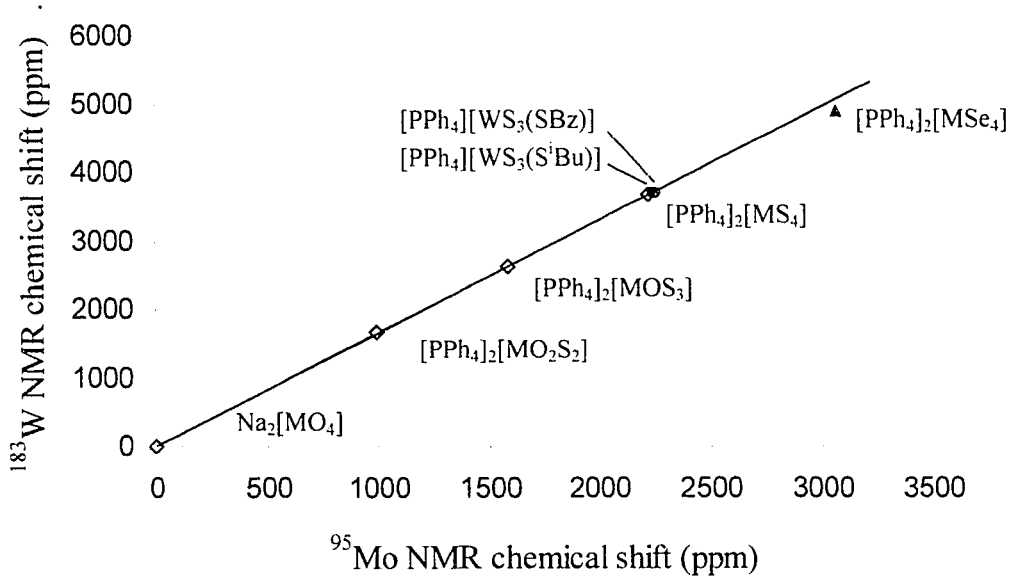

Figure 5.2 Graph representing linear correlation between ^{95}Mo and ^{183}W chemical shifts and extrapolation to predict unknown values.

The chemical shifts for oxothiometallates shown in Figure 5.2 show a linear correlation due to the identical conditions under which data for the respective W and Mo salts were collected. The point representing $[PPh_4]_2[MSe_4]$ is slightly further from the best fit line since different solvents were used for data collection in the W versus the Mo salt. Our data for $[PPh_4][WS_3(SBz)]$ and $[PPh_4][WS_3(S^iBu)]$ were collected at room temperature in THF solvent. If identical conditions were used for ^{95}Mo NMR data acquisition, the signal for $[PPh_4][MoS_3(SBz)]$ would fall at 2242ppm. Variations in solvent alone have shown chemical shift differences of up to 70ppm for $[Et_4N]_2[MoS_4]$,[73] and variation in temperature is also known to significantly affect the chemical shift observed.[108]

5.2.2 $[PPh_4]_2[MoS_4]$

^{95}Mo and ^{1}H NMR data were collected during the reaction of $[PPh_4]_2[MoS_4]$ with a 10-fold excess of BzCl at –20°C. Each ^{95}Mo spectrum was collected over one hour and the ^{1}H spectra in Figure 5.3 were collected over 45 seconds in between each ^{95}Mo data set, making the ^{1}H spectra true snapshots of the reaction and the ^{95}Mo spectra an average over each hour.

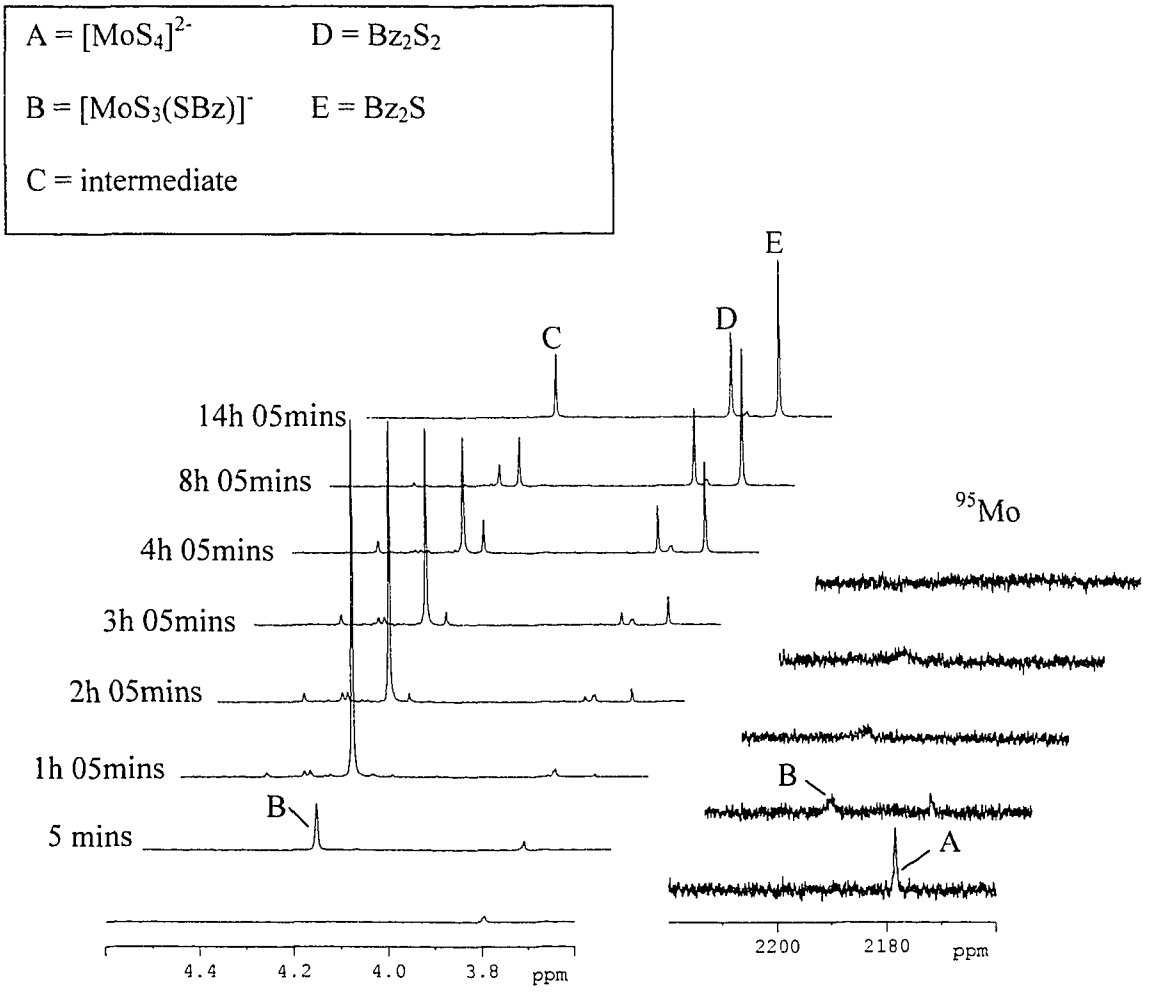

Figure 5.3 Time dependent ^{1}H and ^{95}Mo NMR spectra for the reaction of $[PPh_4]_2[MoS_4]$ and BzCl (1:10) in DMF-d_7 at –20°C.

At the beginning of the experiment, a signal is observed in the ^{95}Mo NMR spectrum corresponding to $[PPh_4]_2[MoS_4]$ at 2178ppm. After injection of BzCl, this signal rapidly disappears and a small broad signal starts to appear at 2197ppm which is well within the range predicted for $[MoS_3(SBz)]^-$. The broadening is expected since the level of symmetry at the metal centre has been reduced. After 4 hours, no trace of this signal can be seen, which correlates to the signal assigned to $[MoS_3(SBz)]^-$ in the ^{1}H NMR spectra at 4.27ppm (signal B). Signal B is at a maximum after approximately one hour, giving the optimum time for isolation of the product from a synthetic scale reaction. Decomposition products start to appear 2 hours into the reaction, with formation of Bz_2S and an intermediate (signal C), which we believe to be a polynuclear Mo species with a coordinated thiolate ligand. Bz_2S_2 also starts to be formed, though Bz_2S remains the major organic sulfur containing product. BzSH is notably absent from the reaction in contrast to the analogous reactions with $[WS_4]^{2-}$, indicating that under the above reaction conditions, residual water does not enhance decomposition of Mo alkylated products. After 14 hours, no alkylated product remains in solution.

Attempts were made to isolate $[PPh_4][MoS_3(SBz)]$ from synthetic scale reactions performed in CH_3CN at –20°C since this solvent is easier than DMF to remove during the work-up procedure. Our studies of $[PPh_4]_2[WS_4]$ and BzCl in CH_3CN versus DMF indicated that the solvent did not significantly change the reaction products formed and, as a result, we were confident in using CH_3CN. However, we consistently encountered significant decomposition of the THF extract with large yields of insoluble black MoS_2/MoS_3. Attempts were made to extract the reaction mixture residue with THF-d_8, after removal of CH_3CN, and immediately perform ^{1}H NMR spectral analysis. However,

this only showed signals corresponding to organic sulfides and $[PPh_4]^+$ (presumably from polythiomolybdates), even when the sample was maintained at low temperature. We also attempted the synthesis in DMF solvent, with precipitation of products by Et_2O after an hour, and filtration and extraction of the solid with THF. Again, black precipitates formed readily and the THF extract was almost colourless.

While we can certainly observe significant quantities of alkylated product *in situ* using both ^1H and ^{95}Mo NMR spectroscopy, we have so far been unsuccessful in isolating this product and characterizing it separately.

5.2.3 $[PPh_4]_2[WSe_4]$

In the related tetraselenotungstate system, we have performed time dependent NMR studies using the ^1H and ^{77}Se nuclei. The narrower linewidths of ^{77}Se compared to ^{95}Mo signals allowed us to acquire suitable spectra over shorter time periods; each spectrum was collected in 30 minutes. Unfortunately, due to the long acquisition times and high concentration requirements for ^{183}W NMR data, we were unable to measure the ^{183}W chemical shift of alkylated $[WSe_4]^{2-}$.

A = $[WSe_4]^{2-}$	C = Bz_2Se_2
B = $[WSe_3(SeBz)]^-$	D = Bz_2Se

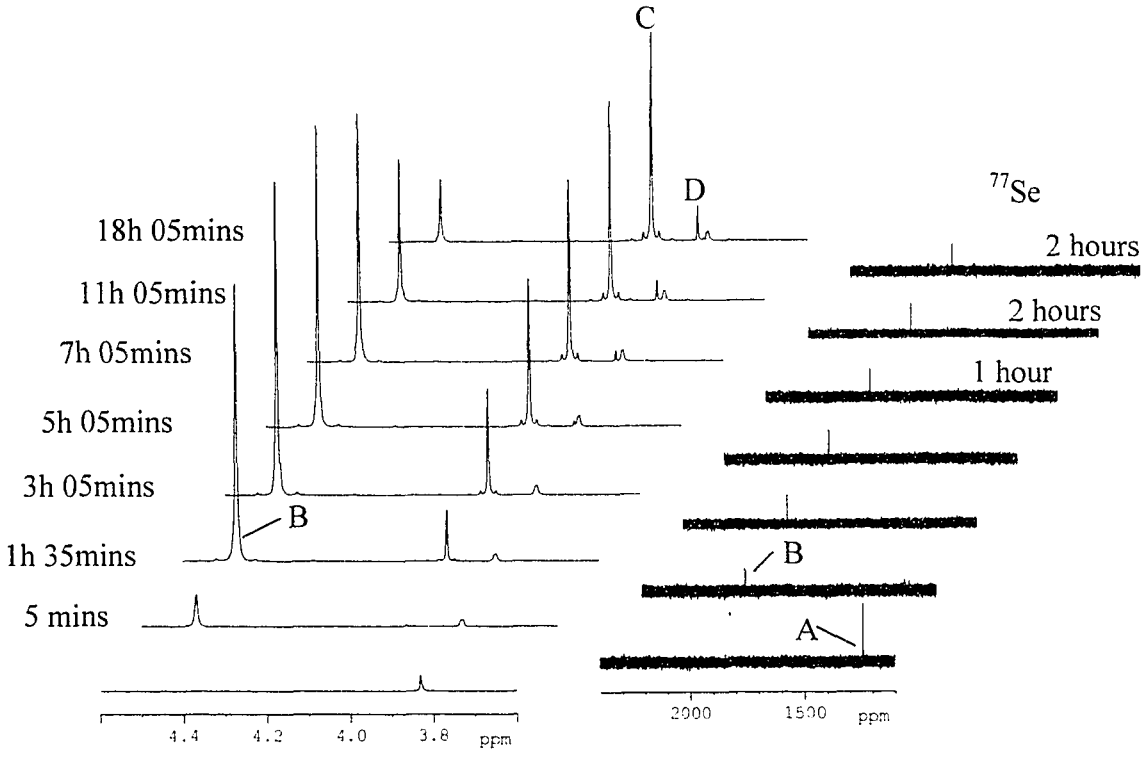

Figure 5.4 Time dependent ^1H and ^{77}Se NMR spectra for the reaction of $[PPh_4]_2[WSe_4]$ and BzCl (1:10) in DMF-d_7 at –20°C.

The first ^{77}Se NMR spectrum shows a signal at 1243ppm corresponding to the four equivalent terminal selenides in $[WSe_4]^{2-}$ ($^1J_{WSe}$ = 48Hz). On addition of BzCl, each subsequent ^{77}Se spectrum was collected over 30 minutes, except for the last three which were collected over 1 or 2 hours as indicated in Figure 5.4, to allow detection of the

signal as it became less intense. Each of these spectra were collected at the times indicated on the left side of the figure and it can clearly be seen that a new signal corresponding to the three equivalent terminal selenides in $[WSe_3(SeBz)]^-$ is observed. This ^{77}Se signal correlates to the methylene signal (B) observed at 4.47ppm in the ^1H NMR spectra, which is at a maximum after 3 hours. No W-Se satellites could be seen for signal B in the ^{77}Se NMR spectra, though broadening at the base of the signal was observed, suggesting their presence. In addition, no resolved Se-H satellites were observed for signal B in the ^1H NMR spectrum, though distinct shoulders separated by approximately 6Hz were seen.

The only decomposition products observed are Bz_2Se_2 and later Bz_2Se, which exhibit $^2J_{SeH}$ values of 15 and 12Hz, respectively. When following the above reaction by ^{77}Se NMR in the range of 500-0ppm, we observe the corresponding signals of the Bz_2Se_2 and Bz_2Se at 331 and 395ppm, respectively. We have attempted to locate the selenolate Se resonance of $[WSe_3(SeBz)]^-$ in this chemical shift region without success, even when using ^1H-decoupled data acquisition. Problems with ^1H-decoupling have previously been reported due to unwanted heating effects, which can alter the chemical shift and result in broadened signals.[80] This observation may account for our inability to locate the selenolate signal in ^1H-decoupled ^{77}Se spectra.

We attempted to isolate $[PPh_4][WSe_3(SeBz)]$ from synthetic scale reactions in acetonitrile after 3 hours of stirring $[PPh_4]_2[WSe_4]$ and a 10-fold excess of BzCl at –20°C. The outcome of our endeavours was the same as for $[PPh_4]_2[MoS_4]$ reactions, and we were only able to isolate insoluble black precipitates of WSe_2/WSe_3.

5.2.4 $[PPh_4]_2[MoSe_4]$

To follow alkylation reactions of the highly reactive $[MoSe_4]^{2-}$ ion we chose to perform our reactions at –30°C to stabilize the alkylated species. In order to increase our chances of observing the rapidly decomposing alkylated species, we chose to follow the reaction by ^{77}Se instead of ^{95}Mo NMR spectroscopy. Under these conditions we had hoped to detect a ^{77}Se signal for $[MoSe_3(SeBz)]^-$ if present in large enough concentrations.

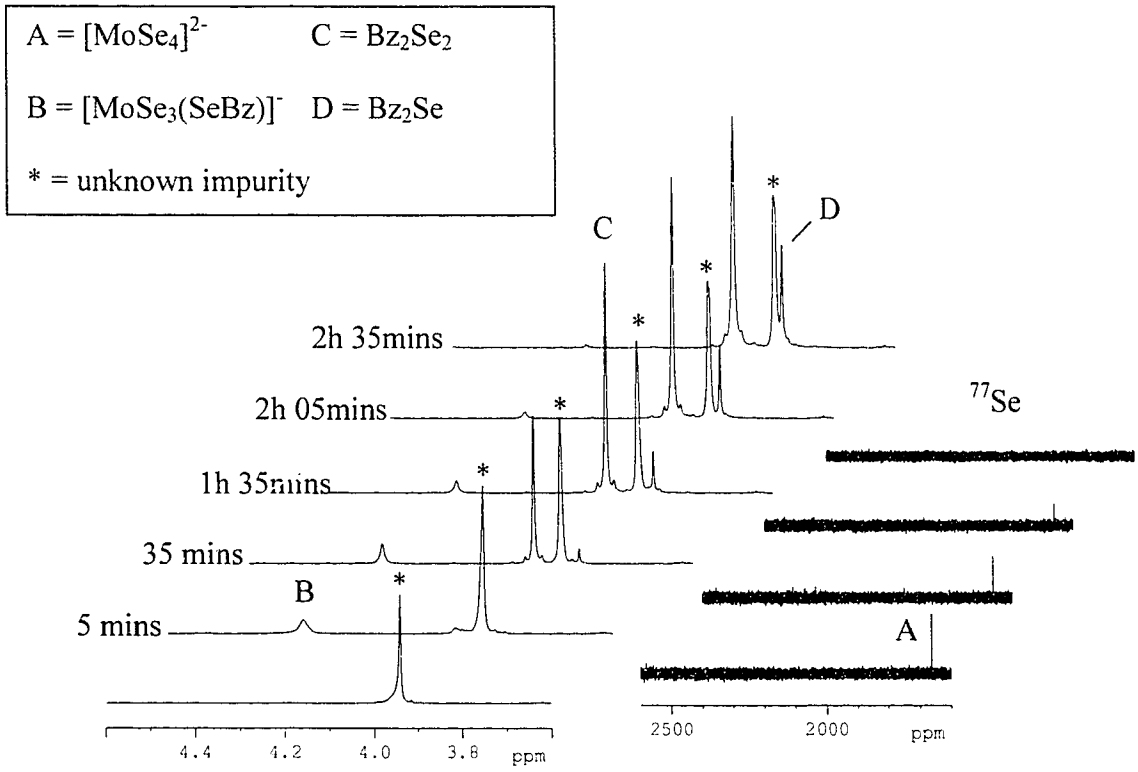

Figure 5.5 Time dependent ^1H and ^{77}Se NMR spectra for the reaction of $[PPh_4]_2[MoSe_4]$ and BzCl (1:10) in DMF-d_7 at –30°C.

We can clearly see from the ^{77}Se spectra that $[MoSe_4]^{2-}$ is being consumed (signal A), but we see no other signals at a higher chemical shift due to $[MoSe_3(SeBz)]^-$. When

we examine the ^{1}H NMR spectra, we see that the amount of $[MoSe_3(SeBz)]^-$ in solution is very small, so it is not surprising that we are unable to observe this species by ^{77}Se NMR. The first organic decomposition formed in solution is Bz_2Se_2 (signal C) and with time we see the formation of Bz_2Se (signal D).

After only two and a half hours, almost no trace of $[MoSe_3(SeBz)]^-$ remains. In the hope of preventing such rapid decomposition, we attempted to perform the experiment at –40°C but found that no reaction occurred until the solution was warmed. Due to the extremely low yields of $[PPh_4][MoSe_3(SeBz)]$ in solution, we did not attempt to isolate this product on a synthetic scale.

5.2.5 $[PPh_4]_2[MoS_4]$ and $[PPh_4]_2[WSe_4]$

Since reactions of $[PPh_4]_2[MoS_4]$ or $[PPh_4]_2[WSe_4]$ with BzCl occur under similar conditions, we were interested in investigating whether the stability of the alkylated products would be altered in the presence of each other. Also, we wanted to see whether cross products would be formed by decomposition, which might also yield mixed Mo/W polymetallates. Using an equal molar ratio of $[PPh_4]_2[MoS_4]$ to $[PPh_4]_2[WSe_4]$, we followed reactions at –20°C by ^{1}H and ^{77}Se NMR, where each ^{77}Se spectrum was collected over one hour due to the lower concentration of $[PPh_4]_2[WSe_4]$ used compared to our previous experiments.

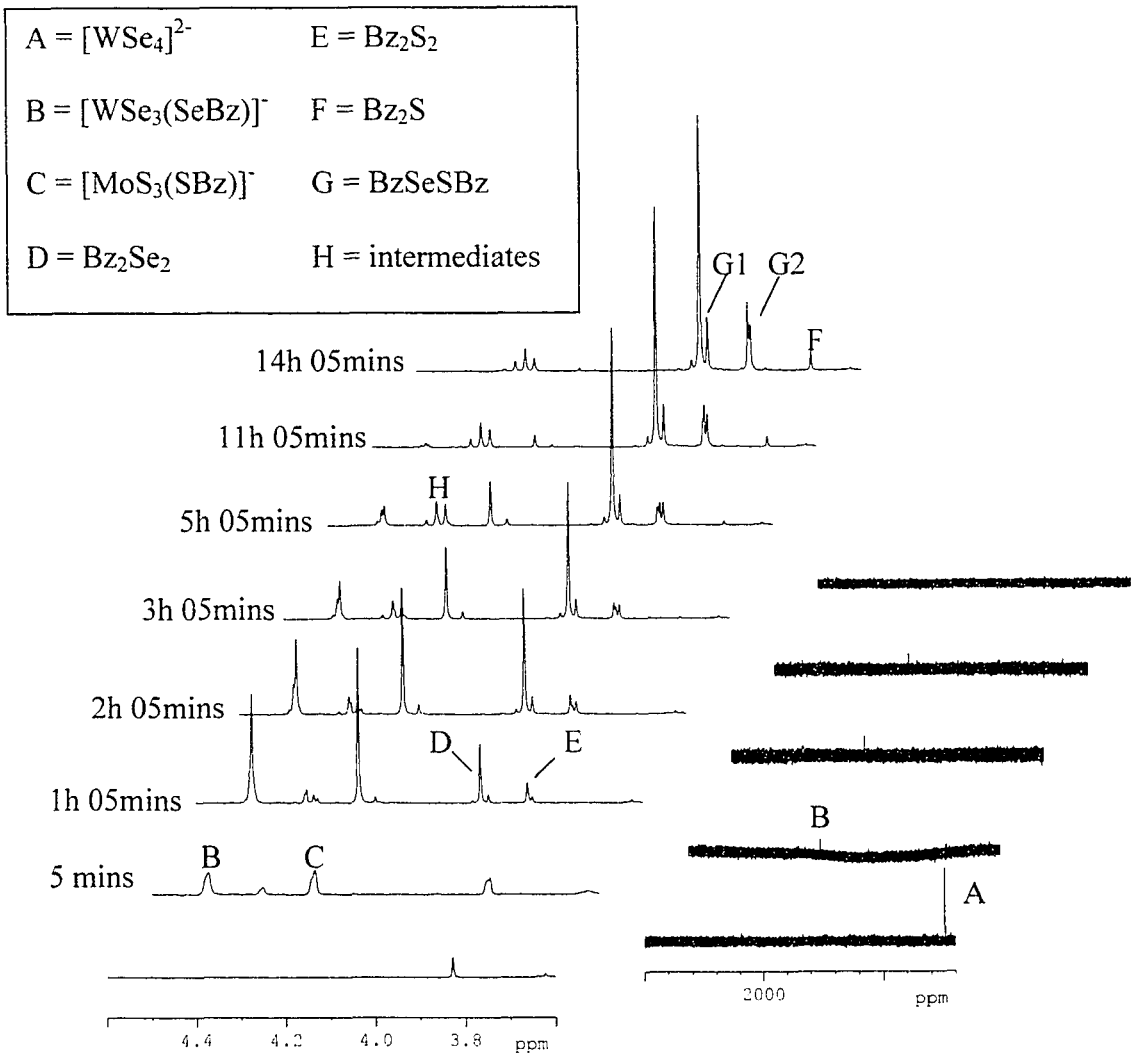

Figure 5.6 Time dependent ^{1}H and ^{77}Se NMR spectra for the reaction of $[PPh_4]_2[MoS_4]$ and $[PPh_4]_2[WSe_4]$ with BzCl (1:1:20) in DMF-d_7 at –20°C.

From the ^{77}Se NMR spectra it is immediately evident that $[WSe_4]^{2-}$ is being consumed and formation of alkylated product is occurring. However, compared to reactions performed in the absence of $[MoS_4]^{2-}$, the intensity of each $[WSe_3(SeBz)]^-$ signal (signal B) in the ^{77}Se NMR spectra is much lower than the initial $[WSe_4]^{2-}$ signal. In addition, the ^{1}H NMR spectra show that $[WSe_3(SeBz)]^-$ is almost completely absent

from the solution after only 5 hours. The ^{1}H NMR spectra show that $[MoS_3(SBz)]^-$ also decomposes more rapidly under these conditions than in the absence of $[WSe_4]^{2-}$. The major organic decomposition products for $[MoS_3(SBz)]^-$ are Bz_2S_2 and Bz_2S, but for $[WSe_3(SeBz)]^-$ only Bz_2Se_2 is observed. Another interesting point is that the integration of Bz_2Se_2 in solution at the end of the experiment far exceeds that of Bz_2S_2 and Bz_2S combined, suggesting that not all $[MoS_4]^{2-}$ was consumed by alkylation. In this region we observe a set of two singlets that correspond to BzSeSBz, where the downfield resonance (signal G1) is due to the methylene protons adjacent to Se. Finally, a set of signals at *ca.* 4.32ppm is observed throughout the experiment and we are uncertain of their origin. Our best explanation is that they correspond to intermediates in the decomposition of both alkylated products and may be due to coordinated thiolate or selenolate ligands on mixed polyselenothiometallates.

5.3 Differences in the Reactions of $[ME_4]^{2-}$ (M = Mo, W; E = S, Se) with BzCl

Certain trends can be seen in the chemical shift data of the tetrathio- and tetraselenometallates, and their respective alkylated products. These are summarized in the following table.

Table 5.2 (a)-(c) Chemical shifts (δ, ppm) for $[PPh_4]_2[ME_4]$ (M = Mo, W; E = S, Se) and $[PPh_4][ME_3(EBz)]$ (M = Mo, W; E = S, Se).

(a) ^{183}W and ^{95}Mo NMR chemical shifts for $[PPh_4]_2[ME_4]$ in ppm

	M = W, δ ^{183}W	M = Mo, δ ^{95}Mo
$[MS_4]^{2-}$	3658 (CH_3CN, RT)	2212 (CD_3CN, RT)
$[MSe_4]^{2-}$	4871 (DMF, RT)	3060 (CD_3CN, RT)

(b) ^{77}Se NMR chemical shifts for $[PPh_4]_2[MSe_4]$ and $[PPh_4][MSe_3(SeBz)]$ in ppm

	M = W, δ ^{77}Se	M = Mo, δ ^{77}Se
$[MSe_4]^{2-}$	1243 (DMF-d_7, –20°C)	1664 (DMF-d_7, –30°C)
$[MSe_3(SeBz)]^-$	1944 (DMF-d_7, –20°C)	not observed

(c) ^1H NMR chemical shifts of methylene protons for $[PPh_4][MS_3(SBz)]$ and $[PPh_4][MSe_3(SeBz)]$ in ppm

	M = W, δ ^1H (CH_2)	M = Mo, δ ^1H (CH_2)
$[MS_3(SBz)]^-$	4.41 (DMF-d_7, RT)	4.23 (DMF-d_7, –20°C)
$[MSe_3(SeBz)]^-$	4.47 (DMF-d_7, –20°C)	4.30 (DMF-d_7, –30°C)

Moving from terminal thio- to seleno-ligands on the metal centre results in a more downfield chemical shift for both the ^{183}W and ^{95}Mo nuclei. This same trend is observed when moving from oxo- to thio-ligands as illustrated in Figure 5.2, and is somewhat counter intuitive based on the electronegativities of the chalcogen ligands involved. The shielding in nuclei such as ^{183}W and ^{95}Mo is not easily predicted compared to lighter elements due to the significant paramagnetic shielding contribution caused in part by non-spherical electron density distribution at the nucleus. The chemical shifts in $[MO_xS_{4-x}]^{2-}$ ions have been predicted based on their average excitation energy, ΔE.[108] As ΔE

decreases, so does the paramagnetic shielding, resulting in more intensely coloured salts at higher chemical shifts.

^{77}Se chemical shifts can be predicted more readily based on the electron withdrawing effects of nearby atoms.[80] In Table 5.2(b) we see a downfield shift for $[MSe_4]^{2-}$ moving from W to Mo, and also a downfield shift for the terminal selenides in $[WSe_3(SeBz)]^-$ compared to $[WSe_4]^{2-}$. One explanation for these observations is that the dπ-pπ orbital overlap for W-Se is less favourable for electron density to be donated to the metal, causing more shielding at Se.[50] This is reflected in the greater stability of W to reduction, compared to Mo, particularly with respect to induced internal redox reactions.[73,74] The greater ^{77}Se terminal selenide deshielding observed in $[WSe_3(SeBz)]^-$ compared to $[WSe_4]^{2-}$ might be explained by the change of terminal selenide formal bond order from 1.5 to 1.67 upon alkylation, causing greater π-overlap of Se with W and consequently more donation to the metal.

Table 5.2(c) illustrates that the methylene protons in $[ME_3(EBz)]^-$ are more deshielded when adjacent to Se versus S, which is reflected in the downfield ^{1}H chemical shifts for organic di(selenides) versus di(sulfides). When the metal in $[ME_3(EBz)]^-$ changes from W to Mo, the chemical shift moves upfield. If related back to the argument for ^{77}Se chemical shifts, Mo withdraws more electron density than W due to the more favourable π-overlap of the metal with terminal selenides. The M-Se(R) bond is predominantly of σ-character, so less of an electron withdrawing effect is felt on the Se and methylene protons, and when M = Mo, this effect is even more pronounced.

On the surface, it appears that despite our predictions of $[MoS_4]^{2-}$ and $[WSe_4]^{2-}$ showing similar reactivity with alkyl halides, we actually observe distinct differences in

their NMR spectral data. By comparing both reactions at the same temperature and in the same solvent, we see that alkylated $[WSe_3(SeBz)]^-$ remains in solution after 18 hours, whereas $[MoS_3(SBz)]^-$ has almost completely disappeared after only 8 hours. Another difference is that the major organic decomposition product in the $[MoS_4]^{2-}$ reactions is benzyl sulfide, in contrast to benzyl *di*selenide from reactions of $[WSe_4]^{2-}$. This suggests two possibilities: a) a different decomposition mechanism is occurring in reactions of each of the above anions, or b) some of the decomposition products that are formed in solution are subsequently reacting with other species and reducing their observed concentration.

Stiefel *et al.* have reported that $[MoS_4]^{2-}$ readily reacts with R_2S_2 in DMF at 90°C, resulting in formation of $[Mo_2S_8]^{2-}$ and $[RS]^-$.[73,74] At -20°C we have observed that $[MoS_4]^{2-}$ reacts with Bz_2S_2, generating a new signal at 3.60ppm, corresponding to $[BzS]^-$. In our alkylation reactions of $[MoS_4]^{2-}$ with BzCl, any Bz_2S_2 formed by decomposition of $[MoS_3(SBz)]^-$ likely further reacts with remaining $[MoS_4]^{2-}$ and forms $[BzS]^-$. Since we do not observe a signal at 3.60ppm, we proposed that the highly reactive $[BzS]^-$ attacks $[MoS_3(SBz)]^-$, either at the Mo-S bond[24] or the S-C bond,[130] and forms polythiometallates and either Bz_2S and/or more Bz_2S_2. As a result, the concentration of $[MoS_3(SBz)]^-$ in solution appears to decrease and the amount of Bz_2S_2 formed appears to be less than Bz_2S.

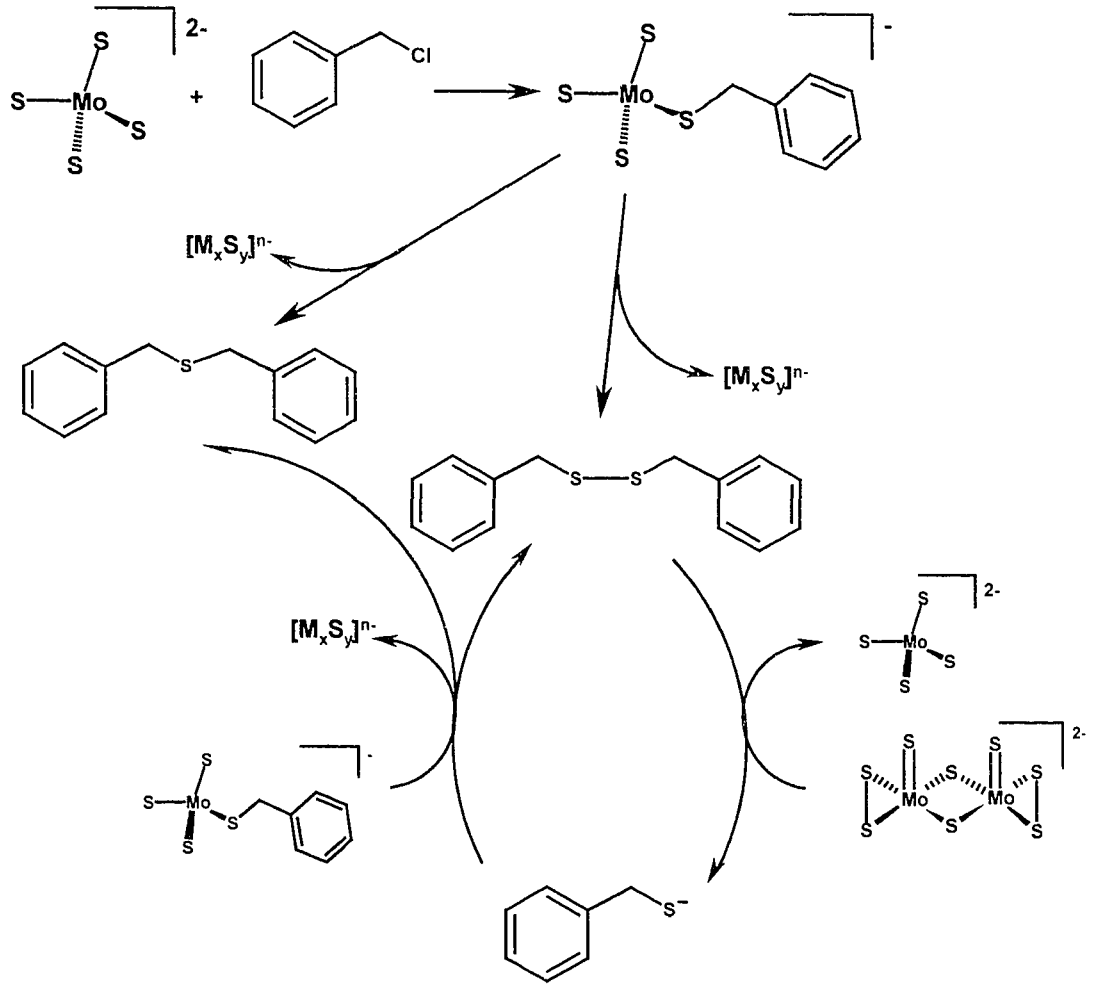

Scheme 5.1 Proposed reaction pathway for the alkylation of $[PPh_4]_2[MoS_4]$ with BzCl.

While the reaction of $[WSe_4]^{2-}$ with Bz_2S_2 has been reported to proceed in a similar manner to the analogous $[MoS_4]^{2-}$,[4] and $[MoS_4]^{2-}$ has been reported to react with R_2Se_2,[5] no comment has previously been made regarding $[WSe_4]^{2-}$ and R_2Se_2. This might explain why we observe greater stability of $[WSe_3(SeBz)]^-$ and higher concentrations of Bz_2Se_2 in reactions of $[WSe_4]^{2-}$ with BzCl.

When $[MoS_4]^{2-}$ and $[WSe_4]^{2-}$ are reacted with BzCl in the presence of each other, it appears that once again Bz_2S_2 is further reacting with $[MoS_4]^{2-}$ in solution. However,

the situation is made even more complex by the possibility that Bz_2S_2 is also reacting with $[WSe_4]^{2-}$ or that Bz_2Se_2 is reacting with $[MoS_4]^{2-}$. From the large amounts of Bz_2Se_2 detected in solution, it appears that the latter possibility is not a predominant process. The smaller combined integration of Bz_2S and Bz_2S_2 to Bz_2Se_2, at the end of the experiment, suggests that not all $[MoS_4]^{2-}$ was alkylated, which is consistent with some $[MoS_4]^{2-}$ reacting directly with Bz_2S_2. Therefore, we believe that the same cycles we proposed in reactions of $[PPh_4]_2[MoS_4]$ with BzCl (see Figure 5.5) are also occurring in the presence of $[PPh_4]_2[WSe_4]$, but that the $[BzS]^-$ generated *in situ* reacts with both $[MoS_3(SBz)]^-$ and $[WSe_3(SeBz)]^-$. This explains their apparent instability in the presence of each other and the formation of organic cross products.

Our reactions with $[MoSe_4]^{2-}$ show that Bz_2Se_2 is the major organic decomposition product, which is the same as in reactions of $[WSe_4]^{2-}$. The major difference is that $[MoSe_3(SeBz)]^-$ is highly unstable compared to $[WSe_3(SeBz)]^-$, likely because of the ease with which the metal can be reduced. Decomposition in both cases probably occurs by an associative mechanism similar to that observed for $[WS_3(SEt)]^-$,[58] resulting in reduction at the metal centres to form a polyselenometallate and elimination of Bz_2Se_2. An interesting observation is that only $[WS_3(SBz)]^-$ shows susceptibility to hydrolysis by small amounts of water, forming organic thiols, whereas reactions of $[MoS_4]^{2-}$, $[WSe_4]^{2-}$ and $[MoSe_4]^{2-}$ with BzCl all show a distinct absence of thiol or selenol formation.

5.4 Summary

Multinuclear NMR has proved to be a valuable tool in the investigation of alkylation reactions of $[PPh_4]_2[ME_4]$ (M = Mo, W and E = S, Se) with BzCl. In addition, the linear correlation between ^{95}Mo and ^{183}W NMR chemical shifts allowed us to easily predict the window in which a signal due to $[PPh_4][MoS_3(SBz)]$ would appear.

We have observed $[PPh_4][MoS_3(SBz)]$ and $[PPh_4][WSe_3(SeBz)]$ *in situ* using ^{95}Mo and ^{77}Se NMR spectroscopy, respectively, and ^1H NMR spectroscopy in both cases, and using time dependent spectra, we have observed differences in their decomposition pathways. While similarities exist between the alkylation of $[MoS_4]^{2-}$ versus $[WSe_4]^{2-}$, as predicted, further reaction of Bz_2S_2 with $[MoS_4]^{2-}$ appears to initiate a chain reaction that ultimately changes the ratio of products in solution compared to $[WSe_4]^{2-}$ reactions. A similar effect is observed when competitive reactions of $[MoS_4]^{2-}$ and $[WSe_4]^{2-}$ with BzCl are studied.

Based on time dependent ^1H NMR studies, we have observed that $[PPh_4][MoS_3(SBz)]$ and $[PPh_4][WSe_3(SeBz)]$ are likely candidates for isolation but that $[PPh_4][MoSe_3(SeBz)]$ is formed in such small quantities that its isolation would be impracticable. Using optimum reaction times measured from the ^1H NMR spectral data, we have attempted to synthesize and isolate these salts at low temperature, but have so far been unsuccessful.

5.5 Experimental

General Procedures

All manipulations were performed under an atmosphere of dry dinitrogen or argon, using standard Schlenk and glovebox techniques. All solvents were distilled over appropriate drying agents[144] onto molecular sieves, and degassed with dinitrogen prior to use. Benzyl chloride was purchased from Aldrich, stored over molecular sieves under dinitrogen and degassed by freeze-pump-thaw techniques prior to use. Benzyl disulfide was purchased from Aldrich and used without further purification. $[PPh_4]_2[MoS_4]$ was prepared as described in Chapter 2 and stored under dinitrogen. $[PPh_4]_2[WSe_4]$ and $[PPh_4]_2[MoSe_4]$ were prepared by Dr. Steve Reid in our laboratory using a variation on a literature procedure.[49]

Physical Measurements

^{183}W NMR measurements were performed by Dr. Deane McIntyre in the Department of Biological Sciences using an identical protocol to that described in Chapter 2. Samples of $[PPh_4][WS_3(SBz)]$ and $[PPh_4][WS_3(S^iBu)]$ were prepared by the respective syntheses described in Chapter 3, except that the concentrated THF extract obtained was directly placed in NMR tubes for analysis at room temperature.

^{95}Mo NMR measurements were performed using Bruker DRX-400 spectrometers operating at a resonance frequency of 26.0 MHz. Samples were run in 5mm tubes and the magnetic field was locked and shimmed using the ^2H resonance of the deuterated solvent. Chemical shifts were referenced externally to 2M $Na_2[MoO_4]$ solution in ^2H_2O by sample replacement. All spectra were acquired at -20 ± 1°C with a pulse length of 23 μs (90°

pulse), a relaxation delay of 0.1s, and a sweep width of 31.2 to 20.8 kHz. 32K data points were used for each pulse. Experiments were repeated at least twice to ensure reproducibility, and data were acquired and processed using both analogue and digital filtering techniques to ensure that reflected signals were not misinterpreted.

^{77}Se NMR measurements were performed using Bruker DRX-400 spectrometers operating at a resonance frequency of 76.3 MHz. Samples were run in 5mm tubes and the magnetic field was locked and shimmed using the ^{2}H resonance of the deuterated solvent. Chemical shifts were referenced externally to a saturated Ph_2Se_2 solution in $CDCl_3$ at 463ppm by sample replacement. Spectra for $[WSe_4]^{2-}$ and $[MoSe_4]^{2-}$ reactions were acquired at -20 ± 1°C and -30 ± 1°C, respectively. A pulse length of 12μs (90° pulse), a relaxation delay of 1.00s, and a sweep width of 99.1 to 38.2 kHz were used. 32K data points were used for each pulse. Experiments were repeated at least twice to ensure reproducibility, and data were acquired and processed using both analogue and digital filtering techniques to ensure that reflected signals were not misinterpreted.

Reactions of $[PPh_4]_2[MoS_4]$ with BzCl

Typical NMR scale reaction were performed as follows: $[PPh_4]_2[MoS_4]$ (15mg, 0.017mmol) was dissolved in *ca.* 0.7ml DMF-d_7 and placed in a 5mm NMR tube fitted with a rubber septum under dinitrogen. ^{1}H and ^{95}Mo spectra were collected on this sample at –20°C as a baseline before commencing the experiment. The sample was removed from the NMR probe and placed in a dry ice/acetone bath, then BzCl (19μl, 0.17mmol) was injected by syringe. The sample was immediately returned to the NMR

probe to warm to –20°C, and data acquisition was started, alternating between ^{1}H and ^{95}Mo spectra, where the latter were each collected over an hour.

A typical synthetic scale reaction was performed as follows: $[PPh_4]_2[MoS_4]$ (0.053g, 0.059mmol) was placed in a Schlenk tube and dissolved in ca. 20ml CH_3CN under dinitrogen to give a bright red solution. The solution was cooled to –40°C in a dry ice/acetone bath and BzCl (67μl, 0.59mmol) was injected by syringe. The solution was allowed to warm to –20 ± 5°C and was maintained with stirring at this level for an hour, during which the solution changed to a red/brown colour. The solvent and volatiles were then removed *in vacuo* and the residue was extracted with THF (1 × 10 ml) to give a brown solution. The solvent and residue were maintained at –20 ± 5°C during work-up, and a small sample of the THF extract was pumped down for analysis by ^{1}H NMR in CD_3CN. The signals could be attributed to $[PPh_4]^+$ (likely from polythiomolybdates) and organic sulfides, with no evidence of an alkylated species. The remainder of the THF extract was layered with Et_2O and stored at –20°C. After two days, all colour had disappeared from the solution leaving a fine black precipitate of MoS_2/MoS_3 on the sides of the tube, indicating significant decomposition had occurred.

Reactions of $[PPh_4]_2[WSe_4]$ with BzCl

NMR scale reactions of $[PPh_4]_2[WSe_4]$ (15mg, 0.014mmol) and BzCl (16μl, 0.14mmol) were performed using an identical procedure to that used for $[PPh_4]_2[MoS_4]$ except that ^{77}Se NMR was used instead of ^{95}Mo NMR spectroscopy, and each ^{77}Se spectrum was collected over 30 minutes.

Typical synthetic scale reactions for $[PPh_4]_2[WSe_4]$ (0.055g, 0.050mmol) and BzCl (57μl, 0.5mmol) were performed using an identical procedure to that used for $[PPh_4]_2[MoS_4]$ except that the reaction was allowed to stir at –20 ± 5°C for three hours instead of one. During this time the solution turned from a deep red to a red/brown colour. After removal of solvent and volatiles and extraction of the residue with THF at –20 ± 5°C, a small sample of the THF extract was pumped down for analysis by ^1H NMR in CD_3CN. The signals could be attributed to $[PPh_4]^+$ (likely from polyselenotungstates) and organic selenides, with no evidence of an alkylated species. The remainder of the THF extract was layered with Et_2O and stored at –20°C. After three days, all colour had disappeared from the solution leaving a fine black precipitate of WSe_2/WSe_3 on the sides of the tube, indicating significant decomposition had occurred.

Reactions of $[PPh_4]_2[MoSe_4]$ with BzCl

NMR scale reactions of $[PPh_4]_2[MoSe_4]$ (15mg, 0.015mmol) and BzCl (17μl, 0.15mmol) were performed using an identical procedure to that used for $[PPh_4]_2[MoS_4]$ except that ^{77}Se NMR was used instead of ^{95}Mo NMR spectroscopy, and each ^{77}Se spectrum was collected over 30 minutes.

Competitive Reactions of $[PPh_4]_2[MoS_4]$ and $[PPh_4]_2[WSe_4]$ with BzCl

Competitive NMR scale reactions of $[PPh_4]_2[MoS_4]$ (7.0mg, 7.8μmol) and $[PPh_4]_2[WSe_4]$ (8.6mg, 7.8μmol) with BzCl (18μl, 16μmol) were performed using a similar procedure to that used for $[PPh_4]_2[MoS_4]$ except that the thiomolybdate and selenotungstate solutions were mixed and subjected to ^1H and ^{77}Se NMR analysis prior to

injection of BzCl to ensure that no reaction was occurring between the two starting materials. Each ^{77}Se spectrum was collected over one hour.

Chapter 6 -- Conclusions and Further Work

6.1 General Comments

We have shown that alkylated intermediates in the condensation reactions of $[ME_4]^{2-}$ (M = Mo, W; E = O, S, Se) can be isolated and characterized when M = W and E = S, but are susceptible to decomposition by aerial oxidation, hydrolysis and high temperatures. By moving to the more reactive Mo/S, W/Se and Mo/Se systems, we are able to observe these alkylated intermediates *in situ* by multinuclear NMR spectroscopy, but have so far been unsuccessful in isolating them as salts, except in the case of $[PPh_4][MoS_3(S^tBu)]$. Mixed oxothiotungstates show a tendency to undergo O/S ligand redistribution upon alkylation and despite using pure samples of *oxo*thiometallate salts for these reactions, the only isolable alkylated products have been of the formula $[PPh_4][WS_3(SR)]$.

6.2 Comparative Reactivities of $[ME_4]^{2-}$ (M = Mo, W; E = O, S, Se) Anions

We have shown that C-E (E = S, Se) bond formation readily occurs in reactions of $[ME_4]^{2-}$ (M = Mo, W; E = O, S, Se) with alkyl halides, and that the W/S system yields the most stable products for isolation and characterization. In mixed oxothiometallates, alkylation occurs at the sulfur and no indication of C-O bond formation is observed. After alkylation, the predominant decomposition pathway is via M-E cleavage and as we move from W to Mo, or O to Se the rate of reaction increases and the stability of the alkylated intermediate decreases. Reactivity can be approximated as $[WS_4]^{2-} < [MoS_4]^{2-} \approx [WSe_4]^{2-} < [MoSe_4]^{2-}$ and stability is in the reverse order.

When we compare W/Se versus Mo/S systems we see similarities in their reactivity, likely due to the ease with which the metal can be reduced. While tungsten ligated by terminal sulfides is more difficult to reduce, replacement by selenides makes this process more facile. Extrapolating to M/O systems suggests that these would be the most difficult to reduce and consequently we see a wide range of M(VI) polynuclear architectures containing oxide ligands.[30]

6.3 Biological Implications of This Work

Some of the bonding distances measured in the crystal structures reported in Chapters 2 and 3 correspond closely with those reported for the first coordination sphere of molybdenum or tungsten in certain enzymes. For instance, the terminal oxide ligands in tungsten aldehyde oxidoreductase and molybdenum DMSO reductase are at distances of 1.74 and 1.75Å, respectively,[28] and compare quite favourably with those in disordered $[PPh_4]_2[WOS_3]$ and $[PPh_4]_2[WO_2S_2]$ at an average of 1.69 and 1.70Å, respectively. Similar variation is observed in the $M\text{-}S_{thiolene}$ distance for molybdenum and tungsten enzymes, where distances generally range from 2.35-2.50Å,[8,12,28] as compared to the slightly shorter $M\text{-}S_{thiolate}$ bonds in alkylated $[MS_4]^{2-}$, ranging from 2.32-2.35Å. These data suggest that the terminal M-O bonds in enzymes are somewhat elongated, possibly to facilitate oxygen atom transfer to a coordinated substrate. In addition, the $M\text{-}S_{thiolene}$ distances are longer than the $M\text{-}S_{thiolate}$ distances observed in our compounds, suggesting that the ligands are more loosely coordinated, possibly to allow flexibility in the metal site during the catalytic cycle. This is supported by the observation that in the disordered

crystal structure of DMSO reductase, one of the independent molecules shows a molybdopterin ligand at a non-bonding distance from the metal centre.[8]

The terminal Mo-S distance in xanthine oxidase is 2.15Å,[17] which falls within the range of average terminal M-S distances for $[PPh_4][MS_3(SR)]$, from 2.146 to 2.155Å. Average M-S bond distances in $[PPh_4]_2[MS_4]$ are slightly longer at 2.180 and 2.195Å, for M = Mo and M = W, respectively. This is particularly important since the active site possesses a combination of $[S]^{2-}$ and $[SR]^-$ ligands on a Mo(VI) centre, which has been reproduced in part by the $[PPh_4][WS_3(SR)]$ salts in the solid state. In addition, these salts have been synthesized from a biologically relevant source of the metal, $[WS_4]^{2-}$.

We have observed that $[ME_3(ER)]^-$ anions are far more reactive than the respective $[ME_4]^{2-}$ anions from which they were derived. It would appear that nature has fine tuned the coordination environment in its active sites by the careful choice of terminal chalcogenide and thiol(selenol)ate ligands, to provide the optimum reactivity for catalytic function.

6.4 Future Work

The synthesis and alkylation reactions of mixed thioselenometallates, $[PPh_4]_2[MS_xSe_{4-x}]$ (M = Mo, W), would certainly be of interest, to determine whether S/Se redistribution would occur. Alkylation would likely occur at the selenide, and if ligand redistribution did not occur, a range of new alkylated intermediates could be investigated. The active centre in formate dehydrogenase contains a terminal selenolate and four $W\text{-}S_{thiolene}$ bonds, so it would be of interest to compare structural data from the

active site to that of a small molecule containing a similar first coordination sphere, such as $[PPh_4][WS_3(SeR)]$.

Isolation of $[WSe_3(SeR)]^-$ is still unaccomplished, and our best approach may be by using ^{t}BuBr, which has shown success in the Mo/S system. It is conceivable that since formation of $[WS_3(S^tBu)]^-$ occurs by a different mechanism than primary alkyl analogues, decomposition may also be by a different mechanism that is perhaps slower. This might explain why $[MoS_3(S^tBu)]^-$ could be isolated, and since ^{1}H NMR studies of reactions of BzCl and $[WSe_4]^{2-}$ show that the W/Se alkylated species is more stable than the Mo/S alkylated species under the same conditions, our chances for the ^{t}Bu analogue are good.

If it were possible to isolate $[WSe_3(SeR)]^-$, where R = allyl, it would be of interest to compare its fluxional behaviour to that of $[WS_3(SR)]^-$ and $[WS_3(SeR)]^-$, to examine differences in alkyl shifts between selenium and sulfur atoms. Since we suggest that the allyl group can migrate over all terminal ligands in $[WS_3(SR)]^-$, we might also propose that such a process could occur in $[WSe_3(SeR)]^-$. In $[WS_3(SeR)]^-$, allyl migration could be hindered at low temperature by the C-S bond formation barrier, preventing fluxionality and providing confirmation our proposed mechanism.

There are many other variations on oxo- thio- and selenometallates that could be investigated with respect to their alkylation chemistry, including the more complex oxothioselenometallate species. Other aspects of alkylated species that have not been fully investigated are their complexation to other metals. So far, we have been unable to perform such reactions without the concomitant loss of the thiolate ligand as organic disulfide. Metal species that have a preference to bind to aromatic or unsaturated

functionalities might be a viable option, to avoid a direct interaction with the molybdenum or tungsten centre. In addition, it would be preferable to choose metals that do not complex to unalkylated $[ME_4]^{2-}$, in an attempt to prevent the behaviour observed with Fe(II), Ag(I) and Cu(I), described in Chapter 4.

As discussed in Chapter 1, the reactivity of dimethylacetylene dicarboxylate (DMAD) has been investigated with mononuclear and polynuclear metal sulfide complexes.[64,80,83] We have performed preliminary investigations into the reactions of $[ME_4]^{2-}$ (M = Mo, W; E = O, S, Se) and DMAD, and believe that polymerization of the acetylene is initiated by C-S(Se) bond formation, resulting in a complex mixture of metal containing polymeric anions. This is clearly an area of chemistry that is poorly understood, and isolation and characterization of a single component of the complex reaction mixture would be a major accomplishment. Possible approaches to this problem might involve the use of column chromatography to separate individual components, or the synthesis of smaller discrete anions that can be easily separated by recrystallization. The latter might be achieved by using a less reactive form of $[ME_4]^{2-}$, for example a copper complexed thio- or selenometallate, where the nucleophilicity of the metallate, and subsequent reaction rate, is lower. This might also allow the reaction to be sufficiently slow to follow by ^{1}H NMR spectroscopy, which has not previously been possible. ^{77}Se NMR spectroscopy could be employed to characterize products from $[MSe_4]^{2-}$ reactions, and ^{95}Mo and ^{183}W NMR could be used to determine the environments of the metal centres.

References

1) Lippard, S. J.; Berg, J. M. *Principles of Bioinorganic Chemistry*; University Science Books: Mill Valley, CA, 1994, p 131.

2) Young, C. G.; Wedd, A. G. In *Encyclopedia of Inorganic Chemistry*; King, R. B., Ed.; Wiley: New York, 1994; pp 2330-2346.

3) Adams, M. W. W. In *Encyclopedia of Inorganic Chemistry*; King, R. B., Ed.; Wiley: New York, 1994; pp 4284-4291.

4) Stiefel, E. I. In *Molybdenum Enzymes, Cofactor, and Model Systems*; Stiefel, E. I.; Coucouvanis, D.; Newton, W. E., Ed.; American Chemical Society: Washington, DC, 1993; pp 1-19.

5) Stiefel, E. I. *Science* **1996**, *272*, 1599-1600.

6) Kramer, S. P.; Johnson, J. L.; Ribero, A. A.; Millington, D. S.; Rajagopalan, K. V. *J. Biol. Chem.* **1987**, *262*, 16357-16363.

7) Schindelin, H.; Kisker, C.; Hilton, J.; Rajagopalan, K. V.; Rees, D. C. *Science* **1996**, *272*, 1615-1620.

8) Li, H.-K.; Temple, C.; Rajagopalan, K. V.; Schindelin, H. *J. Am. Chem. Soc.* **2000**, *122*, 7673-7680.

9) Hille, R. *Chem. Rev.* **1996**, *96*, 2757-2816.

10) Kramer, S. P.; Johnson, J. L.; Ribeiro, A. A.; Millington, D. S.; Rajagopalan, K. V. *J. Biol. Chem.* **1987**, *262*, 16357-16363.

11) Meyer, O.; Frunzke, K.; Tachil, J.; Volk, M. In *Molybdenum Enzymes, Cofactor, and Model Systems*; Stiefel, E. I.; Coucouvanis, D.; Newton, W. E., Ed.; American Chemical Society: Washington, DC, 1993; pp 50-68.

12) George, G. N.; Hilton, J.; Rajagopalan, K. V. *J. Am. Chem. Soc.* **1996**, *118*, 1113-1117.

13) Lippard, S. J.; Berg, J. M. *Principles of Bioinorganic Chemistry*; University Science Books: Mill Valley, CA, 1994, pp 321-322.

14) George, G. N.; Pickering, I. J.; Kisker, C. *Inorg. Chem.* **1999**, *38*, 2539-2540.

15) Garner, C. D.; Armstrong, E. M.; Ashcroft, M. J.; Austerberry, M. S.; Birks, J. H.; Collison, D.; Goodwin, A. J.; Larsen, L.; Rowe, D. J.; Russell, J. R. In *Molybdenum Enzymes, Cofactor, and Model Systems*; Stiefel, E. I.; Coucouvanis, D.; Newton, W. E., Ed.; American Chemical Society: Washington, DC, 1993; pp 98-113.

16) Romão, M. J.; Archer, M.; Moura, I.; Moura, J. J. G.; LeGall, J.; Engh, R.; Schneider, M.; Hof, P.; Huber, R. *Science* **1995**, *270*, 1170-1176.

17) Hille, R. In *Molybdenum Enzymes, Cofactor, and Model Systems*; Stiefel, E. I.; Coucouvanis, D.; Newton, W. E., Ed.; American Chemical Society: Washington, DC, 1993; pp 22-37.

18) Bertini, I.; Gray, H.; Lippard, S.; Valentine, J.; *Bioinorganic Chemistry*; University Science Books: Mill Valley, CA, 1994, pp 412-453.

19) Kim, J.; Rees, D. C. *Science* **1992**, *257*, 1677-1682.

20) Chan, M. K.; Kim, J.; Rees, D. C. *Science* **1993**, *260*, 792-794.

21) Coucouvanis, D.; Demadis, K. D.; Malinak, S. M.; Mosier, P. E.; Tyson, M. A.; Laughlin, L. J. In *Transition Metal Sulfur Chemistry: Biological and Chemical Significance*; Stiefel, E. I.; Matsumoto, K., Ed.; American Chemical Society: Washington, DC, 1996; pp 117-134.

22) Burgess. B. K. In *Molybdenum Enzymes, Cofactor, and Model Systems*; Stiefel, E. I.; Coucouvanis, D.; Newton, W. E., Ed.; American Chemical Society: Washington, DC, 1993; pp 144-169.

23) Laurie, S. H. *Eur. J. Inorg. Chem.* **2000**, 2443-2450.

24) Müller, A.; Diemann, E.; Jostes, R.; Bögge, H. *Angew. Chem. Int. Ed. Engl.* **1981**, *20*, 934-955.

25) Sarkar, S.; Mishra, S. B. S. *Coord. Chem. Rev.* **1984**, *59*, 239-264.

26) Müller, A.; Bögge, H.; Schimanski, U.; Penk. M.; Nieradzik, K.; Dartmann, M.; Krickemeyer, E.; Schimanski, J.; Römer, C.; Römer, M.; Dornfeld, H.; Wienboker, U.; Hellmann, W.; Zimmermann, M. *Monatsh. Chem.* **1989**, *120*, 367-391.

27) Newton, W. E.; Gheller, S. F.; Hedman, B.; Hodgson, K. O.; Lough, S. M.; McDonald, J. W. *Eur. J. Biochem.* **1986**, *159*, 111-115.

28) Johnson, M. K.; Rees, D. C.; Adams, M. W. W. *Chem. Rev.* **1996**, *96*, 2817-2839.

29) Hale, W. G.; Margham, J. P. *The HarperCollins Dictionary of Biology*; HarperCollins Publishers: New York, 1991, p 525.

30) Fraústo da Silva, J. J. R.; Williams, R. J. P. The Biological Chemistry of the Elements; Clarendon Press: Oxford, 1991, pp 431-434.

31) Chan, M. K.; Mukund, S. Kletzin, A.; Adams, M. W. W.; Rees, D. C. *Science*, **1995**, *267*, 1463-1469.

32) Fraústo da Silva, J. J. R.; Williams, R. J. P. *The Biological Chemistry of the Elements*; Clarendon Press: Oxford, 1991, pp 459-462.

33) Böck, A. In *Encyclopedia of Inorganic Chemistry*; King, R. B., Ed.; Wiley: New York, 1994; pp 3700-3709.

34) Boyington, J. C.; Gladyshev, V. N.; Khangulov, S. V.; Stadtman, T. C.; Sun, P. D. *Science* **1997**, *275*, 1305-1308.

35) Cramer, S. P.; Liu, C.-L.; Mortenson, L. E.; Spence, J. T.; Liu, S.-M.; Yamamoto, I.; Ljungdahl, L. G. *J. Inorg. Biochem.* **1985**, *23*, 119-124.

36) Stiefel, E. I. In *Transition Metal Sulfur Chemistry: Biological and Chemical Significance*; Stiefel, E. I.; Matsumoto, K., Ed.; American Chemical Society: Washington, DC, 1996; pp1-40.

37) Donahue, J. P.; Lorber, C.; Nordlander, E.; Holm, R. H. *J. Am. Chem. Soc.* **1998**, *120*, 3259-3260.

38) Berg, J. M.; Hodgson, K. O.; Cramer, S. P.; Corbin, J. L.; Elsberry, A.; Pariyadath, N.; Stiefel, E. I. *J. Am. Chem. Soc.* **1979**, *101*, 2774-2776.

39) Das, S. K.; Biswas, D.; Maiti, R.; Sarkar, S. *J. Am. Chem. Soc.* **1996**, *118*, 1387-1397.

40) Malinak, S. M.; Simeonov, A. M.; Mosier, P. E.; McKenna, C. E.; Coucouvanis, D. *J. Am. Chem. Soc.* **1997**, *119*, 1662-1667.

41) Eagle, A. A.; Thomas, S.; Young, C. G. In *Transition Metal Sulfur Chemistry: Biological and Chemical Significance*; Stiefel, E. I.; Matsumoto, K., Ed.; American Chemical Society: Washington, DC, 1996; pp 324-335.

42) Young, C. G.; Wedd, A. G. In *Molybdenum Enzymes, Cofactor, and Model Systems*; Stiefel, E. I.; Coucouvanis, D.; Newton, W. E., Ed.; American Chemical Society: Washington, DC, 1993; pp 70-82.

43) Xiao, Z.; Young, C. G.; Enemark, J. H.; Wedd, A. G. *J. Am. Chem. Soc.* **1992**, *114*, 9194-9195.

44) Eagle, A. A.; Harben S. M.; Tiekink, E. R. T.; Young, C. G. *J. Am. Chem. Soc.* **1994**, *116*, 9749-9750.

45) A. A. Eagle, Tiekink, E. R. T.; Young, C. G. *Inorg. Chem.* **1997**, *36*, 6315-6322.

46) Pilato, R. S.; Eriksen, K.; Greaney, M. A.; Gea, Y.; Taylor, E. C.; Goswami, S.; Kilpatrick, L.; Spiro, T. G.; Rheingold, A. L.; Stiefel, E. I. In *Molybdenum Enzymes, Cofactor, and Model Systems*; Stiefel, E. I.; Coucouvanis, D.; Newton, W. E., Ed.; American Chemical Society: Washington, DC, 1993; pp 83-97.

47) McDonald, J. W.; Friesen, G. D.; Rosenhein, L. D.; Newton, W. E. *Inorg. Chim. Acta* **1983**, *72*, 205-210.

48) Lenher, V.; Fruehan, A. G. *J. Am. Chem. Soc.* **1927**, *49*, 3076-3080.

49) O'Neal, S. C.; Kolis, J. W. *J. Am. Chem. Soc.* **1988**, *110*, 1971-1973.

50) Wardle, R. W. M.; Mahler, C. H.; Chau, C.-N.; Ibers, J. A. *Inorg. Chem.* **1988**, *27*, 2790-2795.

51) Müller, A.; Diemann, E. *Z. Anorg. Allg. Chem.* **1970**, *373*, 57-63.

52) Müller, A.; Diemann, E.; Schulze, H. *Z. Anorg. Allg. Chem.* **1970**, *376*, 120-124.

53) Gardner, D. R.; Fettinger, J. C.; Eichorn, B. W. *Angew. Chem. Int. Ed. Engl.* **1994**, *33*, 1859-1860.

54) Shibahara, T. *Coord. Chem. Rev.* **1993**, *123*, 73-147.

55) Simonnet-Jegat, C.; Toscano, R. A.; Robert, F.; Daran, J. C.; Sécheresse, F. J. *Chem. Soc., Dalton Trans.* **1994**, 1311-1315.

56) Diemann, E.; Müller, A. *Coord. Chem. Rev.* **1973**, *10*, 79-122.

57) Xin, X.; Jin, G.; Wang, B.; Pope, M. T. *Inorg. Chem.* **1990**, *29*, 553-554.

58) Kruhlak, N. L.; Wang, M.; Boorman, P. M.; Parvez, M.; McDonald, R. *Inorg. Chem.* **2001**. Accepted for publication.

59) Greenwood, N. N.; Earnshaw, A. *Chemistry of the Elements*; Pergamon: Oxford, 1984; pp 1170-1183.

60) Errington, R. J.; Kerlogue, M. D.; Richards, D. G. *J. Chem. Soc., Chem. Commun.*, **1993**, 649-651.

61) Cotton, F. A.; Wilkinson, G.; Murillo, C. A.; Bochmann, M. *Advanced Inorganic Chemistry*; 6th Ed.; Wiley: New York, 1999; pp 946-949.

62) Dance, I. G. *Polyhedron* **1986**, *5*, 1037-1104.

63) Hanewald, K.; Gattow, G. *Z. Anorg. Allg. Chem.* **1981**, *476*, 159-170.

64) Müller, A.; Bögge, H.; Krickemeyer, E.; Henkel, G.; Krebs, B. *Z. Natuforsch.* **1982**, *37b*, 1014-1019.

65) Sécheresse, F.; Lefebvre, J.; Daran, J. C.; Jeannin, Y. *Inorg. Chem.* **1982**, *21*, 1311-1314.

66) Simonnet-Jegat, C.; Jourdan, N.; Robert, F.; Bois, C.; Secheresse, F. *Inorg. Chim. Acta.* **1994**, *216*, 201-207.

67) Coucouvanis, D.; Toupadakis, A.; Koo, S. M.; Hadjikyriacou, A. *Polyhedron*, **1989**, *8*, 1705-1716.

68) Cohen, S. A.; Stiefel, E. I. *Inorg. Chem.* **1985**, *24*, 4657-4662.

69) Chandrasekaran, J.; Ansari, M. A.; Sarkar, S. *Inorg. Chem.* **1998**, *27*, 3663-3665.

70) Coucouvanis, D.; Toupadakis, A.; Hadjikyriacou, A. *Inorg. Chem.* **1988**, *27*, 3272-3273.

71) Coucouvanis, D.; Toupadakis, A.; Lane, J. D.; Koo, S. M.; Kim, C. G.; Hadjikyriacou, A. *J. Am. Chem. Soc.* **1991**, *113*, 5271-5282.

72) Coucouvanis, D.; Koo, S. M. *Inorg. Chem.* **1989**, *28*, 2-5.

73) Pan, W.-H.; Harmer, M. A.; Halbert, T. R.; Stiefel, E. I. *J. Am. Chem. Soc.* **1984**, *106*, 459-460.

74) Gea, Y.; Greaney, M. A.; Coyle, C. L.; Stiefel, E. I. *J. Chem. Soc., Chem. Commun.* **1992**, 160-161.

75) Wang, K.; McConnachie, J. M.; Stiefel, E. I. *Inorg. Chem.* **1999**, *38*, 4334-4341.

76) Afanasiev, P.; Geantet, C.; Thomazeau, C.; Jouget, B. *J. Chem. Soc., Chem. Commun.* **2000**, 1001-1002.

77) Stiefel, E. I.; Halbert, T. R.; Coyle, C. I.; Wei, L.; Pan, W. -H.; Ho, T. C.; Chianelli, R. R.; Daage, M. *Polyhedron* **1989**, *8*, 1625-1629.

78) Mdleleni, M. M.; Hyeon, T.; Suslick, K. S. *J. Am. Chem. Soc.* **1998**, *120*, 6189-6190.

79) York, A. *Chemistry in Britain*, **2000**, *36*, 40-41.

80) Duddeck, H. *Progr. Nucl. Magn. Spectr.* 1995, 27, 1-323.

81) Wardle, R. W. M.; Chau, C.-N.; Ibers, J. A. *J. Am. Chem. Soc.* **1987**, 109, 1859-1860.

82) Kawaguchi, H.; Tatsumi, K. *J. Am. Chem. Soc.* **1995**, *117*, 3885-3886.

83) Kawaguchi, H.; Yamada, K.; Lang, J.-P.; Tatsumi, K. *J. Am. Chem. Soc.* **1997**, *119*, 10346-10358.

84) Kawaguchi, H.; Tatsumi, K. *J. Chem. Soc., Chem. Commun.* **2000**, 1299-1300.

85) Rau, M. S.; Kretz, C. M.; Geoffrey, G. L.; Rheingold, A. L. *Organometallics* **1993**, *12*, 3447-3460.

86) Cousins, M.; Green, M. L. H. *J. Chem. Soc. A* **1969**, 16-19.

87) Coucouvanis, D.; Hadjikyriacou, A.; Toupadakis, A.; Koo, S.-M.; Draganjac, M.; Salifoglou, A. *Inorg. Chem.* **1991**, *30*, 754-767.

88) Callahan, K. P.; Piliero, P. A. *Inorg. Chem.* **1980**, 19, 2619-2626.

89) Potvin, C.; Manoli, J.-M.; Sécheresse, F.; Marzak, S. *Inorg. Chem.* **1987**, *26*, 4370-4374.

90) Clegg, W.; Garner, D. C.; Nicholson, J. R. *Acta. Crystallogr.* **1983**, *C39*, 552-554.

91) Sécheresse, F.; Robert, F.; Marzak, S.; Manoli, J.-M.; Potvin, C. *Inorg. Chim. Acta.* **1991**, *182*, 221-228.

92) Gao, J.; Wu, X.; Zhang, W.; Sheng, T.; Huang, Q.; Lin, P.; Wang, Q.; Lu, J. *Angew. Chem. Int. Ed. Engl.* **1997**, *36*, 2464-2466.

93) Liu, H.; Cao, R.; Lei, X.; Wu, D.; Wei, G.; Huang, Z.; Hong, M.; Kang, B. *J. Chem. Soc., Dalton Trans.* **1990**, 1023-1026.

94) Lang, J.; Li, J.; Bao, S.; Xin, X.; Yu, K. *Polyhedron* **1993**, *12*, 801-806.

95) Hong, M.; Zhang, Q.; Cao, R.; Wu, D.; Chen, J.; Zhang, W.; Liu, H.; Lu, J. *Inorg. Chem.* **1997**, *36*, 6251-6260.

96) Christuk, C. C.; Ibers, J.A. *Inorg. Chem.* **1993**, *32*, 5105-5107.

97) Zhang, Q.; Bao, M.; Hong, M.; Cao, R.; Song, Y.; Xin, X. *J. Chem. Soc., Dalton Trans.* **2000**, 605-610.

98) Liu, Q.; Huang, L.; Liu, H.; Lei, X.; Wu, D.; Kang, B.; Lu, J. *Inorg. Chem.* **1990**, *29*, 4131-4137.

99) Chen, C.; Wen, T.; Li, W.; Zhu, H.; Chen, Y.; Liu, Q.; Lu, J. *Inorg. Chem.* **1999**, *38*, 2375-2379.

100) Osterloh, F.; Segal, B. M.; Achim, C.; Holm, R. H. *Inorg. Chem.* **2000**, *39*, 980-989.

101) Krüss, G., *Liebigs Ann. Chem.* **1884**, *225*, 1-57.C

102) Corleis, E. *Liebigs Ann. Chem.*, **1886**, *232*, 244-270.

103) Quagraine, E. K.; Reid, R. S. *Personal communication.*

104) Harmer, M. A.; Sykes, A. G. *Inorg. Chem.* **1980**, *19*, 2881-2885.

105) Aymonino, P. J.; Renade, A. C.; Diemann, E.; Müller, A. *Z. Anorg. Allg. Chem.* **1969,** *371*, 300-305.

106) Aymonino, P. J.; Renade, A. C.; Müller, A. *Z. Anorg. Allg. Chem.* **1969,** *371*, 295-299.

107) Gheller, S. F.; Hambley, T. W.; Rodgers, J. R.; Brownlee, R. T. C.; O'Connor, M. J.; Snow, M. R.; Wedd, A. G. *Inorg. Chem.* **1984**, *23*, 2519-2528.

108) Minelli, M.; Enemark, J. H.; Brownlee, R. T. C.; O'Connor M. J.; Wedd. A. G. *Coord. Chem. Rev.* **1985**, *68*, 169-278.

109) Gheller, S. F.; Gazzana, P. A.; Masters, A. F.; Brownlee, R. T. C.; O'Connor, M. J.; Wedd, A. G.; Rodgers, J. R.; Snow, M. R. *Inorg. Chim. Acta* **1981**, *54*, L131-132.

110) Brevard, C.; Granger, P. *Handbook of High Resolution Multinuclear NMR*; Wiley: New York, USA, 1981, pp138-193.

111) Quagraine, E. K. *Personal communication.*

112) Ma, Y.; Demou, P.; Faller, J. W. *Inorg. Chem.* **1991**, *30*, 62-64.

113) Youngkyu, D.; Simhon, E. D.; Holm, R. H. *Inorg. Chem.* **1985**, *24*, 1831-1838.

114) Kroneck, P.; Lutz, O.; Nolle, A. *Z. Naturforsch.* **1980**, *35A*, 226-229.

115) Lutz, O.; Nolle, A.; Kroneck, P. *Z. Naturforsch.* **1977**, *32A*, 505-506.

116) Kraatz, H.-B.; Aramini, J. M.; Gao, X.; Boorman, P. M.; Vogel, H. J. *Inorg. Chem.* **1993**, *32*, 3976-3979.

117) O'Neal, S. C.; Kolis, J. W. *Inorg. Chem.* **1989**, *28*, 2780-2783.

118) Wang, M. Ph.D Thesis, 1996, University of Calgary, Canada.

119) Lapasset, J.; Chezeau, N.; Belougne, P. *Acta Crystallogr.* **1976**, *B32*, 3087-3088.

120) Kutzler, F. W.; Scott, R. A.; Berg, J. M.; Hodgson, K. O.; Doniach, S.; Cramer, S. P.; Chang, C. H. *J. Am. Chem. Soc.* **1981**, *103*, 6038-6088.

121) Fuchs, V. J.; Freivald, W.; Hartl, H. *Acta Crystallogr.* **1978**, *B34*, 1764-1770.

122) Hou, H.-W.; Ye, X.; Xin, X.; *Acta Crystallogr.* **1995**, *C51*, 2013-2015.

123) LaRue, W.; Liu, A. T.; Fillipo, J. S. *Inorg. Chem.* **1980**, *19*, 315-320.

124) Parvez, M.; Boorman, P. M.; Langdon, N. L. *Acta Crystallogr.* **1998**, *C54*, 608-609.

125) Bhattacharyya, R.; Biswas, S.; Armstrong, J.; Holt, E. M. *Inorg. Chem.* **1989**, *28*, 4297-4300.

126) Errington, R. J.; Kerlogue, M. D.; Richards, D. G. *J. Chem. Soc., Chem. Commun.* **1993**, 649-651.

127) Kato, M.; Kawano, M.; Taniguchi, H.; Funaki, M.; Moriyama, H.; Sato, T.; Matsumoto, K. *Inorg. Chem.* **1992**, *31*, 26-35.

128) TEXSAN: *Crystal Structure Analysis Package*; Molecular Structure Corporation: The Woodlands, TX, 1985 and 1992.

129) Sheldrick, G. M. *SHELX-97: Program for the Refinement of Crystal Structures*; University of Göttingen: Germany, 1997.

130) Boorman, P. M.; Gao, X.; Fait, J. L.; Parvez, M. *Inorg. Chem.* **1991**, *30*, 3886-3893.

131) Dhar, P.; Chandrasekaran, S. *J. Org. Chem.* **1989**, *54*, 2998-3000.

132) Dhar, P.; Ranjan, R.; Chandrasekaran, S. *J. Org. Chem.* **1990**, *55*, 3728-3729.

133) Boorman, P. M.; Wang, M.; Parvez, M. *J. Chem. Soc., Chem. Commun.* **1995**, 999-1000.

134) Parvez, M.; Wang, M.; Boorman, P. M. *Acta Crystallogr.* **1996**, *C52*, 377-378.

135) Gao, X. Ph.D Thesis, 1992, University of Calgary, Canada.

136) Vollhardt, K. P. C.; Schore, N. E. *Organic Chemistry: Structure and Function*; 3rd Ed.; W. H. Freeman: New York, 1999; p335.

137) Parvez, M.; Boorman, P. M.; Wang. M. *Acta Crystallogr.* **1997**, *C53*, 413-414.

138) Kruhlak, N. L.; Nguyen, P. N.; Boorman, P. M.; Parvez, M. Manuscript in preparation.

139) Listemann, M. L.; Dewan, J. C.; Schrock, R. R. *J. Am. Chem. Soc.* **1985**, *107*, 7207-7208.

140) Otsuka, S.; Kamata, M.; Hitotsu, K.; Higuchi, T. *J. Am. Chem. Soc.* **1981**, *103*, 3011-3014.

141) Vollhardt, K. P. C.; Schore, N. E. *Organic Chemistry: Structure and Function*; 3rd Ed.; W. H. Freeman: New York, 1999; p671.

142) Olah, G.; Kuhn, S.; Olah, J. *J. Chem. Soc.* **1957**, 2174-2176.

143) El-Issa, B. D.; Ali, A. A. M.; Zanati, H. *Inorg. Chem.* **1980**, *28*, 3297-3305.

144) Perrin, D. D.; Amarego, W. L. F. *Purification of Laboratory Chemicals*; 3rd ed.; Pergamon Press: Oxford, 1988.

145) Sheldrick, G. M. *Acta Crystallogr.* **1990**, *A46*, 467-473.

146) Beurskens, P. T.; Beurskens, G.; Bosman, W. P.; de Gelder, R.; Garcia Granda, S.; Gould, R. O.; Israel, R.; Smits, J. M. M. *The DIRDIF-96 Program System*; Crystallography Laboratory, University of Nijmegen: The Netherlands, 1996.

147) Sheldrick, G. M. *SHELXL-93: Program for the Refinement of Crystal Structures*; University of Göttingen: Germany, 1993.

148) Personal communication with Christophe Taeschler.

149) Gimeno, M. C; Jones, P. G.; Laguna, A.; Laguna, M.; Terroba, R. *Inorg. Chem.* **1994**, *33*, 3932-3938.

150) Nakamura, A.; Ueyama, N.; Tatsumi, K. *Pure Appl. Chem.* **1990**, *62*, 1011-1020.

151) King, J. F.; Tsang, G. T. Y.; Abdel-Malik, M. M.; Payne, N. C. *J. Am. Chem. Soc.* **1985**, *107*, 3224-3232.

152) Lag, J.; Li, J.; Bao, S.; Xin, X. *Polyhedron* **1993**, *12*, 801-806.